



**THE UNIVERSITY OF QUEENSLAND**  
AUSTRALIA

# **SENATAXIN IN DNA REPAIR AND MEIOTIC SILENCING**

**Abrey Jie Yeo**

BSc. (Hons) Biochemistry & Molecular Biology

*A thesis submitted for the degree of Doctor of Philosophy at  
The University of Queensland in 2014*

School of Medicine

## ABSTRACT

Hereditary ataxias are a group of rare neurological genetic disorders characterized by debilitating signs and symptoms that include progressive lack of coordination of gait and is also often associated with poor coordination of hands, speech, and eye movements. The different forms of ataxia are diagnosed by family history, physical examination, neuroimaging, and molecular genetic testing. To date, no specific treatments exist for hereditary ataxias. Oculomotor apraxia type 2 (AOA2) is part of a subgroup of autosomal recessive cerebellar ataxias (ARCA) characterized by defects in genes responsible for the recognition and/or repair of DNA damage. AOA2 is caused by mutations in the gene *SETX* (coding for senataxin), and cells from these patients have been characterized by the presence of oxidative stress, defects in the repair of oxidative DNA lesions, and abnormal RNA processing and termination of transcription.

Recent studies suggest that senataxin is involved in coordinating events between DNA replication and ongoing transcription. To further understand the physiological role of senataxin, we generated the first *Setx*<sup>-/-</sup> mouse model. In this Report, the phenotypic characterization of this mouse model is discussed. An essential role for senataxin in spermatogenesis was demonstrated by showing that the absence of senataxin led to the persistence of DNA double strand breaks, disruption of homologous recombination and an incomplete diffusion of DNA damage response proteins on the broader XY chromatin. Senataxin localized to the XY body during the pachytene stage of spermatogenesis and this was dependent on *Brca1*, which functions early in meiotic sex chromosome inactivation (MSCI) to recruit other DNA damage response proteins to the XY body. We observed that there was no diffusion of *Atr*, a key regulator of the DNA damage response during MSCI, to the broader XY chromatin in *Setx*<sup>-/-</sup> pachytene-staged spermatocytes, indicating abnormal *Atr* activity and signalling during MSCI. The persistent activity of RNA polymerase II on the XY body, the disrupted localization of heterochromatin markers such as *ubH2A*, as well as the abnormal expression of XY genes demonstrated an essential role for senataxin at the interface of replication and transcription, and in coordinating MSCI. The end result was sterility in male *Setx*<sup>-/-</sup> mice due to defects in MSCI, increased apoptosis, and a failure to complete meiosis during spermatogenesis.

Recent reports have also shown a role for senataxin in resolving R-loops, which are DNA/RNA hybrids that occur naturally during transcription behind elongating RNA Polymerase II. Here, the *in vivo* accumulation of R-loops in the testes of *Setx*<sup>-/-</sup> mice as well as in that of other ARCA mouse models (*Atm*, *Aptx* and *Tdp1*) is reported. This represents the first evidence of R-loop accumulation in such mouse models and demonstrates that R-loops can contribute significantly towards genome

instability. This correlates with the perturbed fertility observed in these disorders. Additionally, we also provide further evidence that R-loop formation requires both the activity of replication and transcription, and that genomic instability is a consequence of disrupted transcription in the presence of DNA double strand breaks that arise during DNA replication or recombination. While R-loops have been identified as a substrate for senataxin, the absence of R-loops in post-mitotic tissues may reflect a regulatory role for senataxin in transcription and/or RNA processing that does not involve the resolution of R-loops *per se*. AOA2 may represent a novel “RNAopathy” in which defects in senataxin can affect the fidelity of the transcriptome. Altogether, these findings reveal a complex and coordinated network between transcription, RNA processing, and DNA repair pathways, and support the emerging importance of RNA processing factors, such as senataxin, in maintaining genome stability.

## **DECLARATION BY AUTHOR**

This thesis is composed of my original work, and contains no material previously published or written by another person except where due reference has been made in the text. I have clearly stated the contribution by others to jointly-authored works that I have included in my thesis.

I have clearly stated the contribution of others to my thesis as a whole, including statistical assistance, survey design, data analysis, significant technical procedures, professional editorial advice, and any other original research work used or reported in my thesis. The content of my thesis is the result of work I have carried out since the commencement of my research higher degree candidature and does not include a substantial part of work that has been submitted to qualify for the award of any other degree or diploma in any university or other tertiary institution. I have clearly stated which parts of my thesis, if any, have been submitted to qualify for another award.

I acknowledge that an electronic copy of my thesis must be lodged with the University Library and, subject to the General Award Rules of The University of Queensland, immediately made available for research and study in accordance with the *Copyright Act 1968*.

I acknowledge that copyright of all material contained in my thesis resides with the copyright holder(s) of that material. Where appropriate I have obtained copyright permission from the copyright holder to reproduce material in this thesis.

## PUBLICATIONS DURING CANDIDATURE

**R-Loops in Proliferating Cells but Not in the Brain: Implications for AOA2 and Other Autosomal Recessive Ataxias.** Yeo AJ, Becherel OJ, Luff JE, Cullen JK, Wongsurawat T, Jenjaroenpoon P, Kuznetsov VA, McKinnon PJ, Lavin MF. 2014. *PLoS One*. 9(3): e90219.

**Senataxin Protects the Genome: Implications for Neurodegeneration and other Abnormalities.** Lavin MF, Yeo AJ and Becherel OJ. 2013. *Journal of Rare Diseases*. Vol I (Addendum): e25230.

**Senataxin saves Sperm- World of Reproduction Biology.** Feature article written by Charlotte Shubert. Becherel OJ, Yeo AJ, Stellati A, Heng EY, Luff J, Suraweera AM, Woods R, Fleming J, Carrie D, McKinney K, Xu X, Deng C, Lavin MF. 2013. *Biology of Reproduction*. 89 (1) 1, 1-2.

**Senataxin Plays an Essential Role with DNA Damage Response Proteins in Meiotic Recombination and Gene Silencing.** Becherel OJ, Yeo AJ, Stellati A, Heng EY, Luff J, Suraweera AM, Woods R, Fleming J, Carrie D, McKinney K, Xu X, Deng C, Lavin MF. 2013. *PLoS Genetics*. 9(4): e1003435.

## PUBLICATIONS INCLUDED IN THIS THESIS

Publication citation – incorporated as Chapter 5.

**R-Loops in Proliferating Cells but Not in the Brain: Implications for AOA2 and Other Autosomal Recessive Ataxias.** Yeo AJ, Becherel OJ, Luff JE, Cullen JK, Wongsurawat T, Jenjaroenpun P, Kuznetsov VA, McKinnon PJ, Lavin MF. 2014. *PLoS One*. 9(3): e90219.

Contribution of Authors:

Contributor	Statement of Contribution
Author (Abrey J Yeo)	Designed experiments (60%) Performed experiments (80%) Analysed the data (70%) Wrote the paper (60%)
Author (Olivier J Becherel)	Designed experiments (20%)

	Performed experiments (15%) Analysed the data (20%) Wrote paper (15%)
Author (John E. Luff)	Managed mouse breeding program
Author (Jason K. Cullen)	Performed experiments (5%)
Author (Thidathip Wongsurawat)	Provided prediction program Contributed to Figure 4
Author (Piroon Jenjaroenpoon)	Provided prediction program
Author (Vladimir A. Kuznetsov)	Wrote the paper (5%)
Author (Peter J. McKinnon)	Provided <i>Tdp1</i> and <i>Aptx</i> mice
Author (Martin F. Lavin)	Designed experiments (20%) Analysed the data (20%) Wrote paper (20%)

## **CONTRIBUTIONS BY OTHERS TO THE THESIS**

**Prof. Martin F. Lavin** was the Principal Investigator for the Project and contributed to discussion on study design, data interpretation and provided comments on the Thesis and publications.

**Dr. Olivier J. Becherel** was the co-supervisor and contributed to discussion on study design, data interpretation and provided comments on the Thesis and publications.

**Dr. Mark Graham** performed the liquid chromatography mass spectrometry and assisted in interpreting the data.

**Mr. John Luff** was in charge of the mouse-breeding program.

## **STATEMENT OF PARTS OF THE THESIS SUBMITTED TO QUALIFY FOR THE AWARD OF ANOTHER DEGREE**

None.

## ACKNOWLEDGEMENTS

I would first like to thank God for everything. He has blessed me with so much throughout my Ph.D.

I would next like to thank my supervisors, Prof. Martin F. Lavin and Dr. Olivier J. Becherel for their guidance and support these few years. A big thank you to Martin for taking me in when I was a green horn during my Honours, for believing in me that I could complete a Ph.D. and for inspiring me to always be steadfast in my research. I would also like to say a special thank you to Olivier, who has always been there for me not only as a mentor but also as a dear friend. Thank you for all your encouragement and patience, and for making this journey more fun to travel on. I would also like to acknowledge the financial support provided to me by the University of Queensland, the QIMR Berghofer Medical Research Institute, the BrAshA-T Foundation, the Australian National Health & Medical Research Council (NHMRC) and the Australian Research Council (ARC), without which I would not have been able to embark on this course.

To my parents, Anthony and Jane, thank you so much for giving me the opportunity and support to study in Australia. Thank you for always being there for me all these years and for all your sacrifices and prayers from afar. Dad, thank you for all your encouragement, practical advice and for keeping me on track. Mum, thank you for always being my sounding board, for your nurturing love and support. I love you both so much and no words can express the heartfelt gratitude I have for you both. Appreciation also goes out to my one and only sister, Audrey, who has shared in my many moments of tears and joy.

I would also like to thank my fiancé, Clement, for always being there for me through thick and thin. Thank you for your patience and for understanding my Ph.D.-related mood swings during this time.

Lastly, I would like to thank all my colleagues at UQCCR and QIMR, Dr. Amanda Kijas, Dr. Sergei Kozlov, Dr. Magtouf Gatei, Dr. Yi Chieh Lim, Ms. Aine Farrell, Mr. John Luff, Mr. Romal Stewart and Ms. Hazel Quek for being part of my journey, and for all the advice, fun and laughter shared with me during this time.



## **KEYWORDS**

senataxin, mouse model, meiosis, R-loops, DNA damage repair, spermatogenesis, transcription.

## **AUSTRALIAN AND NEW ZEALAND STANDARD RESEARCH CLASSIFICATIONS (ANZSRC)**

ANZSRC code: 060103 Cell Development, Proliferation and Death, 40%

ANZSRC code: 060199, Biochemistry and Cell Biology not elsewhere classified, 40%

ANZSRC code: 060408 Genomics, 20%

## **FIELDS OF RESEARCH (FOR) CLASSIFICATION**

FoR code: 0601, Biochemistry and Cell Biology, 70%

FoR code: 0699, Other Biological Sciences, 20%

FoR code: 0604, Genomics, 10%

## LIST OF FIGURES

### Chapter 1:

- 1.1 ATM activation and signalling to downstream substrates in response to DNA DSBs
- 1.2 Mechanism of action of Topo I
- 1.3 Aprataxin removes 5'-AMP from abortive DNA ligation intermediates
- 1.4 Distribution of mutations along *SETX*
- 1.5 Schematic domain organization of SETX and related proteins
- 1.6 Role for senataxin in R loop resolution
- 1.7 Role of senataxin in relations to neurodegeneration
- 1.8 Effects of ROS/RNS on cells
- 1.9 Models of DNA repair pathways
- 1.10 DNA strand break repair pathways during nervous system development
- 1.11 Process of spermatogenesis
- 1.12 Schematic time line of the first wave of spermatogenesis
- 1.13 Different stages of synaptonemal complex (SC) formation in mouse spermatocytes
- 1.14 Schematic diagram of DNA repair proteins in meiotic recombination
- 1.15 The initiation of MSCI
- 1.16 Alternative splicing mechanism
- 1.17 Potential models of transcriptional R-loops mediated DNA damage
- 1.18 R-loops prevent methylation of CpG island promoters

### Chapter 3:

- 3.1 Targeted disruption of mouse *Setx* gene
- 3.2 Disruption of the *Setx* gene in *Setx*<sup>-/-</sup> mice
- 3.3 Absence of neurological phenotype and ataxia in *Setx*<sup>-/-</sup> mice
- 3.4 No gross cellular or structural differences in brain or cerebellum of *Setx*<sup>-/-</sup> mice
- 3.5 *Setx*<sup>-/-</sup> mice have normal Purkinje cell arrangement
- 3.6 Defect in spermatogenesis in *Setx*<sup>-/-</sup> mice
- 3.7 Normal ovarian structure in *Setx*<sup>-/-</sup> mice
- 3.8 Block in meiosis at pachytene stage in *Setx*<sup>-/-</sup> spermatocytes
- 3.9 Increased apoptosis in germ cells in *Setx*<sup>-/-</sup> mice
- 3.10 Persistence of DNA DSBs ( $\gamma$ H2AX) in *Setx*<sup>-/-</sup> spermatocytes

- 3.11 Persistence of DNA DSBs (Rad51) in *Setx*<sup>-/-</sup> spermatocytes
- 3.12 Absence of crossing-over in *Setx*<sup>-/-</sup> spermatocytes
- 3.13 Similar expression levels of Rad51 and Mlh1 in *Setx* mice
- 3.14 Senataxin localizes to the XY chromosomes during meiosis
- 3.15 Aberrant meiotic sex chromosome inactivation (MSCI) in *Setx*<sup>-/-</sup> spermatocytes

#### Chapter 4:

- 4.1 SUMO is confined to the axial element of the XY chromosomes in *Setx*<sup>-/-</sup> spermatocytes
- 4.2 Senataxin interacts with SUMO-1 at the XY chromosomes in *Setx*<sup>+/+</sup> spermatocytes
- 4.3 Excision of bands following SUMO-1 immunoprecipitation from *Setx*<sup>+/+</sup> and *Setx*<sup>-/-</sup> testes
- 4.4 Atrp is SUMOylated in spermatocytes of *Setx*<sup>+/+</sup> but not *Setx*<sup>-/-</sup> mice
- 4.5 Normal recruitment of Brca1 in *Setx*<sup>+/+</sup> and *Setx*<sup>-/-</sup> spermatocytes
- 4.6 Recruitment of senataxin is dependent on Brca1
- 4.7 No direct interaction between senataxin and Brca1
- 4.8 Decreased levels of TopBP1 on XY chromosomes of *Setx*<sup>-/-</sup> spermatocytes
- 4.9 Lack of diffusion of Atr over XY chromosomes in *Setx*<sup>-/-</sup> spermatocytes
- 4.10 Lack of diffusion of p-Atr (S428) over XY chromosomes in *Setx*<sup>-/-</sup> spermatocytes
- 4.11 Decreased levels of Atrp on XY chromosomes in *Setx*<sup>-/-</sup> spermatocytes
- 4.12 Lack of diffusion of p-Rpa (S33) over XY chromosomes in *Setx*<sup>-/-</sup> spermatocytes
- 4.13 Decreased levels of p-Chk1 (S317) on XY chromosomes in *Setx*<sup>-/-</sup> spermatocytes
- 4.14 DDR protein levels in *Setx*<sup>+/+</sup> and *Setx*<sup>-/-</sup> testes
- 4.15 Mis-localization of Nek1 in *Setx*<sup>-/-</sup> spermatocytes
- 4.16 Differential localization of ubH2A in *Setx*<sup>-/-</sup> spermatocytes
- 4.17 Differential formation of heterochromatin of XY chromosomes in *Setx*<sup>-/-</sup> spermatocytes
- 4.18 Lack of recruitment of Chd4 over XY chromosomes in *Setx*<sup>-/-</sup> spermatocytes
- 4.19 *In-situ* interaction of senataxin with Chd4 at the XY chromosomes in *Setx*<sup>+/+</sup> spermatocytes during MSCI
- 4.20 Molecular mechanism of MSCI failure in *Setx*<sup>-/-</sup> mice

#### Chapter 5:

- 5.1 Treatment of *Atm* and *Aptx* mice with topotecan hydrochloride induces severe weight loss
- 5.2 Induction of R-loops in proliferating cells after topotecan hydrochloride treatment

- 5.3 Topotecan hydrochloride treatment does not induce R-loop formation in post-mitotic nervous tissues in *Atm*<sup>-/-</sup> mice
- 5.4 Increased R-loop formation in topotecan hydrochloride-treated *Atm*<sup>-/-</sup> and *Aptx*<sup>-/-</sup> mice
- 5.5 Increased R-loop formation at Fra8E1 in testes of *Setx*<sup>-/-</sup> mice
- 5.6 R-loop formation sites predicted by QuadFinder on the mouse XY genes *Ube1y* and *Tkt1l*
- 5.7 PCR amplification of predicted R-loop formation sites from DRIP assay performed in *Setx* mice
- 5.8 Problems that can arise from R-loop accumulation

## **Chapter 6:**

- 6.1 Senataxin in proliferating and post-mitotic cells

## **LIST OF TABLES**

### **Chapter 1:**

- 1.1 Genetic and clinical features of ARCAs associated with defects in DNA repair
- 1.2 Neurological disorders associated with RNA processing defects

### **Chapter 2:**

- 2.1 Description of primers for genotyping of animals
- 2.2 Description of primary antibodies for immunofluorescence
- 2.3 Description of secondary antibodies for immunofluorescence
- 2.4 Description of primary antibodies for PLA
- 2.5 Description of primers for RT-PCR
- 2.6 Description of primary antibodies for immunoblotting
- 2.7 Description of secondary antibodies for immunoblotting
- 2.8 Description of primers for DRIP assay

### **Chapter 3:**

- 3.1 Essential role for senataxin in spermatogenesis and germ cell maturation

## LIST OF COMMONLY USED ABBREVIATIONS

8-oxo-dG	8'-oxo-2'-deoxy guanosine
$\gamma$ H2AX	Phosphorylated histone H2AX
ALS4	Amyotrophic lateral sclerosis type 4
AOA1	Ataxia oculomotor apraxia type I
AOA2	Ataxia oculomotor apraxia type II
ARCA	Autosomal recessive cerebellar ataxia
A-T	Ataxia Telangiectasia
A-TLD	Ataxia telangiectasia-like Disorder
ATM	Ataxia-telangiectasia mutated
ATR	Ataxia telangiectasia and Rad3 related
ATRIP	ATR interacting protein
bp	Base pair
BRCA1	Breast cancer 1
C3ABR	Control lymphoblastoid cell line
CHD4	Chromodomain helicase DNA binding protein 4
CHK1	Checkpoint kinase 1
DDR	DNA damage repair
DMC1	DNA Meiotic Recombinase 1
DRIP	DNA:RNA immunoprecipitation
DSB	Double strand break
dsDNA	Double-stranded DNA
H3K4me1	Histone H3 Lysine 4 (mono-methylated)
H&E	Haematoxylin & Eosin
HR	Homologous recombination
IP	Immunoprecipitation
iPSCs	Induced pluripotent stem cells
kb	Kilo base
LCL	Lymphoblastoid cell line
MDC1	Mediator of DNA-damage checkpoint 1
MLH1	MutL homolog 1
MRN	MRE11-RAD50-NBS
MS	Mass spectrometry
MSCI	Meiotic sex chromosome inactivation

MSH4/5	MutS Homolog 4/5
NuRD	Nucleosome remodeling deacetylase
ONSCs	Olfactory neural stem cells
PCR	Polymerase chain reaction
RLFS	R-loop forming site
RNAPII	RNA polymerase II
RPA	Replication protein A
RT-PCR	Reverse-transcriptase polymerase chain reaction
SCAN1	Spinocerebellar ataxia with axonal neuropathy type I
SCP3	Synaptonemal complex protein 3
SDS-PAGE	Sodium dodecyl sulfate-polyacrylamide gel electrophoresis
SETX	Senataxin
SSB	Single strand break
ssDNA	Single-stranded DNA
SUMO	Small ubiquitin-like modifier
TopBP1	DNA topoisomerase 2-binding protein 1
TAE	Tris-Acetate-EDTA
TDP1	Tyrosyl-DNA phosphodiesterase 1
TUNEL	Terminal deoxynucleotidyl transferase dUTP nick end labelling
ubH2A	Ubiquitinated histone H2A
WT	Wild type

## TABLE OF CONTENTS

ABSTRACT.....	ii
DECLARATION BY AUTHOR.....	iv
PUBLICATIONS DURING CANDIDATURE .....	v
PUBLICATIONS INCLUDED IN THIS THESIS.....	v
CONTRIBUTIONS BY OTHERS TO THE THESIS.....	vii
STATEMENT OF PARTS OF THE THESIS SUBMITTED TO QUALIFY FOR THE AWARD OF ANOTHER DEGREE.....	vii
ACKNOWLEDGEMENTS .....	viii
KEYWORDS .....	ix
AUSTRALIAN AND NEW ZEALAND STANDARD RESEARCH CLASSIFICATIONS (ANZSRC).....	ix
FIELDS OF RESEARCH (FOR) CLASSIFICATION .....	ix
LIST OF FIGURES .....	x
LIST OF COMMONLY USED ABBREVIATIONS.....	xiv
<b>CHAPTER 1 Literature Review .....</b>	<b>1</b>
1.1 Autosomal recessive cerebellar ataxias.....	3
1.1.1 Ataxia-Telangiectasia (A-T).....	4
1.1.2 Ataxia-Telangiectasia-related disorders .....	6
1.1.3 Spinocerebellar ataxia with axonal neuropathy (SCAN1).....	8
1.1.4 Ataxia oculomotor apraxia type I (AOA1).....	9
1.1.5 Ataxia oculomotor apraxia type II (AOA2).....	10
1.2 DNA damage and DNA repair.....	14
1.2.1 Oxidative stress and DNA damage.....	14
1.2.2 DNA strand break repair.....	16
1.2.2.1 Single strand break (SSB) repair .....	16
1.2.2.2 Double strand break (DSB) repair.....	16



1.3 DNA Repair & Spermatogenesis .....	19
1.3.1 Spermatogenesis .....	19
1.3.2 Meiotic Sex Chromosome Inactivation (MSCI) .....	24
1.4 Transcription regulation & disease .....	25
1.4.1 Aberrant splicing & neurodegeneration.....	25
1.4.2 Transcription regulation & genomic instability.....	28
1.4.2.1 R-loops accumulation can cause genomic instability.....	28
1.4.2.2 R-loops & gene expression (CpG methylation) .....	31
1.4.2.3 G-quadruplexes & R-loop formation.....	32
1.5 Aims of Project .....	33
<b>CHAPTER 2: Materials &amp; Methods .....</b>	<b>35</b>
2.1 Animal husbandry & genotyping.....	36
2.2 Cell culture.....	37
2.3 Senataxin immunoprecipitation .....	37
2.4 Histological analyses of <i>Setx</i> mouse tissues .....	38
2.5 Immunofluorescence .....	38
2.6 TUNEL assay.....	40
2.7 Spermatocyte spreads.....	41
2.8 Proximity ligation assay (PLA).....	41
2.9 RT-PCR & gene expression analyses .....	42
2.10 Immunoprecipitation of SUMOylated proteins from <i>Setx</i> <sup>+/+</sup> and <i>Setx</i> <sup>-/-</sup> testes.....	43
2.11 Tryptic digestion of SUMOylated proteins from mice spermatocytes for Mass Spectrometry.....	44
2.12 Immunoblotting for DDR proteins from <i>Setx</i> <sup>+/+</sup> and <i>Setx</i> <sup>-/-</sup> testes .....	44
2.13 Transfection of HeLa and U2OS cells with Stealth <sup>TM</sup> siRNA.....	46
2.14 Treatment of HeLa and U2OS cells with Camptothecin and Actinomycin D.....	46
2.15 DNA:RNA immunoprecipitation assay (DRIP) .....	47
2.16 PCR analyses for DRIP assay .....	48

<b>CHAPTER 3 Characterization of the <i>Setx</i><sup>-/-</sup> Mouse</b> .....	49
3.1 Introduction.....	50
3.2 Results.....	52
3.2.1 Generation of <i>Setx</i> <sup>-/-</sup> mice .....	52
3.2.2 Absence of neurological phenotype in <i>Setx</i> <sup>-/-</sup> mice.....	53
3.2.4 Senataxin is essential for male germ cell development and fertility .....	56
3.2.5 Defects in homologous recombination in <i>Setx</i> <sup>-/-</sup> spermatocytes .....	60
3.2.6 Defect in meiotic sex chromosome inactivation (MSCI) in <i>Setx</i> <sup>-/-</sup> spermatocytes .....	65
3.3 Discussion .....	69
<b>CHAPTER 4: Senataxin regulates Atr activity and chromatin remodeling during MSCI</b> .....	72
4.1 Introduction.....	73
4.2 Results.....	74
4.2.1 Defect in SUMOylation in spermatocytes of <i>Setx</i> <sup>-/-</sup> mice during MSCI .....	74
4.2.2 Senataxin is SUMOylated.....	76
4.2.3 Identification of SUMOylated proteins- Candidate selected: Atrip .....	78
4.2.4 Normal recruitment of Brca1 and TopBP1 observed in spermatocytes of <i>Setx</i> <sup>-/-</sup> mice during MSCI.....	81
4.2.5 Defect in Atr-Atrip signaling in <i>Setx</i> <sup>-/-</sup> mice.....	84
4.2.6 Defect in XY heterochromatin formation in <i>Setx</i> <sup>-/-</sup> mice.....	92
4.3 Discussion.....	97
<b>CHAPTER 5: Senataxin &amp; R-loop Resolution</b> .....	104
5.1 Introduction.....	105
5.3 Results (continued) .....	106
5.3.1 DNA damage induces R-loop accumulation in proliferative tissues in <i>Atm</i> <sup>-/-</sup> and <i>Aptx</i> <sup>-/-</sup> mice .....	106
5.3.2 R-loops accumulate along the mouse WWOX and XY genes in <i>Setx</i> <sup>-/-</sup> spermatocytes .....	110

5.4 Discussion .....	114
<b>CHAPTER 6: General Discussion &amp; Future Directions .....</b>	<b>118</b>
6.1 General discussion .....	119
6.2 Future directions .....	126
<b>REFERENCES.....</b>	<b>129</b>
<b>APPENDIX.....</b>	<b>151</b>

## **APPENDIX I**

**Senataxin Plays an Essential Role with DNA Damage Response Proteins in Meiotic Recombination and Gene Silencing.** Becherel OJ, Yeo AJ, Stellati A, Heng EY, Luff J, Suraweera AM, Woods R, Fleming J, Carrie D, McKinney K, Xu X, Deng C, Lavin MF. 2013. *PLoS Genetics*. 9(4): e1003435.

## **APPENDIX II**

**Senataxin saves Sperm- World of Reproduction Biology.** *Feature article written by Charlotte Shubert.* Becherel OJ, Yeo AJ, Stellati A, Heng EY, Luff J, Suraweera AM, Woods R, Fleming J, Carrie D, McKinney K, Xu X, Deng C, Lavin MF. 2013. *Biology of Reproduction*. 89 (1) 1, 1-2.

## **APPENDIX III**

**Senataxin Protects the Genome: Implications for Neurodegeneration and other Abnormalities.** Lavin MF, Yeo AJ and Becherel OJ. 2013. *Journal of Rare Diseases*. Vol I (Addendum): e25230.

# **CHAPTER 1 Literature Review**

## 1.1 Autosomal recessive cerebellar ataxias

Autosomal recessive cerebellar ataxias (ARCAs) are a diverse group of rare neurodegenerative disorders that result from cerebellar atrophy and spinal tract dysfunction, and can cause various neurological, ophthalmological, and in some cases, systemic symptoms<sup>1-3</sup>. Several distinguishable groups of ARCAs, based on causal pathological mechanisms include congenital ataxias, degenerative ataxias, ataxias associated with metabolic dysfunction and ataxias with DNA damage repair defects<sup>4</sup>.

This study focuses on a subset of ARCAs associated with defective DNA damage repair mechanisms, and we aim to understand how gene transcription regulation and aberrant RNA processing may contribute to neurodegeneration as observed in patients suffering from these disorders. This subset of related ARCAs include Ataxia Telangiectasia (A-T), Ataxia Telangiectasia-like Disorder (A-TLD), Ataxia Oculomotor Apraxia Types 1 and 2 (AOA1 and AOA2), juvenile onset of Amyotrophic Lateral Sclerosis 4 (ALS4), and Spinocerebellar Ataxia with Axonal Neuropathy Type 1 (SCAN1)<sup>5,6</sup>, which will be introduced in the following sections. The focus of the present study is AOA2 and its clinical, biochemical and genetic aspects will be discussed in greater detail in this report.

<b>Disease</b>	<b>Gene/Protein</b>	<b>Age of onset (years)</b>	<b>Clinical features</b>
Ataxia Telangiectasia (A-T)	<i>ATM</i> ATM	2-6	Cerebellar ataxia, oculomotor apraxia, predisposition to cancer, immunodeficiency, radiosensitivity, increased $\alpha$ -feto protein levels
Ataxia Telangiectasia-like Disorder (A-TLD)	<i>MRE11A</i> MRE11	2-6	Cerebellar ataxia, oculomotor apraxia, peripheral neuropathy, radiosensitivity
Nijmegen Breakage Syndrome (NBS)	<i>NBS1</i> NBS1	1-4	Microcephaly, peripheral neuropathy, growth retardation, immunodeficiency, predisposition to cancer, radiosensitivity
Nijmegen Breakage Syndrome-Like (NBS-like) Disorder	<i>RAD50</i> RAD50		Microcephaly, growth retardation, chromosomal instability, ataxia

Ataxia Oculomotor Apraxia Type 1 (AOA1)	<i>APTX</i> Aprataxin	2-6	Cerebellar ataxia, oculomotor apraxia, peripheral neuropathy, hypoalbuminaemia, hypercholesterolaemia
Ataxia Oculomotor Apraxia Type 2 (AOA2)	<i>SETX</i> Senataxin	11-22	Cerebellar ataxia, oculomotor apraxia, elevated $\alpha$ -feto protein levels, peripheral neuropathy
Spinocerebellar Ataxia with Axonal Neuropathy Type 1 (SCAN1)	<i>TDP1</i> Tyrosyl-DNA phosphodiesterase I	10-20	Cerebellar ataxia, axonal neuropathy with progressive loss of sensation in the hands and legs, decreased serum levels of albumin and cholesterol

**Table 1.1: Genetic and clinical features of ARCAs associated with defects in DNA repair.**

Name of disorder, mutated gene, dysfunctional protein, age of onset of disorder and symptoms of disorder listed. *Table adapted from Palau 2006<sup>4</sup>.*

### 1.1.1 Ataxia-Telangiectasia (A-T)

Ataxia Telangiectasia (A-T) is a multi-systemic disorder characterized by ataxia resulting from cerebellar degeneration, in particular, from the loss of Purkinje cells<sup>7</sup>. Clinical symptoms of A-T include oculocutaneous telangiectasia, apraxia, immunodeficiency, predisposition to cancers (in particular lymphoid cancers), hypersensitivity to ionizing radiation (IR) and increased  $\alpha$ -feto protein levels<sup>8,9</sup>. Other characteristics of A-T include dysarthric speech, choreoathetosis, hypogonadism and sterility, growth and mental retardation<sup>10</sup>. The incidence of A-T is estimated to be 1 in every 40,000 to 100,000 live births in the US and has an early onset of between 2 to 3 years, with children almost always requiring wheelchairs by the age of 10<sup>10,11</sup>. A-T patients often succumb to respiratory infections such as pneumonia. These infections can occur during ingestion of food due to the inability of A-T patients to coordinate breathing and swallowing<sup>12</sup>.

The causative gene for A-T is *Ataxia Telangiectasia Mutated (ATM)*<sup>13</sup> and most mutations (e.g. nonsense, frameshift, point mutations) giving rise to A-T destabilizes ATM protein<sup>14</sup>. Patients with less clinically severe A-T display either reduced levels of functional protein or normal levels of ATM with significantly reduced activity<sup>15</sup>. *ATM* is mapped to chromosome 11q22-23, and encodes a ~350 kDa serine-threonine protein kinase that belongs to the phosphoinositide 3-kinase related

protein kinase (PI3KK) family<sup>2,13</sup>. ATM is predominantly found in the nucleus, although low levels of cytoplasmic forms have also been reported<sup>2,16</sup>.

The most well characterized role of ATM is its participation in a signaling cascade that occurs in response to DNA double-strand breaks (DSBs) caused by damaging agents, and in cell-cycle checkpoints activation<sup>17</sup>. Upon the occurrence of DSBs, inactive dimeric ATM undergoes auto-phosphorylation and becomes an active monomer which subsequently phosphorylates and activates various protein substrates such as p53, breast cancer-associated 1 (BRCA1) and checkpoint kinase 2 (CHK2), all of which are involved in cell-cycle regulation<sup>16,18</sup> (Fig 1.1). ATM is also involved in physiological DSB events such as that occurring in meiosis, during the maintenance of telomeres, and during DNA homologous recombination (HR) in immune system maturation<sup>13</sup>. Cells cultured from A-T patients show sensitivity to IR and radio-resistant DNA synthesis with abnormal G<sub>1</sub>/S and G<sub>2</sub>/M checkpoints<sup>19</sup>. Induction of p53, a key player involved in IR-induced apoptosis, was found to be decreased in these cells after irradiation as compared to wildtype cells, further supporting the signaling role for ATM in DSB repair<sup>20</sup>.

ATM also interacts directly with the MRN complex, a heterotrimeric group of proteins which consists of MRE11, RAD50 and NBS1, which is involved in maintaining genome stability by initiating DNA damage signaling during DSB events<sup>13,21</sup>. Deficiency in ATM results in chromosomal instability and early senescence as seen in cells cultured from A-T patients<sup>20</sup>. The importance of the interaction between ATM and the MRN complex is observed in other A-T-related syndromes that result from mutations in NBS1 (causing Nijmegen Breakage Syndrome), RAD50 (causing Nijmegen Breakage Syndrome-like disorder)<sup>22</sup> and MRE11 (causing Ataxia-Telangiectasia-Like Disorder)<sup>13</sup> which will be discussed in sections 1.1.2.

Several *Atm*<sup>-/-</sup> mouse models have been generated previously and some phenotypical similarities between these models and A-T patients were observed. *Atm*<sup>-/-</sup> mice displayed growth retardation, infertility, sensitivity to IR, immunological abnormalities and high incidences of thymic lymphomas<sup>7,20,23,24</sup>. However, neither histological evidences of ocular telangiectasia nor neurodegeneration were observed despite mild abnormalities in motor function<sup>7,20,25</sup>.

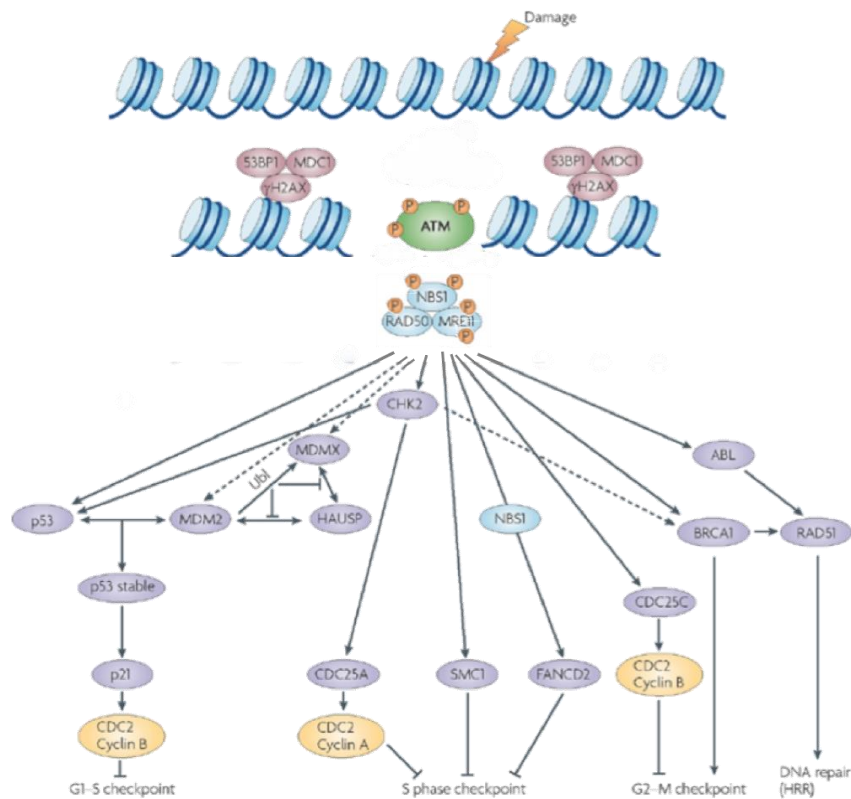


**Fig 1.1: ATM activation and signaling to downstream substrates in response to DNA DSBs.** Upon formation of a DNA DSB, ATM is recruited to break sites by the MRN complex, a DNA DSB sensor. It then undergoes autophosphorylation and subsequently initiates the DNA damage response by phosphorylating downstream substrates such as 53BP1, BRCA1, FANCD2 and MDC1, which are proteins involved in DNA damage repair and cell cycle checkpoints. *Image taken from Lavin 2008<sup>2</sup>.*

### 1.1.2 Ataxia-Telangiectasia-related disorders

*MRE11A* encodes the MRE11 protein which is the 1<sup>st</sup> component of the MRN complex that acts upstream of ATM to detect DSBs<sup>15</sup>. MRE11 contains a nuclease domain which is one of the most highly conserved components of DNA damage repair (DDR) factors, with orthologues observed even in organisms such as the bacteriophage T4<sup>26</sup>. A deficiency in MRE11 destabilizes the MRN complex and thus compromises genomic integrity<sup>13</sup>. Mutations in the *MRE11A* gene that lead to a loss of protein function results in Ataxia Telangiectasia-Like Disorder (A-TLD). Clinical symptoms of A-TLD are similar to but not as severe as that seen in A-T. A-TLD has a later onset and slower disease progression as compared to A-T. Patients with A-TLD display neurodegeneration, peripheral neuropathy and oculomotor apraxia but neither telangiectasia, cancer predisposition nor



immune deficiencies<sup>27</sup>. Null mutants for *Mre11* in mice are embryonic lethal, indicating that it is required for development<sup>28</sup>. Knock-in mutant mice for *Mre11* harboring different point mutations display a range of defects that include DNA damage sensitivity, reduced fertility, early cellular senescence, a reduction in class-switch recombination and impaired DNA DSB repair in B cells<sup>28,29</sup>.

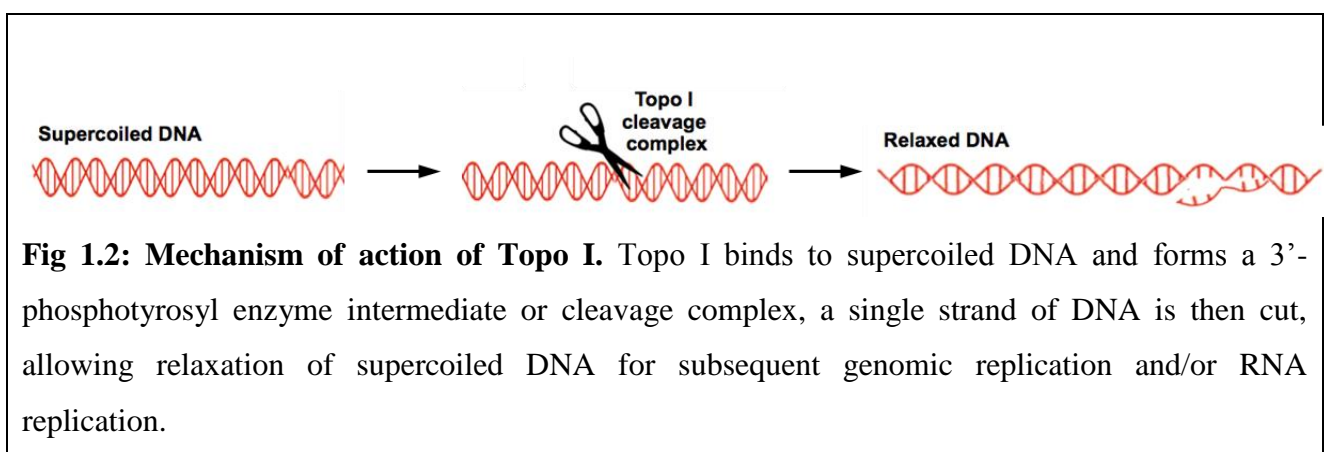
NBS1 is the 2<sup>nd</sup> component of the MRN complex and is also an ATM substrate involved in the S phase checkpoint of the cell cycle following DNA damage<sup>30</sup>. Hypomorphic mutations in the *NBS1* gene result in Nijmegen Breakage Syndrome (NBS). Clinical symptoms of NBS are also similar to that seen in A-T and include immunodeficiency, chromosomal instability, sensitivity to IR and a predisposition to hematopoietic cancers<sup>31</sup>. However, NBS patients display neither neurological abnormalities, ocular telangiectasia nor increased  $\alpha$ -feto protein levels<sup>31</sup>. Patients instead display microcephaly as a neurological hallmark instead of neurodegeneration<sup>31</sup>. Similar to *Mre11*, null mutants for *Nbs1* in mice were also found to be embryonic lethal<sup>28</sup>. Mice expressing mutant NBS1 with N- or C-terminal truncations display various defects including intra-S and G2/M checkpoint defects, DNA damage sensitivity, chromosomal instability, decreased ATM activity, defects in immune system development and reduced fertility<sup>32-35</sup>.

RAD50 is the 3<sup>rd</sup> component of the MRN complex, and mutations in this gene lead to an NBS-like disorder. To date, only two patients have been described with this disorder<sup>36</sup>. These patients displayed microcephaly and mental retardation without immunodeficiency or predisposition to malignancies. Patients' cells were reported to show chromosomal instability, sensitivity to radiation, failure to form DNA damage-induced MRN foci, and decreased activation of ATM and its subsequent downstream signaling pathway. These cells also showed impaired G1/S cell-cycle-checkpoint activation and displayed radio-resistant DNA synthesis and G2-phase accumulation<sup>22</sup>. Several *Rad50* mutant mouse models have been made and like the null mutants for *Mre11* and *Nbs1*, null mutants for *Rad50* were embryonic lethal<sup>37</sup>. It was observed that mice with hypomorphic mutations in *Rad50* had short lifespans of approximately three months, gradual loss of germ cells and died with bone marrow failure<sup>38</sup>. These mice also displayed chromosomal instability, sensitivity to topoisomerase poisons and cancer predisposition<sup>39</sup>.

### 1.1.3 Spinocerebellar ataxia with axonal neuropathy (SCAN1)

Spinocerebellar ataxia with axonal neuropathy (SCAN1) is a very rare disorder caused by a mutation in the tyrosyl-DNA phosphodiesterase (*TDP1*) gene<sup>40</sup>. Only one family originating from Saudi Arabia has been described with this disorder<sup>40</sup>. SCAN1 is characterized by an adolescent onset, ataxia, axonal neuropathy with progressive loss of sensation in the hands and legs, and decreased serum levels of albumin and cholesterol<sup>41</sup>. No significant extra-neurological symptoms have been observed. However, detailed clinical studies have not been possible due to the rarity of this disease and the lack of relevant phenotype observed in the animal models<sup>5</sup>.

*TDP1* has been mapped to chromosome 14q32 and codes for tyrosyl-DNA phosphodiesterase I (TDP1) and is a protein involved in the repair of DNA single strand breaks (SSB) generated by abortive topoisomerase I DNA cleavage complexes (Topo 1)<sup>5,42</sup>. Topo I acts to relieve super-helical torsion in DNA by introducing a transient, reversible nick in which it is attached covalently to the 3'-terminus<sup>42</sup>. Following the release of torsional stress, the Topo I cleavage complex is removed, allowing the repair of the nick and thereby maintaining genomic integrity<sup>43</sup> (Fig 1.2). However, Topo I cleavage complexes can become trapped on DNA if they collide with the replication fork or transcription machinery, or if they encounter lesions along the DNA. In normal individuals, TDP1 removes the bound Topo I cleavage complex and allows repair of DNA SS- or DSBs. In the absence of TDP1, bound Topo I cleavage complexes remain trapped on DNA, preventing the efficient repair of DNA breaks<sup>42,44</sup>.



Several *Tdp1*<sup>-/-</sup> mice generated independently failed to elicit any obvious behavioural deficits. Additionally, gross histological analyses of brain and cerebellar tissues from these mice did not show any significant differences in comparison to their wild type littermates either<sup>45,46</sup>. Katyal *et al.* 2007 and Hirano *et al.* 2007 both showed an *in vivo* hypersensitivity of *Tdp1*<sup>-/-</sup> mice to

camptothecin and topotecan (an analogue of camptothecin), two Topo I inhibitors. However, doses of these compounds even up to a lethal level, failed to stimulate SCAN1-type symptoms<sup>5,46</sup>. These data show that the phenotype of the *Tdp1*<sup>-/-</sup> mouse model does not recapitulate that seen in humans. It was suggested that rather than a complete loss of TDP1, the unique features of mutant TDP1 in humans contribute to the SCAN1 phenotype in response to high levels of Topo I complexes found in the Purkinje cells of adolescents instead<sup>45,47</sup>.

#### 1.1.4 Ataxia oculomotor apraxia type I (AOA1)

Ataxia Oculomotor Apraxia Type I (AOA1), also known as early onset ataxia with hypoalbuminemia (EAOH), has an onset from between 2 to 6 years of age<sup>48</sup>. Clinical symptoms of AOA1 include progressive ataxia resulting from cerebellar atrophy, oculomotor ataxia, peripheral neuropathy, loss of reflexes, mild mental retardation, hypoalbuminemia and hypercholesterolemia<sup>4</sup>.

The gene mutated in AOA1 is *APTX* and has been mapped to chromosome 9q13<sup>49</sup>. *APTX* encodes the protein aprataxin, which is a 342 amino acid-long nuclear protein that belongs to the histidine triad (HIT) domain superfamily of nucleotide hydrolases/transferases<sup>50</sup>. The N-terminus of aprataxin shares homology with that of PNK, a protein involved in SSB repair, and upon closer inspection, was found to contain a putative fork-head associated (FHA) domain<sup>50,51</sup>. This domain was found to mediate interaction with other proteins involved in DNA repair such as the X-ray repair cross-complementing group 1 and 4 proteins (XRCC1 and XRCC4) and mediator of DNA damage checkpoint 1 (MDC1), all of which are scaffold proteins involved in SS- and DSB repair respectively. An interaction with Poly(ADP-ribose) polymerase I (PARP-1), a nick sensor in DNA SSB repair was also found<sup>52,53</sup>. Aprataxin possesses 5' DNA adenylate hydrolase activity that is essential for the resolution of abortive DNA ligation intermediates that occur at sites of SSBs<sup>54</sup> (Fig 1.3). The presence of unrepaired SSBs with blocked termini may hinder the progression of RNA polymerases, thereby inhibiting transcription and leading to cellular collapse<sup>55</sup>. Becherel *et al.* 2006 also found an interaction between aprataxin and nucleolar proteins such as nucleolin, nucleophosmin and UBF-1, and suggested a role for aprataxin in DDR in the nucleolus where high rates of transcription occur<sup>56</sup>.

Although several roles for aprataxin have been described, conflicting results have been observed in attempts to demonstrate a defect in DNA strand break repair in the absence of aprataxin. Some studies showed SSB repair defects<sup>6,57</sup> while others do not<sup>58</sup>. It was suggested that the lack of

consistent data was due to low frequencies of breaks with 5'-AMP, or that there are other factors to repair these breaks<sup>59</sup>.

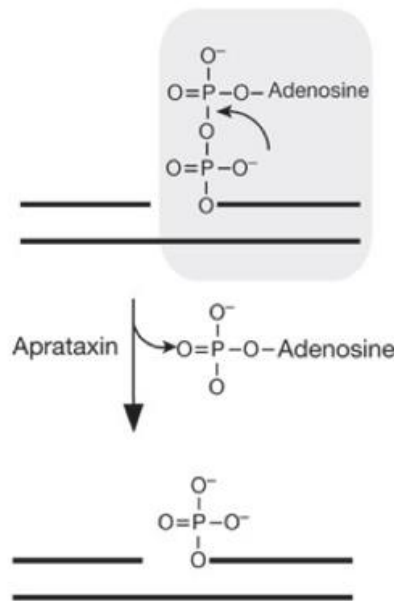


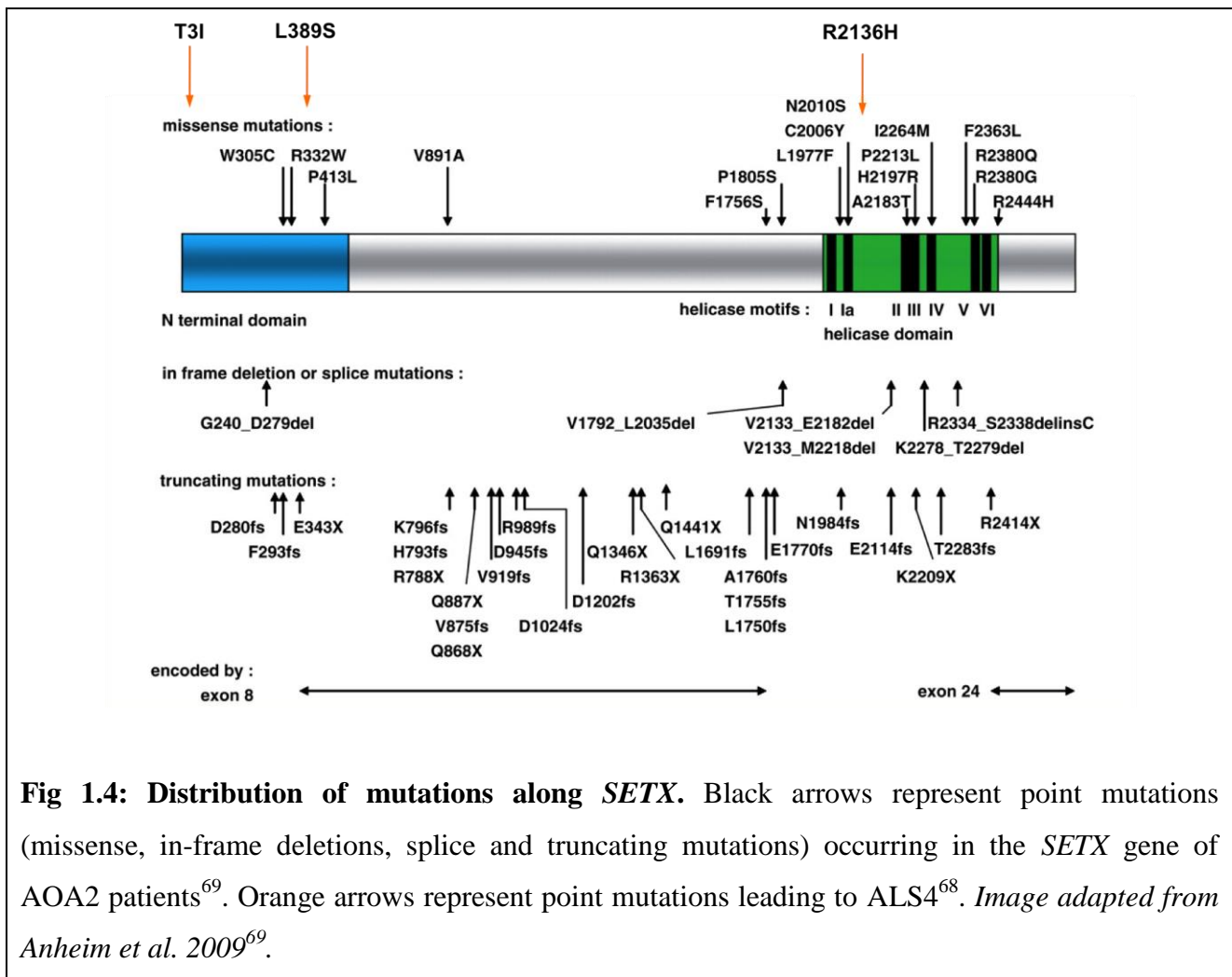
**Fig 1.3: Aprataxin removes 5'-AMP from abortive DNA ligation intermediates.** As a consequence of abortive ligation at sites of SSB, an AMP moiety remains covalently attached to the 5' end of the break. Aprataxin removes the resulting 5'-adenylate group at the SSB to allow subsequent repair. *Image taken from Ahel et al. 2006<sup>54</sup>.*

### 1.1.5 Ataxia oculomotor apraxia type II (AOA2)

Ataxia oculomotor apraxia type II (AOA2) is characterized by progressive cerebellar atrophy and peripheral sensorimotor neuropathy (~93% of patients) with a late onset of between 11 to 22 years of age, oculomotor apraxia (~47% of patients), dysarthria, and elevated  $\alpha$ -feto-protein (AFP),  $\gamma$ -globulin and creatine kinase serum levels<sup>60,61</sup>. Neither mental retardation, immunodeficiency nor predisposition to cancers have been reported<sup>62</sup>

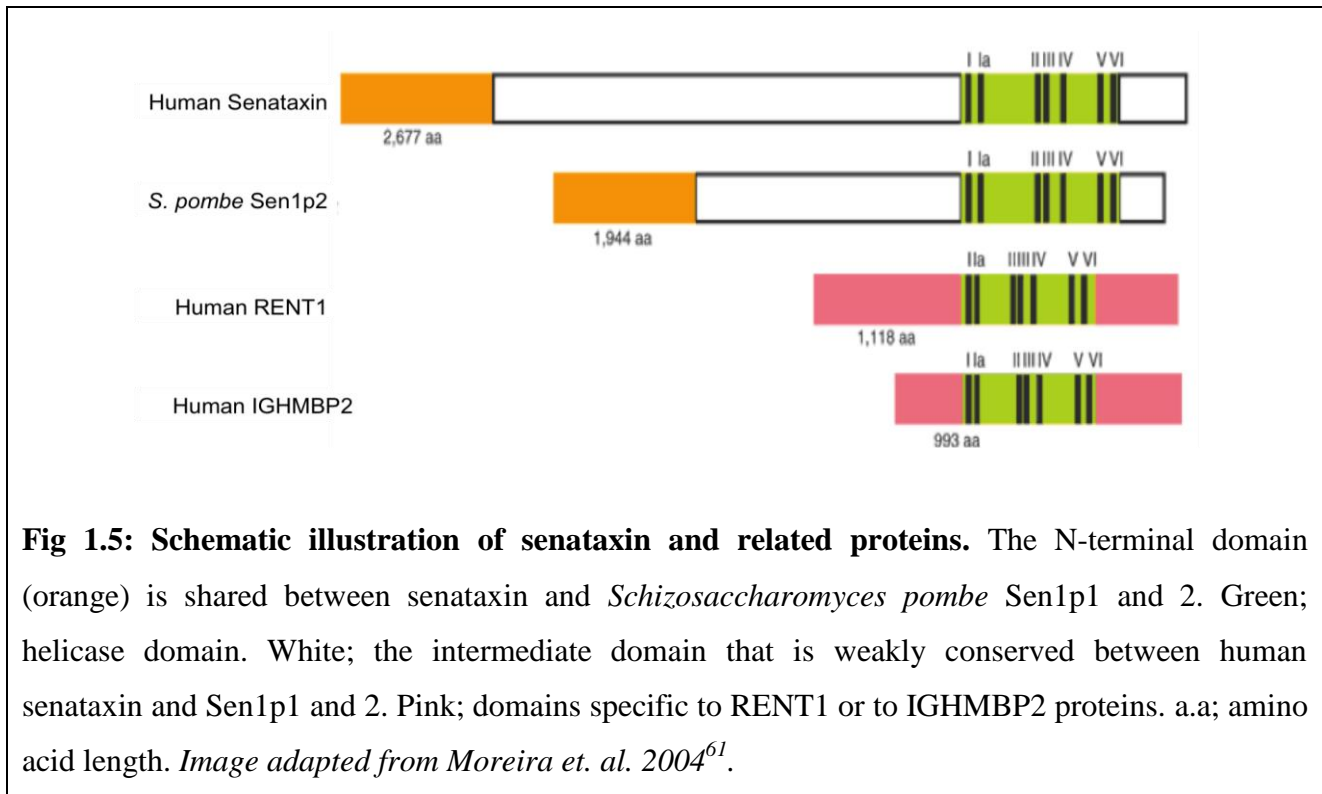
The gene mutated in AOA2 is *SETX* which has been mapped to chromosome 9q34<sup>61</sup>. *SETX* encodes for the protein senataxin which is approximately 2,667 amino acid-long. Senataxin contains a highly conserved C-terminal seven-motif domain found in the superfamily I of DNA/RNA helicases, and an N-terminal domain believed to be important for protein-protein interaction<sup>60,63</sup>. Additionally, senataxin is related to other DNA/RNA helicases such as RENT1/Upf1 and

IGHMBP2 (Fig 1.4 and 1.5)<sup>63</sup>. Interestingly, RENT1/Upf1 has been implicated in nonsense-mediated RNA decay and IGHMBP2, dysfunctional in spinal muscular atrophy, is thought to be a DNA-binding protein with transcriptional *trans*-activating activity<sup>64,65</sup>. *SETX* is highly polymorphic and >95% of individuals harbour benign mutations<sup>66</sup>. Pathogenic mutations in AOA2 patients include point mutations, frameshift mutations, premature truncation and splicing mutations, leading to a deficiency in senataxin<sup>61,67</sup>. Mutations in *SETX* have also been associated with amyotrophic lateral sclerosis type 4 (ALS4), a juvenile-onset form of an autosomal dominant disorder<sup>68</sup> (Fig 1.4).



Senataxin shares homology with the yeast *Saccharomyces cerevisiae* splicing endonuclease 1 protein (Sen1p) that has RNA helicase activity and is involved in splicing and termination of tRNA, small nuclear and nucleolar RNA<sup>61</sup>. Sen1p also interacts with Rpo21p (a subunit of RNA polymerase II), Rad2 (required for DNA repair) and Rnt1p (an endoribonuclease required for RNA maturation), suggesting that Sen1p is involved RNA processing, transcription and transcription-coupled DNA repair<sup>70</sup>. Sen1p1 and Sen1p2, which are homologs of Sen1p in *Schizosaccharomyces*

*pombe* include (Fig 1.5), also show DNA/RNA helicase activity and have been implicated in RNA metabolism<sup>61</sup>.



Similarly, senataxin interacts with proteins involved in RNA transactions that include Sit4 associated protein (SAP155), polyadenylate-binding protein 1 and 2 (PABP1/2), survival motor neuron 1 (SMN1), nucleolin, heterogenous ribonucleoprotein 1 (hnRNPA1) and RNA Polymerase II (RNAPII), and has also been found to play a role in transcription regulation by modulating RNA Pol II binding to various gene loci<sup>71</sup>. mRNA splicing efficiency, alternative splicing, splice site selection and transcription termination were altered in senataxin-deficient cells<sup>71</sup>. This was in agreement with studies with the yeast homolog Sen1p<sup>72</sup>. A recent study has described an additional role for senataxin in transcription elongation and termination<sup>73</sup> (Fig 1.6). An increase in RNA read-through and Pol II concentration downstream of the poly(A) site was detected in cells deficient in senataxin. Furthermore, increased levels of R-loop formation were also reported<sup>73</sup>. R-loops are DNA:RNA hybrids that form over transcriptional pause sites by the interaction of nascent mRNA with a ssDNA template behind an elongating RNA Polymerase II. These structures can cause genomic instability if left unresolved<sup>73-75</sup>. Incidentally, it has also been shown that the yeast orthologue of senataxin, Sen1p, protects its highly-transcribed genome from R-loop-mediated DNA damage, suggesting that Sen1p function in transcription elongation and termination may be associated with R-loop resolution<sup>76</sup>.

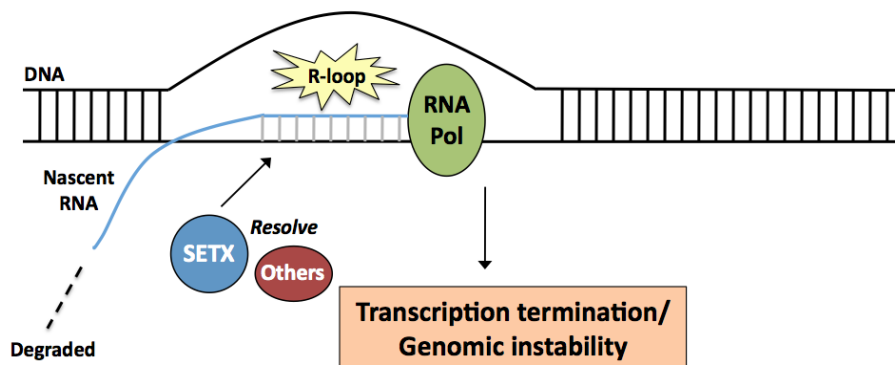


**Fig 1.6: Role for senataxin in R-loop resolution.** R-loops are DNA:RNA hybrids that form over transcription pause sites (usually GC-rich regions or with specific pause sequences), behind elongating RNA Polymerase. Proteins such as senataxin and several other factors (e.g. RNase H, DHX9) resolve these structures, thereby allowing for the efficient termination of transcription. *Image adapted from Skourti-Stathaki et. al. 2011<sup>73</sup>.*

Although the precise mechanism by which mutant senataxin causes neurodegeneration in AOA2/ALS4 patients remains unclear, a deregulation in the various roles of senataxin such as RNA processing, DNA repair and transcription regulation, may account for the neurodegenerative phenotype observed in AOA2 patients (Fig 1.7).

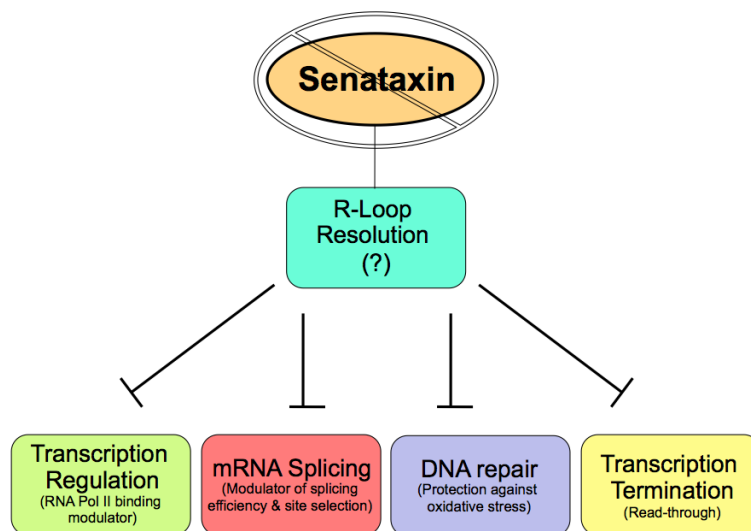


**Fig 1.7: Roles of senataxin in relation to neurodegeneration.** Defects in senataxin lead to an accumulation of R-loops, which can affect several cellular functions that include transcription

regulation, mRNA splicing, DNA repair and transcription termination, which may then contribute to the neurodegenerative phenotype observed in AOA2/ ALS4 patients<sup>71</sup>. *Image adapted from Suraweera et al. 2009.*

## **1.2 DNA damage and DNA repair**

### *1.2.1 Oxidative stress and DNA damage*

Reactive oxygen and nitrogen species (ROS/RNS), are free radicals which are byproducts of cellular metabolism. These free radicals possess redox activities that have detrimental effects on cellular components such as protein, DNA and lipids, if left unresolved<sup>77,78</sup> (Fig 1.8). This is evident in many neurodegenerative disorders such as Alzheimer's disease, Parkinson's disease and ALS, where post-mortem brain examinations of patients show an increase in oxidative stress in affected regions of the brain<sup>79</sup>. Post-mortem brain sections of AOA1 patients have also shown evidence of increased oxidative DNA damage (8-oxo-dG staining)<sup>80</sup>. Studies on several neurodegenerative mouse models have also suggested an association of oxidative stress with neuronal cell death<sup>78</sup>. Given the high metabolic rates in neuronal cells and high oxygen concentration in nervous tissues such as the brain and cerebellum, it is possible that oxidative stress could significantly contribute neuronal cell degeneration<sup>81</sup>.

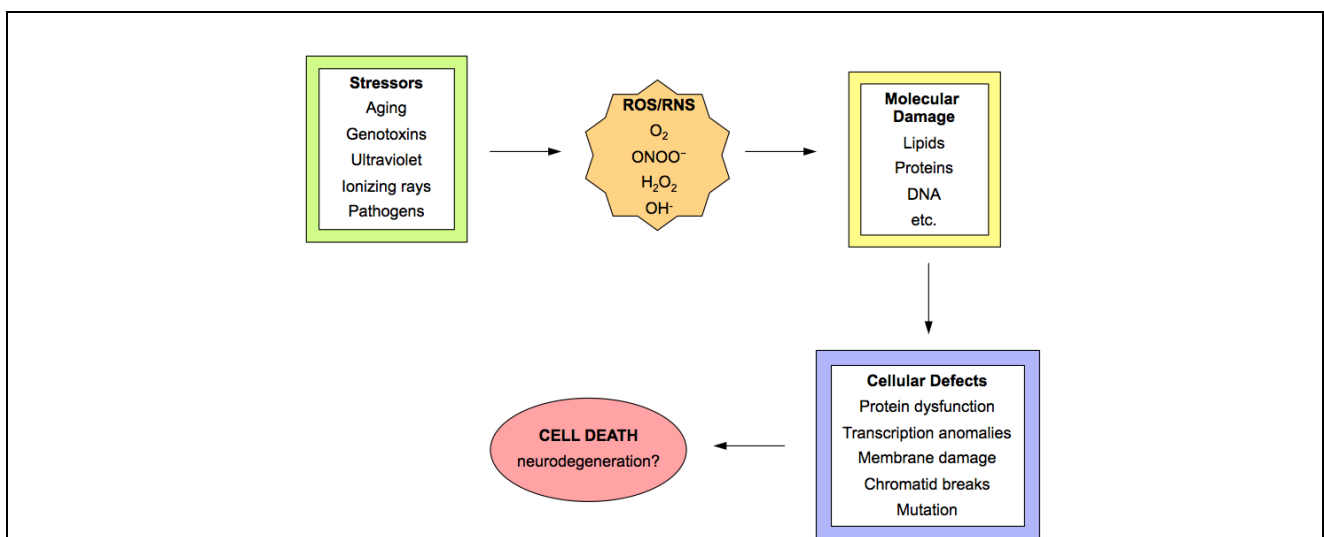


**Fig 1.8: Effects of ROS/RNS on cells.** Free radicals (ROS/RNS) resulting from by endo- or exogenous insults can react with biomolecules such as lipids, proteins and nucleic acids (DNA) and



in turn lead to a variety of physiological dysfunctions and ultimately to cell death. *Image adapted from Scandalios 2005*<sup>82</sup>.

Although the body has several antioxidant defense mechanisms to counter the effects of ROS/RNS, a slight perturbation in these homeostatic operations can potentially cause extensive damage especially in the brain, which is extremely sensitive to oxidative damage<sup>83</sup>. Abnormal control of ROS has been observed in cells of A-T patients, where the cells show sensitivity to oxidative stress and have less effective antioxidant systems<sup>81</sup>. Oxidative stress can also lead to DNA damage, as observed in cells of SCAN-1 patients<sup>84</sup>. Incidentally, defects in repair of these DNA breaks are also thought to contribute to neurodegeneration<sup>83</sup>. Cells from AOA2 patients were found to be sensitive to H<sub>2</sub>O<sub>2</sub> and the repair of H<sub>2</sub>O<sub>2</sub>-induced DNA DSB was compromised in these cells. These data indicate that senataxin also exerts a protective function against oxidative DNA damage<sup>63</sup>.

A-T provided one of the first direct links between DNA damage repair and neurodegeneration. The protein defective in A-T, ATM, responds directly to endogenous DNA damage in the nervous system, as shown by the requirement of ATM for DNA damage-induced apoptosis arising from Lig IV deficiency<sup>85,86</sup>. It was suggested that loss of ATM function in eliminating neural cells that acquire DNA damage can result in cell death and subsequent neurodegeneration<sup>87</sup>. Other diseases associated with neuropathology have further strengthened the connection between DNA damage and perturbation of neural homeostasis. As aforementioned, hypomorphic mutations in both MRE11 and NBS1 leading to A-TLD and NBS respectively, have overlapping clinical phenotypes with A-T and are each a result of defects in different stages of DNA DSB repair. The sensitivity of AOA2 cells to oxidizing agents and the repair defect of ROS-induced DNA DSB in AOA2 cells further support the contribution of DNA damage and oxidative stress to neurodegeneration<sup>71</sup>. Not only has DSB repair defects been implicated in such disorders, defective SSB repair has also been implicated in neurodegenerative diseases such as AOA1 and SCAN-1<sup>87</sup>.

DNA is subject to continuous modifications from both endogenous reactive compounds such as free radicals and exogenous factors such as industrial genotoxins, ultraviolet (UV) rays and ionizing radiation (IR) that can cause base modifications, single- and/or double-strand breaks (SSB/DSB)<sup>88</sup>. DNA is also characterized by spontaneous base loss and deamination of uracil occurring at high frequencies<sup>89</sup>. While many DNA repair systems exist, defects in proteins involved in these systems can lead to less efficient repair and mutagenesis, resulting in genomic instability, apoptosis or malignant transformations<sup>3,90</sup>. In the nervous system, defective DNA repair can lead to pronounced

neuropathologies as observed in several ARCAAs described above. The following sections will briefly describe DNA SSB and DSB repair mechanisms.

### *1.2.2 DNA strand break repair*

#### *1.2.2.1 Single strand break (SSB) repair*

SSBs are one of the most common DNA lesions and there has been four repair pathways reported for SSB repair (SSBR)- direct SSBR, mismatch repair (MMR), nucleotide excision repair (NER) and base excision repair (BER). BER repairs damage to bases caused by hydrolysis oxidation, deamination and/or alkylation. Damaged bases are excised by DNA glycosylases and the gaps are filled in by DNA polymerases<sup>91</sup> (Fig 1.9). In BER, the endonuclease APEX-1 initiates base excision, poly(ADP-ribose) polymerase (PARP-1), a multi-functional protein associated with DNA repair, subsequently recruits other proteins such as DNA ligase 3 $\alpha$  and PNKP, and processes the damaged termini<sup>92</sup>. Gap filling by DNA polymerase and ligation then occurs<sup>93</sup>. MMR corrects errors that occur during DNA replication and recombination where incorrect nucleotides may be inserted and produce mismatched nucleotides. Conversely, the exact mechanism of how nucleotides are excised and repaired remains unclear<sup>94</sup>. NER recognizes DNA structure-distorting lesions, such as pyrimidine dimers, and recruits repair factors which excise ~30 nucleotides from the affected region, leaving a gap that is consequently filled in by DNA polymerases.

#### *1.2.2.2 Double strand break (DSB) repair*

DNA DSBs are lethal lesions, therefore mammalian cells have evolved two DNA repair pathways that include: (1) homologous recombination (HR) and (2) non-homologous end joining (NHEJ) (Fig 1.9). Briefly, HR is a high fidelity repair pathway that utilizes the undamaged, homologous DNA strand as a template and ensures the accurate repair of DSBs. Some proteins involved in HR include BRCA1/2, RAD51 and RAD52<sup>95</sup>. HR occurs primarily during early embryogenesis and in proliferating cells in late S to G2 phase<sup>87,96</sup>. Upon occurrence of DSBs, RAD52 binds rapidly to the ends of DNA and subsequently recruits RAD51-family proteins (e.g. XRCC2/3, RAD51B/C/D). The MRN complex is subsequently recruited and resection of the termini by MRE11 occurs. RAD51 then promotes strand invasion between the damaged and undamaged homologous DNA strands. This results in the formation of Holliday Junctions, where nascent DNA is synthesized by DNA Polymerase. Upon completion, the Holliday Junction is resolved and DNA nicks are re-sealed by DNA ligases<sup>97</sup>.

In contrast, NHEJ is a low fidelity repair pathway that is the primary method of DSB repair in non-proliferating, G<sub>1</sub> phase cells, repairing DSBs by end-processing and ligation of the ends<sup>98</sup>. NHEJ is initiated by DNA-end binding heterodimer proteins, Ku70 and Ku80. The Ku proteins align broken DNA ends and together with scaffold protein, XRCC4, stabilize the interaction of PI3KK DNA-dependent Protein Kinase catalytic subunit (DNA-PK<sub>cs</sub>) with the termini. DNA ends are then processed by nucleases that include the WRN helicase and Artemis complex (as a result of end processing, NHEJ often results in microdeletions of DNA). Finally, Lig IV ligates the DNA ends and the DSB is repaired<sup>87,99</sup>.

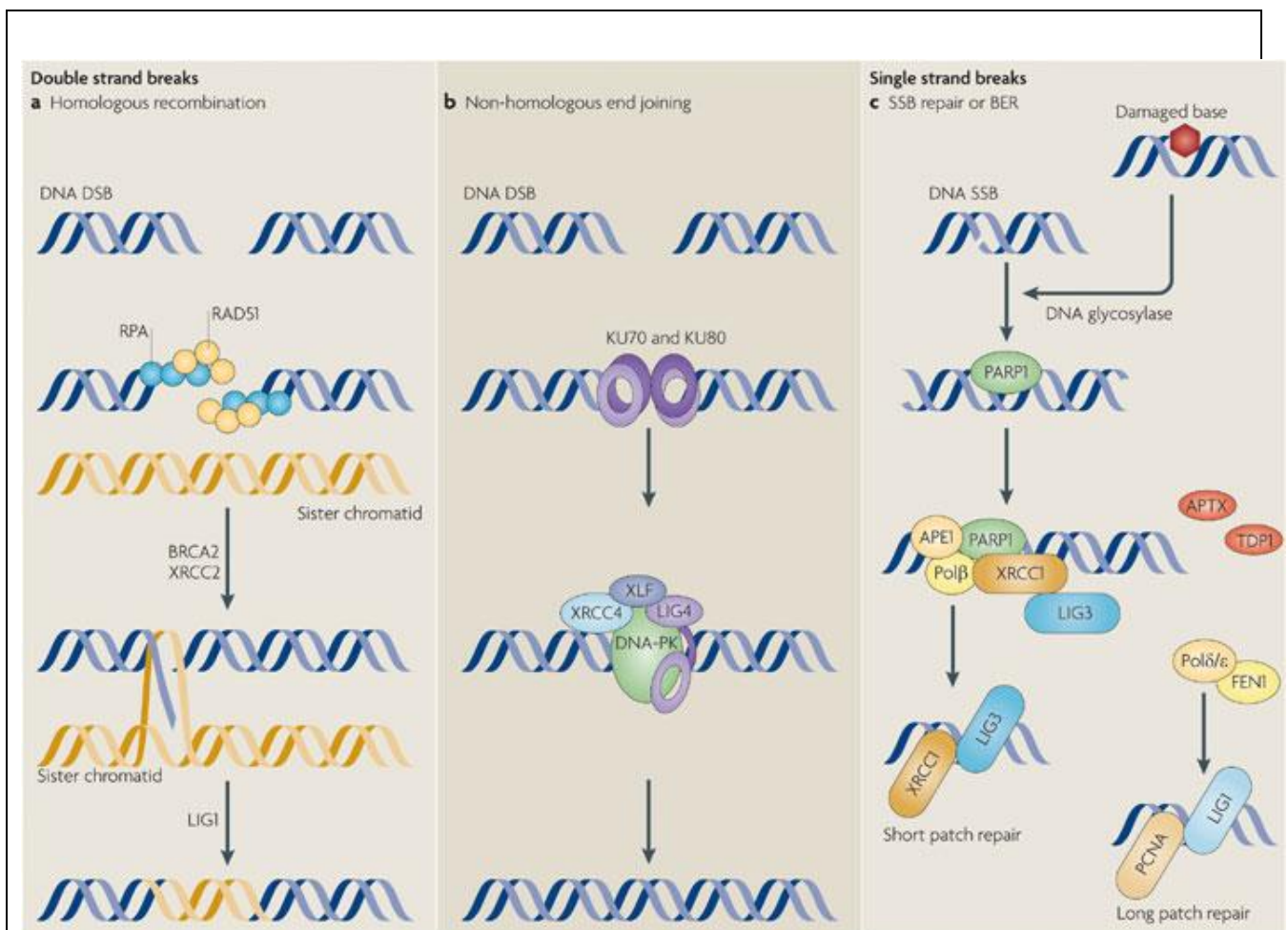


**Fig 1.9: Model of DNA repair pathways.** DNA DSBs are repaired via homologous recombination (HR) or non-homologous end joining (NHEJ). In HR repair, RAD52 bind to DSBs and recruits RAD51. RAD51 facilitates crossing over of undamaged homologous chromosomes, forming a repair bubble (also known as Holliday junction) where nascent DNA is synthesized by DNA Pols. In NHEJ, DSBs are recognized by heterodimeric Ku proteins, which recruit DNA-PK<sub>cs</sub> and the XRCC4/Lig IV complex. Nucleases such as Artemis and WRN process DNA ends to generate blunt

termini, which are subsequently ligated by the XRCC4/Lig IV complex. DNA SSBs repaired via base excision repair (BER) is shown here. SSBs lead to the accumulation of poly ADP-ribose polymerase 1 (PARP1) which recruits other repair factors that modify DNA ends for ligation. *Image taken from Mckinnon 2009<sup>93</sup>.*

In summary, these repair pathways utilize different repair complexes, have different levels of repair fidelity and occur preferentially at different stages of the cell cycle<sup>87</sup> (Fig 1.10). Both oxidative stress and defective DNA damage repair may play a role in neurodegeneration. The brain utilizes ~20% of total consumed oxygen due to high levels of metabolic and transcriptional activities occurring in neurons but contains a lower capacity to neutralize free radicals, making neurons especially vulnerable to oxidative stress<sup>100</sup>. High oxidative loads in neurons can generate DNA breaks, and if left unrepaired, cells can undergo apoptosis once it has acquired too much damage. DNA breaks can also interfere with the transcriptional machinery, thereby resulting in cell death<sup>87</sup>.

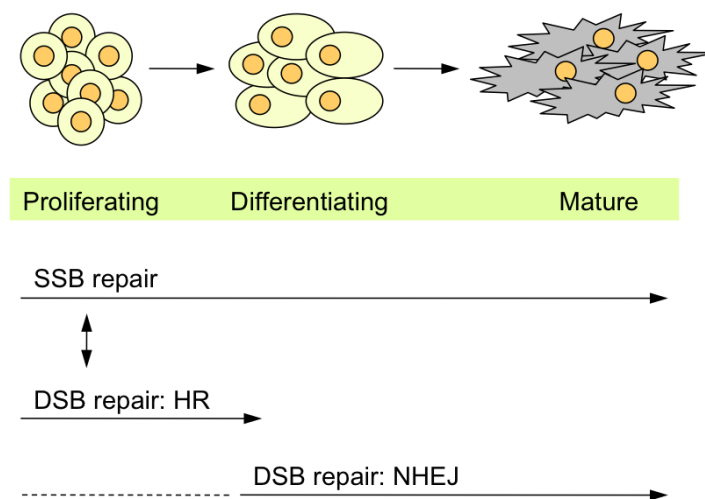


**Fig 1.10: DNA strand break repair pathways during nervous system development.** Development occurs via proliferation, differentiation/migration and maturation. Three major pathways repair DNA breaks during development. DSBR occurs via NHEJ or HR, with HR primarily occurring in proliferating and replicating cells. SSB repair occurs during development through to maturity. In some cases, HR can repair SSBs during replication (black arrow). Together, these pathways maintain genomic integrity throughout the development and maintenance of the nervous system. Various neuropathologies can result if these systems are defective. *Image adapted from Katyal and Mckinnon 2007<sup>87</sup>.*

### **1.3 DNA Repair & Spermatogenesis**

DNA damage response proteins such as Brca1, Rad51 and Atr function not only in response to inadvertent cellular damage but also in programmed DNA damage, where the repair of DNA DSBs is required for the recombination of parental genomes during meiosis in order to generate mature germ cells<sup>101,102</sup>. This Report will focus on spermatogenesis, the process by which male germ cells (spermatozoa) are produced.

#### *1.3.1 Spermatogenesis*

Spermatogenesis is necessary for male fertility and continues during the course of adult life in most mammals, ensuring a continuous supply of mature germ cells. This intricate process involves cell proliferation and differentiation, and occurs in the seminiferous tubules of the testes containing an epithelium populated by a mixture of germ cells and Sertoli cells<sup>103</sup>. Sertoli cells serve a fundamental nourishing role for germ cells and are involved in coordinating important events during spermatogenesis<sup>104</sup>. Mammalian spermatogenesis is a continuous process in which 3 major phases can be discerned, namely- (1) spermatogonial renewal and proliferation, (2) meiosis and (3) spermiogenesis, with the germ cells moving from the peripheral region to the lumen of the seminiferous tubules. Spermatogenesis is initiated by the mitotic division of stem cells (type A spermatogonia), which give rise to daughter cells that either remain as type A spermatogonia (self-renewal) or differentiate to form type B spermatogonia also known as primary spermatocytes.

Primary spermatocytes enter meiosis prophase I where sister chromatids assemble and the exchange of genetic material via homologous recombination (HR) occur. This process is then followed by meiotic prophase II, where sister chromatids separate and give rise to round, haploid spermatids<sup>105</sup>. These round spermatids subsequently enter spermiogenesis, forming elongating spermatids that eventually develop into mature spermatozoa (Fig 1.11).

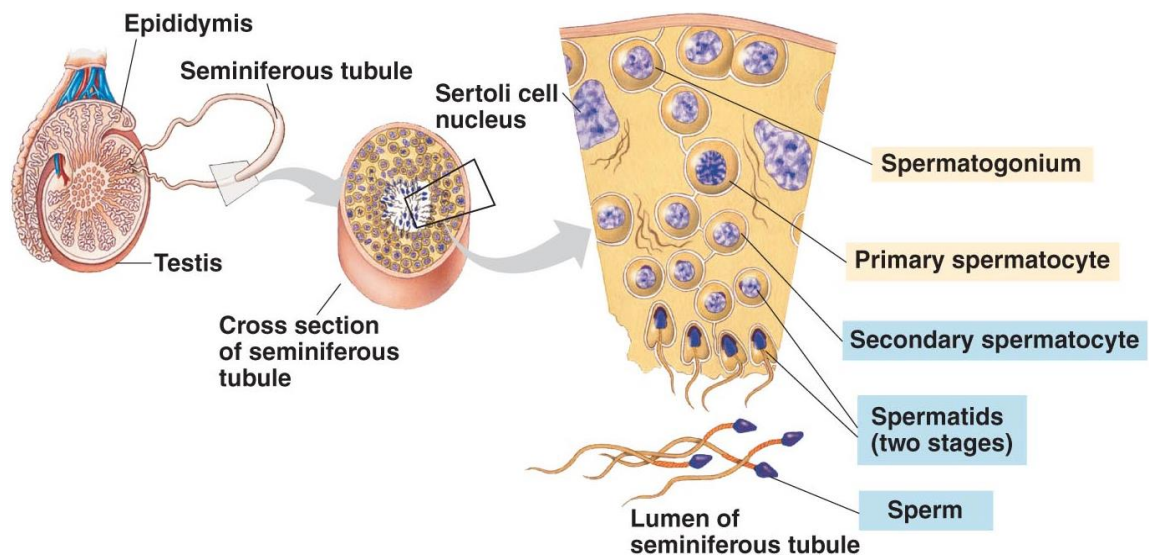


**Fig 1.11: Process of spermatogenesis.** The process of germ cell development in the seminiferous tubules of mammalian males from the primordial germ cells, through spermatogonia, spermatocytes, spermatids to mature spermatozoa. Image taken from Campbell et. al. 1999 (Fig 46.1, p922 in Biology, 5<sup>th</sup> Edition).

In mice, this entire process spans approximately 35 days, where the mitotic, meiotic and post-meiotic phase lasts about 11, 10 and 14 days respectively. Spermatogenesis also begins approximately every 8-9 days<sup>106</sup> (Fig 1.12). This multi-faceted, highly-ordered process is orchestrated by many proteins that play essential roles during the specific phases of germ cell development. Additionally, the temporal, stage-specific expression of these proteins is regulated by both the transcriptional and translation control mechanisms of these cells<sup>107</sup>. In this Report, the events that occur during meiosis prophase I will be focused on.

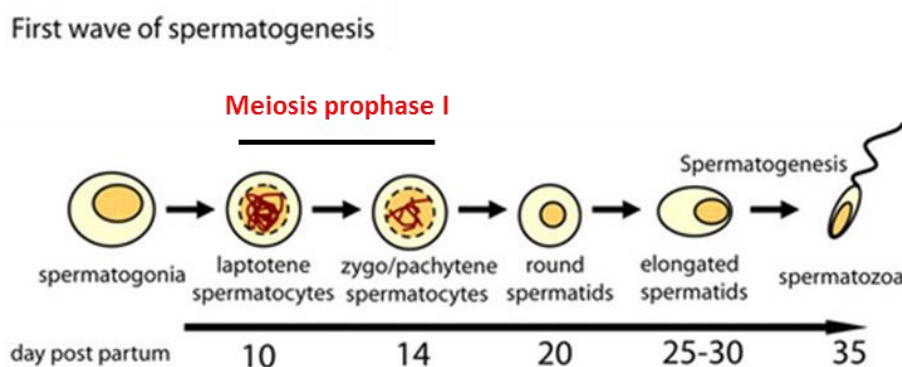
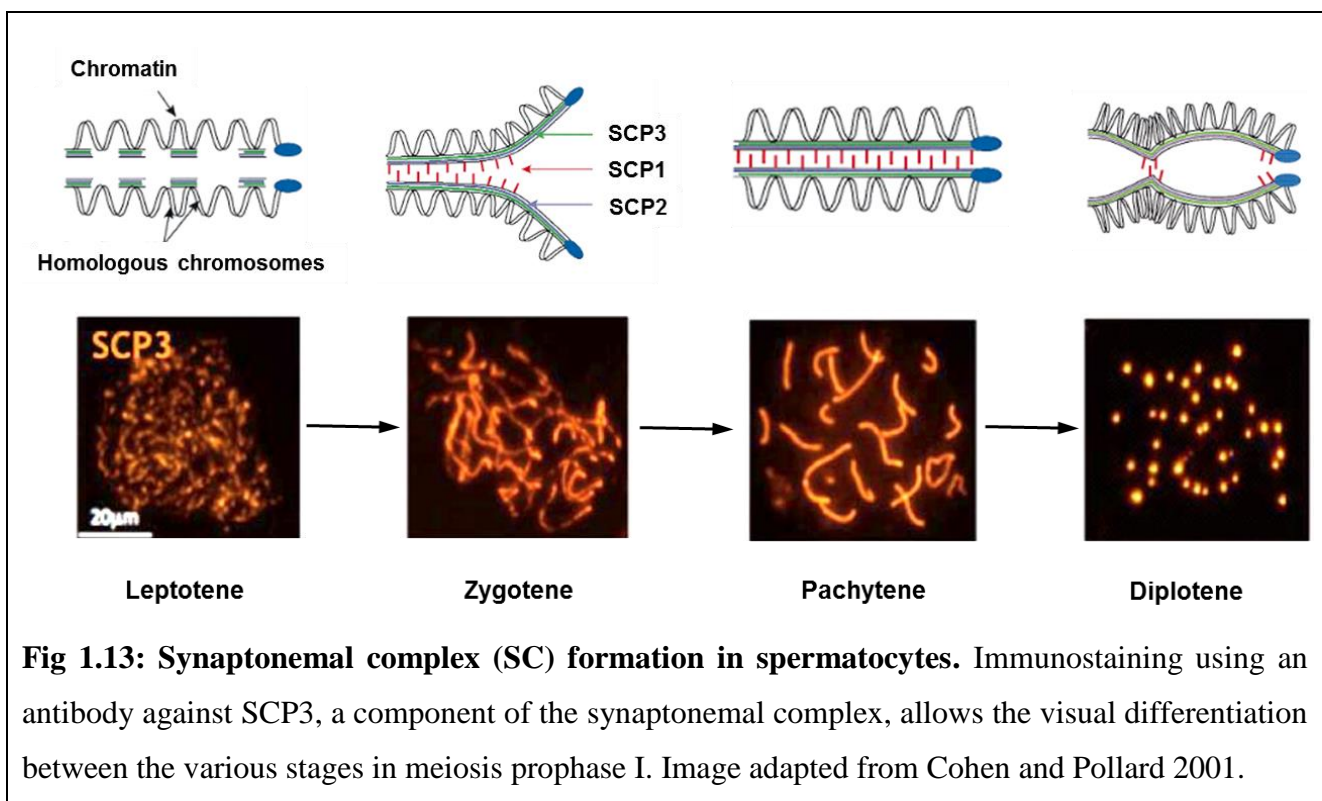


**Fig 1.12: Schematic time line of the first wave of spermatogenesis.** Spermatogenesis can be divided into 3 distinct phases- mitotic, meiotic and post-meiotic phase, lasting approximately 11, 10 and 14 days respectively. Image taken from Yu et al. 2009<sup>108</sup>.

Meiotic recombination is a crucial stage in spermatogenesis whereby diploid germ cells divide and differentiate into haploid spermatids. This promotes genetic diversity and it also helps promote accurate segregation of homologous sister chromosomes for the generation of haploid gametes<sup>109</sup>. Meiotic prophase I can be divided into 4 distinct cytological stages- leptotene (chromatin condensation and initiation of programmed DNA DSBs), zygotene (initiation of synapsis of homologous chromosomes), pachytene (full synapsis, development of crossing over sites on homologous chromosomes) and diplotene (de-synapsis)<sup>105,110</sup>. During these stages, homologous chromosomes are bound by cohesion complex proteins and the synapsis of these chromosomes is achieved by the formation of a large zipper-like arrangement known as the synaptonemal complex (SC)<sup>111</sup>. The SC is made up of two parallel lateral elements, the synaptonemal complex protein 3 (SCP3) and the synaptonemal complex protein 2 (SCP2), that is connected by transverse filaments made up of synaptonemal complex protein 1 (SCP1) (Fig 1.13)<sup>112</sup>. Proper formation of the SC between homologous chromosomes is vital for meiotic recombination to occur<sup>111,113</sup>.

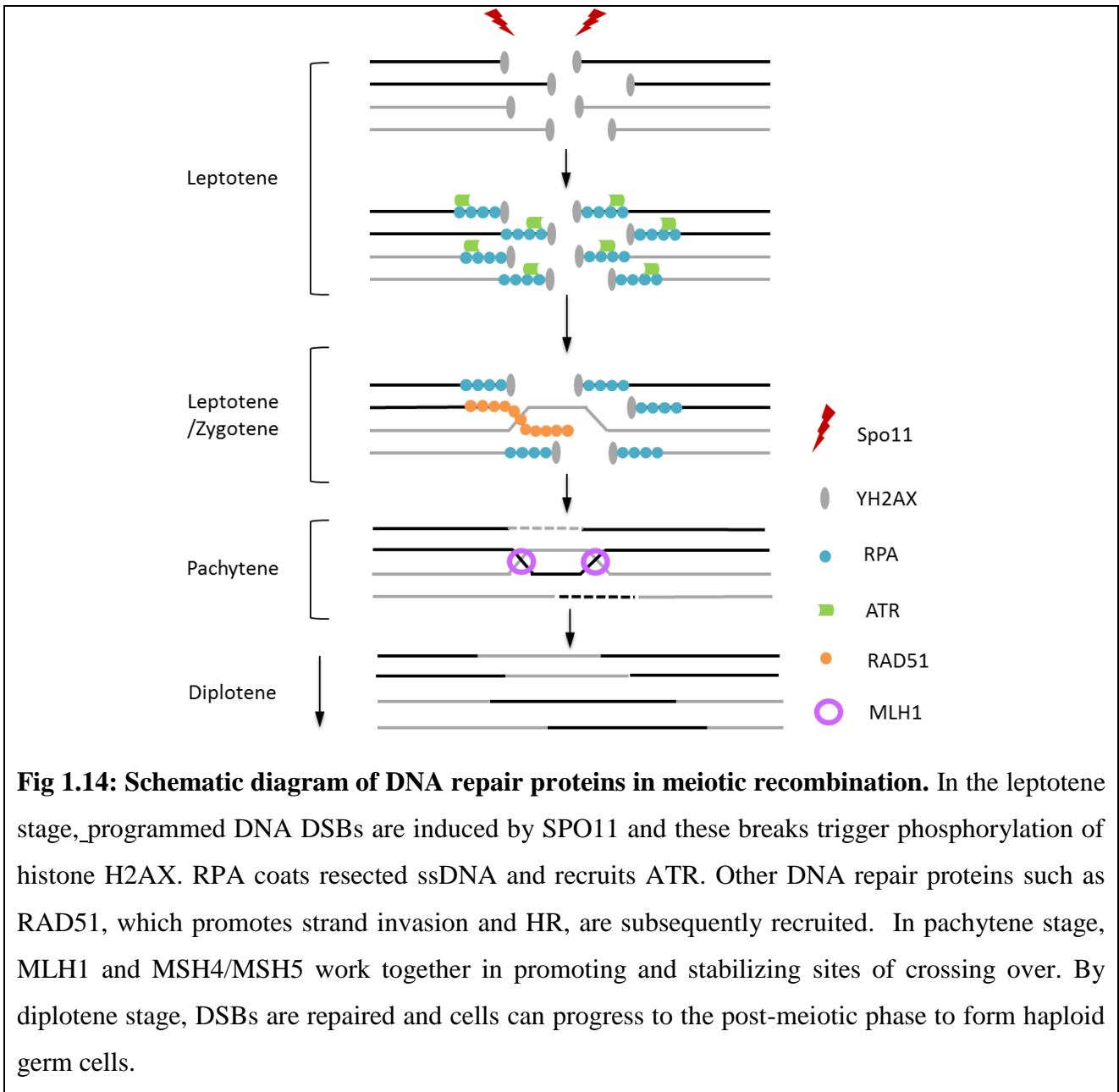


As illustrated in Fig 1.14, initiation of meiotic recombination occurs when the endonuclease SPO11, a DNA topoisomerase II-like protein, induces programmed DNA DSBs during the leptotene stage<sup>114</sup>. These breaks then initiate the phosphorylation of histone H2AX at Ser139<sup>115,116</sup>. Histone H2AX is a variant of the core histone H2A and is distributed widely throughout the genome<sup>117</sup>. Upon DNA damage, histone H2A becomes phosphorylated on Ser139 ( $\gamma$ H2AX) and this is

commonly used as a marker to observe for DNA DSBs in cells<sup>118</sup>. During the zygotene stage, these DSBs initiate the pairing and synapsis of homologous chromosomes<sup>119</sup>. DNA strands containing DSBs introduced by SPO11 have their 5' ends resected to produce 3' single-stranded tails and these ssDNA are bound by replication protein A (RPA), which in turn recruit other DNA repair proteins such as RAD51 and meiosis-specific DMC1<sup>109,120</sup>. Given the fundamental role of DNA DSB formation and repair that occur normally during meiosis, it is not surprising that these DNA damage repair proteins play important roles during meiosis<sup>121</sup>.

Both RAD51 and DMC1 subsequently promote strand invasion between homologous chromosomes which is required for HR and repair<sup>109,120</sup>. These DNA DSBs are gradually repaired during the zygotene stage and  $\gamma$ H2AX phosphorylation intensity decreases. By the pachytene stage,  $\gamma$ H2AX phosphorylation is no longer detectable on autosomal chromosomes due to the effective repair of DNA breaks and  $\gamma$ H2AX phosphorylation becomes restricted only to the XY chromosomes. This 2<sup>nd</sup> wave of  $\gamma$ H2AX phosphorylation occurs only on the XY chromosomes and is important for silencing during the pachytene stage<sup>122</sup>. The two major events that occur during the pachytene stage are (1) chromosomal crossing over and homologous recombination, and (2) meiotic sex chromosome inactivation (MSCI; which will be discussed in more detail in section 1.3.2). Stabilization of the Holiday junctions during meiotic recombination is ensured by the mismatch repair heterodimer MutS Homologs 4 and 5 (MSH4/MSH5) which then recruits MutL Homolog 1 (MLH1) to sites of crossing over<sup>123</sup>. During crossing over, MLH1 localizes to sites of reciprocal recombination on meiotic chromosomes and is regularly used as a marker of chiasmata, which is the physical connection between homologous chromosomes during strand invasion<sup>124</sup>.





By diplotene, crossing over is complete and the SC begins to degrade, allowing the uncoupling of homologous chromosomes<sup>125</sup>. These homologs however, remain tightly bound at the chiasmata, appearing as foci when visualized with SCP3 (Fig 1.13). These homologs will remain bound at the chiasmata until segregation into haploid cells<sup>125</sup>. These spermatocytes then enter into the second phase of meiosis, spermiogenesis, where they further divide into haploid cells, before undergoing cytological transformation to form mature spermatozoa<sup>107</sup>.

### 1.3.2 Meiotic Sex Chromosome Inactivation (MSCI)

During meiosis prophase I, an important phenomena known as meiotic sex chromosome inactivation (MSCI) occurs in the pachytene stage. Due to the lack of homology, the X and Y chromosomes remain largely unpaired with exception to the pseudo-autosomal region (PAR), and this leads to the formation of the XY body<sup>111</sup>. MSCI is essentially the transcriptional silencing of the X and Y chromosomes following large-scale, epigenetic changes to the chromatin. Failure in MSCI has been shown to lead to active sex-linked gene expression and ultimately, spermatocyte death via apoptosis<sup>126</sup>. The X and Y chromosomes remain transcriptionally active during the leptotene and zygotene stages, however they are rapidly silenced and compartmentalized into a peripheral subdomain within the nucleus during the pachytene stage<sup>127</sup>. MSCI then persists through to the diplotene stage<sup>126</sup>. Although the exact function of MSCI is still unknown, it has been postulated that MSCI may act to suppress any illegitimate recombination between the non-homologous X and Y chromosomes<sup>128</sup>, suppress expression of sex-linked genes that may be toxic to cells during spermatogenesis and/or act as a driving force for trans-generational epigenetic inheritance<sup>129,130</sup>, in order for successful meiotic recombination to occur and for the production of mature germ cells<sup>131</sup>.

Silencing is attained through the remodeling of chromatin into a highly condensed structure (heterochromatin) and this renders the chromatin inaccessible to the transcription machinery<sup>126,132</sup>. Although the exact mechanism of how MSCI occurs remains unclear, several DNA damage repair (DDR) factors such as the breast cancer susceptibility 1 (BRCA1) and ataxia-telangiectasia and Rad3-related kinase (ATR) proteins have been shown to play critical roles in this phenomenon<sup>133</sup>. Prior to MSCI, BRCA1 has been shown to localize and associate with the axial element of the unsynapsed XY chromosomes (Fig 1.15). ATR is then recruited in a BRCA1-dependent manner and localizes to the axial element as well. ATR subsequently translocates from the axial element and into the chromatin loops, creating a diffused staining pattern over the XY chromosomes<sup>126,134</sup>. It then phosphorylates histone H2AX on the XY chromosomes and this contributes to the XY silencing that is required for MSCI<sup>126</sup>.

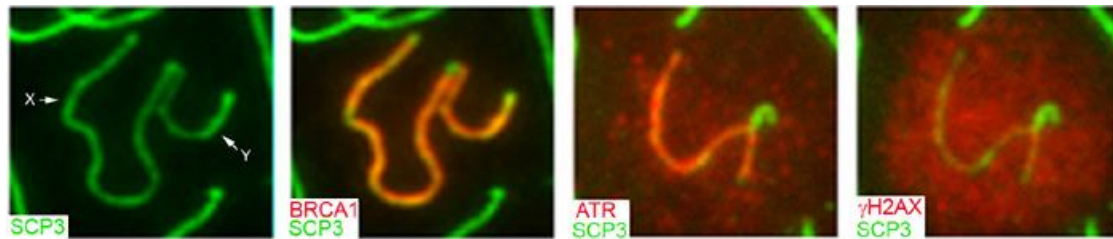


**Fig 1.15: The initiation of MSCI.** The initiation of MSCI occurs when BRCA1 is recruited to the axial element of the X and Y chromosomes (white arrow). This is followed by a BRCA1-dependent recruitment of ATR to the axial element before translocating into the chromatin loops and phosphorylating histone H2AX ( $\gamma$ H2AX). Silencing occurs as soon as phosphorylation is initiated. *Image taken from Turner et al. 2004.*

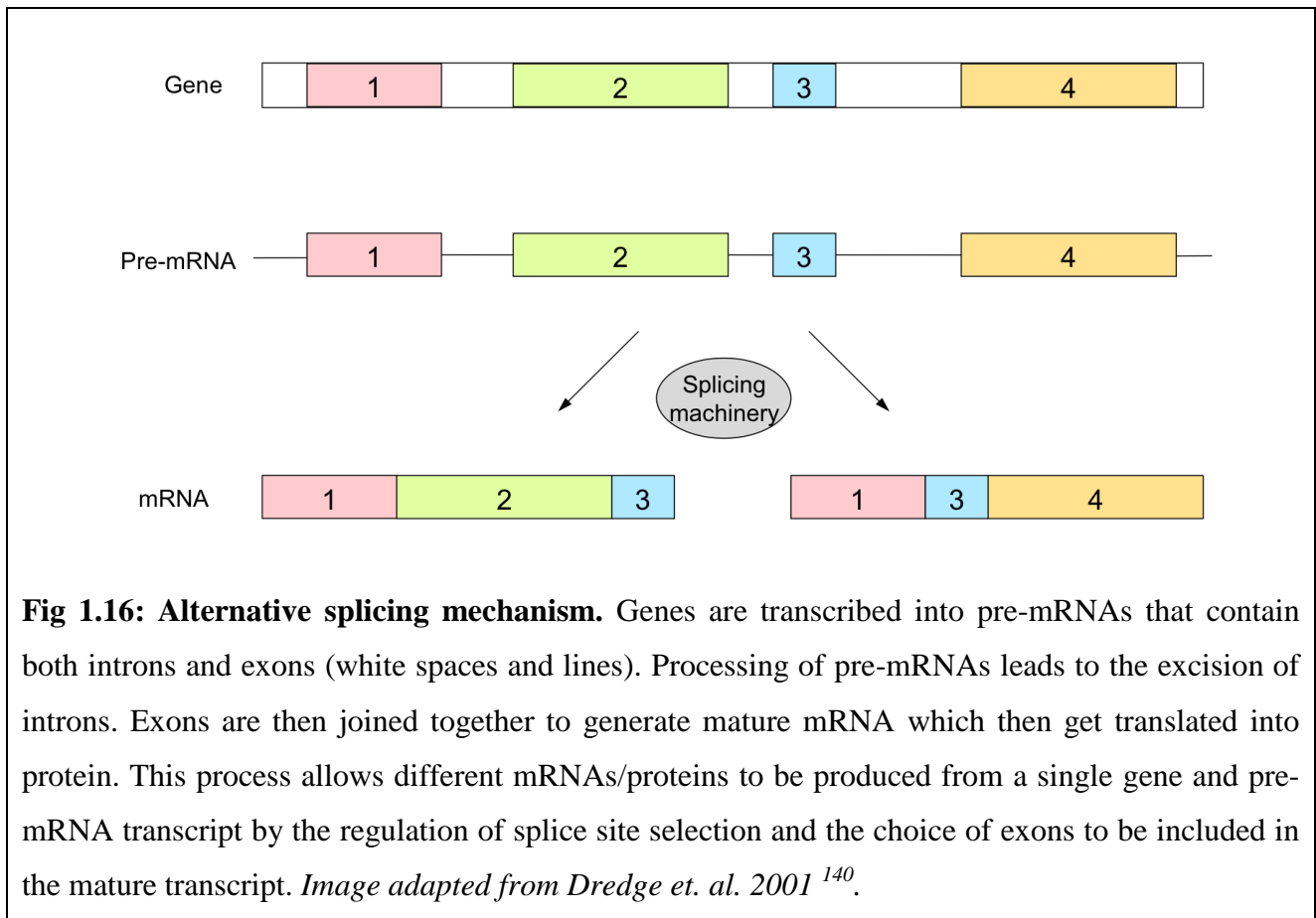
The progression of meiotic events and XY body formation are also tightly regulated by various post-translational modifications. SUMOylation (covalent modification by small ubiquitin-like modifiers; SUMO) has been implicated in a range of cellular pathways, such as protein-protein interactions, transcription regulation (repression, in most cases), DNA repair, and formation of specific heterochromatic nuclear subdomains<sup>131,135,136</sup>. There are four different members of the SUMO family in mammals, namely SUMO-1, -2, -3 and -4. SUMO-1 shares about 45% homology with SUMO-2 and -3 (which are approximately 96% identical, commonly termed SUMO-2/3) and SUMO-4 shares 87% homology to SUMO 2/3<sup>137</sup>. While SUMO-1 and -2/3 are expressed ubiquitously, SUMO-4 has been identified as a kidney-specific protein<sup>137</sup>. Interestingly, SUMO-1 and -2/3 have been shown to localize to the XY chromosomes during the pachytene stage, suggesting roles in MSCI<sup>138,131</sup>. However the exact role of each of the different SUMO isoforms during MSCI remains unclear.

## **1.4 Transcription regulation & disease**

### *1.4.1 Aberrant splicing & neurodegeneration*

In recent years, the contribution of aberrant RNA metabolism to neurodegeneration has become increasingly clear<sup>139</sup>. Following its transcription from DNA, RNA undergoes a series of complex processing that include capping, splicing, editing and association with various proteins that changes its function, stability and subcellular localization. Of particular interest is the process of alternative splicing, a mechanism that generates a versatile repertoire of functionally different proteins within

individual cells<sup>140</sup> (Fig 1.16). The importance of alternative splicing is evidently clear in highly specialized cells such as neurons<sup>141,142</sup>. For example, all of the main neurotransmitter receptors contain subunits, which influence their localization, ligand-binding, signal-transducing and electrophysiological properties, and the synthesis of neurotransmitters and their subunits are generated through alternative splicing<sup>140</sup>.



Aberrant splicing of mRNAs encoding proteins that are critical for the proper function of neuronal cells has been associated with several neurological diseases<sup>140,142</sup>. An example of such a phenomenon is observed in spinal muscular atrophy (SMA), an autosomal recessive disorder resulting from the dysfunction of lower motor neurons<sup>143</sup>. The causative gene for SMA is *SMN1*, where mutations lead to a loss of the motor neuron protein, SMN<sup>144</sup>. The loss of SMN is due to a mutation in the last exon of the *SMN1* gene that affects its splicing, thereby resulting in a predominantly truncated, unstable form of SMN. SMA is a disease caused by defects in RNA processing as SMN itself is an RNA-binding protein involved in several facets of RNA functions such as splicing and mRNA localization to the axon<sup>139,140</sup>. Interestingly, SMN also interacts with senataxin, which as mentioned previously, is another protein involved in RNA metabolism that can cause AOA2 if mutated<sup>145</sup>. Senataxin also interacts with several key proteins that include RNA Pol

II, SAP155, Nucleolin, PABP1/2, and hnRNPA1 which are all involved in RNA processing, splicing and transport<sup>71</sup>. Additionally, alternative splicing in the nervous system coordinates the activity of protein networks at the synapse and is important for genes encoding for receptors, signal transduction proteins, and splicing regulators<sup>146</sup>. Alternative splicing can also lead to the alteration of functional properties of neuronal receptors by modifying their affinity to agonists or by changing their localization<sup>139</sup>.

Other neurological disorders associated with aberrant RNA processes such as RNA editing, polyadenylation, nuclear mRNA export, mRNA stabilization and localization, as well as aberrant regulation by non-coding regulatory RNAs such as small-interfering RNAs (siRNAs) and microRNAs (miRNAs)<sup>147-149</sup>, are summarized in the table below (Table 1.2).

<b>Aberrant RNA process</b>	<b>Neurological disorder</b>	<b>Details</b>
RNA editing	Amyotrophic lateral sclerosis (ALS) Alzheimer's disease (AD) Huntington's disease (HD)	Reduced editing efficiency off the GluR2 AMPA receptor subunit at Q/R site
	Epilepsy	Increased editing efficiency of the GluR2 AMPA receptor subunit at the R/G site
Alternative splicing	Spinal muscular atrophy (SMA)	Truncated protein via exon skipping
	Spinocerebellar ataxias (SCA) type 2, 8, 10, 12	Splicing factors interact with several ataxia-causing proteins
	Rett syndrome (RTT)	Mutations in causative gene, <i>MECP2</i> , affects splicing of target mRNAs
Polyadenylation	Oculopharyngeal muscular dystrophy (OPMD)	Polyalanine expansion and aggregation of polyadenylation binding protein nuclear 1 (PABPN1)
Nuclear mRNA transport	Fragile X syndrome (FXS)	Deletion of fragile X mental retardation protein (FMRP) prevents its interaction with export factor, NXF2
	Lethal congenital contracture	Disease-causing mutations in the

	syndrome type 1 (LCCS1)	gene encoding mRNA export protein, GLE1
mRNA stabilization and localization	SMA	Defect in the localization of $\beta$ -actin mRNA to the growth cones of motor neurons
	ALS	TDP43 stabilizes human low molecular weight neurofilament (hNFL) mRNA by binding directly to 3'UTR
Regulation by noncoding RNAs	SCA1	miRNAs miR-19, -101 and -130 co-regulate ataxin 1 (ATXN1) levels in Purkinje cells and inhibition of these proteins enhances cytotoxicity of polyglutamine-expanded ATXN1

**Table 1.2: Neurological disorders associated with RNA processing defects.** *Table adapted from Anthony and Gallo 2010<sup>139</sup>.*

#### 1.4.2 Transcription regulation & genomic instability

##### 1.4.2.1 R-loops accumulation can cause genomic instability

R-loops are naturally occurring DNA:RNA hybrid structures that form behind elongating RNA Polymerase (*cis*) by the interaction between the nascent mRNA and its ssDNA template from which it was transcribed from, over transcriptional pause sites<sup>150</sup>. R-loops can also form when an RNA transcript hybridizes into an opened bubble that arises from negative DNA supercoils<sup>151,152</sup>. Wahba *et al.* 2013 also showed that R-loops can form in *trans* where RNA was found to invade DNA duplexes at a distant genomic loci in yeast. Interestingly, they also reported that Rad51, a DDR protein involved in promoting strand invasion during homologous recombination, promoted R-loop formation<sup>153</sup>. Although the exact function of R-loops is unclear, it is believed that these structures allow for efficient transcription initiation and termination through RNA Polymerase stalling<sup>73</sup>, induce transcription-associated recombination<sup>74</sup> or mutagenic events such as class-switch recombination and somatic hyper-recombination in B lymphocytes<sup>75</sup>.

Wongsurawat *et al.* 2011 mapped R-loop forming sequences (RLFS, as defined by Roy and Lieber 2009<sup>154</sup>) on 66,083 sequences defined by the UCSC Genome Bioinformatics database (<http://genome.ucsc.edu/>) as “known” genes and found that ~59% of these transcribed sequences contain at least 1 RLFS<sup>155</sup>. It was predicted that many oncogenes, tumour suppressor genes (e.g. *p53*, *BRCA1 and 2*, *Kras*) and neurodegenerative disease-related genes (e.g. *ATM*, *Park2*, *Ptprd*) are also susceptible to significant R-loop formation<sup>155</sup>. The formation of these stable secondary structures can potentially pose a threat to genomic integrity<sup>73</sup> and reports have shown that R-loops are often associated with neurodegenerative diseases caused by trinucleotide repeats such as spinocerebellar ataxia type 1 (SCA1), myotonic dystrophy (DM1) and fragile X type A (FRAXA)<sup>156-158</sup>.

Unresolved R-loops can cause DNA DSBs and chromosomal rearrangements as observed in a study by Li and Manley 2005, where cells depleted of the protein-splicing factor ASF/SF2 led to an accumulation of R-loops which subsequently resulted in hypermutagenic cells with high molecular weight DNA fragmentation<sup>75,159</sup>. Although little is known about the molecular mechanisms by which transcriptional R-loops influence genome stability, several hypotheses have been raised. First, because ssDNA is known to be more susceptible to mutations than dsDNA, it has been proposed that extensive R-loop formation may expose highly transcribed regions of the genome to more DNA damage by increasing the incidence of single-stranded DNA (Fig 1.17A). Second, it has been proposed that protein factors that specifically recognize R-loops may be involved in the generation of mutagenic and/or recombinant DNA lesions (Fig 1.17B). One instance of this is seen in G-rich class-switch recombination (CSR) sites in B lymphocytes where R-loop formation preferentially occur<sup>160</sup>. An example of a protein involved in CSR is activation-induced (cytidine) deaminase (AID)<sup>161</sup>. AID deaminates cytidine to form uracil preferentially on single-stranded non-template DNA, and the resulting mismatch is subsequently processed by uracil DNA glycolase (UNG) and/or apurinic/apyrimidinic endonuclease (APE), components of the base excision repair machinery, thereby generating DNA nicks in the region. These nicks are then converted into DSBs by mismatch repair proteins to initiate recombination<sup>159</sup>. Hence, an accumulation of R-loops at inappropriate gene regions may then cause illegitimate hyper-recombination to occur. Third, G-rich ssDNA regions are prone to folding and forming stable parallel four-stranded DNA structures called G-quadruplexes (further discussed in section 1.4.2.3)<sup>73,159</sup>. Hence, it was suggested that these higher order structures generate susceptible sites for specific nucleases (Fig 1.17C). These nucleases such as DNA2 and GQN1 have been found to cleave specifically DNA in single-stranded regions 5' of G-quadruplex structures<sup>162,163</sup>. Lastly, it was hypothesized that R-loops may block or collide with oncoming or stalled replication machinery, consequently leading to DNA DSBs, aberrant

recombination and cell death<sup>164,165</sup> (Fig 1.17D). Such a phenomenon has been observed in yeast and bacteria, where transcription-dependent replication fork collisions have been shown to induce recombination and DSBs<sup>159</sup>. Therefore, an accumulation of R-loops may disturb the gene expression or repression balance in cells and further contribute to abnormal transcription regulation that could lead to genomic instability<sup>166</sup>.

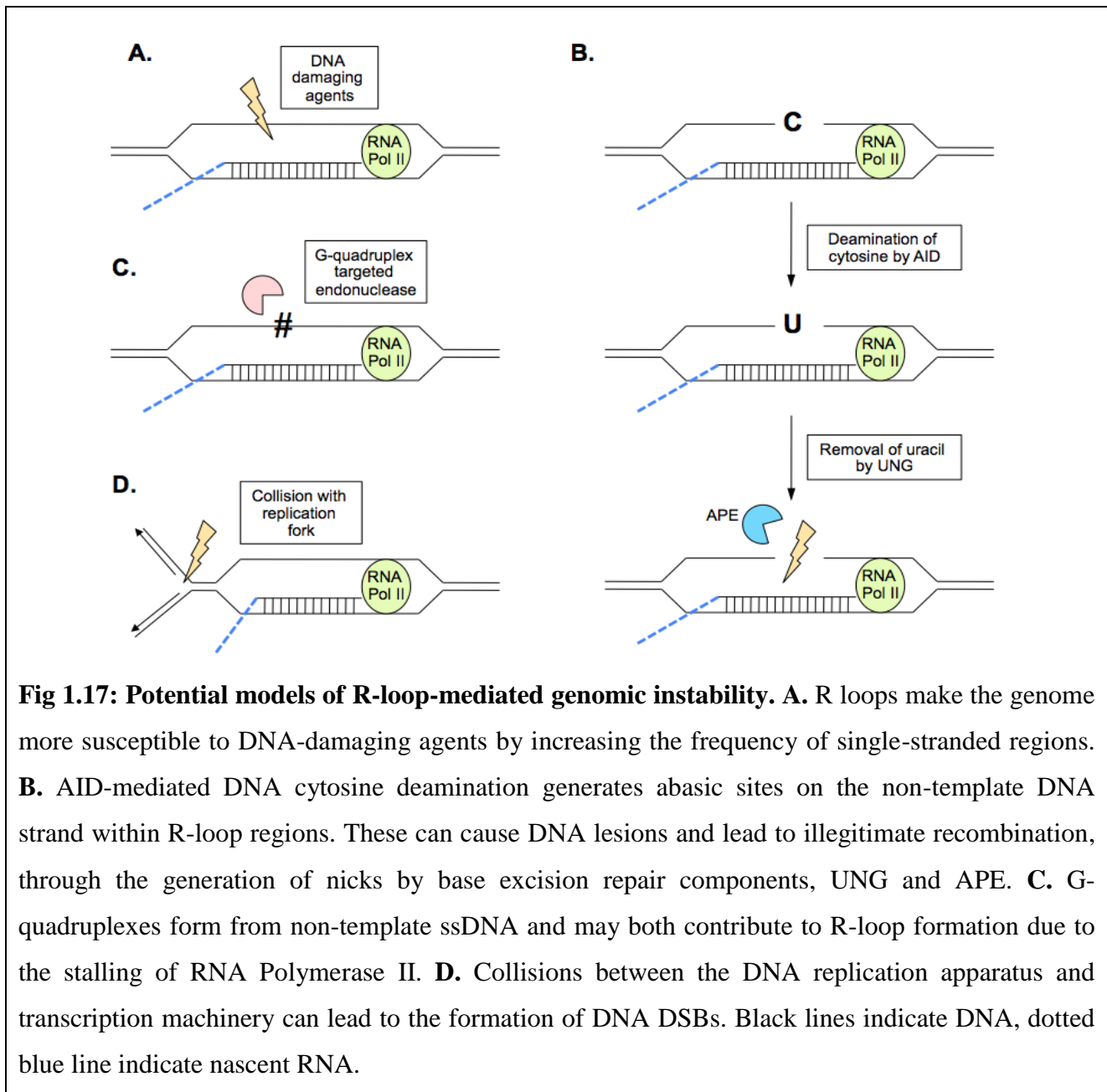


**Fig 1.17: Potential models of R-loop-mediated genomic instability.** **A.** R loops make the genome more susceptible to DNA-damaging agents by increasing the frequency of single-stranded regions. **B.** AID-mediated DNA cytosine deamination generates abasic sites on the non-template DNA strand within R-loop regions. These can cause DNA lesions and lead to illegitimate recombination, through the generation of nicks by base excision repair components, UNG and APE. **C.** G-quadruplexes form from non-template ssDNA and may both contribute to R-loop formation due to the stalling of RNA Polymerase II. **D.** Collisions between the DNA replication apparatus and transcription machinery can lead to the formation of DNA DSBs. Black lines indicate DNA, dotted blue line indicate nascent RNA.

The resolution of R-loop structures is dependent on several DNA/RNA helicases, enzymes that act to unwind the DNA and/or RNA duplexes in an ATP-dependent manner. The uncoupling of DNA or RNA complementary strands is an essential requirement for many metabolic processes in cells. The unwinding of these duplexes allows the access of proteins of the transcription, recombination,



replication and repair machineries to the DNA template<sup>167</sup>. Generally, helicases possess specific polarity, moving in 3'-5' or 5'-3' direction depending upon the strand on which they act on<sup>167</sup>. An example of a helicase that can unwind R-loop structures is the human DHX9 helicase, also known as the nuclear DNA helicase II or RNA helicase A<sup>168</sup>. DHX9 belongs to the superfamily II of DNA/RNA helicase and has been shown to dissociate DNA duplexes, RNA duplexes as well as R-loops with a 3'-5' polarity; despite this little is known about its substrate specificity<sup>168</sup>. Other well-characterized R-loop-resolving enzymes include RNase H1/H2, where they act by removing the RNA component of R-loops<sup>169</sup>. It is also possible that senataxin is another protein that resolves R-loop structures as reported by Skourti-Stathaki *et al.* 2011, as it contains a predicted DNA/RNA helicase domain<sup>61,73</sup>.

#### 1.4.2.2 R-loops & gene expression (CpG methylation)

CpG islands are short interspersed DNA sequences that are GC-rich regions, which function as promoter regions for about 60% of human genes and are predominantly maintained in a non-methylated state<sup>170</sup>. Silencing of these CpG promoters is achieved through methylation and are therefore capable of influencing local chromatin structure and modify regulation of gene activity<sup>171</sup>. In 2011, Deaton *et al.* reported that R-loops structures form over these CpG islands and prevent their methylation<sup>171</sup>. It was also shown that the formation of R-loops could be a new mechanism in the retention of CpG islands in its non-methylated state (Fig 1.18)<sup>170</sup>. Wongsurawat *et al.* 2011 reported the presence of RLFS in the *Dazl* gene, which encodes potential RNA binding proteins that are expressed in pre- and postnatal germ cells of males and females. Due to the negative effect of R-loop formation on the methylation of promoters, it is interesting to note that the incorrect methylation of the *Dazl* gene has been associated with defective human sperm<sup>155</sup>. This is reminiscent of the recently observed role of R-loops on the inhibition of CpG island methylation (Fig 1.17)<sup>172</sup>.

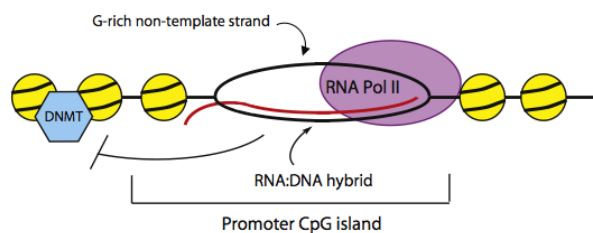


**Fig 1.18: R-loops prevent methylation of CpG island promoters.** Formation of R-loops at CpG island promoters is favored by the GC-sequence skew and these structures can inhibit the actions of DNA methyltransferases. *Image adapted from Vertino and Wade 2012.*

### 1.4.2.3 *G-quadruplexes & R-loop formation*

Genomic DNA is generally maintained in a duplex formation, but DNA also can form other structures and one such sequence motif particularly susceptible to tertiary structure formation is a guanine-run<sup>173</sup>. Sequences containing continuous guanine bases readily fold into four-stranded structures stabilized by planar arrays of four hydrogen-bonded guanines, and these tertiary structures are known as G-quadruplexes<sup>174</sup>.

Although the exact functions of these structures remains unknown, there have been reports associating G-quadruplexes to several essential cellular processes that include DNA replication, transcription regulation and overall genomic stability<sup>175</sup>. Several chromosomal regions contain G-rich sequences that form G-quadruplexes in the genome and indeed, these G-quadruplexes which have also been linked with R-loop formation, have been shown to affect transcription termination, alternative splicing and gene expression<sup>175-177</sup>. G-rich chromosomal domains include four classes of repetitive regions—telomeres, rDNA, immunoglobulin heavy chain switch regions, and G-rich minisatellites<sup>178</sup>. Telomeric repeats in almost all eukaryotes contain runs of guanines and these telomeric sequences form have been reported to form G-quadruplexes *in vitro*<sup>179</sup>. Mammalian rDNA, which encodes ribosomes, also contain large stretches of over 40kb of G-rich repeats, on the non-template DNA strand<sup>180</sup>. These structures can form both within the region that is transcribed into mature rRNA and within spacers<sup>181</sup>. The immunoglobulin heavy chain class switch regions, which are required for class-switch recombination, consists too of numerous G-rich repeats that range from 2kb to 10 kb in length and conform to a loose consensus<sup>161</sup>. Overall, the human genome contains many repetitive minisatellites, and among those that exhibit the most marked instability are G-rich sequences that form G-quadruplexes<sup>182,183</sup>.

## **1.5 Aims of Project**

Mutations in several proteins involved in DNA damage repair (DDR) such as ataxia-telangiectasia (ATM), senataxin (SETX), aprataxin (APTX) and tyrosyl-DNA phosphodiesterase 1 (TDP1), lead to autosomal recessive cerebellar ataxias (ARCA). Mutant senataxin was identified to cause the human ARCA, ataxia oculomotor apraxia type 2 (AOA2). Senataxin is a putative DNA/RNA helicase that, in addition to its role in DDR, has been reported to be involved in several RNA metabolic processes such as splice site selection, transcription initiation and termination, and R-loop resolution<sup>71,73</sup>. Additionally, senataxin-deficient cells display sensitivity to several DNA damaging agents such as hydrogen peroxide and camptothecin, exhibit constitutive oxidative DNA damage and chromosomal instability<sup>63</sup>.

To better understand the role of senataxin *in vivo*, the first *Setx*<sup>-/-</sup> mouse model was generated and this Project represents the characterization of this mouse model. The specific aims of this Project are as follows:

### **1. To characterize the *Setx*<sup>-/-</sup> mouse model.**

This involves the overall phenotypic characterization and behavioral analyses of these mice, followed by the morphological analyses of nervous tissue as well as the structural analyses of Purkinje cells in the cerebellum, which is the affected cell type in ARCAs.

### **2. To investigate the role of senataxin in DDR during meiotic sex chromosome inactivation (MSCI)**

Several ARCA mouse models do not show neurological defects but display fertility issues as a common feature. Here, the role of senataxin in DDR in spermatogenesis, more specifically, during meiotic sex chromosome inactivation in male *Setx*<sup>-/-</sup> mouse will be investigated.

### **3. To investigate the role of R-loop as a form of transcription deregulation in ARCA mouse models.**

This involves the investigation of how senataxin influences R-loop formation and resolution, and how this impacts gene expression in *Setx*<sup>-/-</sup> mice. Furthermore, given the association of these DDR proteins (ATM, APTX and TDP1 in addition to SETX) in transcription regulation, the prevalence of

R-loop structures in these respective ARCA mouse models will also be examined to investigate the impact of R-loop accumulation and its effect on transcription deregulation in other systems, including the nervous system. Because these models do not recapitulate the neurodegenerative phenotype observed in human patients, attempts to induce such a phenotype via DNA damage exposure will be performed to determine whether a correlation between DNA damage and R-loop accumulation exists.

## **CHAPTER 2: Materials & Methods**

## **2.1 Animal husbandry & genotyping**

All animal experiments were approved by the QIMR Berghofer Medical Research Institute (aka QIMR) Animal Ethics Committee. The mice were weaned at 21 days post-partum and ear clipped for identification. Genotyping was carried out via PCR on genomic DNA isolated from tail tips. See Table 2.1 for description of primers for genotyping the animals.

To genotype *Setx* mice, primers used were In3F, In3R and LoxPR. PCR cycling conditions were as follows: 35 cycles, denaturation at 95°C for 30 sec, annealing at 49 °C for 30 sec, extension at 72°C for 1 min, with a final cycle and extension of 7 min at 72°C. Two PCR products were generated, a wild type PCR product of 600 bp, and the targeted PCR product of 339 bp.

To genotype *Atm* mice, primers used were KO1F, KO1R and KO2R. PCR cycling conditions were as follows: 35 cycles, denaturation at 94°C for 45 sec, annealing at 62 °C for 45 sec, extension at 72°C for 1 min, with a final cycle and extension of 5 min at 72°C. Two PCR products were generated, a wild type PCR product of 344 bp, and the targeted PCR product of 402 bp.

To genotype *Tdp1* mice, primers used were TDP1F, TDP1R and GEOR. PCR cycling conditions were as follows: 35 cycles, denaturation at 94°C for 30 sec, annealing at 60 °C for 45 sec, extension at 72°C for 45 sec, with a final cycle and extension of 6 min at 72°C. Two PCR products were generated, a wild type PCR product of 300 bp, and the targeted PCR product of 550 bp.

To genotype *Aptx* mice, primers used were APTX1F, APTX1R and APTX2R. PCR cycling conditions were as follows: 35 cycles, denaturation at 94°C for 30 sec, annealing at 60 °C for 45 sec, extension at 72°C for 45 sec, with a final cycle and extension of 6 min at 72°C. Two PCR products were generated, a wild type PCR product of 224 bp, and the targeted PCR product of 300 bp.

PCR products were electrophoresed at 100V for 30 min on 2% TAE Agarose (Boehringer Mannheim, Amresco, Lewes, UK) stained with Ethidium bromide and visualised with UV transillumination using a GelDoc<sup>TM</sup>XR (Biorad Laboratories Inc, California, USA).

<b>Mouse model</b>	<b>Primer name</b>	<b>Primer sequence</b>
<i>Atm</i>	KO1F	5'-TGGTCAGTGTAACAGTCATTGTGC-3'
	KO1R	5'-AAGGTTGTAGATAGGTCAGCATTG-3'

	KO2R	5' AACGAGATCAGCAGCCTCTGTTCC-3'
<i>Setx</i>	In3F	5'-TTTAAGGAACAGTGCTGC-3'
	In3R	5'-ATGAAGCAGGTAGGATT-3'
	LoxPR	5'-CGAAGTTATATTAAGGGT-3'
<i>Tdp1</i>	TDP1F	5'-TCTTCCAGTTCTTAGCCTCCTCTGC-3'
	TDP1R	5'-TGGCCTGGATCTCACTCTGGAGGC-3'
	GEOR3	5'-GAGTTCCCAGGAGGAGCCAAGGC-3'
<i>Aptx</i>	APT1F	5'-TTCTCTCCATGACTGGTCATGGC-3'
	APT1R	5'-TATACTCAGAGCCGGCCT-3'
	APT2R	5'-TCCTCGTCGTTTACGGTATC-3'

**Table 2.1: Primers for genotyping animals**

## **2.2 Cell culture**

Lymphoblastoid cell lines (LCLs) from control (C3ABR) and AOA2 patients (SETX2RM) were cultured in RPMI 1640 medium (Gibco BRL, Life Technologies, California, USA) containing 6% fetal calf serum (JRH Biosciences, Kansas, USA), 2mM L-glutamine (Life Technologies, California, USA), 100U/ml penicillin (Gibco BRL, Life Technologies, California, USA) and 100U/ml streptomycin (Gibco BRL, Life Technologies, California, USA). Cells were maintained in a humidified incubator at 37°C/5% CO<sub>2</sub>.

HeLa and U2OS cell lines were cultured under identical conditions with DME medium (Gibco BRL, Life Technologies, California, USA) containing 10% foetal calf serum, 100U/ml penicillin (Gibco BRL, Life Technologies, California, USA) and 100U/ml streptomycin (Gibco BRL, Life Technologies, California, USA). Cells were maintained in a humidified incubator at 37°C/5% CO<sub>2</sub>.

## **2.3 Senataxin immunoprecipitation**

LCLs and testes from 35 day-old mice (ground with a pestle to disrupt their structure) were lysed for 1 h at 4°C on a rotating wheel with 1 ml of lysis buffer (50 mM Tris-HCl pH 7.4, 150 mM NaCl, 2 mM EGTA, 2mM EDTA, 25 mM β-glycerophosphate, 0.1 mM sodium orthovanadate (Na<sub>3</sub>VO<sub>4</sub>), 0.1 mM PMSF, 25 mM sodium fluoride (NaF), 0.2% Triton X-100, 0.3% NP-40 and 1X EDTA-free Complete Protease inhibitor (Roche, Basel Switzerland)). Cellular debris were pelleted by

centrifugation at 16,100 x g at 4°C for 10 min, and protein concentration was determined using the Lowry Assay (Biorad Laboratories Inc, California, USA). 2 mg of total protein extract were pre-cleared with 10 µl of Protein G beads (50:50 slurry) (Merck Millipore, Massachusetts, USA) for 3 h at 4°C on a rotating wheel. Extracts were centrifuged for 5 min at 2000 x g, beads were removed, and 10 µg of anti-human senataxin antibody (Ab-1 #OB 1) was added to the extract. Extracts and antibody were incubated overnight at 4°C on a rotating wheel to allow binding of the antibody to senataxin. The next day, 20 µl of Protein G beads (50:50 slurry) (Merck Millipore, Massachusetts, USA) were added to the protein extract and incubated for 2 h at 4°C on a rotating wheel. Protein extracts were centrifuged for 5 min at 2000 x g and the beads were removed. The immunoprecipitate was subsequently washed 3 times with lysis buffer and the beads were resuspended in SDS loading buffer containing 2X DTT and separated via 5% SDS-PAGE at constant current (20 mA) per gel for 1.5 h. Once separated, proteins were transferred onto an Amersham Hybond-C nitrocellulose membrane (GE Healthcare, Queensland, Australia) for 1 h at 4°C with constant voltage (100 Volts). Immunoblotting with anti-senataxin (Ab-1) antibody was performed as described in section 2.12.

## **2.4 Histological analyses of Setx mouse tissues**

Testes, ovaries, brains and cerebellums from 35-day-old and 20-month-old mice were collected and fixed in PBS containing 10% formalin, embedded in paraffin blocks and sectioned at 4 µm by the Histology Department at the QIMR Berghofer Medical Research Institute (aka QIMR). Sections were stained with Hematoxylin and Eosin (H&E). Slides were examined under light microscope and then scanned using Scanscope CS system (Aperio Technologies, Vista, USA). Images corresponding to ×10 and ×20 magnifications were captured and assembled in Adobe Photoshop CS5 (Adobe Systems Inc, USA).

## **2.5 Immunofluorescence**

Tissue sections embedded in paraffin and mounted onto glass slides were dewaxed and rehydrated with Shandon Varistain® Gemini ES (Thermo Scientific, Massachusetts, USA). Briefly, slides were first immersed twice for 2 min each in xylene, dipped into absolute ethanol, 90% ethanol, then 70% ethanol for 2 min and rinsed with distilled water. Enzymatic antigen retrieval was performed by incubating the sections with 1:10 trypsin dilution in PBS for 20 min at 37°C. Slides were washed 3 times for 5 min with PBS on an orbital shaker at room temperature for 5 min each. Spermatocyte spreads that were fixed onto glass slides by PFA did not require dewaxing. Slides were blocked in



20% FCS, 2% BSA, 0.2% Triton X-100 in 1 X PBS for 1 h at room temperature. Slides were incubated with primary antibody (Table 2.2) overnight at 4°C in a humidified chamber. The next day, slides were washed 5 times with 1 X PBS containing 0.5% Triton X-100 for 5 min each at room temperature on an orbital shaker. Alexa-Dye-conjugated secondary antibody (Life Technologies, California, USA) (Table 2.3) was added and slides were incubated for 1 h at 37°C in a humidified chamber. Subsequently, slides were washed 3 times as before and Hoechst 33342 (1:10,000) (Life Technologies, California, USA) was added for 10 min to stain nuclei. Slides were finally washed twice and glass coverslips were mounted for imaging. Images were captured using a digital camera (AxioCam Mrm, Carl Zeiss Microimaging Inc., Jena, Germany) attached to a fluorescent microscope (Axioskop 2 mot plus, Carl Zeiss Microimaging Inc., Jena, Germany) equipped with the appropriate filters, and the AxioVision 4.8 software (Carl Zeiss Microimaging Inc., Jena, Germany). The objective employed was an EC Plan-Neofluar 10x/0.3 (Carl Zeiss Microimaging Inc, Jena, Germany).

<b>Primary antibody</b>	<b>Species</b>	<b>Dilution</b>	<b>Catalogue number</b>	<b>Manufacturer</b>
Scp3	Rabbit	1:100	NB300-230	Novus Biologicals
Scp3	Mouse	1:100	AB97672	Abcam
Atr	Goat	1:100	SC-1887	Santa Cruz Biotechnology
Nek1	Rabbit	1:100	BS-7814R	Bioss Inc.
Atrip	Rabbit	1:100	A300-670	Bethyl Laboratories Inc.
Chk1	Mouse	1:100	2360	Cell Signaling Technology
Chd4	Rabbit	1:100	AB72418	Abcam
Rad51	Rabbit	1:100	SC-6862	Santa Cruz Biotechnology
Mlh1	Mouse	1:10	SC-56161	Santa Cruz Biotechnology
Setx	Sheep	1:300	-	In-house
Brcal	Rabbit	1:300	-	With courtesy, David Livingstone (Dana Farber Cancer Institute, MA, USA)
TopBp1	Rabbit	1:100	AB2402	Abcam
SUMO-1	Rabbit	1:100	AB32058	Abcam
SUMO-2/3	Rabbit	1:100	A3742	Abcam
Phospho-Atr (S428)	Rabbit	1:100	2853	Cell Signaling Technology

Phospho-RNAPII (S2)	Rabbit	1:100	AB24758	Abcam
Phospho-Rpa (S33)	Rabbit	1:100	A300-246A	Bethyl Laboratories Inc.
Phospho-Chk1 (S317)	Rabbit	1:100	2344	Cell Signaling Technology
$\gamma$ H2AX	Mouse	1:100	Y-91016	Merck Millipore
H3K4me1	Rabbit	1:100	AB8895	Abcam
Gapdh	Rabbit	1:500	GTX100118	Genetex
$\alpha$ -tubulin	Rabbit	1:500	GTX112141	Genetex
S9.6 (R-loop)	Mouse	1:100	-	With courtesy, Stephen Leppla (National Institute of Health, MD, USA)

**Table 2.2: Description of primary antibodies used for immunofluorescence.**

Secondary antibodies	Dilution	Catalogue number	Manufacturer
Alexa 488-labeled chicken anti-mouse	1:250	A-21200	Life Technologies
Alexa 594-labeled donkey anti-rabbit	1:250	A-11032	Life Technologies
Alexa 594-labeled donkey anti-goat	1:250	A-11058	Life Technologies
Alexa 350-labeled anti-mouse	1:100	A-11045	Life Technologies

**Table 2.3: Description of secondary antibodies used for immunofluorescence.**

## **2.6 TUNEL assay**

Slides with tissue sections were de-waxed as previously described. TUNEL assay was performed using the Fluorescence *in situ* Cell Death Detection Kit (Roche, Basel, Switzerland) following the manufacturer's instructions. Slides were visualised under a fluorescent microscope and images were captured as previously described. The objective employed was an EC Plan-Neofluar 10x/0.3 (Carl Zeiss, Jena, Germany). For double staining, TUNEL was carried out before immunostaining as described in section 2.5.

## **2.7 Spermatocyte spreads**

All spreads were made from testes collected from adult 35-day-old mice. Briefly, testes were decapsulated, finely chopped and rinsed in 1 ml of GIBCO serum-free DME medium (Life Technologies, California, USA) containing 1X Complete Protease inhibitor (Roche, Basel, Switzerland). 6 ml of GIBCO serum-free DME medium (Life Technologies, California, USA) was then added and tubes were allowed to stand on ice for 5 min to allow large clumps and cellular debris to settle. 6 ml of the remaining supernatant from each sample was subsequently aliquoted into Eppendorf tubes, with each tube containing 1 ml of suspension. Tubes were then centrifuged for 5 min at 5000 xg to pellet the cell suspension. The pellet was then resuspended in 0.1 M sucrose and applied onto glass slides pre-wetted with 1% paraformaldehyde and 0.1% Triton X-100 in PBS. Cells were fixed on the glass slides and allowed to air-dry for 3 h at room temperature. The slides were subsequently washed with 1:250 Kodak Photo-Flo 200 (Kodak Professional, New York, USA) in 1X PBS and air-dried for 1 h. Once dried, spreads were stored at  $-80^{\circ}\text{C}$ .

## **2.8 Proximity ligation assay (PLA)**

Proximity Ligation Assay (PLA) (Duolink, Olink Bioscience, Uppsala, Sweden) was performed according to the manufacturer's protocol using the relevant primary antibodies (Table 2.4) and their corresponding PLA PLUS and MINUS probes. Identification of pachytene stage spermatocytes was determined by counterstaining with SCP3 antibody. Slide mounting and imaging was performed as described in section 2.5.

<b>Primary antibodies</b>	<b>Species</b>	<b>Dilution</b>	<b>Catalogue number</b>	<b>Manufacturer</b>
Brcal	Rabbit	1:300	-	With courtesy, David Livingstone (Dana Farber Cancer Institute, MA, USA)
Atr	Goat	1:100	SC-1887	Santa Cruz Biotechnology
Senataxin	Sheep	1:100	-	In-house
Chd4	Rabbit	1:100	AB72418	Abcam
SUMO-1	Rabbit	1:100	AB32058	Abcam

**Table 2.4: Description of primary antibodies used for PLA.**

## **2.9 RT-PCR & gene expression analyses**

Total RNA was isolated from 35-day-old *Setx*<sup>+/+</sup> and *Setx*<sup>-/-</sup> mice testes using the RNeasy mini kit (Qiagen, Limburg, Netherlands) according to the manufacturer's protocol. RNA concentrations were determined by UV spectrophotometry using a NanoDrop ND-1000 (Thermo Scientific, Massachusetts, USA). cDNA was made from 5 µg of purified RNA. Briefly, RNA was mixed with 1 µl of random hexamer primers (Bio-Rad Laboratories Inc. USA), 1 µl of 10 mM dNTP mix and DEPC-treated water (Life Technologies, California, USA) up to a 14 µl volume. The mixture was heat-denatured at 65°C for 5 min. 4 µl of First Strand buffer (Life Technologies, California, USA), 1 µl of 1 mM DTT, 1 µl of RNAaseIN (Promega, Wisconsin, USA), and 1 µl of SuperScriptIII Reverse Transcriptase enzyme (Life Technologies, California, USA) was added to the mixture, and incubated for 10 min at 25°C, then 60 min at 50°C, 15 min at 70°C, and chilled on ice. 1 µl of RNase H was subsequently added to each tube and incubated for 20 min at 37°C, followed by heat inactivation for 20 min at 65°C. The resulting cDNA were stored at -20°C prior to use.

Gene expression analysis was performed by PCR in a 2720 Thermal Cycler (Life Technologies, California, USA). 25 µl reactions contained 14.5 µl of sterile water, 50 ng of cDNA template, 1X PCR Buffer II (Roche, Basel, Switzerland), 2.5 mM MgCl<sub>2</sub> (Roche, Basel, Switzerland), 20 µM dNTPs, 1 µM of each primer, and 5 µl of AmpliTaq Gold DNA Polymerase (Roche, Basel, Switzerland) (Table 2.5). Amplification was for 30 cycles and cycling conditions were as follows: denaturation for 5 min at 95°C for 30 sec, annealing at 55°C for 30 sec, elongation for 1 min at 72°C followed by a final extension step of 7 min at 72°C.

PCR products were electrophoresed at 100V for 30 min on 2% TAE Agarose (Boehringer Mannheim, Lewes, UK) stained with ethidium bromide (Sigma Aldrich, Missouri, USA) and visualised with UV transillumination using a GelDoc<sup>TM</sup> XR (Biorad Laboratories Inc, California, USA).

<b>Regions</b>	<b>Primer name</b>	<b>Primer sequence</b>
<i>Ube1y</i>	Ube1yF	5'-ATTGACTTTGAGAAGGATGAC-3'
	Ube1yR	5'-CAGACACSCSSGGCCAACTAT-3'
<i>Ube1x</i>	Ube1xF	5'-GTGCATTCCCCTAAGCCCCA-3'
	Ube1xR	5'-GGGTAATTATCCTTTTATTGGGAT-3'
<i>Rbmy</i>	RbmyF	5'-AACCGAAGTAACATATACTCA-3'

	RbmyR	5'-ATCTGCTTTCTCCACGACCTC-3'
<i>Fthl17</i>	Fth17F	5'-TACTTTGACCGTGATGACGTG-3'
	Fth17R	5'-AGTTTTGCTCCAGGAAATGGC-3'
<i>Usp26</i>	Usp26F	5'-AATGTAACGAAGGGAGAAGTG-3'
	Usp26R	5'-AGGCTTTGCCTTCTTATCGAG-3'
<i>Tktl1</i>	Tktl1F	5'-TCAAAGGGACTACCATTTGTT-3'
	Tktl1R	5'-AACAGGGGGCGAAGTCATACA-3'
<i>Dazl</i>	DazlF	5'-TTCAGGCATATCCTCCTTATC-3'
	DazlR	5'-ATGCTTCGGTCCACAGACTTC-3'
<i>Setx</i>	SetxF	5'-CCGGGATTCATTATTAAGACCAGTGACCC-3'
	SetxR	5'-GATGGCCTCGAGCTATAGAAATTGTCTCCTC-3'
<i>β-actin</i>	ActbF	5'-GCGGACTGTTACTGAGCTGCGT-3'
	ActbR	5'-GAAGCAATGCTGTACCTTCCC-3'

**Table 2.5: Description of primers used for RT-PCR**

### **2.10 Immunoprecipitation of SUMOylated proteins from *Setx*<sup>+/+</sup> and *Setx*<sup>-/-</sup> testes**

Testes of 35 day-old mice (ground with a pestle to disrupt their structure) were lysed for 1 h at 4°C on a rotating wheel with 1 ml of lysis buffer [50 mM Tris-HCl pH 7.4, 150 mM NaCl, 2 mM EGTA, 2mM EDTA, 25 mM β-glycerophosphate, 0.1 mM Sodium Orthovanadate, 0.1 mM PMSF, 25 mM Sodium Fluoride, 0.2% Triton X-100, 0.3% NP-40 and 1 X EDTA-free Complete Protease inhibitor (Roche, Basel, Switzerland) 25 μM NEM (Sigma Aldrich, Missouri, USA)]. Cellular debris were pelleted by centrifugation at 16,100 x g at 4°C for 10 min, and protein concentration was determined using Lowry Assay (Bio-Rad Laboratories, Inc, California, USA). 3 mg of total cell extract were pre-cleared with 20 μl of Protein A beads (50:50 slurry) (Merck Millipore, Massachusetts, USA) for 3 h at 4°C on a rotating wheel. Extracts were centrifuged for 5 min at 2000 x g, beads were removed, and 10 μg of anti-SUMO antibody (Abcam, Cambridge, UK) was added to the extract. Extracts and antibody were incubated overnight at 4°C on a rotating wheel to allow binding of the antibody to SUMOylated protein. The next day, 40 μl of Protein A beads (50:50 slurry) (Merck Millipore, Massachusetts, USA) was added to the extract and incubated for 2 h at 4°C on a rotating wheel. Extracts were centrifuged for 5 min at 2000 x g and the beads were removed. The immunoprecipitate was subsequently washed 3 times with lysis buffer and the beads were resuspended in SDS loading buffer containing 2X DTT and separated via 4-12% SDS-PAGE

using Novex Tris-Glycine gels (Life Technologies, California, USA) at 110V for 1.5 h. Once separated, gel was stained with G-250 Colloidal Coomassie (Life Technologies, California, USA) overnight. Gel was subsequently de-stained using Milli-Q water.

### **2.11 Tryptic digestion of SUMOylated proteins from mice spermatocytes for Mass Spectrometry**

Bands were excised from gel using a sterile scalpel and were left to de-stain (50% acetonitrile, 50% ammonium bicarbonate) for 4 hours. Trypsin (Promega, Wisconsin, USA) was added 1:20 by weight in 50 mM ammonium bicarbonate until gel pieces were covered and left to digest overnight. Subsequently, 100% acetonitrile was added and tube was vortexed for 10 min. Liquid in the tube was then transferred into a fresh Eppendorf tube. 50% acetonitrile was added to the gel pieces and vortexed again for 10 min. Liquid was combined with the liquid collected in the previous step. Tubes were spun in a Speedy-Vac for 30 min to dry liquid to approximately 5  $\mu$ l. This volume was reconstituted to 20  $\mu$ l 0.1% TFA and applied to a C18 STAGE tip (Thermo Scientific, Massachusetts, USA) by pipetting up and down for approximately 10 times. Tips were then washed with 10  $\mu$ l of 0.1% TFA and peptides were eluted with 50% acetonitrile into a fresh Eppendorf tube. Eluant was frozen at -20°C and shipped to Dr. Mark Graham (Children's Medical Research Institute, University of Sydney, Australia) for Liquid Chromatography Mass Spectrometry analyses.

### **2.12 Immunoblotting for DDR proteins from *Setx*<sup>+/+</sup> and *Setx*<sup>-/-</sup> testes**

Testes of 35 day-old mice (ground with a pestle to disrupt their structure) were lysed for 1 h at 4°C on a rotating wheel with 1 ml of lysis buffer [50 mM Tris-HCl pH 7.4, 150 mM NaCl, 2 mM EGTA, 2mM EDTA, 25 mM  $\beta$ -glycerophosphate, 0.1 mM Sodium Orthovanadate, 0.1 mM PMSF, 25 mM Sodium Fluoride, 0.2% Triton X-100, 0.3% NP-40 and 1 X EDTA-free Complete Protease inhibitor (Roche, Basel, Switzerland)]. Cellular debris was pelleted by centrifugation at 16,100 x g at 4°C for 10 min, and protein concentration was determined using Lowry Assay (Bio-Rad Laboratories, Inc, California, USA). 30  $\mu$ g of total cell extract were resuspended in SDS loading buffer containing 2X DTT and separated via 4-12% SDS-PAGE using Novex Tris-Glycine gels (Life Technologies, California, USA) at 110V for 1.5 h. The proteins were then transferred onto a Hybond-C nitrocellulose membrane (Pall Life Sciences, NY, USA) using a high molecular weight transfer buffer (100mM Tris, 40mM Glycine, 0.05% SDS, 20% Methanol) at 100V for 1 h at 4°C in a mini-protean gel rig (Biorad, CA, USA). The membrane was the blocked in 5% skim milk in TBS/Tween 20 or 5% BSA/TBS/Tween 20 and immunoblotting was performed with various

antibodies (Table 2.6). Membranes were incubated with primary antibody in 5% skim milk/TBS/Tween 20 or 5% BSA/TBS/Tween 20 overnight at 4°C and washed thrice the following day with TBS/Tween 20 for 5 min each. Secondary antibody conjugated with horseradish peroxidase (HRP) (Table 2.7) in 5% skim milk/TBS/Tween 20 or 5% BSA/TBS/Tween 20 was then applied to the membrane for 1 h at room temperature. Membranes were then analysed using the Western Lightning Plus Enhanced Chemiluminescence (ECL) reagent (Perkin Elmer, MA, USA).

Primary antibody	Species	Dilution	Catalogue number	Manufacturer
Atr	Goat	1:1000	SC-1887	Santa Cruz Biotechnology
Nek1	Rabbit	1:1000	BS-7814R	Bioss Inc.
Atrip	Rabbit	1:1000	A300-670	Bethyl Laboratories Inc.
Chk1	Mouse	1:1000	2360	Cell Signaling Technology
Chd4	Rabbit	1:1000	AB72418	Abcam
Rad51	Rabbit	1:1000	SC-6862	Santa Cruz Biotechnology
Mlh1	Mouse	1:500	SC-56161	Santa Cruz Biotechnology
Setx	Sheep	1:500	-	In-house
TopBp1	Rabbit	1:1000	AB2402	Abcam
SUMO-1	Rabbit	1:1000	AB32058	Abcam
Phospho-Atr (S428)	Rabbit	1:1000	2853	Cell Signaling Technology
Phospho-Chk1 (S317)	Rabbit	1:1000	2344	Cell Signaling Technology
Gapdh	Rabbit	1:2000	GTX100118	Genetex
$\alpha$ -tubulin	Rabbit	1:2000	GTX112141	Genetex

**Table 2.6: Description of primary antibodies used for immunoblotting**

Secondary antibodies	Dilution	Catalogue number	Manufacturer
HRP-conjugated donkey anti-sheep	1:5000	AP184P	Merk Millipore
HRP-conjugated donkey anti-mouse	1:5000	AP192P	Merk Millipore
HRP-conjugated donkey anti-rabbit	1:5000	AP182P	Merk Millipore

**Table 2.7: Description of secondary antibodies used for immunoblotting.**

### **2.13 Transfection of HeLa and U2OS cells with Stealth™ siRNA**

HeLa and U2OS cells were transfected with Stealth™ siRNA negative control LO GC (#12935200) (Life Technologies, California, USA) and Stealth™ siRNA specific for the knockdown of *SETX* (CCAUCUAACUCUGUACAACUUGCUU, Life Technologies, California, USA). Lipofectamine™ 2000 (Life Technologies, California, USA) was used for the transfections. Briefly, 2.5-10x10<sup>5</sup> cells were seeded in a 6-well plate and upon transfection, cells were washed with 2X OPTIMEM® I Reduced Serum Medium (Life Technologies, California, USA). For transfection with Stealth™ siRNA negative control, 5 µl of a 20 µM stock of oligoribonucleotide was diluted in 250 µl of OPTIMEM® I Reduced Serum Medium and for the transfection Stealth™ siRNA *SETX*, 5 µl of a 20 µM stock of oligoribonucleotide was diluted in 250 µl of OPTIMEM® I Reduced Serum Medium. For each transfection, 10 µl of Lipofectamine™ 2000 was diluted in 250 µl of OPTIMEM® I Reduced Serum Medium and the mixture was incubated at room temperature for 5 min. Subsequently, the diluted oligoribonucleotides (either control or *SETX* RNAi) were combined with the diluted Lipofectamine™ 2000 (total volume 500 µl) and incubated at room temperature for 20 min. The oligoribonucleotide- Lipofectamine™ 2000 complexes were added to the corresponding well of a 6-well plate to be transfected with the siRNA. The plate was then centrifuged at 500 x g for 5 min at room temperature, and cells were incubated in a humidified incubator at 37°C/5% CO<sub>2</sub>. 8 h later, 2 ml of DME medium containing 10% FCS (Gibco BRL, Life Technologies, California, USA) was added to each well and the cells were incubated in a humidified incubator at 37°C/5% CO<sub>2</sub> for 24 h.

To determine the knockdown efficiency of *SETX* with siRNA, 24 h post-transfection with control and *SETX* siRNA, total cell extracts were made and immunoblotted as described in section 2.12. Immunostaining using anti-senataxin (Ab-1) antibody was also performed as described in section 2.5.

### **2.14 Treatment of HeLa and U2OS cells with Camptothecin and Actinomycin D**

U2OS cells transfected with control (Ctrl siRNA) and *SETX* siRNAs were first treated with 5µg/ml of Actinomycin D (Sigma Aldrich, Missouri, USA) and incubated in a humidified incubator at 37°C/5% CO<sub>2</sub> for 2 h. After the 2 h incubation, 25 µM of camptothecin (Sigma Aldrich, Missouri, USA) was added to the cells and incubated in a humidified incubator at 37°C/5% CO<sub>2</sub> for another 2 h. Subsequently, cells were fixed with 4% PFA in 1 X PBS, immunostained with R-loop antibody



(S9.6, gift from Dr. Stephen Leppla, USA) and imaged using a 63X Plan Achromat 1.4 oil differential interference contrast objective (Carl Zeiss, Jena, Germany).

## **2.15 DNA:RNA immunoprecipitation assay (DRIP)**

Genomic DNA and RNA extraction from *Setx*<sup>+/+</sup> and *Setx*<sup>-/-</sup> mice testes, LCLs and HeLa cells were performed using the DNeasy Blood & Tissue Kit (Qiagen, Limburg, Netherlands) following the manufacturers' instructions. Protein extracts were sonicated (maximum voltage, constant output, microtip limit) for 3 min with 1 min incubation on ice within each min. 40 µl of Protein G beads (50:50 slurry) (Merck Millipore, Massachusetts, USA) was added to the extracts and pre-cleared. In a separate tube, 15 µg of anti-R-loop antibody (S9.6) and 40 µl of Protein G beads (50:50 slurry) (Merck Millipore, Massachusetts, USA) were added together and incubated at 4°C overnight on a rotating wheel to allow binding of antibody to beads. Anti-c-Abl antibody (Cell Signaling Technology, Massachusetts, USA) and 40 µl of Protein G beads (50:50 slurry) (Merck Millipore, Massachusetts, USA) were also added together to serve as a non-specific (species-specific) control for our experiment. The next day, the tubes were centrifuged at 5400 x g for 2 min to pellet the beads. The supernatant was then divided equally into 3 tubes- 1 was left untreated, 1 was treated with 200 U of S1 Nuclease (Promega, Wisconsin, USA) and the other was treated with 10 U of RNase H (New England BioLabs, Massachusetts, USA). Extracts were incubated at 37°C for 2 h, heat inactivated for 20 min at 65°C then added on to the antibody-bound Protein G beads and incubated at 4°C overnight on a rotating wheel to allow binding of R-loops fragments to antibody-bound beads. The next day, the beads were pelleted at 5400 x g for 2 min and the supernatant was discarded. The beads were washed once with the IP Wash Buffer 1 (20 mM Tris-HCl pH 8.1, 2 mM EDTA, 50 mM NaCl, 1% Triton X-100, 0.1% SDS), twice with the High Salt Wash Buffer (20 mM Tris-HCl pH 8.1, 2 mM EDTA, 500 mM NaCl, 1% Triton X-100, 0.1% SDS), once with the IP Wash Buffer 2 (10 mM Tris-HCl pH 8.1, 1 mM EDTA, 0.25 M LiCl, 1% NP-40, 1% Deoxycholic Acid) and twice with TE Buffer (20 mM Tris-HCl pH 8.0, 1mM EDTA). The immunoprecipitates were incubated at 4°C on a rocker for 3 min between each wash. The nucleic acids were then eluted twice with 100 µl of Elution Buffer (100 mM NaHCO<sub>3</sub>, 1% SDS). 3 µl of Proteinase K (20 mg/ml) was then added to each sample and incubated at 55°C. The samples were then diluted to 400 µl with TE Buffer and 3 µl of Glycogen (20 mg/ml) (Roche, Basel, Switzerland) was added. The nucleic acids were extracted using 400 µl of phenol-chloroform (1:1) (Life Technologies, California, USA) and vortexed for 1 min. The samples were centrifuged at 16,000 x g for 5 min and the aqueous phase containing the nucleic acids were retained. These were extracted again using 400 µl of chloroform (Life Technologies, California, USA) under the same conditions. 2.5X of 100% EtOH

was added to the samples and these were incubated at -80°C for 20 min. The samples were centrifuged at 16, 000 x g for 20 min and the supernatant was decanted. The pellet was washed with 70% EtOH, centrifuged at 16, 000 x g for 20 min and the supernatant was decanted. The pellet was air-dried and resuspended in EB Buffer (Qiagen, Limburg, Netherlands).

## **2.16 PCR analyses for DRIP assay**

Primers for the RLFS region in mouse *Ube1y1* gene were Ube1y1F and Ube1y1R. PCR cycling conditions were as follows: 35 cycles, initial denaturation at 95°C for 3 min, denaturation at 95°C for 45 sec, annealing at 58 °C for 45 sec, extension at 72°C for 1 min, with a final cycle and extension of 7 min at 72°C. The PCR product size for the RLFS region in *Ube1y1* was 183 bp. Primers for the RLFS region in mouse *Tktl1* gene were Tktl1F and Tktl1R. PCR cycling conditions were as follows: 35 cycles, initial denaturation at 95°C for 3 min, denaturation at 95°C for 45 sec, annealing at 55 °C for 45 sec, extension at 72°C for 1 min, with a final cycle and extension of 7 min at 72°C. The PCR product size for the RLFS region in *Tktl1* was 179 bp. See table 2.8 for description of primers used for DRIP assay.

PCR products were electrophoresed at 100V for 30 min on 2% TAE Agarose (Boehringer Mannheim, Amresco, Lewes, UK) stained with Ethidium bromide and visualised with UV transillumination using a GelDoc™ XR (Biorad Laboratories Inc, California, USA).

<b>Regions</b>	<b>Primer name</b>	<b>Primer sequence</b>
<i>Ube1y1</i>	Ube1y1F	5'-CACAGAAGTTCAGGGCATGA-3'
	Ube1y1R	5'-GCCCAGTCTGCTGTGAAAAGT-3'
<i>Tktl1</i>	Tktl1F	5'-CATAAGCCTCCATAAGCAAGC-3'
	Tktl1R	5'-CTGCTTGCCTCAGCTTCC-3'
<i>Wwox</i>	Wwox1F	5'-GACCGAGGGTGGAGCTGTAG-3'
	Wwox1R	5'-AGCCAAGTGTTACATGGAGTTAGT-3'
<i>HS44.2</i>	mHS44.2 1F	5' AGCGGGTTTACGGAATGCTT-3'
	mHS44.2 1R	5'-AGTCTTCAGAGAGGAGATTAGAGGA-3'
<i>Foxo4</i>	mFoxo4 F	5'-GGTTTCTGGTTTCTGCTGCC-3'
	mFoxo4 R	5'-AGGGCTGGAGTGAACACTTG-3'

**Table 2.8 Description of primers used for DRIP assay.**

## **CHAPTER 3 Characterization of the *Setx*<sup>-/-</sup> Mouse**

### **3.1 Introduction**

Ataxia oculomotor apraxia type 2 (AOA2) belongs to a wide class of autosomal recessive cerebellar ataxias (ARCA), and is a neurological disorder characterized by the onset of progressive cerebellar degeneration and oculomotor apraxia during adolescence<sup>49,69</sup>. AOA2 patients also display axonal sensorimotor neuropathy and elevated alpha-fetoprotein serum levels<sup>184</sup>.

The protein mutated in AOA2 is senataxin (SETX), which is encoded on chromosome 9q34<sup>61</sup>. Senataxin is approximately 300kDa in size and contains a classical seven-motif domain belonging to the superfamily I of helicases<sup>61</sup>. These helicases are motor proteins involved in the unwinding of DNA or RNA strands and play central roles in nucleic acid metabolic activities such as DNA replication, recombination and repair, as well as transcription and mRNA splicing<sup>185</sup>. It has previously been reported that cells lacking senataxin showed higher levels of oxidative damage, increased chromosomal instability following treatment with DNA damaging agents such as H<sub>2</sub>O<sub>2</sub>, camptothecin and mitomycin C, as well as impaired DNA repair<sup>63</sup>. Senataxin deficient cells were also reported to show defects in transcription termination, splicing efficiency and splice site selection<sup>71</sup>.

To further investigate the role of senataxin *in vivo*, our lab generated the first *Setx*<sup>-/-</sup> mouse model. This was achieved by using a highly-efficient recombineering-based method<sup>186</sup> and deleting exon 4 of the *Setx* gene. This creates an unstable transcript that is quickly degraded.

Briefly, a *loxP-F3-PGK-EM7-Neo-F3 (Neo)* selection cassette was inserted into a bacterial artificial chromosome (BAC) clone (RP23-389D11, Children's Hospital Oakland Research Institute) corresponding to mouse chromosome 2 and covering the mouse *Setx* genomic sequence. The *Neo* cassette, which provides positive selection in embryonic stem cells (ESC), was flanked by a 5'-homology arm of 6.8 kb and a 3'-homology arm of 3 kb. ESCs were then transfected with the linearized targeting vector and selected with 150 µg/ml of G418. Successful recombinant ESC clones were determined by Southern Blotting with a specific probe as well as with PCR genotyping. Targeted cells (+*Neo*) were subsequently microinjected into C57BL6/129Sv mouse blastocysts, generating chimeras. Excision of the Neo cassette was obtained by crossing the chimeras with a *Cre* deleter strain, generating *Setx*<sup>-/-</sup> mice containing only a single *LoxP* site (Fig 3.1).

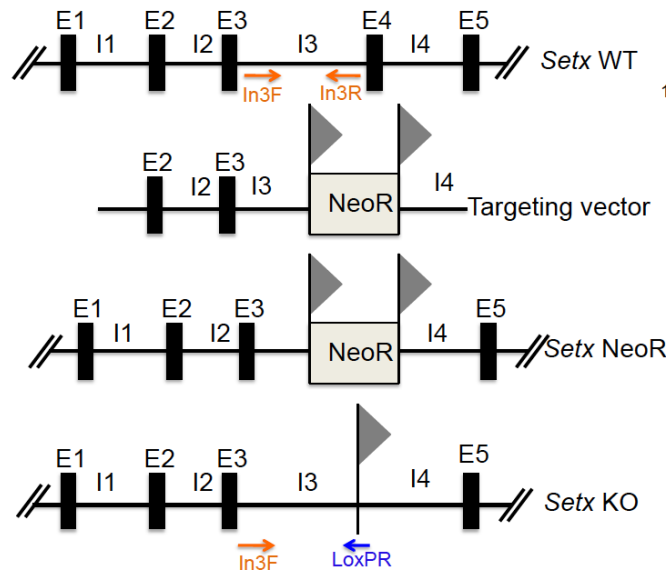


**Fig 3.1: Targeted disruption of mouse *Setx* gene.** Diagram of the *Setx* wild type allele (WT), targeting vector, and mutant alleles (*neo*<sup>+</sup> and KO). Primers used for PCR genotyping (In3F, In3R, LoxPR). E, exon; I, intron. *NeoR* represents the neomycin cassette, and triangles represent the *LoxP* sites.

While no neurological defects were observed in *Setx*<sup>-/-</sup> mice, multiple attempts to breed male *Setx*<sup>-/-</sup> mice with each other or with *Setx*<sup>+/+</sup> mice were unsuccessful. Male *Setx*<sup>-/-</sup> mice had normal development of secondary sexual characteristics and were capable of the mechanics of mating, but were completely sterile. This Chapter describes the essential role of senataxin in DNA repair and meiotic recombination in spermatogenesis.

## **3.2 Results**

### *3.2.1 Generation of $Setx^{-/-}$ mice*

To show the disruption of the *Setx* gene in our mouse model, an immunoprecipitation (IP) using an antibody against senataxin from total cell extracts made from  $Setx^{+/+}$  and  $Setx^{-/-}$  mouse testes was performed (Fig 3.2A). As a positive control for the IP, human lymphoblastoid cell (hLCLs) protein extracts from a normal subject (C3ABR) and an AOA2 patient (SETX2RM) were used to confirm a similar-sized protein. Indeed, the mouse senataxin protein is only 31 amino acids shorter (2646 aa) compared to human senataxin protein (2677 aa), therefore a difference in protein migration by SDS-PAGE electrophoresis is not detectable. As expected, senataxin was immunoprecipitated from WT mouse testes and normal hLCLs. In contrast, senataxin was not detected in the  $Setx^{-/-}$  mouse extracts. A strong signal was observed in C3ABR as compared to that observed in  $Setx^{+/+}$  mouse testes extracts, indicating a greater sensitivity for the human protein due to the fact that the anti-senataxin antibody was raised against human senataxin. A weak signal was observed in SETX2M cell extracts, indicating that the mutant senataxin protein is expressed at very low levels in the AOA2 patient. As expected, senataxin was not detected in the  $Setx^{-/-}$  mouse testes extracts, confirming the disruption of the *Setx* gene and the lack of senataxin protein production. Additionally, the non-specific (NS) sheep IgG used as a negative control did not pull down senataxin from  $Setx^{+/+}$  mouse testes extracts.

As expected, crosses between *Setx* heterozygotes produced all 3 genotypes (wild type, heterozygotes and homozygote knockouts) (Fig 3.2B) and a Mendelian inheritance pattern was observed (wild type 25%; heterozygote 54%; knockout 21%; n = 87). Primers used for genotyping were In3F, In3R and LoxPR (Table 2.1). Disruption of the *Setx* gene was also confirmed by Reverse-Transcriptase Polymerase Chain Reaction (RT-PCR) where the expression of *Setx* mRNA was observed only in  $Setx^{+/+}$  mice (Fig 3.2C).

It was observed that  $Setx^{-/-}$  mice were of normal body sizes and weights with comparable life spans to those of their wild type and heterozygote littermates.

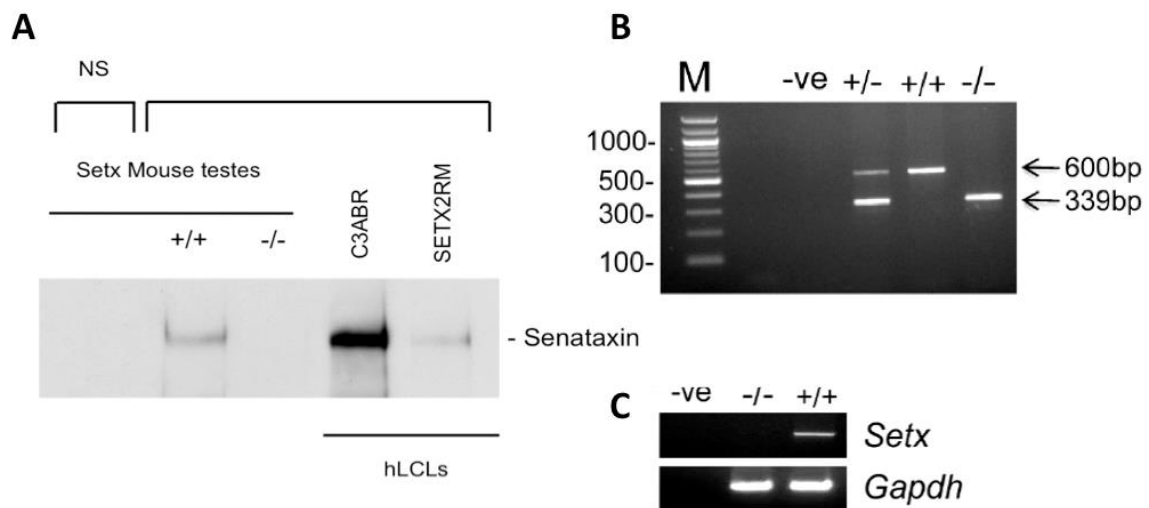


**Fig 3.2: Disruption of the *Setx* gene in *Setx*<sup>-/-</sup> mice.** **A.** Senataxin immunoprecipitation (IP) from total cell extracts from *Setx*<sup>+/+</sup> and *Setx*<sup>-/-</sup> mouse testes. Extracts from human lymphoblastoid cells (hLCLs) from a normal subject (C3ABR) and an AOA2 patient (SETX2RM) were used as positive controls during the immunoprecipitation and to confirm a similar sized protein for the mouse and the human senataxin. A species-matched, sheep non-specific IgG (NS) was used as a negative control. **B.** Representative image of *Setx* PCR genotyping using In3F, In3R and LoxPR primers. Wild type (+/+), heterozygotes (+/-) and knockout (-/-) alleles generate PCR products of 600 bp, 600 bp and 339 bp, and 339 bp, respectively. A negative control (-ve, no template) for the PCR reaction is also shown. M, 100 bp marker. **C.** RT-PCR of total RNA extracted from 35 day-old *Setx*<sup>+/+</sup> and *Setx*<sup>-/-</sup> mouse testes using primers specific to *Setx* cDNA indicated the absence of *Setx* expression in *Setx*<sup>-/-</sup> testes. *Gapdh* was used as an internal standard for loading control.

### 3.2.2 Absence of neurological phenotype in *Setx*<sup>-/-</sup> mice

Because AOA2 is characterized by ataxia, behavioral analyses on these mice using a phenotypic scoring system that is commonly used to evaluate mouse models of neurodegeneration was performed<sup>187</sup>. This system has been used previously to assess several models of neurological disorders such as spinocerebellar ataxias, Huntington's disease and spinobulbar muscular atrophy<sup>188,189</sup>.

These analyses include the ledge test, observation of hindlimb claspings, overall gait and kyphosis. Briefly, the ledge test is a direct measure of balance and coordination, and is the most comparable test to human symptoms of cerebellar degeneration. This test involves placing a mouse on the ledge of their cage, and their overall balance while crossing the ledge and their descent back into their

cage is observed. A normal mouse does not lose balance and would descend into their cage landing first on their front paws without difficulty. The hindlimb clasp test is an indicator of the progression of cerebellar degeneration. A mouse is picked up by the base of its tail and held up in the air for approximately 10 seconds. During this time, a normal mouse would have its hindlimbs fully splayed outwards and not withdrawn towards its abdomen. The gait test looks at muscle function and coordination. A mouse is placed on a flat surface facing away from the investigator, and its walking pattern is observed. A normal mouse should have its weight evenly distributed on all 4 paws without its abdomen dragging on the surface. Lastly, kyphosis of the mouse is observed. This test looks at the curvature of the dorsal spine of a mouse due to loss of muscle tone. To do this, a mouse is placed on a flat surface and its ability to straighten out its spine easily is observed<sup>187</sup>. These tests were repeated thrice and a score of between 0 to 3 is assigned to each mouse, with 0 being the score for mice without the relevant ataxic phenotype and 3 being the score for mice displaying the most severe manifestation of the phenotype<sup>187</sup>. The average cumulative scores of these tests for mice aged between 3 and 17 months was tabulated and no behavioral differences was observed between *Setx*<sup>+/+</sup> and *Setx*<sup>-/-</sup> mice (Fig 3.3).

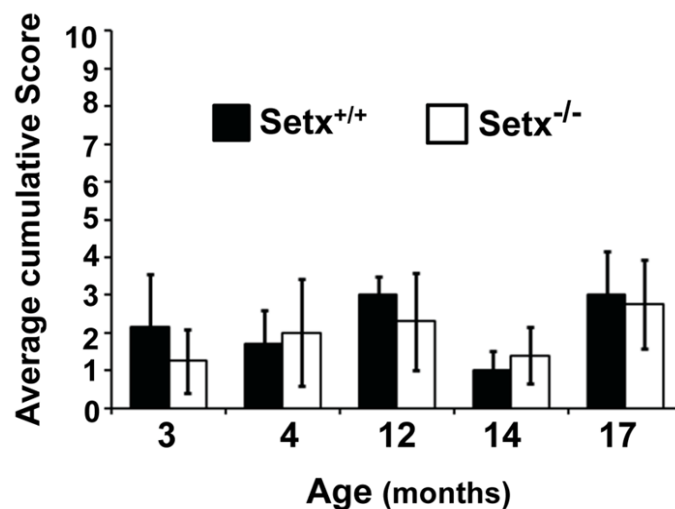


**Fig 3.3: Absence of neurological phenotype and ataxia in *Setx*<sup>-/-</sup> mice.** Behaviour analyses include ledge test, hindlimb clasp test, gait and kyphosis. Each mouse was scored between 0 and 3, with 0 representing the absence of the relevant phenotype and 3 being most severe manifestation of the phenotype. The average cumulative score for *Setx*<sup>+/+</sup> and *Setx*<sup>-/-</sup> mice at the various age was calculated. Neither abnormal behaviour nor ataxic phenotype progression was observed in *Setx*<sup>-/-</sup> mice. Number of animals (n ≥ 3).



Given the lack of abnormal motor behavior in *Setx*<sup>-/-</sup> mice, the overall morphological structure of the brain and cerebellum of both *Setx*<sup>+/+</sup> and *Setx*<sup>-/-</sup> mice was determined to assess for the presence of a subtle neurological phenotype. As shown in Fig 3.4, no gross cellular and structural differences between the mice were observed.

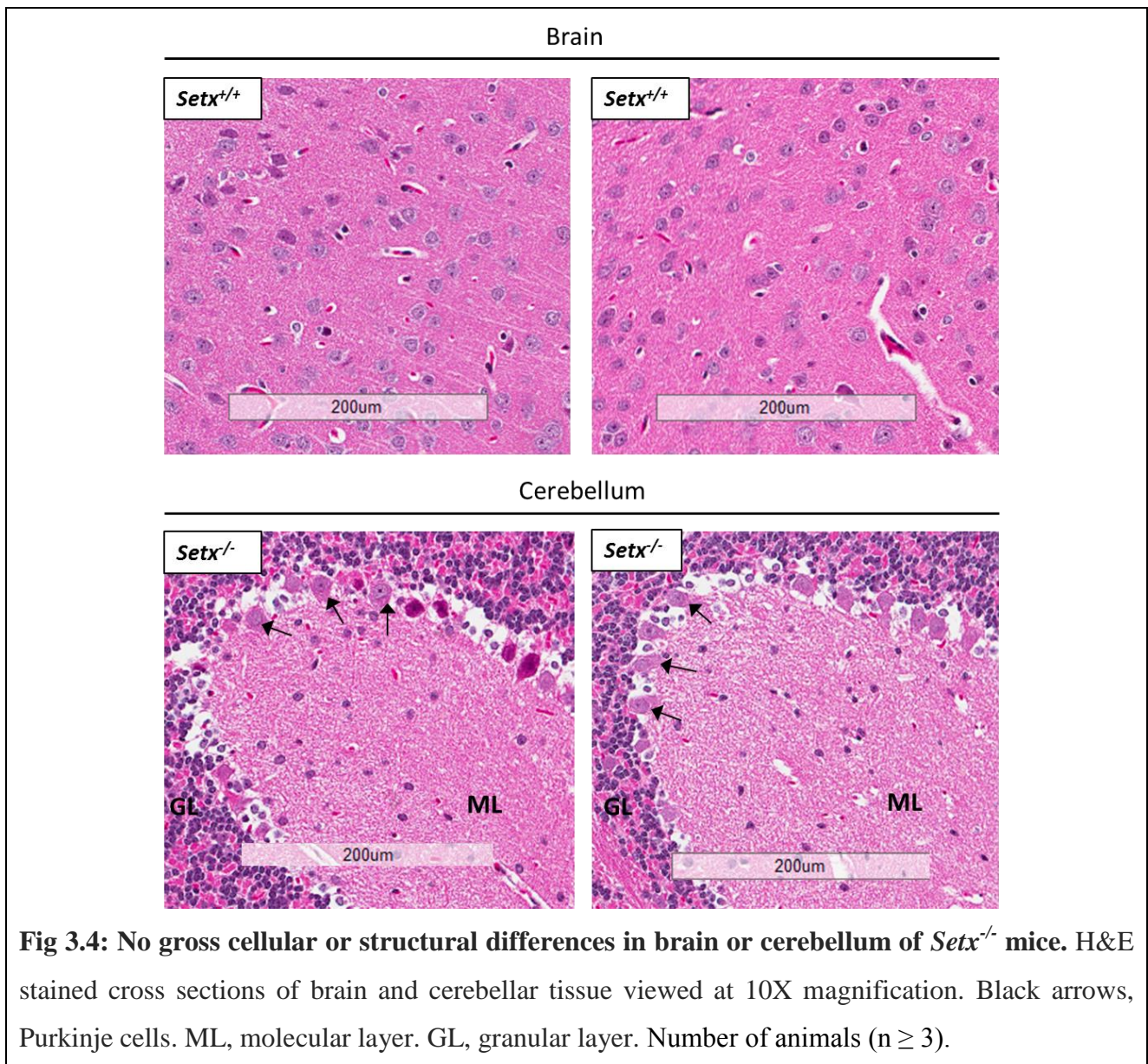
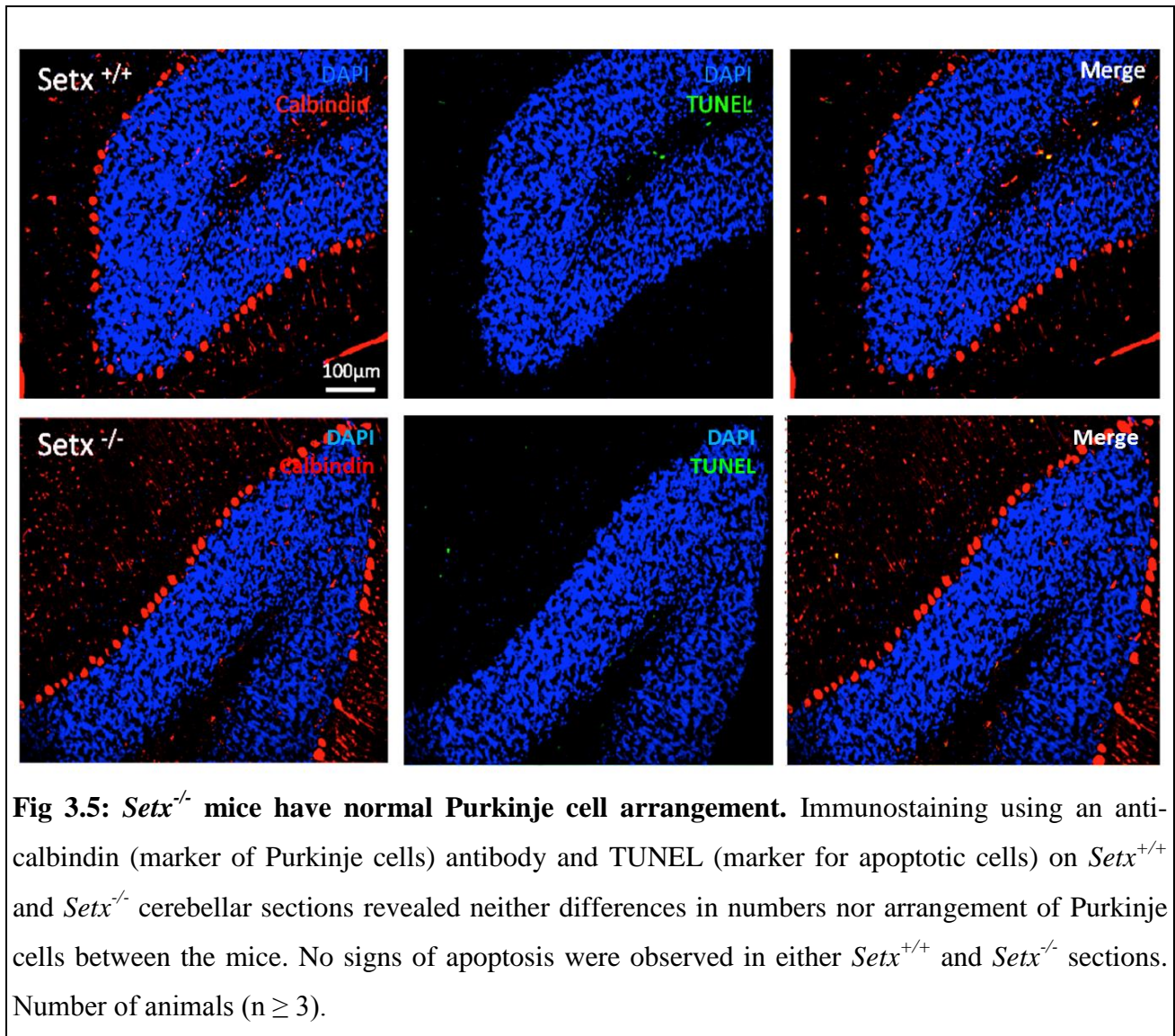


**Fig 3.4: No gross cellular or structural differences in brain or cerebellum of *Setx*<sup>-/-</sup> mice.** H&E stained cross sections of brain and cerebellar tissue viewed at 10X magnification. Black arrows, Purkinje cells. ML, molecular layer. GL, granular layer. Number of animals (n ≥ 3).

As aforementioned, progressive cerebellar degeneration is characteristic of patients suffering from AOA2 due to the loss of Purkinje cells, which are neurons in the cerebellum that control motor movement<sup>61,69</sup>. To observe whether this phenomenon was occurring in our *Setx*<sup>-/-</sup> mice, an immunofluorescence assay was performed using an antibody against calbindin, a marker for Purkinje cells, on cerebellar tissue sections taken from *Setx*<sup>+/+</sup> and *Setx*<sup>-/-</sup> mice. TUNEL staining, a marker for apoptotic cells was performed simultaneously. However, no structural alterations,

general cerebellar degeneration, nor the specific loss of Purkinje cells in *Setx*<sup>-/-</sup> mouse cerebella was detected (Fig 3.5).

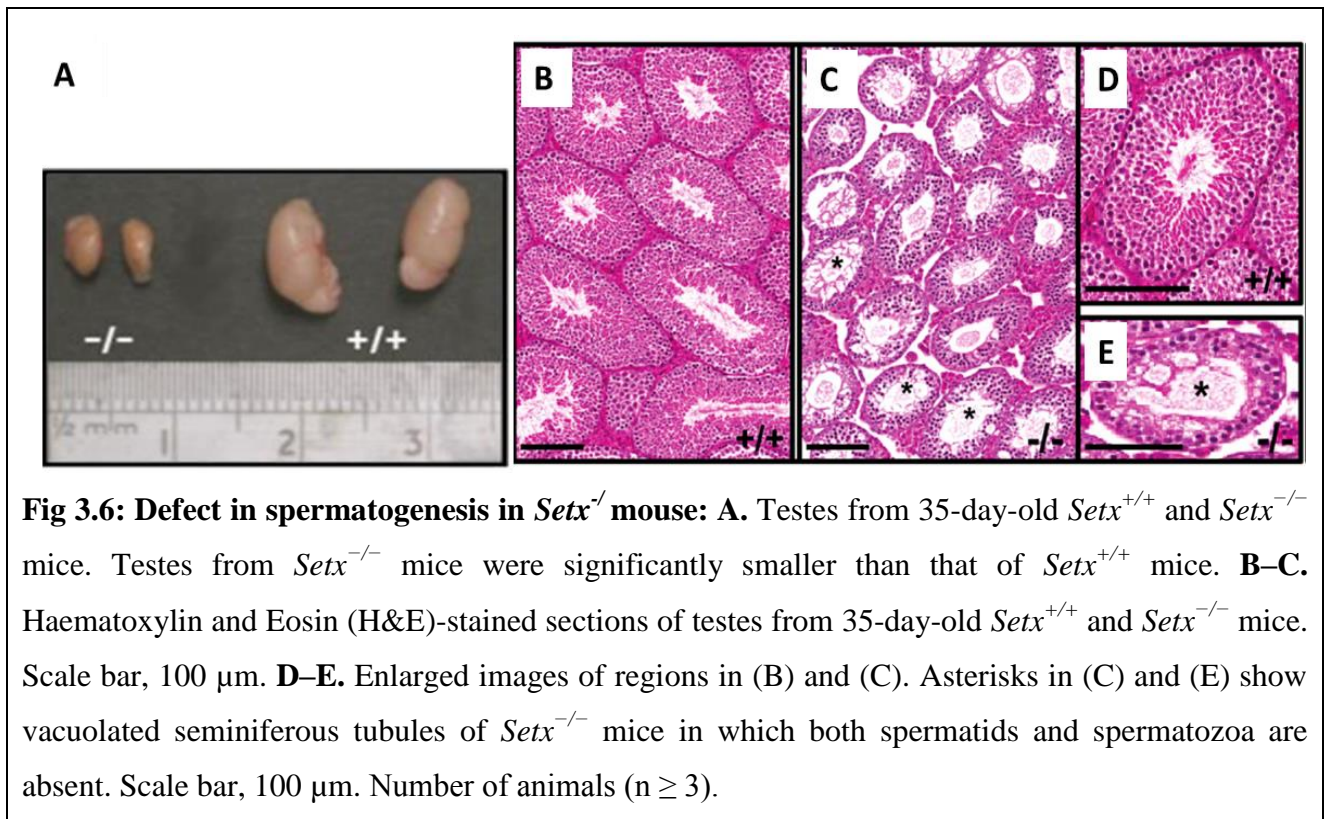


Both behavioral studies and molecular analysis of brain and cerebellum structure and architecture provided evidence for an absence of neurological phenotype in *Setx*<sup>-/-</sup> mice.

### 3.2.4 *Senataxin is essential for male germ cell development and fertility*

Common findings in ARCA patients as well as in their corresponding mouse models are oligospermia and testicular abnormalities<sup>20</sup>. Therefore, whether these phenomena also occur in the *Setx*<sup>-/-</sup> mice was investigated. Multiple attempts to breed male *Setx*<sup>-/-</sup> mice with female *Setx*<sup>+/+</sup> or *Setx*<sup>-/-</sup> mice were unsuccessful. *Setx*<sup>-/-</sup> male mice exhibited normal development of secondary

sexual characteristics and were capable of the mechanics of mating, but were infertile. The development of the testes and seminiferous tubules from *Setx*<sup>-/-</sup> mice with those from *Setx*<sup>+/+</sup> mice was subsequently compared. It was observed that testes from *Setx*<sup>-/-</sup> mice were smaller in size (50–60% reduction) than their *Setx*<sup>+/+</sup> littermates (Fig 3.6A). Histological examination of testes sections from 35 day-old adult *Setx*<sup>-/-</sup> males also revealed a severe disruption of the seminiferous tubules and the absence of mature germ cells as compared to *Setx*<sup>+/+</sup> males (Fig 3.6B-E).



In contrast to male *Setx*<sup>-/-</sup> mice, female *Setx*<sup>-/-</sup> mice were fertile. Histological examination of ovarian sections from female *Setx*<sup>-/-</sup> mice did not exhibit any gross morphological differences from their *Setx*<sup>+/+</sup> littermates. Normal ovarian structure, presence of follicles at various stages and the ability to ovulate was observed (Fig 3.7). However, a closer inspection of this revealed the sub-fertility of female *Setx*<sup>-/-</sup> mice. Superovulation and timed-mating to harvest embryos at the fertilized, one-cell stage [0.5 days post coital (dpc)] was carried out. It was observed that the yield of these viable embryos was very low. A > 3.5-fold reduction in the yield of 0.5 dpc embryos from female *Setx*<sup>-/-</sup> mice (10–20 embryos) was detected as compared to *Setx*<sup>+/+</sup> mice (50–70 embryos). Furthermore, only approximately 23% of these viable embryos from *Setx*<sup>-/-</sup> mice survived in culture, indicating that *Setx*<sup>-/-</sup> females have a reduced fertility. These data are in line with previous reports on female AOA2 patients presenting with fertility issues such as premature ovarian failure<sup>66,190</sup>.

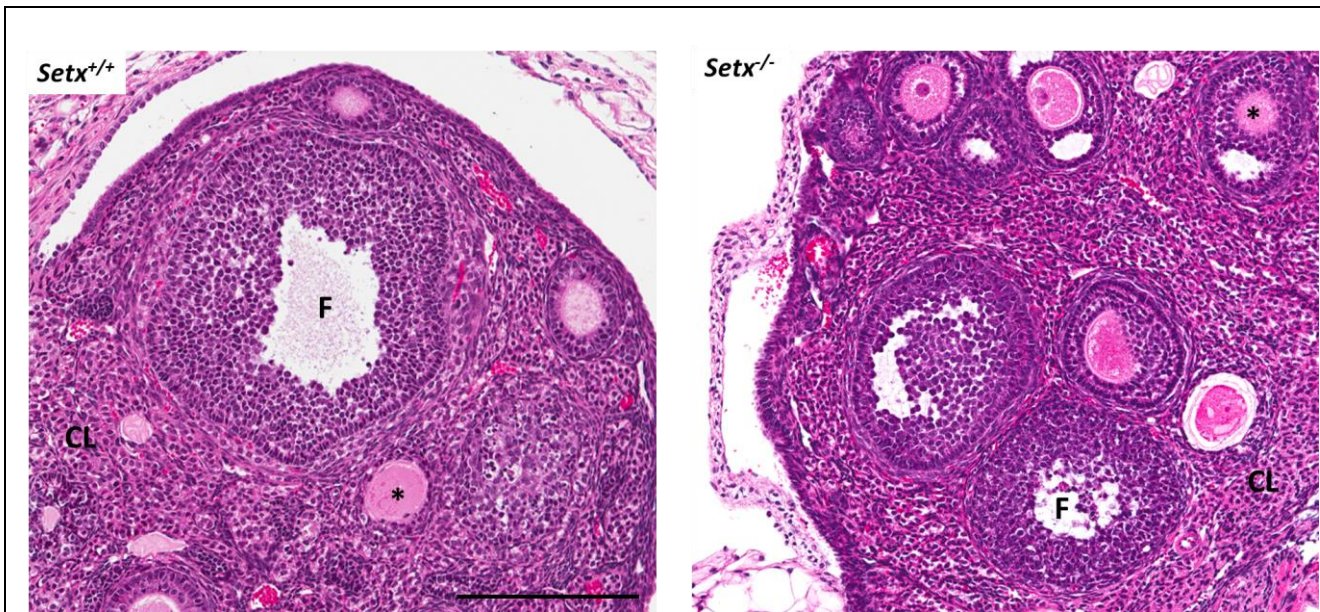


**Fig 3.7: Normal ovarian structure in *Setx*<sup>-/-</sup> mice:** A. Haematoxylin and Eosin (H&E)-stained sections ovarian tissue sections from adult, 35-day-old female *Setx*<sup>+/+</sup> and *Setx*<sup>-/-</sup> mice. Pre-antral and antral follicles (F) are present in all sections and many follicles contain oocytes (asterisks). All sections also contain corpora lutea (CL), suggesting ovulation has occurred. Scale bar, 200  $\mu$ m. Number of animals (n  $\geq$  3).

In this report, focus will be on the infertility phenotype observed in male *Setx*<sup>-/-</sup> mice, which is the most apparent phenotype observed in these mice.

Spermatogonia, or primordial germ cells, undergo 4 stages during meiotic prophase I of spermatogenesis, namely leptotene, zygotene, pachytene and diplotene, before entering spermiogenesis to form mature spermatids. These various stages can be visualized by staining for synaptonemal complex protein 3 (SCP3), a protein member of the axial element on chromatin essential for the synapsis of homologous chromosomes required for recombination (Fig 3.8A)<sup>112</sup>. Briefly, during the leptotene and zygotene stages, sister chromatids start to come together and condense into visible threads within the nucleus. In the pachytene stage, sister chromosomes are fully synapsed and the exchange of genetic material through homologous recombination (HR) occurs. Finally, in the diplotene stage, HR is completed, the synaptonemal complex degrades and sister chromatids begin to separate from one another, leaving only the sites of crossing over visible<sup>113</sup>.

Immunostaining using an antibody against SCP3 revealed that *Setx*<sup>-/-</sup> mice did not carry diplotene-staged spermatocytes (Fig 3.8B). *Setx*<sup>-/-</sup> mice displayed a significant decrease in the percentage of

leptotene- and zygotene-staged spermatocytes but had comparable levels of pachytene-staged spermatocytes as compared to *Setx*<sup>+/+</sup> mice. No diplotene-stage spermatocytes were observed in *Setx*<sup>-/-</sup> mice. These data indicate that the disruption of meiosis is due to a block at the pachytene-diplotene transition, contributing to the defect in spermatogenesis observed in the *Setx*<sup>-/-</sup> male mice.

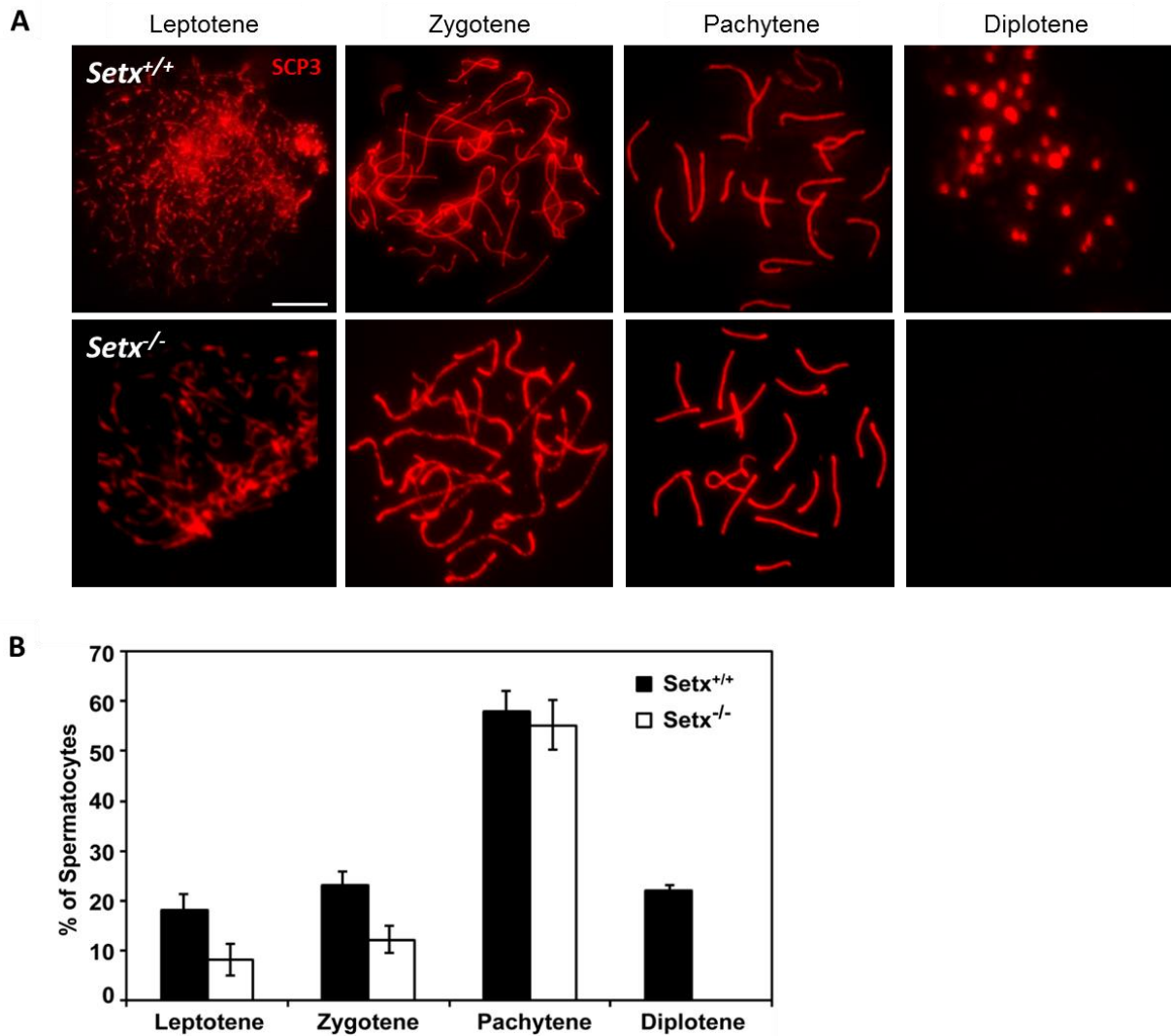
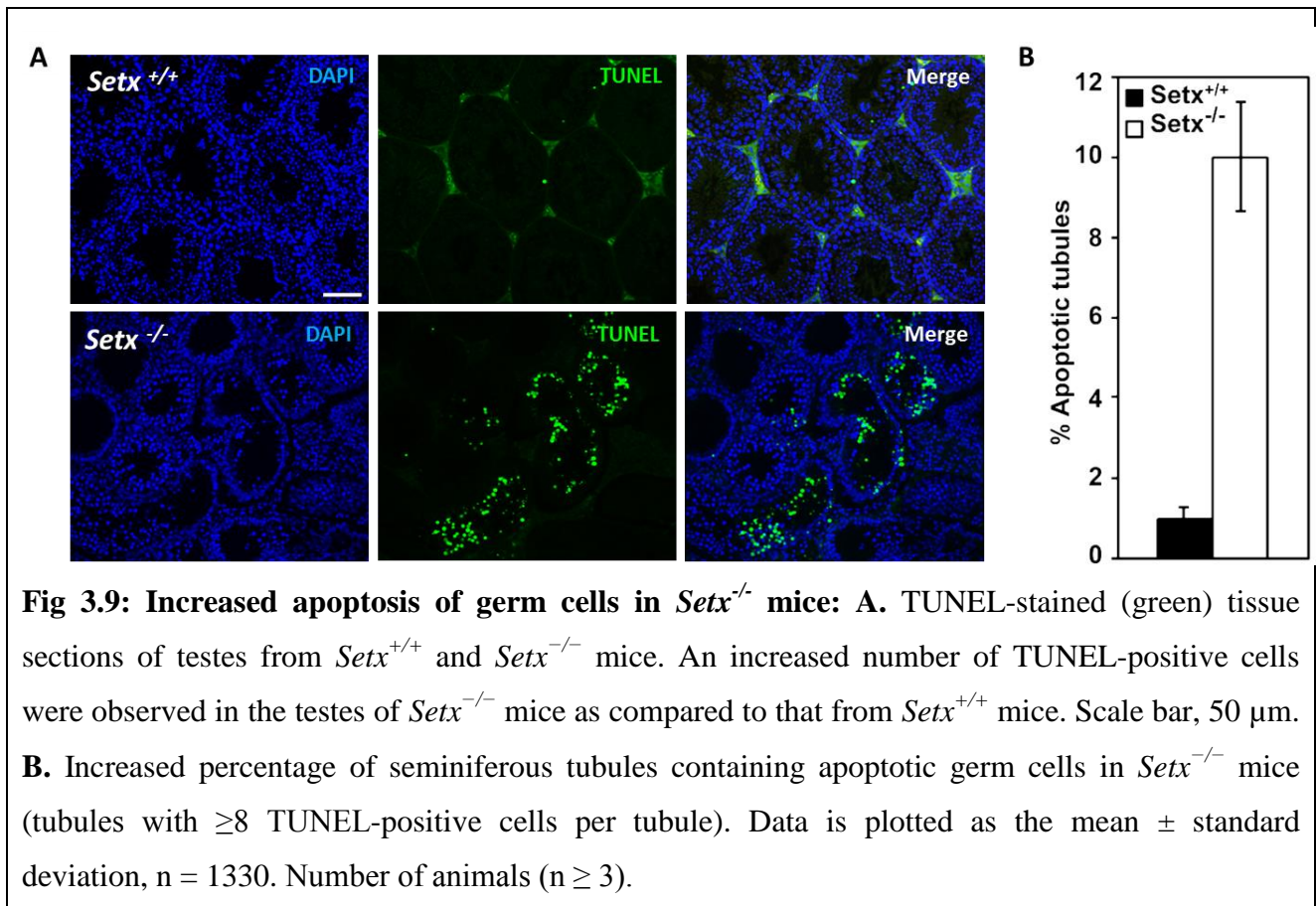


**Fig 3.8: Block in meiosis at pachytene stage in *Setx*<sup>-/-</sup> spermatocytes.** **A.** Immunostaining for SCP3 on spermatocyte spreads made from *Setx*<sup>+/+</sup> and *Setx*<sup>-/-</sup> mouse testes show the various stages in meiosis prophase I. Organisation and structure of the synaptonemal complex allows clear distinction between the different meiotic phases. Scale bar, 20  $\mu$ m. **B.** Graph showing the distribution of the different meiotic prophase I stages (leptotene, zygotene, pachytene, diplotene) in adult 35-day-old *Setx*<sup>+/+</sup> and *Setx*<sup>-/-</sup> mice. A comparable number of leptotene-, zygotene- and pachytene-staged spermatocytes were observed in both mouse types, but a complete absence of diplotene-staged spermatocytes in *Setx*<sup>-/-</sup> mice was observed, indicating a block at pachytene stage. Data is plotted as the mean  $\pm$  standard deviation obtained from 3 mice. 2000 spermatocytes were

counted for each *Setx*<sup>+/+</sup> and *Setx*<sup>-/-</sup> mouse. Student's t-test,  $p < 0.01$ . Data was plotted by Evelyn Y.H. Heng as the mean  $\pm$  standard error,  $n = 6000$ . \* indicates  $p < 0.01$ .

Using the TUNEL assay as a marker for apoptotic cells, elevated levels of apoptosis were detected in seminiferous tubules of *Setx*<sup>-/-</sup> mice (Fig 3.9), suggesting that these arrested spermatocytes are eliminated via this pathway.



### 3.2.5 Defects in homologous recombination in *Setx*<sup>-/-</sup> spermatocytes

To better understand the meiotic defect that is observed in *Setx*<sup>-/-</sup> male mice, differences between the meiotic prophase I stages in spermatocyte in both *Setx*<sup>+/+</sup> and *Setx*<sup>-/-</sup> mice was analyzed, using different key markers involved in homologous recombination (HR).

Briefly, the initiation of HR during spermatogenesis begins with the induction of programmed DNA DSBs by the SPO11 endonuclease during the leptotene and zygotene stage in meiosis prophase I<sup>120</sup>. Proper formation and repair of these programmed DSBs ensures legitimate pairing and segregation of homologous chromosomes<sup>191</sup>. These DNA DSBs subsequently trigger the phosphorylation of

histone H2AX at Ser139 and phosphorylated H2AX ( $\gamma$ H2AX) is a well-established marker for DNA DSBs<sup>116</sup>.  $\gamma$ H2AX immunostaining has also been used extensively to monitor the formation and kinetics of DNA DSB repair in various cell types including human and mouse cells<sup>118</sup>. By the pachytene stage, the majority of DSBs on the autosomes have been repaired, leaving only breaks marked by  $\gamma$ H2AX on the XY chromosomes that are required for meiotic sex chromosomes inactivation (MSCI) (which will be discussed further in section 3.2.6).

In order to determine whether there were differences in the initial production and repair of programmed DNA DSBs in *Setx*<sup>-/-</sup> mice, immunostaining using an antibody against  $\gamma$ H2AX was performed on *Setx*<sup>+/+</sup> and *Setx*<sup>-/-</sup> spermatocytes. As expected, DNA DSBs were induced in *Setx*<sup>+/+</sup> spermatocytes during the leptotene and zygotene stages (Fig 3.10). These DSBs were repaired by the pachytene stage, leaving only  $\gamma$ H2AX staining on the XY body. This 2<sup>nd</sup> wave of H2AX phosphorylation on the XY chromosomes occurs as a natural phenomenon that is essential for XY silencing during MSCI<sup>126</sup>. In contrast, while DNA DSBs were also induced in leptotene- and zygotene-staged spermatocytes of *Setx*<sup>-/-</sup> mice, residual breaks were still observed on the autosomes during the pachytene stage, indicating the persistence of unrepaired DNA DSBs (Fig 3.10).

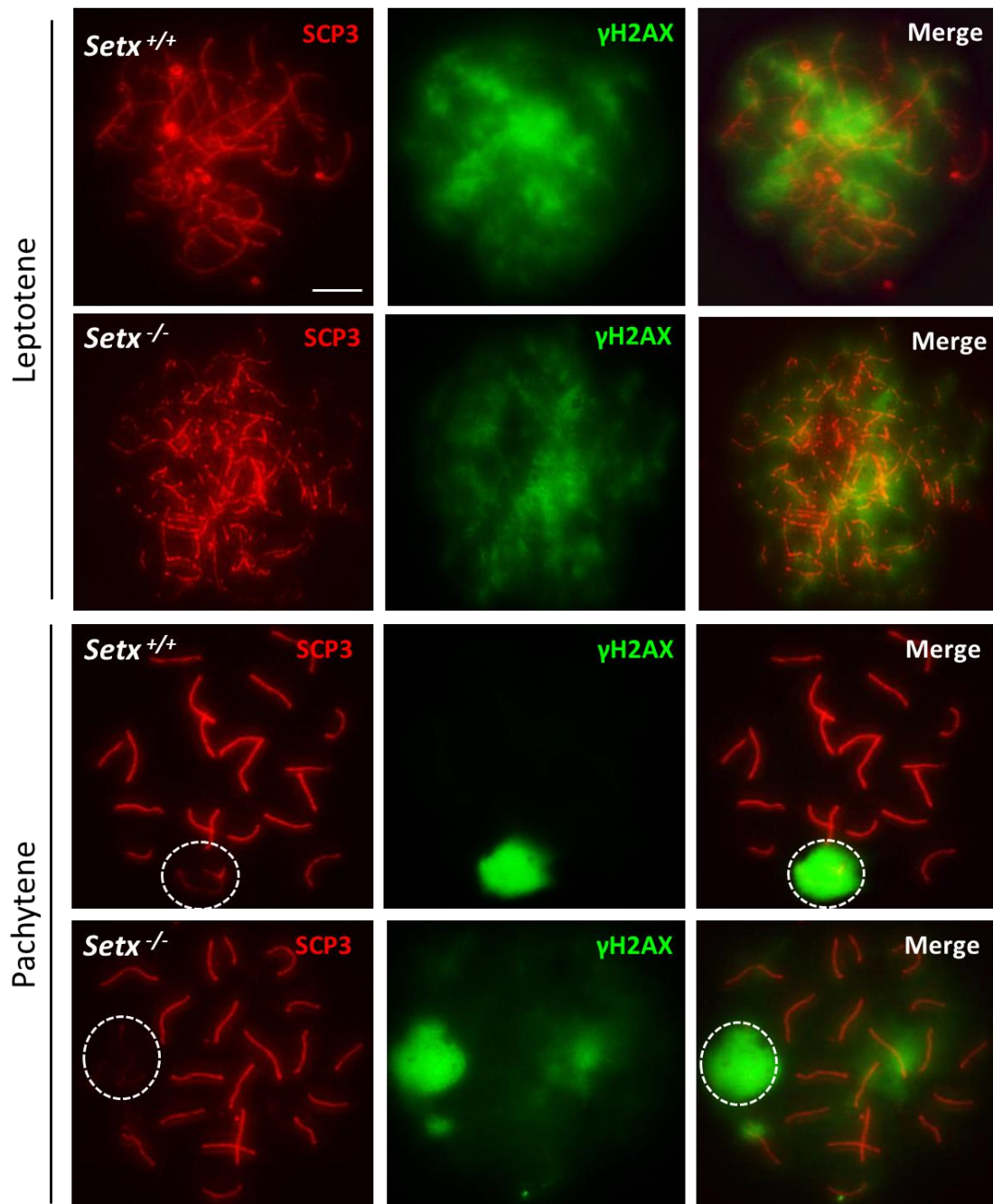
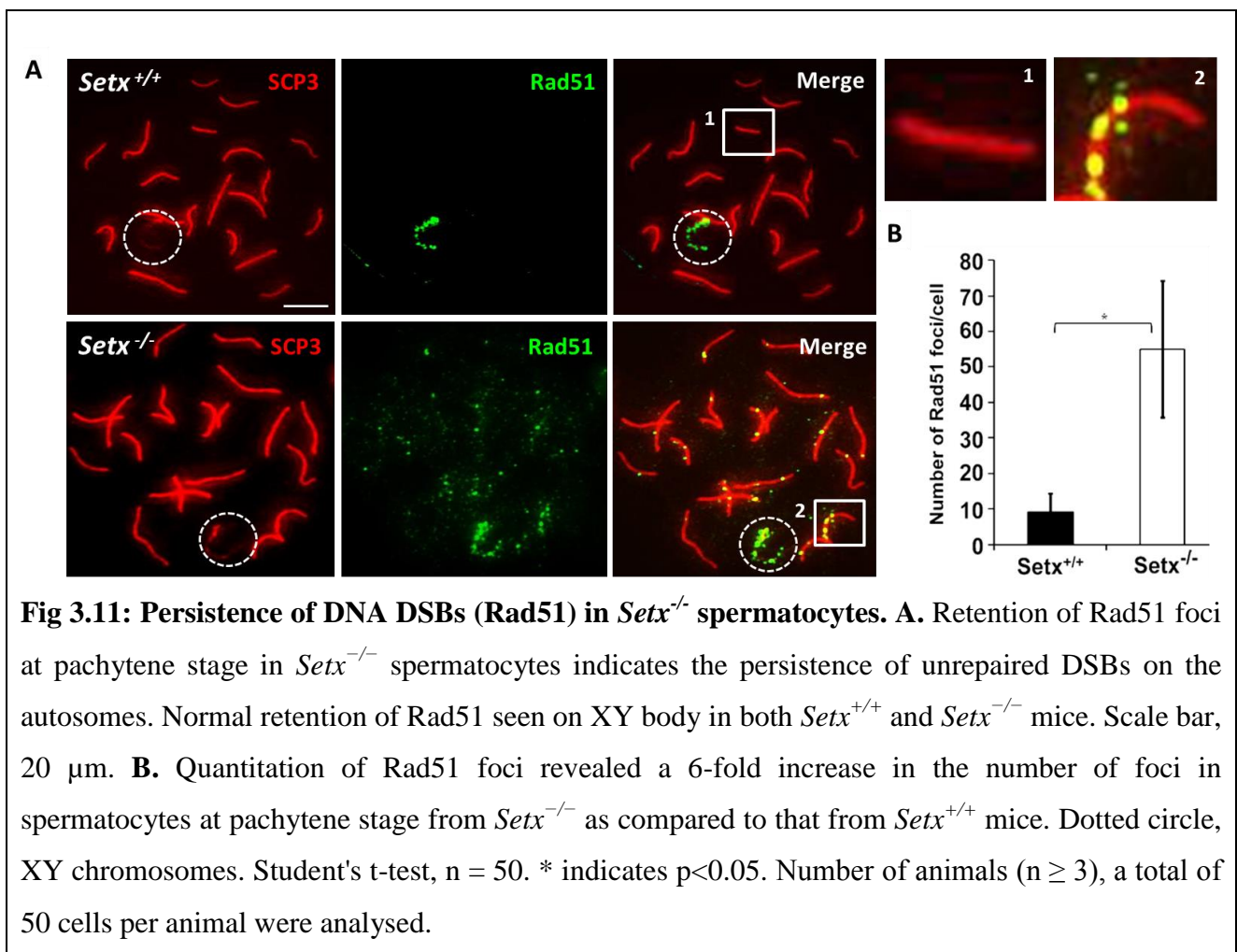


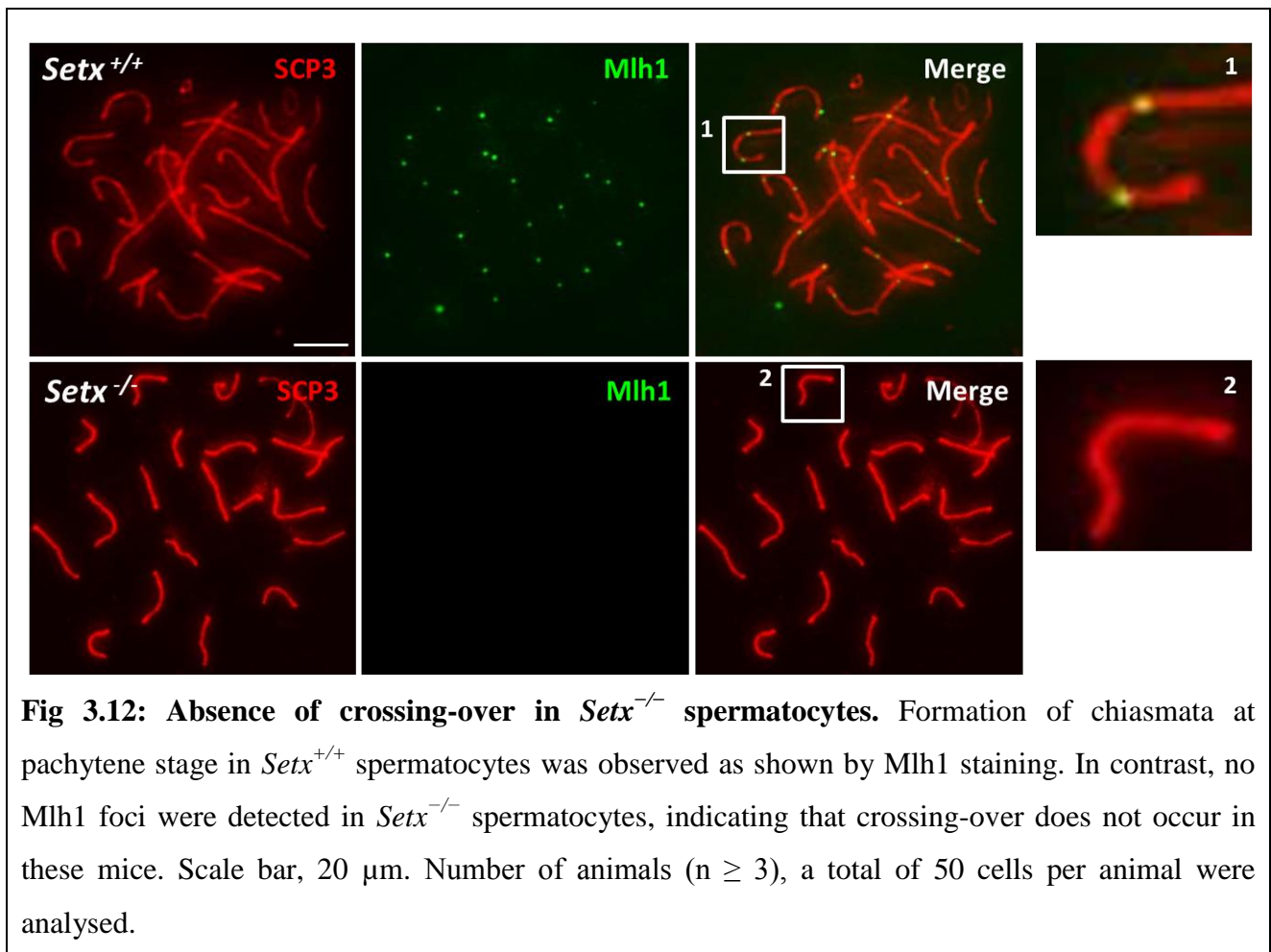
**Fig 3.10: Persistence of DNA DSBs ( $\gamma$ H2AX) in *Setx*<sup>-/-</sup> spermatocytes.** DNA DSBs as denoted by  $\gamma$ H2AX staining of spermatocytes spreads from *Setx*<sup>+/+</sup> and *Setx*<sup>-/-</sup> mice. Initiation of programmed DNA DSBs occurs normally in both *Setx*<sup>+/+</sup> and *Setx*<sup>-/-</sup> mice. At pachytene stage, DSBs on the autosomes are repaired, leaving only  $\gamma$ H2AX staining restricted to the XY chromosomes in *Setx*<sup>+/+</sup> spermatocytes required for meiotic sex chromosome silencing. In contrast,  $\gamma$ H2AX staining remained on the autosomes of *Setx*<sup>-/-</sup> mice during the pachytene stage, indicating the persistence of unrepaired DSBs. Normal  $\gamma$ H2AX staining of the XY chromosomes was observed in both *Setx*<sup>+/+</sup> and *Setx*<sup>-/-</sup> pachytene stage spermatocytes. Dotted circle, XY chromosomes. Scale bar, 20  $\mu$ m. Number of animals ( $n \geq 3$ ), a total of 50 cells per animal were analysed.



The repair of these programmed meiotic DNA DSBs subsequently occurs via homologous recombination (HR) and this involves the participation of various DNA repair factors including RPA, DMC1 and RAD51<sup>125</sup>. Both RAD51 and DMC1 play key roles in the initial steps of HR by mediating strand invasion and homologous pairing. These proteins are normally observed as multiple foci along the chromosomes, first appearing during the leptotene stage then sharply decreasing by the pachytene stage<sup>192</sup>. As expected, normal activity of Rad51 in spermatocytes from *Setx*<sup>+/+</sup> mice was observed, with foci labelling only observed along the axial element of the unsynapsed XY chromosomes (Fig 3.11A). In contrast, multiple Rad51 foci along the SC of autosomal chromosomes still persisted during the pachytene stage in spermatocytes from *Setx*<sup>-/-</sup> mice. Quantitation of the number of Rad51 foci on the autosomes at pachytene stage revealed a 6-fold increase of these foci in *Setx*<sup>-/-</sup> mice compared to *Setx*<sup>+/+</sup> mice (Fig 3.11B). These data indicate a defect in the disassembly of Rad51 filaments potentially hindering the repair of DNA DSBs. This is then likely to interfere with the progression of HR in *Setx*<sup>-/-</sup> mice.



Next, to assess whether meiotic recombination proceeds normally in the spermatocytes of *Setx*<sup>-/-</sup> mice despite the persistence of DNA DSBs, the distribution of the mismatch repair protein Mlh1 was examined. Mlh1 normally forms foci and marks the sites of chiasmata corresponding to sites of crossing over. An average of 22 foci per pachytene-staged spermatocyte in *Setx*<sup>+/+</sup> mice was observed, and this is in agreement with previous reports<sup>193,194</sup>. In contrast, no Mlh1 foci were observed in *Setx*<sup>-/-</sup> pachytene-staged spermatocytes (Fig 3.12), indicating the absence of crossing over.



Given the increased staining of Rad51 and the lack of Mlh1 foci observed in the spermatocytes of *Setx*<sup>-/-</sup> mice, reverse transcription polymerase chain reaction (RT-PCR) was performed to investigate the expression levels of these genes.

It was observed that the retention of Rad51 foci in spermatocytes of *Setx*<sup>-/-</sup> mice was not due to an overexpression of *Rad51* since comparable *Rad51* mRNA levels were observed in both *Setx*<sup>+/+</sup> and *Setx*<sup>-/-</sup> mice (Fig 3.13A). Interestingly, immunoblotting of total protein extracts revealed reduced levels of Rad51 protein in *Setx*<sup>-/-</sup> mice testes as compared to *Setx*<sup>+/+</sup> mice. This indicates that the

absence of senataxin affects the synthesis or stability of Rad51 protein (Fig 3.13B). Although there are less Rad51 molecules in the *Setx*<sup>-/-</sup> spermatocytes, these appear to be sufficient for coating sites of DNA DSB to initiate HR repair. Furthermore, the lack of Mlh1 foci in spermatocytes of *Setx*<sup>-/-</sup> mice does not appear to be due to the low expression of the *Mlh1* gene as similar levels of *Mlh1* mRNA were detected in both *Setx*<sup>+/+</sup> and *Setx*<sup>-/-</sup> mouse testes (Fig 3.13A). In contrast to Rad51, similar levels of Mlh1 protein in both *Setx*<sup>+/+</sup> and *Setx*<sup>-/-</sup> mice were observed as shown by immunoblotting of total protein extracts from testes (Fig 3.13B), indicating that Mlh1 protein is not the limiting factor for crossing-over formation. The lack of senataxin prevents completion of meiosis which in turn is likely to result into germ cell apoptosis. This is in agreement with our observation of increased apoptosis levels in *Setx*<sup>-/-</sup> testes section. Overall, these results thus confirm an essential role for senataxin in meiotic recombination during spermatogenesis.

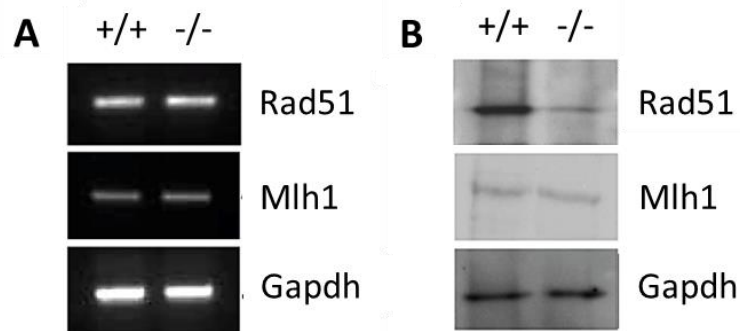


**Fig 3.13: Similar expression levels of Rad51 and Mlh1 in *Setx* mice.** **A.** Expression of *Rad51* and *Mlh1* via RT-PCR revealed that the increased staining of Rad51 foci in *Setx*<sup>-/-</sup> spermatocytes was not due to an upregulation of the *Rad51* gene as similar levels of *Rad51* mRNA were detected in both *Setx*<sup>+/+</sup> and *Setx*<sup>-/-</sup> testes. Likewise, the absence of *Mlh1* foci in *Setx*<sup>-/-</sup> spermatocytes was not due to a downregulation of the *Mlh1* gene as similar levels of *Mlh1* mRNA were detected in both *Setx*<sup>+/+</sup> and *Setx*<sup>-/-</sup> testes. **B.** Immunoblotting of total protein extracts from both *Setx*<sup>+/+</sup> and *Setx*<sup>-/-</sup> mouse testes for either Rad51 or Mlh1 showed reduced levels of Rad51 protein in *Setx*<sup>-/-</sup> mice as compared to *Setx*<sup>+/+</sup> mice whereas similar protein levels for Mlh1 were observed for both *Setx*<sup>+/+</sup> and *Setx*<sup>-/-</sup> mice. Gapdh was used as a loading control for both assays.

### 3.2.6 Defect in meiotic sex chromosome inactivation (MSCI) in *Setx*<sup>-/-</sup> spermatocytes

During pachytene, another important event known as meiotic sex chromosome inactivation (MSCI) takes place. This is when the X and Y chromosomes are transcriptionally silenced and compartmentalized within the peripheral nuclear region known as the XY- or sex body<sup>126</sup>. Although

the exact mechanism and reason as to how and why MSCI occurs remains unclear<sup>126,129</sup>, it has been hypothesized that the silencing of the X and Y chromosomes is essential to prevent the illegitimate recombination of the non-homologous chromosomes<sup>128</sup>, or that the expression of certain X genes may be toxic to the cell<sup>195</sup>. Additionally, defects in or failure of MSCI can cause germ cell elimination via apoptosis<sup>196,197</sup>.

The arrest at pachytene stage observed in the spermatocytes of *Setx*<sup>-/-</sup> male mice led us to investigate whether this was partially caused by the failure of MSCI. Hence, to first observe whether senataxin has a role MSCI, its localization was investigated by performing immunostaining on *Setx*<sup>+/+</sup> mouse spermatocyte spreads. It was observed that senataxin localized mostly over the XY chromosomes as a diffused cloud during the pachytene stage (Fig 3.14). Some background staining was also observed over the autosomes, consistent with a role for senataxin in meiotic recombination. As expected, no senataxin labeling was detected in spermatocytes of *Setx*<sup>-/-</sup> mouse (Fig 3.14).

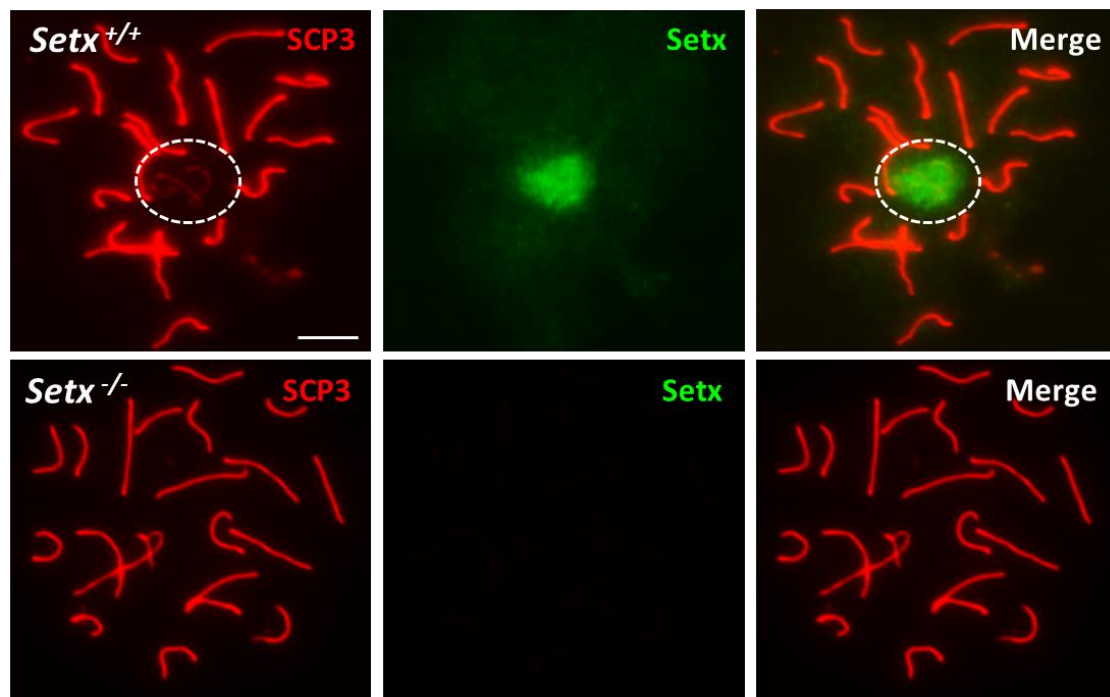


**Fig 3.14: Senataxin localizes to the XY chromosomes during meiosis.** A. Immunostaining for senataxin (Setx) revealed its localization to the XY chromosomes as a diffused cloud during the pachytene stage in spermatocytes of *Setx*<sup>+/+</sup> mice. Some background staining was also observed on the autosomes. As expected, no senataxin was detected in *Setx*<sup>-/-</sup> spermatocytes. Dotted circle, XY chromosomes. Number of animals ( $n \geq 3$ ), a total of 50 cells per animal were analysed.

The preferential localization of senataxin to the XY chromosomes thus indicated a possible role for senataxin in MSCI. To investigate whether the absence of senataxin has an effect on the silencing of the XY body during MSCI, active transcription via immunostaining using an antibody against the activated form (Phospho-S2) of RNA polymerase II was studied. Studying the localization of RNA Pol II is commonly performed to look at XY silencing during MSCI<sup>198,199</sup>. The results revealed a lack of staining over the XY body in *Setx*<sup>+/+</sup> spermatocytes, confirming transcriptional silencing (Fig 3.15A), whereas staining was observed over the XY body in *Setx*<sup>-/-</sup> spermatocytes (Fig 3.15A), indicating that active transcription was still occurring on the XY body in these mice. A graph plot (Fig 3.15B) of the fluorescence intensity of RNA Pol II S2 from the representative image showed similar levels of the protein over the autosomes in both *Setx*<sup>+/+</sup> and *Setx*<sup>-/-</sup> spermatocytes, with an abnormal 5 fold increase over the XY chromosomes in *Setx*<sup>-/-</sup> spermatocytes.

Investigating the expression levels of sex-linked genes is also another commonly employed method for looking at MSCI defects<sup>200,201</sup>. To confirm that aberrant transcription of XY genes was occurring in the spermatocytes of *Setx*<sup>-/-</sup> mice, the expression levels of several XY genes in both *Setx*<sup>+/+</sup> and *Setx*<sup>-/-</sup> spermatocytes was analyzed using reverse transcription polymerase chain reaction (RT-PCR). Shown in Fig 3.15C and D, an anomalous increase in the expression of X-linked genes such as *Usp26* (2.55 fold), *Fthl17* (2.33 fold), *Tktl1* (10.98 fold) and *Ube1x* (1.48 fold), was observed in spermatocytes of *Setx*<sup>-/-</sup> mice as compared to that from *Setx*<sup>+/+</sup> mice. Similar results were also observed for several Y-linked genes such as *Ube1y* (1.82 fold) and *Rbmy* (2.15 fold). These data thus confirmed a defect in the silencing of XY chromosomes in *Setx*<sup>-/-</sup> mice during MSCI. Comparable expression of autosomal genes that include *Actinb*, *Dazl*, and *Gapdh* were observed in spermatocytes from both *Setx*<sup>+/+</sup> and *Setx*<sup>-/-</sup> mice, serving as loading controls as well as confirming the specific nature of the MSCI defect observed in *Setx*<sup>-/-</sup>.

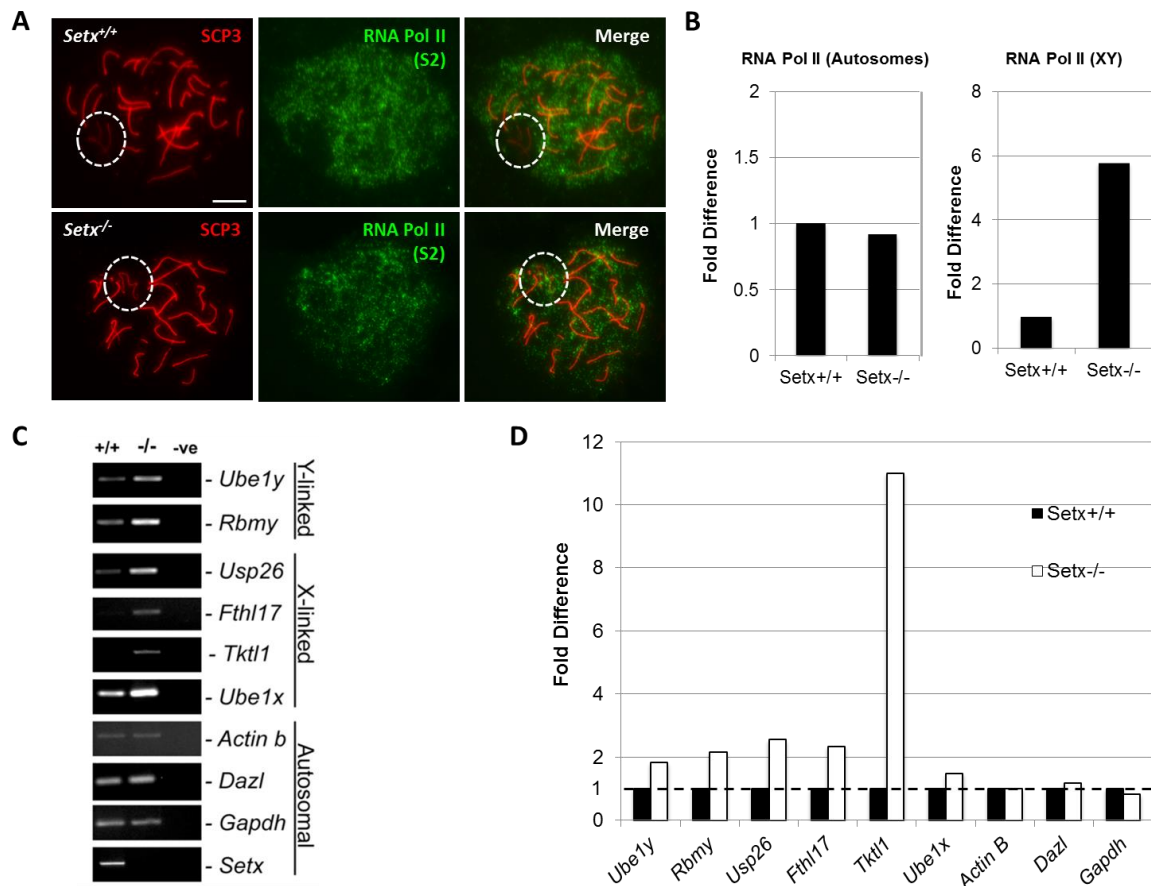


**Fig 3.15: Aberrant meiotic sex chromosome inactivation (MSCI) in *Setx*<sup>-/-</sup> spermatocytes** **A.** Immunostaining for the transcriptionally-active form of RNA Pol II (phospho-S2) revealed active transcription occurring over the XY chromosomes in *Setx*<sup>-/-</sup> spermatocytes. In contrast, no signal for active Pol II was visible over the XY chromosomes in *Setx*<sup>+/+</sup> spermatocytes confirming the normal, programmed silencing of the XY chromosomes during MSCI. Scale bar, 20  $\mu$ m. Dotted circle, XY chromosomes. Number of animals ( $n \geq 3$ ), a total of 50 cells per animal were analysed. **B.** A representative graph plot of the fold difference in RNA Pol II fluorescence intensity between autosomes and XY chromosomes in *Setx*<sup>+/+</sup> and *Setx*<sup>-/-</sup> mice. **C.** Levels of mRNA transcripts of X & Y-linked germ cell specific genes from *Setx*<sup>+/+</sup> and *Setx*<sup>-/-</sup> testes were determined by RT-PCR to assess MSCI. mRNA transcript levels of *Actb*, *Dazl* and *Gapdh* were used as loading controls. **D.** A representative graph plot of the fold differences in genes used for the RT-PCR. Dotted line across represents baseline expression.

### **3.3 Discussion**

In this Chapter, the characterization of the *Setx*<sup>-/-</sup> mouse model was reported. No neurological phenotype in the *Setx*<sup>-/-</sup> mouse was observed as shown by behavioural analyses and histological examinations of tissues of the central nervous system. Gross morphology of the brain and cerebellum as well as the Purkinje cell distribution was comparable between *Setx*<sup>+/+</sup> and *Setx*<sup>-/-</sup> mice.

The major phenotype observed was the sterility of *Setx*<sup>-/-</sup> male mice and this study has provided compelling evidence for an essential role of senataxin in spermatogenesis. Loss of senataxin leads to the persistence of DNA DSBs, which subsequently prevents homologous recombination between sister chromosomes, as well as failure in MSCI that lead to germ cell apoptosis. Testicular atrophy, depletion of germ cells and sterility are common features of animal models with defects in meiotic proteins such as Spo11<sup>193,202</sup>, strand exchange protein Dmc1<sup>203,204</sup>, Brca1<sup>205</sup>, mismatch repair proteins Msh4, Msh5, Mlh3 and Mlh1<sup>206-208</sup>. The phenotype observed in *Setx*<sup>-/-</sup> male mice overlaps with but is distinct from that described for these mutant mice. Unlike that in *Setx*<sup>+/+</sup> mice where DNA DSBs were confined to the XY chromosomes during the pachytene stage, breaks were still present in the autosomes as well as on the XY body in *Setx*<sup>-/-</sup> mice, indicating a defect in repair of DNA DSBs and consequently a defect in meiotic recombination. This was confirmed by persistence of the DNA damage repair protein Rad51 on autosomes and a failure to detect chiasmata via Mlh1 staining at late meiotic stages in pachytene-staged cells from *Setx*<sup>-/-</sup> mice. Failure to remove Rad51, as seen in *Setx*<sup>-/-</sup> mouse spermatocytes, could possibly have prevented the completion of meiotic DNA DSB repair via crossing over and homologous recombination. The persistence of Rad51 foci on the autosomes may influence the recruitment of certain DDR proteins to the XY chromosomes and therefore titrate those proteins which would lead to a defect in MSCI due to a lack of/reduced recruitment of those DDR proteins. Given also that Rad51 has been implicated in R-loop formation, the persistence of Rad51 foci on the chromosomes may also influence transcription regulation of certain genes involved in XY silencing. We cannot exclude the possibility that the 2 phenotypes (Rad51 removal and MSCI defect) are related as both homologous recombination and MSCI involve common DDR proteins.

During meiosis, two waves of H2AX phosphorylation occur. The first wave results from the programmed induction of DNA DSBs by the endonuclease Spo11 and are processed and repaired through homologous recombination, to allow the exchange of genetic material between sister chromatids as mentioned above. The second wave of phosphorylation occurs only on the XY

chromosomes and is completely essential for meiotic sex chromosome inactivation (MSCI)<sup>122,192</sup>. In the leptotene and zygotene stages of meiosis prophase I, the XY chromosomes are transcriptionally active<sup>126</sup>. However, at pachytene stage when meiotic chromosomal synapsis is complete, MSCI occurs and the XY chromosomes are silenced<sup>127,128</sup>. MSCI then persists throughout the pachytene and diplotene stages<sup>126</sup>. Although this second wave of H2AX phosphorylation occurs normally on the XY chromosomes in spermatocytes of *Setx*<sup>-/-</sup> mice, a failure in MSCI is still observed. This is possibly due to the lack of XY silencing in spermatocytes of *Setx*<sup>-/-</sup> mice as observed by RNA Pol II (phospho-S2; active form of elongating RNA Pol II) staining where active transcription was observed over the XY chromosomes. This was subsequently confirmed by the aberrant transcription of selected X- and Y-linked genes thus indicating a defect in MSCI in *Setx*<sup>-/-</sup> mice. Thus, the compounding effects of having defective meiotic recombination due to the persistence of unrepaired DNA DSBs, the lack of crossing-over formation, together with the failure of MSCI appear to be responsible for the increased rate of germ cell apoptosis observed in the seminiferous tubules of *Setx*<sup>-/-</sup> mice, and consequently the sterility in *Setx*<sup>-/-</sup> male mice. This defect in MSCI will be discussed in greater detail in Chapter 4.

The findings in this chapter are briefly summarized in Table 3.1.

<i>Setx</i> <sup>+/+</sup>	Features	<i>Setx</i> <sup>-/-</sup>
✗	Neurodegeneration	✗
✗	Male sterility	✓
✗	Accumulation of DNA DSBs	✓
✓	Crossing-over	✗
✓	MSCI	✗
✗	Germ cell apoptosis	✓

**Table 3.1: Essential role for senataxin in spermatogenesis and germ cell maturation.**

Although it would be worthwhile to corroborate the male sterility observed in the *Setx*<sup>-/-</sup> mouse with that in AOA2/ALS4 patients, there is however a lack of fertility data in the human population for this disorder. Indeed, there are no records till date about male AOA2/ALS4 patients fathering children. Interestingly, there have been reports on female patients having early onset



menopause<sup>62,67</sup>, premature ovarian failure<sup>190,209</sup> and hypogonadotropic hypogonadism<sup>69</sup>, supporting our observation of sub-fertility in the female *Setx*<sup>-/-</sup> mice.

It was previously shown that senataxin is involved in RNA transactions such as transcriptional regulation and RNA processing<sup>71</sup>. Senataxin was found to interact with RNA polymerase II and the lack of senataxin altered RNA polymerase II binding to specific gene loci<sup>71</sup>. Similar observations have been found with the yeast homolog of senataxin (Sen1p). Use of a ChIP–Chip analysis of RNA polymerase distribution, showed that a single amino acid substitution of Sen1p, within its helicase domain, altered the genome-wide distribution of RNA polymerase II in non-coding and protein-coding genes<sup>72</sup>. Furthermore, mutant senataxin has previously been reported to alter gene expression in a disease-specific manner in cells derived from patients with AOA2 and these changes in gene expression likely underlie the phenotypic difference between AOA2 and ALS4<sup>210</sup>. Novel genes and cellular pathways related to senataxin function in nervous tissues have also been recently identified<sup>210</sup>. In collaboration with Dr Brent Fogel (UCLA, USA) evidence for differential gene expression from *Setx*<sup>+/+</sup> and *Setx*<sup>-/-</sup> testes using genome-wide microarray analysis have been obtained (Dr Brent Fogel, Dr Olivier Becherel, unpublished data). Differential gene expression analysis revealed that 72.5% (174/240) of X-linked genes were up-regulated in *Setx*<sup>-/-</sup> as compared to *Setx*<sup>+/+</sup> demonstrating on a genome-wide scale the MSCI defect, thus providing compelling evidence for a role for senataxin in transcriptional regulation. It is possible that the transcriptional regulation that occurs during meiosis is specific to the XY chromosomes. The most apparent feature of the XY body is its chromatin structure, which is visibly different even at the light microscope level, from that of the autosomal domain of the spermatocyte nucleus. Although the exact mechanism of this regulation remains unclear, it has been hypothesized that an aspect of this unique chromatin domain sequesters an interesting array of proteins, many of which are not found elsewhere in the nucleus and are typically associated with heterochromatin, and some of which are post-translationally modified<sup>132</sup>.

**CHAPTER 4: Senataxin regulates Atr activity and chromatin remodeling during MSCI**

## **4.1 Introduction**

Given that the absence of senataxin leads to defects in meiotic sex chromosome inactivation (MSCI), further dissection of the mechanism was necessary. As previously mentioned, meiotic sex chromosome inactivation (MSCI) is the process during meiosis in which the X and Y chromosomes are transcriptionally silenced<sup>126</sup>. This phenomenon has been shown to be critical for the completion of spermatogenesis<sup>126</sup>. Indeed, defects in MSCI can trigger germ cell apoptosis during pachytene stage<sup>211</sup>.

MSCI is initiated by the recruitment and accumulation of Brca1 (breast cancer, early onset) to the unsynapsed axes of the XY chromosomes<sup>192,196</sup>, however the mechanism of this recruitment remains unclear<sup>212</sup>. Brca1 subsequently recruits Atr (Ataxia-telangiectasia and Rad3 related kinase), which then phosphorylates histone variant H2AX ( $\gamma$ H2AX)<sup>126</sup>. Phosphorylated H2AX plays a central role during spermatogenesis, not only by recruiting DNA damage repair proteins to sites of programmed DNA DSBs induced by the Spo11 endonuclease during the leptotene and zygotene stages, but also by controlling gene expression via post-translational modifications (PTM) and the subsequent altering of chromatin structure<sup>122</sup>. MSCI consists of two genetically separable steps that involve a series of DNA damage repair (DDR) proteins. The first step is the MDC1-independent recognition of the unsynapsed axes by DDR factors such as ataxia telangiectasia and Rad3-related (ATR), TOPBP1, and  $\gamma$ H2AX<sup>213</sup>. The second step is the MDC1-dependent chromosome-wide spreading of DDR factors to the entire chromatin<sup>213</sup>.

SUMO (small ubiquitin-like modifiers) are covalently-attached post-translational modifications (PTM) that are involved in numerous cellular activities such as transcription regulation, intracellular transport, heterochromatin formation, protein-protein interaction and stability, and DNA damage recognition and repair<sup>121,125,126</sup>. Evidence that SUMOylation precedes accumulation of phosphorylated H2AX on sex chromosomes during their meiotic inactivation was provided by a very early appearance of SUMO-1, which preceded  $\gamma$ H2AX accumulation on the XY chromosomes, suggesting a possible specific role for SUMO-1 in the initiation of MSCI<sup>131</sup>. In this chapter, the localization and recruitment of SUMO-1, SUMO-2/3 and other key DDR factors involved in XY silencing were compared between *Setx*<sup>+/+</sup> and *Setx*<sup>-/-</sup> spermatocytes, as a way of studying the molecular events that take place during MSCI.

## **4.2 Results**

### *4.2.1 Defect in SUMOylation in spermatocytes of $Setx^{-/-}$ mice during MSCI*

The progression of meiotic events via DDR factors as well as XY chromosome silencing are also tightly regulated by SUMOylation, where SUMO-1 and 2/3 have been shown to localize as a diffuse cloud over the XY chromosomes<sup>138</sup>. Given the preferential localization of senataxin over the XY body and the MSCI defect observed in  $Setx^{-/-}$ , whether the lack of senataxin would affect SUMOylation signaling was investigated.

To observe for differences in SUMOylation patterns of the XY chromosomes between  $Setx^{+/+}$  and  $Setx^{-/-}$  spermatocytes, immunostaining against SUMO-1 and 2/3 was performed on spermatocytes spreads. As expected, diffuse SUMO-1 (Fig 4.1A) and 2/3 (Fig 4.1B) localization to the XY chromosomes in spermatocytes of  $Setx^{+/+}$  mice was observed as a cloud, which is in agreement with the staining pattern reported in wild type mouse models<sup>138</sup>. Conversely, it was observed that in  $Setx^{-/-}$  spermatocytes, decreased signals of SUMO-1 and 2/3 were detected and localized only to the axial element of the XY chromosomes, indicating that the absence of senataxin affects SUMOylation *per se* and/or SUMOylated-molecules distribution over the XY chromosomes.

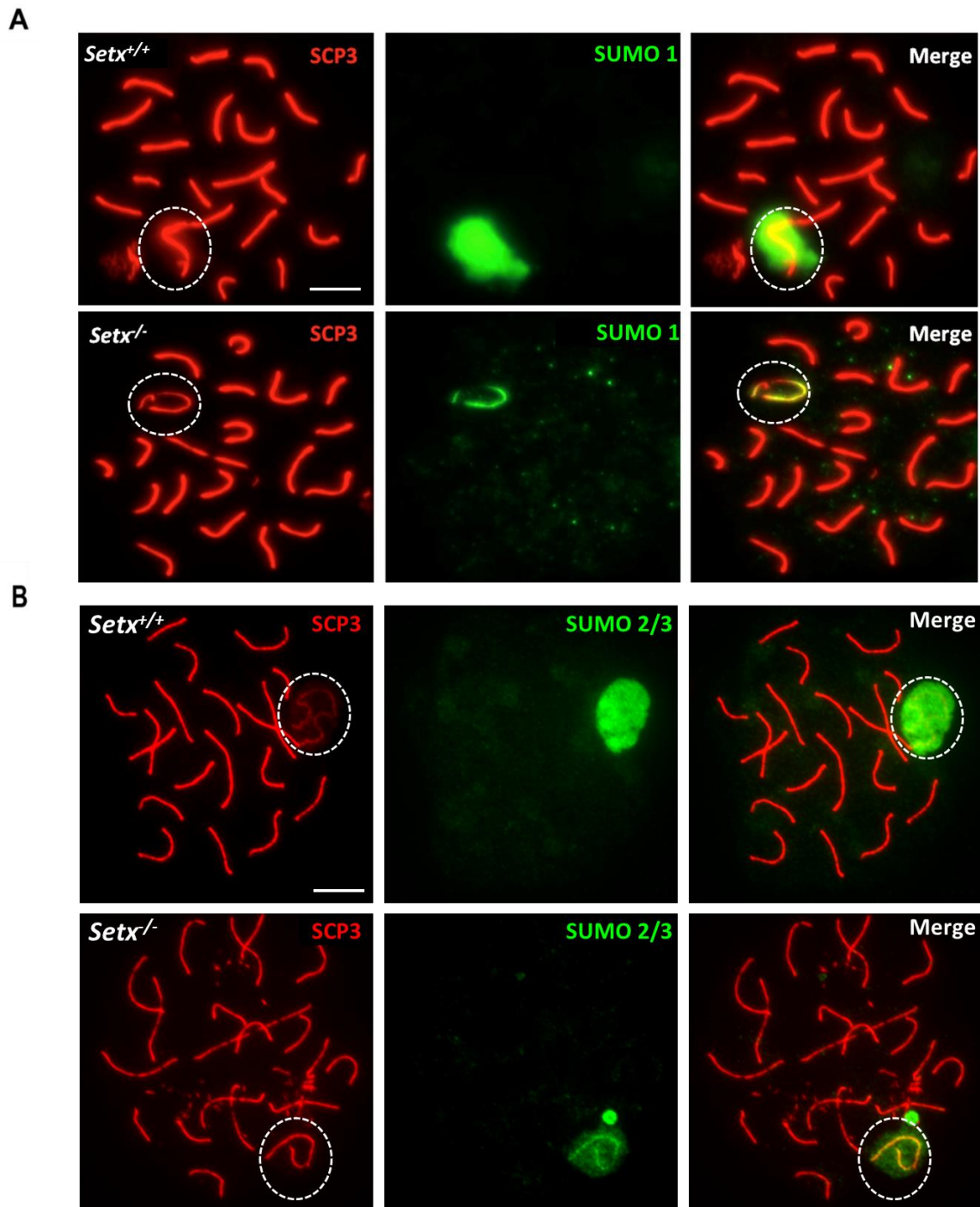


**Fig 4.1: SUMO is confined to the axial element of the XY chromosomes in *Setx*<sup>-/-</sup> spermatocytes.** Immunostaining for SUMO-1 (A) and SUMO-2/3 (B) in *Setx*<sup>+/+</sup> and *Setx*<sup>-/-</sup> spermatocytes revealed a diffuse staining over the XY chromosomes in *Setx*<sup>+/+</sup> spermatocytes. In contrast, staining was largely restricted to the axes of the XY chromosomes in *Setx*<sup>-/-</sup> spermatocytes. Interesting, a similar staining pattern was observed for both SUMO-1 and SUMO-2/3. Dotted circle, XY chromosomes. Scale bar, 20  $\mu$ m. Number of animals ( $n \geq 3$ ), a total of 50 cells per animal were analysed.

#### 4.2.2 *Senataxin is SUMOylated*

Since senataxin is also observed to localize over the XY body, whether senataxin is SUMOylated during MSCI was investigated. A bioinformatics tool, GPS-SUMO (<http://sumosp.biocuckoo.org/>), which predicts sites of SUMOylation and SUMO-interacting motifs (SIM) based on consensus sequences<sup>214</sup> was employed. This program predicted three sites of SUMOylation and three SIMs for senataxin (Fig 4.2A). Further evidence for the SUMOylation of senataxin has also been provided by Hecker *et al.* 2006 whereby senataxin was identified via a yeast two-hybrid screen as a novel SUMO-interacting partner that binds to both SUMO-1 and SUMO-2/3<sup>215</sup>. However, the early appearance of SUMO-1, preceding the accumulation of  $\gamma$ H2AX on the sex chromosomes, and the lack of SUMO-2/3 detection in zygotene spermatocytes, suggested a more specific role for SUMO-1 in the initiation of XY inactivation<sup>131</sup>. Therefore, SUMO-1 was chosen for further investigation.

To study this phenomenon *in vivo*, co-immunoprecipitation of senataxin and SUMO-1 was first performed on total cell extracts made from *Setx*<sup>+/+</sup> and *Setx*<sup>-/-</sup> testes. Results showed the SUMOylation of endogenous senataxin in *Setx*<sup>+/+</sup> spermatocytes (Fig 4.2B). Subsequently, a proximity ligation assay (PLA) for both senataxin and SUMO-1 on *Setx*<sup>+/+</sup> spermatocyte spreads was performed to observe for this interaction. Briefly, PLA allows the visualization of *in situ* endogenous protein-protein interactions via fluorescent dots due to the amplification and subsequent incorporation of fluorescent nucleotides on complementary strands that are conjugated to target antibodies. Results showed that senataxin and SUMO-1 interacted with one another on the XY chromosomes with the majority of the positive signals (red spots) focused over the XY chromosomes (Fig 4.2C). A negative control without primary antibody was included. Altogether, this is consistent with a preferential XY localization pattern of both SUMO-1 and senataxin. In addition, several positive signals were also observed over the autosomes in agreement with the diffuse localization of senataxin over the autosomes and its role in meiotic recombination.

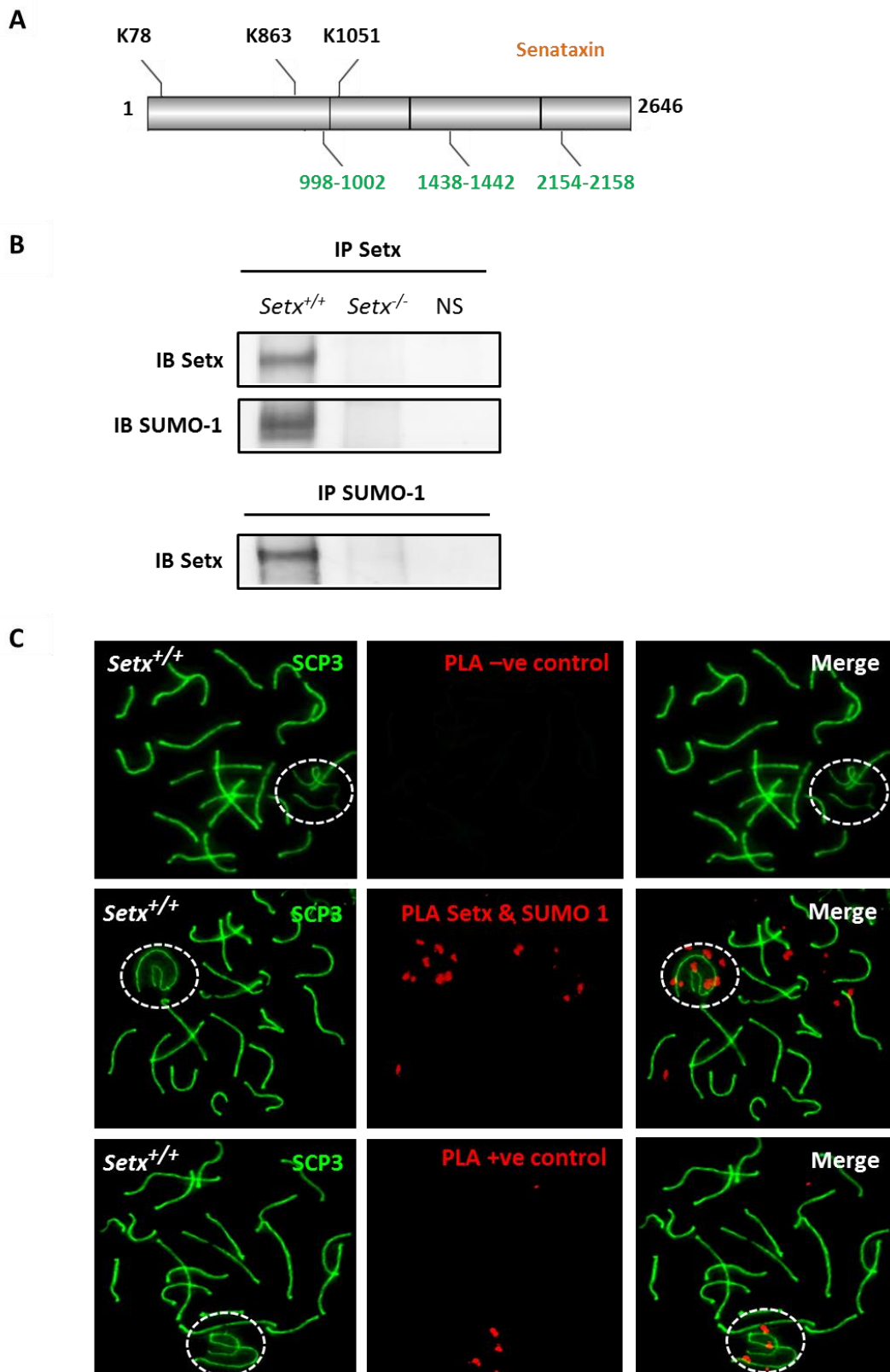


**Fig 4.2: Senataxin interacts with SUMO-1 at the XY chromosomes in *Setx*<sup>+/+</sup> spermatocytes.**  
**A.** GPS-SUMO, a bioinformatics tool, performed an *in silico* prediction and found three potential SUMOylation sites (labeled in black) and three SUMO-interaction motifs (labeled in green) for senataxin. **B.** Endogenous senataxin and SUMO-1 were co-immunoprecipitated and immunoblotted

separately, showing the SUMOylation of senataxin in *Setx*<sup>+/+</sup> spermatocytes. C. Through a Proximity Ligation Assay (PLA), an interaction between Setx and SUMO-1 was observed over the XY chromosomes as red foci (middle panels). Red foci were also observed over the autosomes. A negative control without primary antibody (top panels) as well as a positive control (bottom panels) using antibodies against Brca1 and Atr, two proteins known to interact directly<sup>216</sup> was performed alongside. Dotted circle, XY chromosomes. Scale bar, 20  $\mu$ m. Number of animals ( $n \geq 3$ ), a total of 50 cells per animal were analysed.

#### 4.2.3 Identification of SUMOylated proteins- Candidate selected: Atrip

Based on the differential SUMO staining patterns between *Setx*<sup>+/+</sup> and *Setx*<sup>-/-</sup> spermatocytes, and given that senataxin associates with SUMO-1, the identification of various SUMOylated proteins in these mice was carried out.

To identify these proteins, SUMO-1 immunoprecipitation (IP) from *Setx*<sup>+/+</sup> and *Setx*<sup>-/-</sup> testes protein extracts followed by mass spectrometry (MS) identification were performed. Immunoprecipitates were electrophoresed on a SDS-PAGE denaturing gradient gel and ten bands of interest were excised (Fig 4.3). Following tryptic digest, the bands were sent to Dr. Mark Graham (Children's Medical Research Institute, University of Sydney) for liquid chromatography MS (LC-MS/MS) analysis.



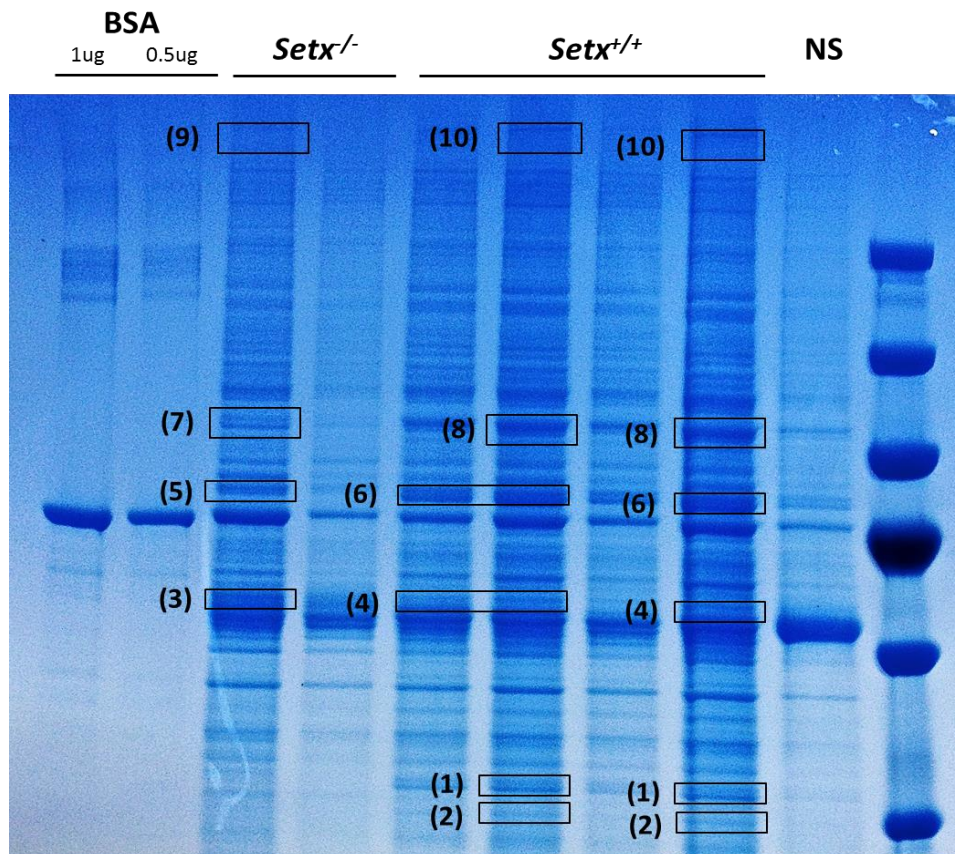


**Fig 4.3: Excision of bands following SUMO-1 immunoprecipitations from *Setx*<sup>+/+</sup> and *Setx*<sup>-/-</sup> testes extracts.** SUMO-1 immunoprecipitates from *Setx*<sup>+/+</sup> and *Setx*<sup>-/-</sup> testes extracts were separated on a 4-12% SDS-PAGE denaturing gradient gel and stained using Coomassie Blue (R250). 10 bands that were different in abundance or presence between *Setx*<sup>+/+</sup> and *Setx*<sup>-/-</sup> were excised, digested and sent for identification via liquid chromatography mass spectrometry (LC-MS/MS) (Dr. Mark Graham, CMRI, NSW). A non-specific sample (NS) using rabbit IgG was performed alongside as a control. Bovine serum albumin (BSA) was also separated on the gel for protein concentration estimation.

According to proteomic standards for protein identification via LC-MS/MS, a stringent threshold for protein was set at 99%, the false discovery rate (FDR) was set at 0.02% and the minimum number of peptides for each protein was set at 2. The software used to display the protein/peptide identification results from tandem MS was Scaffold Q+S (Proteome Software, Portland, OR, USA)<sup>217</sup>.

Several candidates involved in chromatin remodeling (such as Atrx and Ruvb2) and transcription regulation (such as Dhx15 and Ybox3) were identified to be SUMOylated in *Setx*<sup>+/+</sup> spermatocytes

but not in *Setx*<sup>-/-</sup> spermatocytes. However in this Report, the focus will be on Atrip, a protein that was found to be SUMOylated in *Setx*<sup>+/+</sup> but not in *Setx*<sup>-/-</sup> spermatocytes (Fig 4.4).

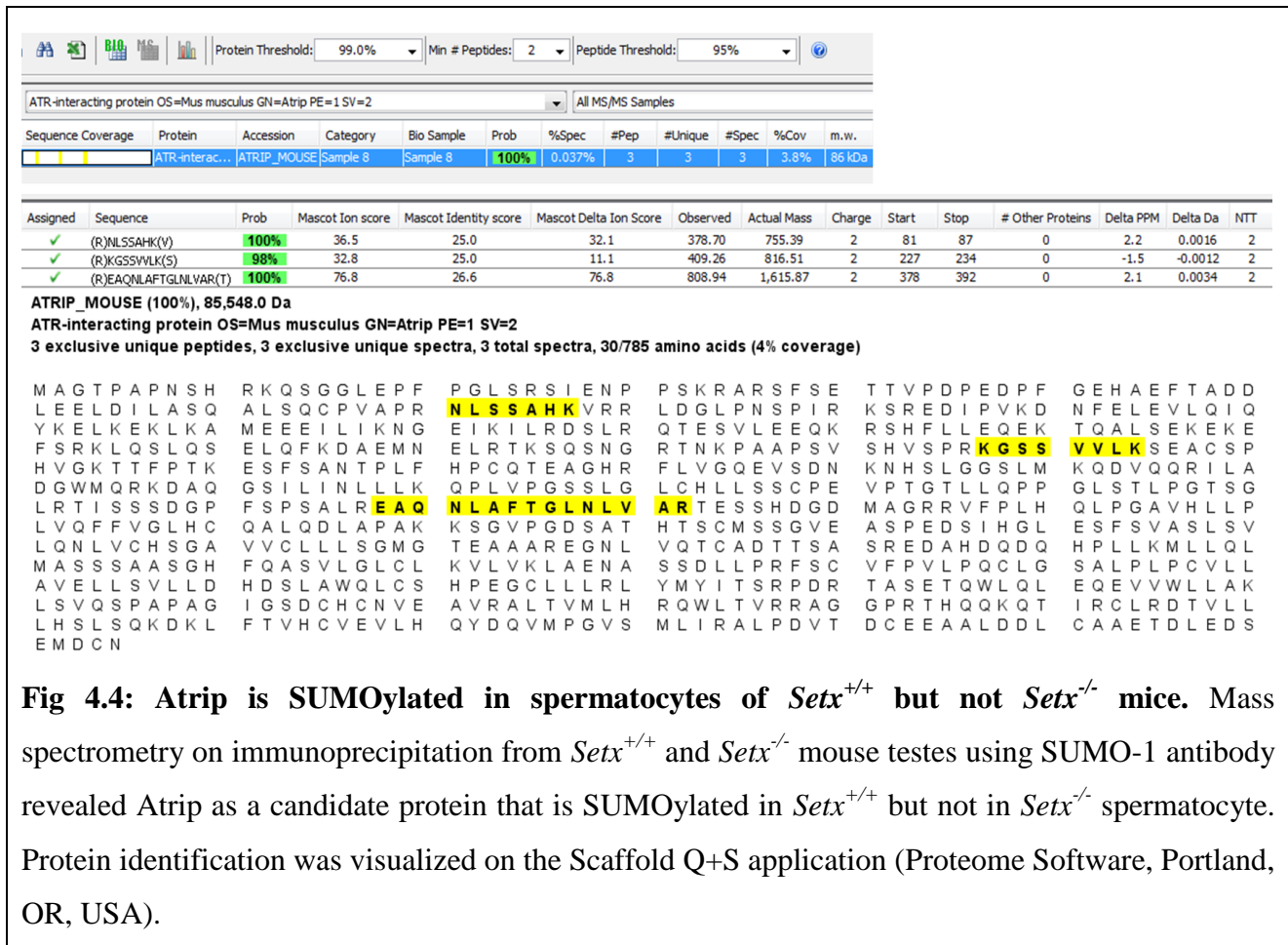


**Fig 4.4: Atrip is SUMOylated in spermatocytes of *Setx*<sup>+/+</sup> but not *Setx*<sup>-/-</sup> mice.** Mass spectrometry on immunoprecipitation from *Setx*<sup>+/+</sup> and *Setx*<sup>-/-</sup> mouse testes using SUMO-1 antibody revealed Atrip as a candidate protein that is SUMOylated in *Setx*<sup>+/+</sup> but not in *Setx*<sup>-/-</sup> spermatocyte. Protein identification was visualized on the Scaffold Q+S application (Proteome Software, Portland, OR, USA).

Atrip (Atr interacting protein) is the binding partner of Atr (Ataxia-telangiectasia and Rad3 related kinase), and the Atr-Atrip heterodimer plays an important role in DDR by signalling the presence of damage and activating cell cycle checkpoints<sup>218</sup>. The Atr signaling pathway is activated during replication fork stalling and is recruited by Atrip to replication protein A (Rpa)-coated ssDNA<sup>219</sup>. Atr is subsequently activated by DNA topoisomerase-2 binding protein 1 (TopBp1), triggering the cascade of phosphorylation of other downstream effector proteins such as Chk1<sup>220</sup>. The Atr-Atrip dimer is also essential for MSCI, where it is required for the phosphorylation of histone H2AX on the XY chromosomes, an epigenetic event that leads to silencing<sup>132</sup>. It was recently reported that the SUMOylation of Atrip plays an essential role in the Atr signaling pathway by facilitating the interactions between several DDR factors, such as Rpa, TopBP1, the MRN (Mre11, Rad50, Nbs1) complex as well as with Atr itself, during DNA repair<sup>221</sup>. Wu et al. 2014 also showed that the SUMOylation of Atrip is required for proper localization to sites of DNA damage and function following DNA damage<sup>221</sup>. During MSCI, the initial recruitment and activation of Atr-Atrip is

dependent on Brca1 and TopBP1 respectively<sup>211</sup>, and the following sections will dissect the Atr-Atrip DDR pathway involved in MSCI to elucidate the mechanistic defect leading to abnormal MSCI observed in *Setx*<sup>-/-</sup> mice.

#### 4.2.4 Normal recruitment of Brca1 and TopBP1 observed in spermatocytes of *Setx*<sup>-/-</sup> mice during MSCI

The initiation of MSCI begins with the crucial recruitment of the tumor suppressor protein, Brca1 to the axial element of the XY chromosomes. To observe whether this initial recruitment occurs normally in the spermatocytes of *Setx*<sup>-/-</sup> mice, immunostaining using an antibody against Brca1 was performed. The results showed a normal recruitment of Brca1 to the axes of the XY chromosomes in the spermatocytes of both *Setx*<sup>+/+</sup> and *Setx*<sup>-/-</sup> mice (Fig 4.5), indicating that the initiation of MSCI occurs normally in these mice and suggesting that the defect in MSCI leading to germ cell apoptosis in *Setx*<sup>-/-</sup> spermatocytes lies further downstream.

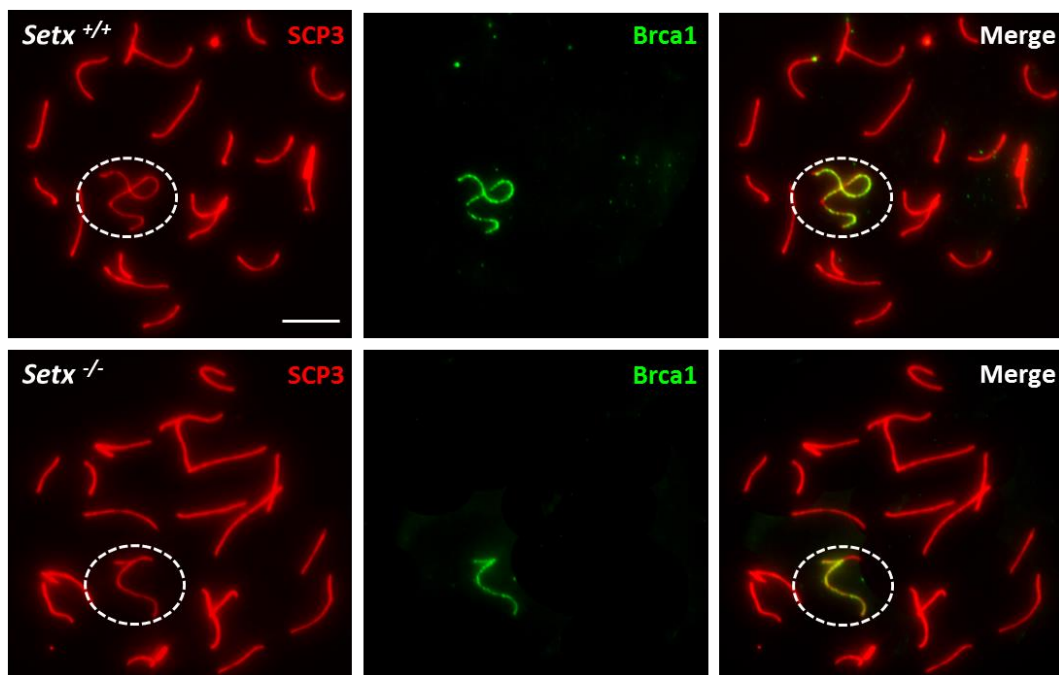


**Fig 4.5: Normal recruitment of Brca1 in *Setx*<sup>+/+</sup> and *Setx*<sup>-/-</sup> spermatocytes.** Immunostaining for Brca1 revealed the normal accumulation of Brca1 along the axial element of the XY chromosomes in the spermatocytes of *Setx*<sup>+/+</sup> and *Setx*<sup>-/-</sup> mice. Scale bar, 20  $\mu$ m. Dotted circle, XY chromosomes. Number of animals ( $n \geq 3$ ), a total of 50 cells per animal were analysed.

Given that both senataxin and Brca1 were observed to localize to the XY chromosomes during the pachytene stage and its essential role in initiating MSCI, whether the recruitment of senataxin to the

XY chromosomes was dependent on Brca1 was subsequently performed via immunostaining using spermatocyte spreads obtained from *Brca1*<sup>Δ11/Δ11</sup> (*p53*<sup>+/-</sup>) mutant mice. Incidentally, *Brca1*<sup>Δ11/Δ11</sup> mice show an overlapping phenotype with *Setx*<sup>-/-</sup> mice where the males are sterile due to a defect in MSCI<sup>222</sup>. The results in Fig 4.6 show that while senataxin localized to the XY chromosomes in *Brca1*<sup>+/+</sup> mice, it failed to do so in the *Brca1*<sup>Δ11/Δ11</sup> mutant mice. Thus, the recruitment of senataxin to the XY chromosomes during MSCI depends on functional Brca1.

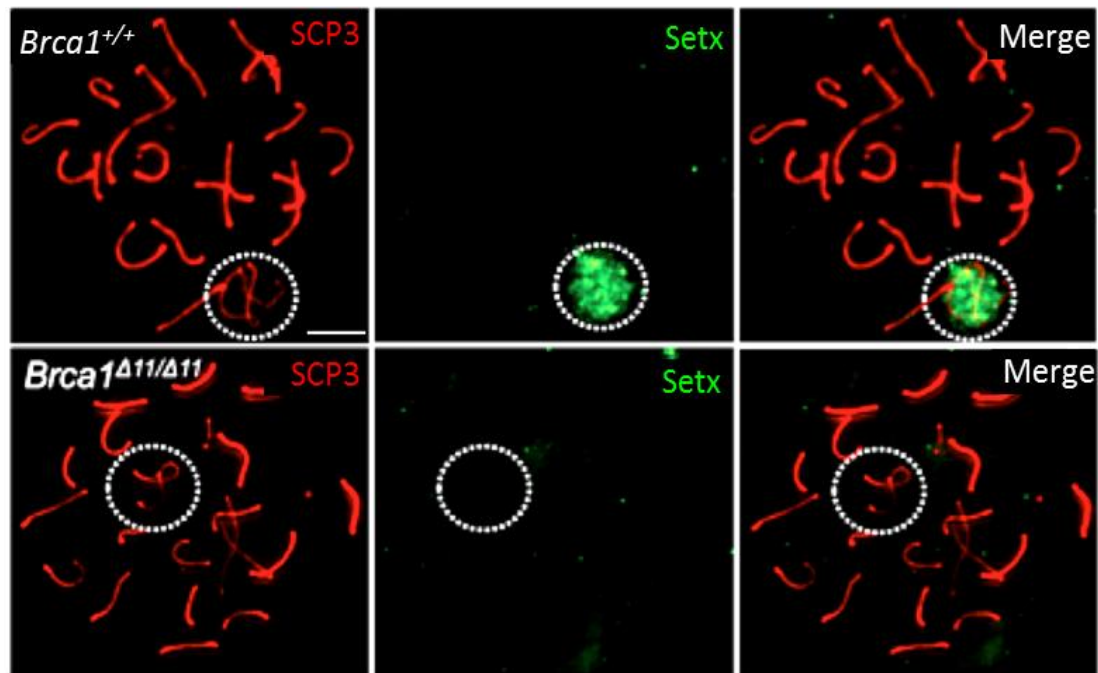


**Fig 4.6: Recruitment of senataxin is dependent on Brca1.** Immunostaining for senataxin in spermatocytes of *Brca1*<sup>+/+</sup> *Brca1*<sup>Δ11/Δ11</sup> mice showed that without functional Brca1, senataxin was not localized to the XY chromosomes. Scale bar, 20 μm. Dotted circle, XY chromosomes. Number of animals ( $n \geq 3$ ), a total of 50 cells per animal were analysed.

Consequently, to determine whether senataxin and Brca1 interacted with one another, a Proximity Ligation Assay (PLA), which allows for the *in situ* detection of endogenous protein-protein interactions was performed. However, a direct interaction between these two proteins was not observed (Fig 4.7). Attempts to co-immunoprecipitate endogenous senataxin and Brca1 also did not reveal an interaction between these proteins (data not shown). Although the recruitment of senataxin to the XY chromosomes is dependent on Brca1, it does not appear to be through a direct protein-protein interaction between the two proteins.

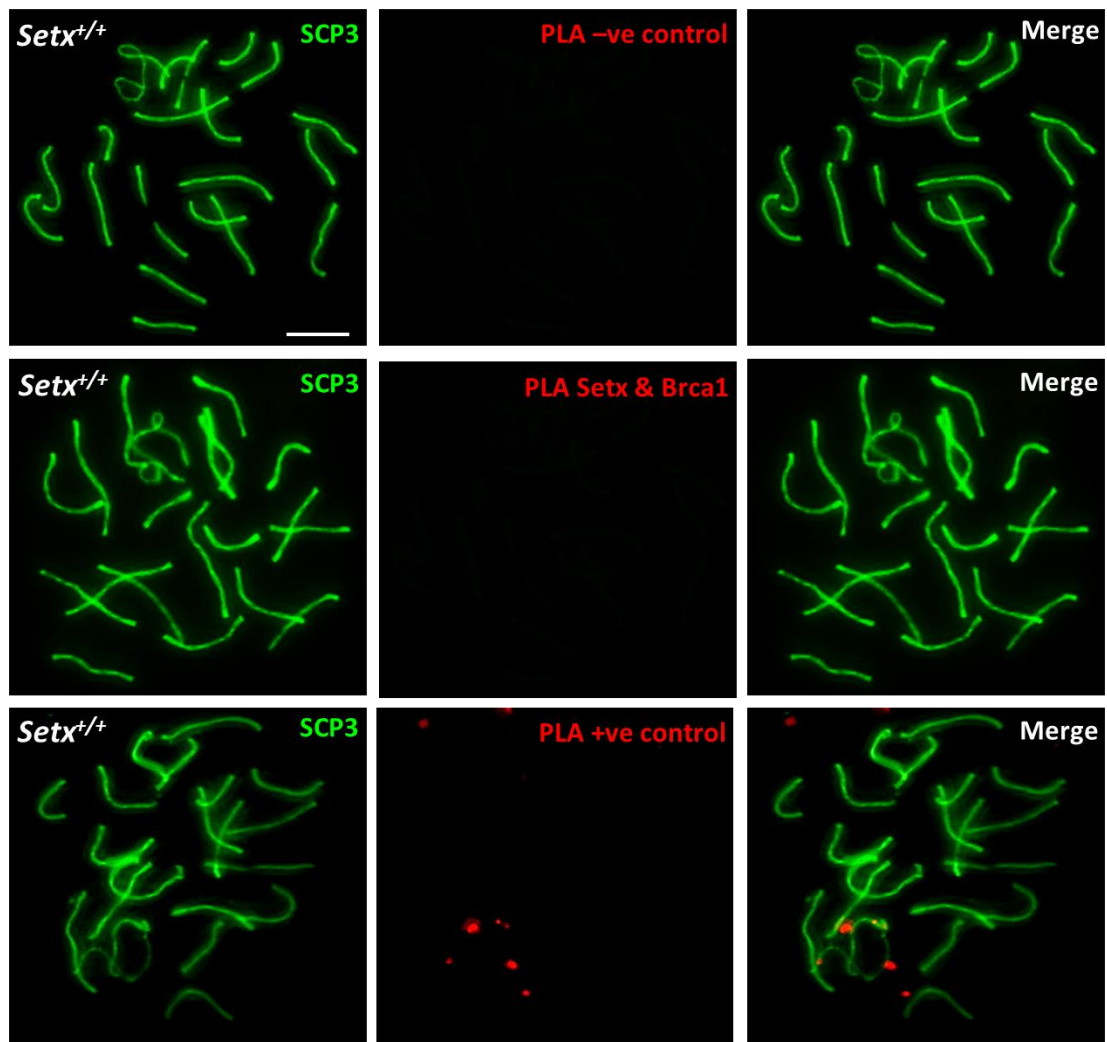


**Fig 4.7: No direct interaction between senataxin and Brca1.** PLA using antibodies against senataxin and Brca1 showed no direct interaction between these 2 proteins (middle panels). An appropriate negative control containing no primary antibodies (top panels) as well as a positive control using antibodies against Brca1 and Atr, two proteins known to interact directly<sup>216</sup>, was used (bottom panels). Scale bar, 20  $\mu$ m. Dotted circle, XY chromosomes. Number of animals ( $n \geq 3$ ), a total of 50 cells per animal were analysed.

Given that Brca1 recruitment was normal despite the absence of senataxin, TopBP1, a regulator and an activator of Atr<sup>211,223</sup>, was subsequently investigated. During meiosis, TopBP1 was shown to localize with Atr on the unsynapsed chromosomes during pachytene. It was also shown to be required in DDR, meiotic recombination and Atr binding to chromatin<sup>223</sup>. Immunostaining on *Setx*<sup>+/+</sup> mice showed that TopBP1 localized predominantly on the unsynapsed XY chromosomes in *Setx*<sup>+/+</sup> spermatocytes as expected whereas a much fainter signal was observed in *Setx*<sup>-/-</sup> spermatocytes, despite a similar localization to *Setx*<sup>+/+</sup> (Fig 4.8). These results gave the first indication of a potential defect in Atr function and other downstream signaling pathways.

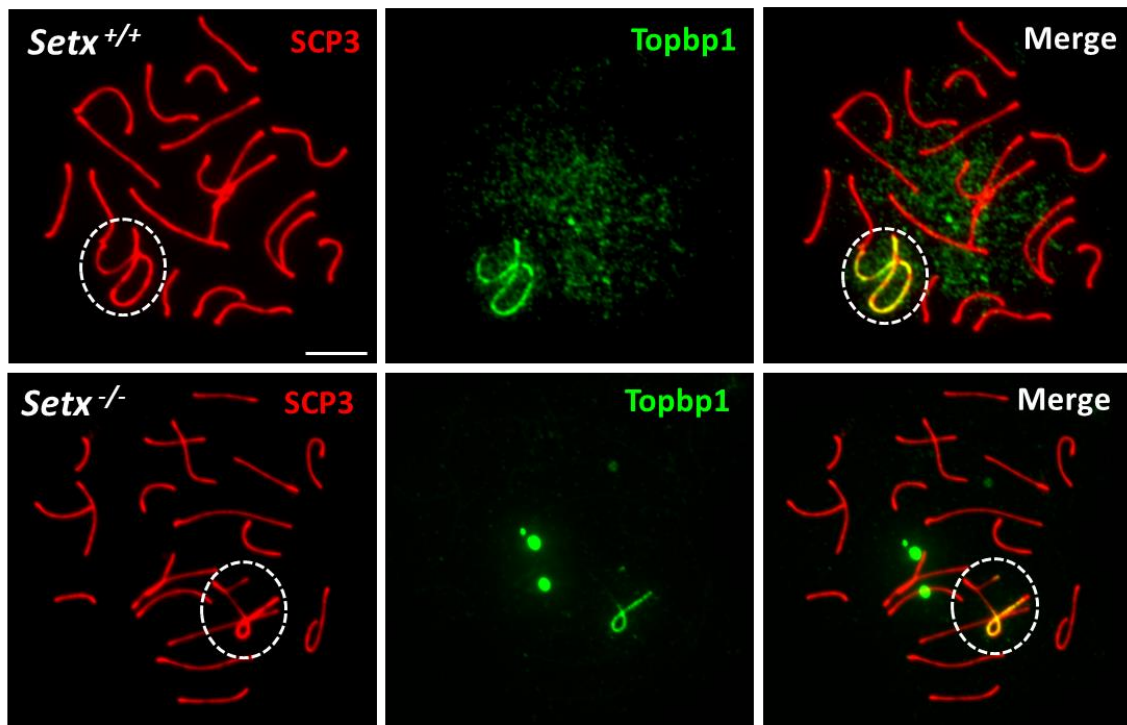


**Fig 4.8: Decreased levels of TopBP1 on XY chromosomes in *Setx*<sup>-/-</sup> spermatocytes.** TopBP1 was observed to localize predominantly to the axial element of the XY chromosomes in *Setx*<sup>+/+</sup> spermatocytes. In contrast, decreased staining intensity for TopBP1 was observed in *Setx*<sup>-/-</sup> spermatocytes. Scale bar, 20  $\mu$ m. Dotted circle, XY chromosomes. Number of animals ( $n \geq 3$ ), a total of 50 cells per animal were analysed.

#### 4.2.5 Defect in Atr-Atrip signaling in *Setx*<sup>-/-</sup> mice

Apart from coordinating DNA damage repair, Atr is required for the phosphorylation of histone H2AX on the XY chromosomes during MSCI<sup>134</sup>. Although the exact purpose of this phosphorylation remains unclear, it has been hypothesized that it is necessary for initiating chromatin condensation and repression of transcription<sup>115</sup>.

Since the localization of Brca1, which is required for the subsequent recruitment of Atr, was normal, Atr localization was then studied. It was observed that in *Setx*<sup>+/+</sup> spermatocytes, Atr formed a diffuse cloud over the XY chromosomes as previously reported<sup>224</sup> whereas Atr was localized predominantly over the axial element of the XY chromosomes in *Setx*<sup>-/-</sup> spermatocytes (Fig 4.9). Thus the absence of senataxin affects the diffusion of Atr on the XY chromosomes which may ultimately impact on MSCI.

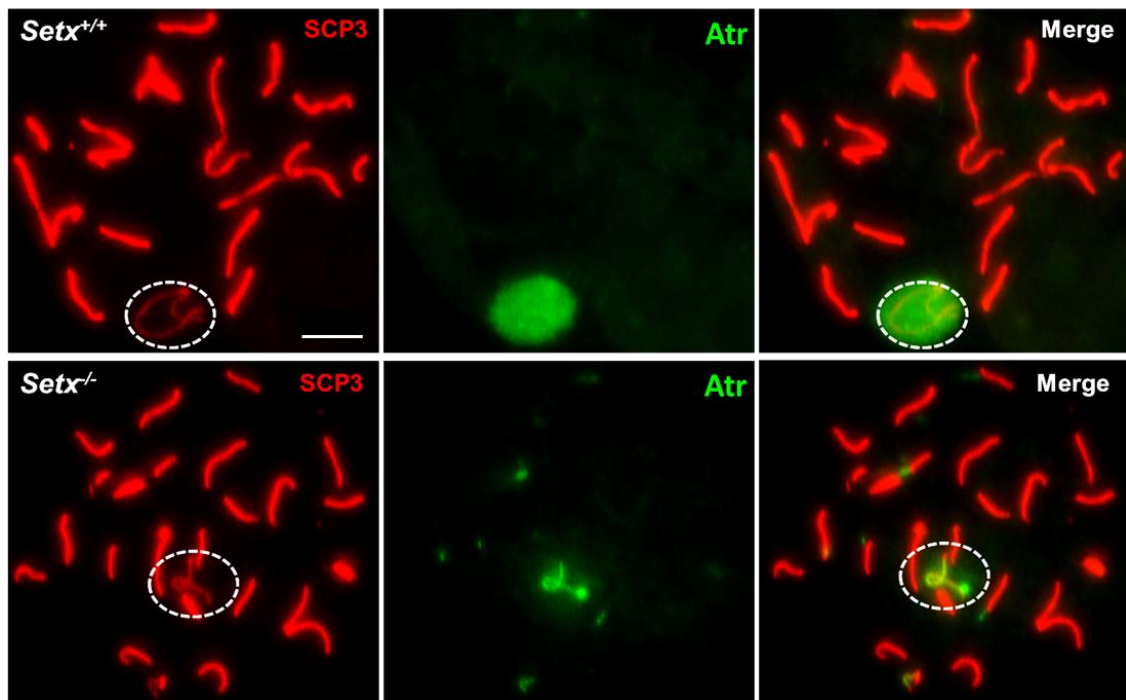


**Fig 4.9: Lack of diffusion of Atr over XY chromosomes in *Setx*<sup>-/-</sup> spermatocytes.** Immunostaining for Atr showed a cloud over the XY chromosomes in *Setx*<sup>+/+</sup> spermatocytes as expected, whereas Atr was largely retained on the axial element of the XY chromosomes in *Setx*<sup>-/-</sup> spermatocytes. Scale bar, 20  $\mu\text{m}$ . Dotted circle, XY chromosomes. Number of animals ( $n \geq 3$ ), a total of 50 cells per animal were analysed.

To determine whether the altered localization of Atr may reflect a difference in its activity, immunostaining against the active form of Atr, phospho-Atr S428 (p-Atr) was performed. Results showed that similar to total Atr, p-Atr formed a cloud over the XY chromosomes in *Setx*<sup>+/+</sup> spermatocytes whereas p-Atr was retained on the axial element of the XY chromosomes in *Setx*<sup>-/-</sup> spermatocytes (Fig 4.10). These data indicate a defect in the diffusion of Atr as well as its active form, p-Atr which could lead to alterations in the downstream DDR signaling that occurs during MSCI.

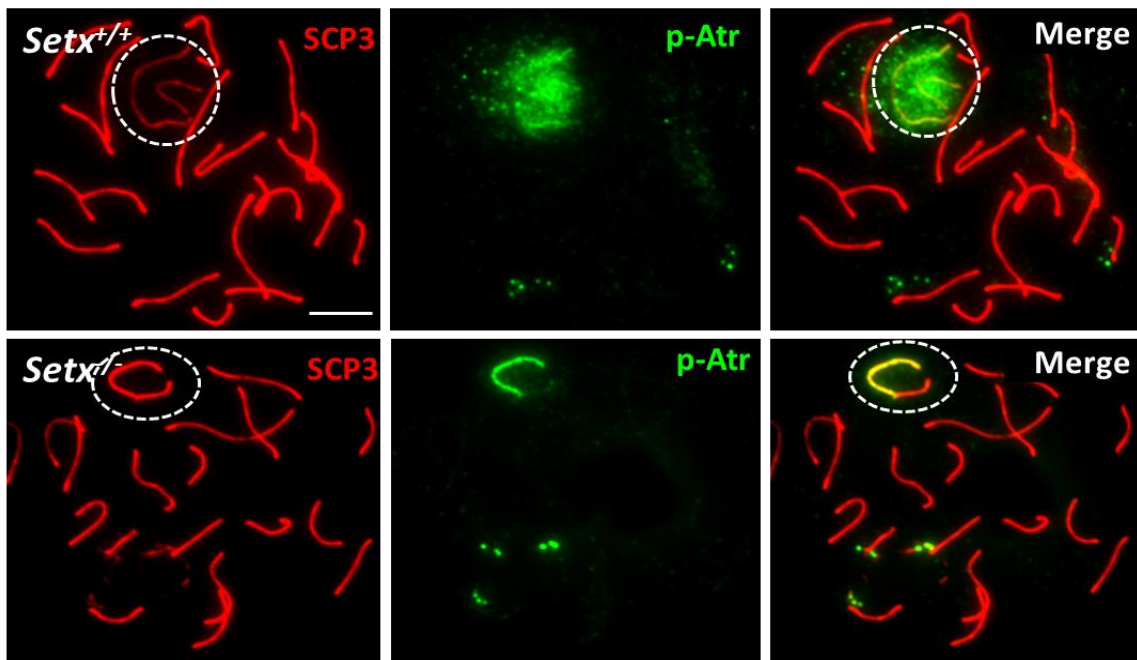


**Fig 4.10: Lack of diffusion of p-Atr (S428) over XY chromosomes in *Setx*<sup>-/-</sup> spermatocytes.** Immunostaining for p-Atr showed a cloud over the XY chromosomes in *Setx*<sup>+/+</sup> spermatocytes as expected, whereas p-Atr was retained on the axial element of the XY chromosomes in *Setx*<sup>-/-</sup> spermatocytes. Scale bar, 20  $\mu$ m. Dotted circle, XY chromosomes. Number of animals ( $n \geq 3$ ), a total of 50 cells per animal were analysed.

The stability and activity of Atr is modulated by its binding partner, Atrip<sup>218</sup>, hence the status of Atrip in spermatocytes of these mice was investigated. A strong signal for Atrip that localized largely to the axial element of the XY chromosomes in *Setx*<sup>+/+</sup> pachytene spermatocytes was observed. Additionally, some background staining for Atrip was observed on the autosomes. Although the localization of Atrip was similar to that observed in *Setx*<sup>+/+</sup> spermatocytes, a much fainter signal was observed in *Setx*<sup>-/-</sup> spermatocytes (Fig 4.11). Furthermore, a lack of background staining was also observed in *Setx*<sup>-/-</sup> spermatocytes. Thus, a reduction in Atrip protein levels and/or a lack of recruitment to the XY chromosomes appear to occur in *Setx*<sup>-/-</sup> pachytene-staged spermatocytes. This data combined with the defect in Atr diffusion in *Setx*<sup>-/-</sup> spermatocytes could possibly lead to deficiencies in the Atr signaling pathway and in turn account for the MSCI defect observed in *Setx*<sup>-/-</sup> mice.



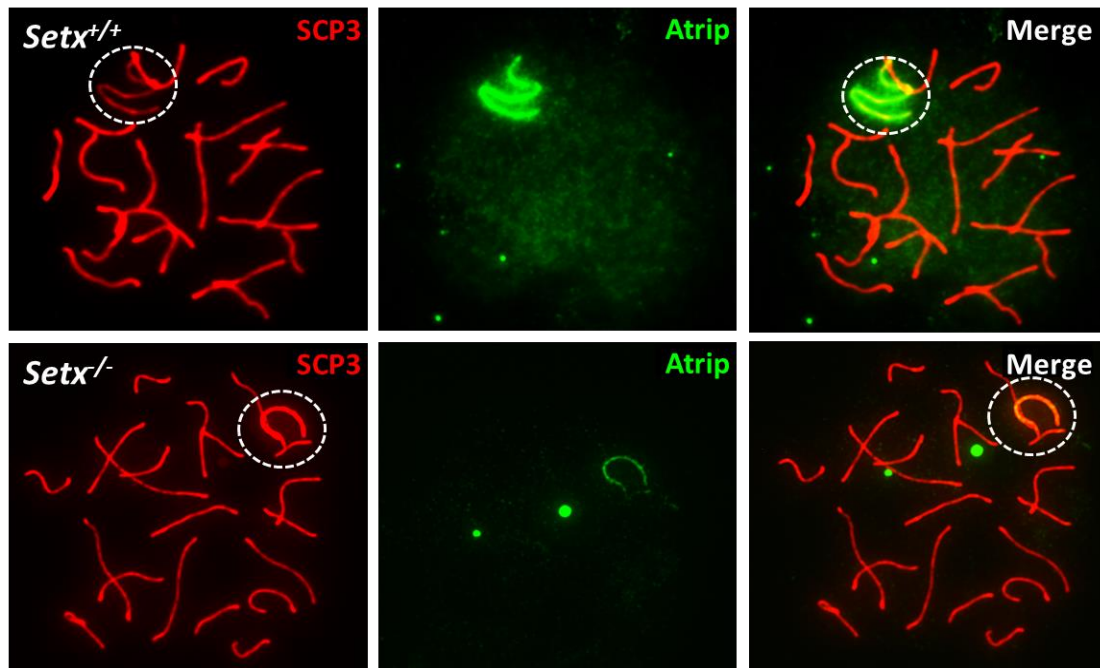


**Fig 4.11: Decreased levels of Atrip on XY chromosomes in *Setx*<sup>-/-</sup> spermatocytes.** Immunostaining for Atrip revealed a strong signal on the axial element of the XY chromosomes in *Setx*<sup>+/+</sup> spermatocytes. On the other hand, decreased staining intensity for Atrip was observed in *Setx*<sup>-/-</sup> spermatocytes. Scale bar, 20  $\mu$ m. Dotted circle, XY chromosomes. Number of animals ( $n \geq 3$ ), a total of 50 cells per animal were analysed.

Atr and Atrip play key roles in the DNA damage response and are mutually dependent partners in cell cycle checkpoint signaling pathways<sup>218</sup>. Atrip has been shown to be phosphorylated by Atr and also to regulate Atr expression<sup>218</sup>.

Given the abnormal localization of Atr and Atrip on the XY chromosomes, defective MSCI may be expected due to impaired Atr signaling. To ascertain this possibility, the functionality of the Atr pathway during MSCI in the absence of senataxin was investigated. To do this, immunostaining for three DDR proteins substrates that are phosphorylated by Atr, namely Rpa, Chk1 and Smc1<sup>225,226</sup>, was performed.

Phospho-Rpa S33 (p-Rpa) was observed to form a diffuse cloud over the XY chromosomes in *Setx*<sup>+/+</sup> spermatocytes whereas p-Rpa was found to localize predominantly on the axial element of the XY chromosomes instead in *Setx*<sup>-/-</sup> spermatocytes (Fig 4.12). This staining pattern is reminiscent of the Atr and p-Atr staining patterns observed in Fig 4.9 and Fig 4.10 and are not unexpected, given that Atr phosphorylates Rpa.

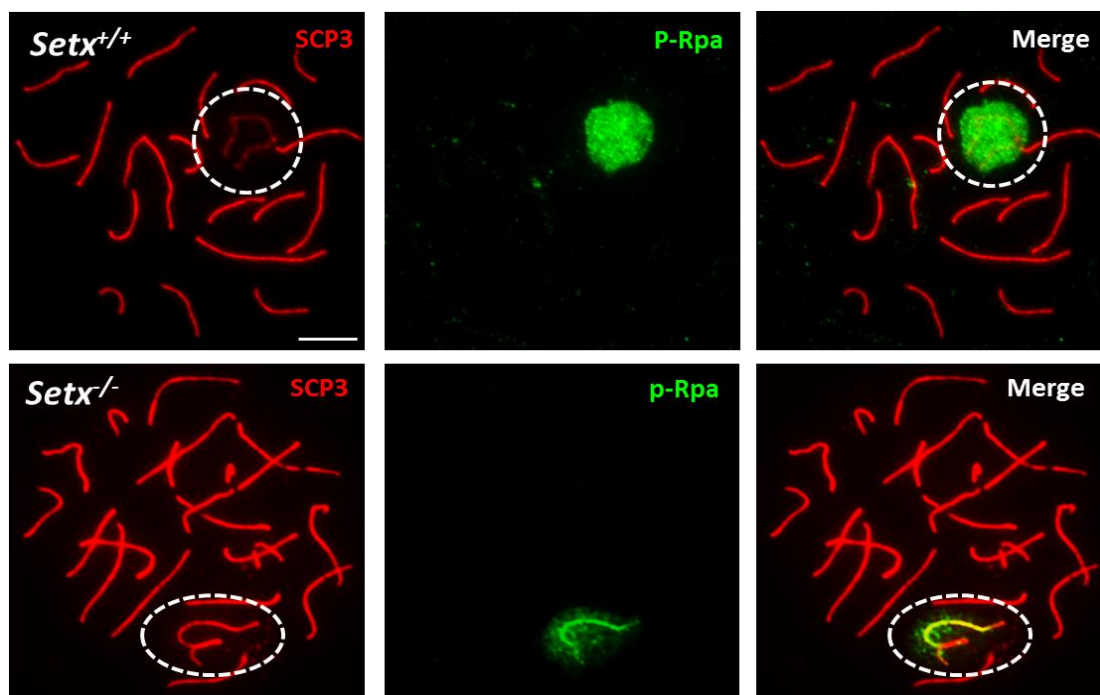


**Fig 4.12: Lack of diffusion of p-Rpa (S33) over XY chromosomes in *Setx*<sup>-/-</sup> spermatocytes.** Immunostaining for p-Rpa showed a cloud over the XY chromosomes in *Setx*<sup>+/+</sup> spermatocytes as expected, whereas p-Rpa was largely retained on the axial element of the XY chromosomes in *Setx*<sup>-/-</sup> spermatocytes; a pattern similar to those of Atr and p-Atr. Scale bar, 20  $\mu$ m. Dotted circle, XY chromosomes. Number of animals ( $n \geq 3$ ), a total of 50 cells per animal were analysed.

The localization of Chk1, a kinase required for cell cycle checkpoint activation and a well-documented downstream target of Atr for phosphorylation<sup>227,228</sup>, was next studied. Here, both unphosphorylated and the Atr-phosphorylated forms of Chk1 (S317) was investigated. Unphosphorylated Chk1 localization pattern was comparable between *Setx*<sup>+/+</sup> and *Setx*<sup>-/-</sup> spermatocytes (Fig 4.13A). However, while the localization of phospho-Chk1 (p-Chk1) formed a diffuse cloud over the XY chromosomes in *Setx*<sup>+/+</sup> spermatocytes, a reduced signal that was largely retained on the axial element was observed in *Setx*<sup>-/-</sup> spermatocytes (Fig 4.13B). Again, as expected, p-Chk1 staining pattern resembled that of Atr and p-Atr. Taken together, these data indicate a defect in Atr downstream signaling that could potentially contribute to the failure in MSCI observed in *Setx*<sup>-/-</sup> mice.

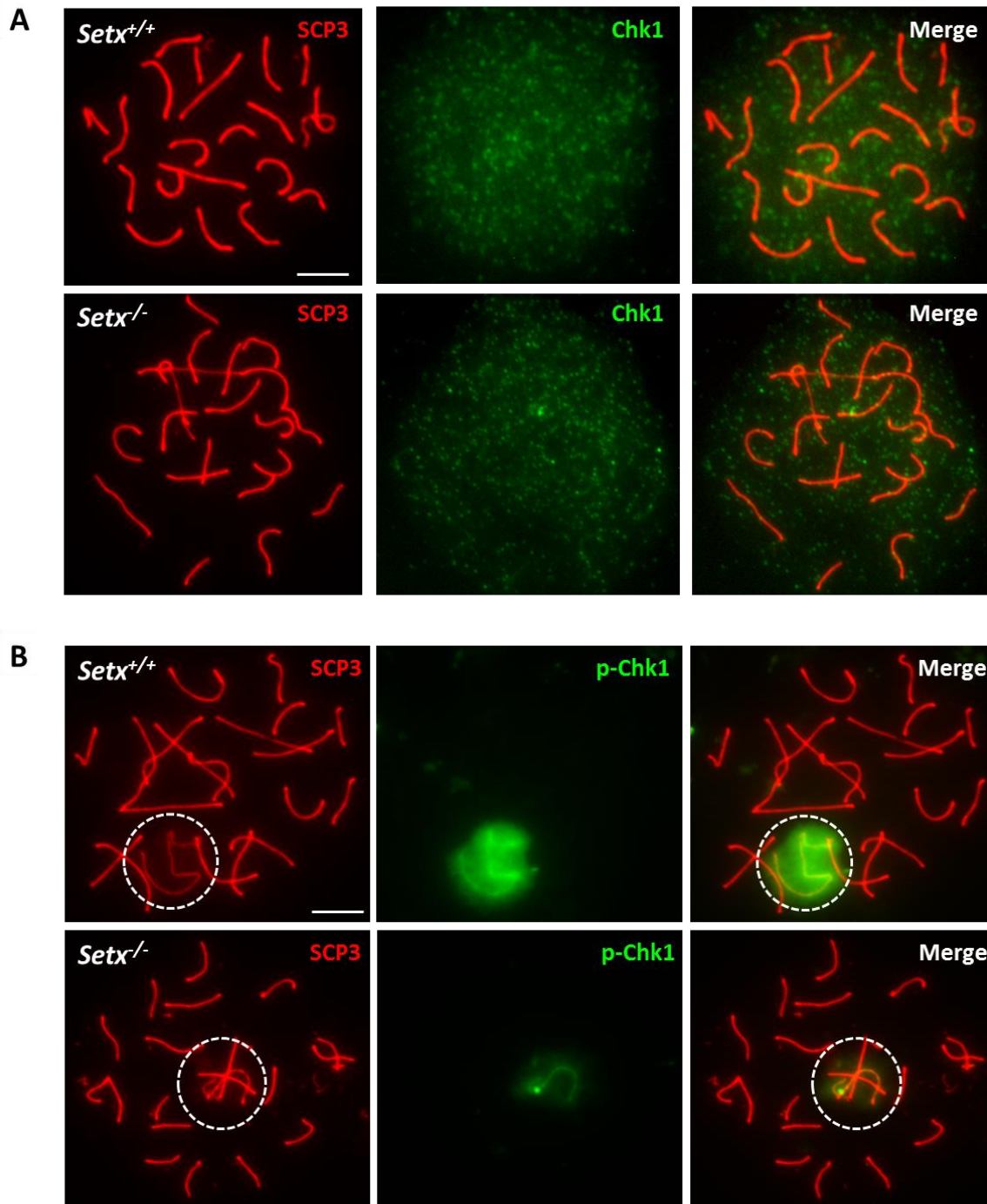


**Fig 4.13: Decreased levels of p-Chk1 over XY chromosomes in *Setx*<sup>-/-</sup> spermatocytes.** **A.** Unphosphorylated Chk1 localization pattern was comparable in spermatocytes of both *Setx*<sup>+/+</sup> and *Setx*<sup>-/-</sup> mice. **B.** Reduced levels of active Chk1, p-Chk1 (S317), over the XY chromosomes in *Setx*<sup>-/-</sup> spermatocytes were observed, localizing mainly to the axes of the XY chromosomes, a pattern similar to that of Atr and p-Atr. Scale bar, 20  $\mu$ m. Dotted circle, XY chromosomes. Number of animals ( $n \geq 3$ ), a total of 50 cells per animal were analysed.

Given the differences in the labeling pattern and intensity of the various DDR proteins involved in MSCI investigated thus far, whether or not these were caused by changes in protein levels was

examined. Western blotting on total cell extracts from *Setx*<sup>+/+</sup> and *Setx*<sup>-/-</sup> mice testes was performed. A slight reduction in Atr and p-Atr protein levels and a marked reduction in TopBP1 protein levels was observed in *Setx*<sup>-/-</sup> as compared to *Setx*<sup>+/+</sup> spermatocytes, which is in agreement with the previous immunostaining data (Fig 4.9 and 4.10). Additionally, differential gene expression data obtained from microarray analyses revealed no significant differences in the levels of TopBP1 gene expression germ cells of *Setx*<sup>+/+</sup> and *Setx*<sup>-/-</sup> mice (unpublished data). Strikingly Atrip was not detected in *Setx*<sup>-/-</sup> testes extracts (Fig 4.14). Note that a faint Atrip protein signal was detected by immunostaining in *Setx*<sup>-/-</sup> indicating a greater sensitivity for the antibody for immunostaining as compared to western blotting. Similar to TopBP1, RT-PCR performed for Atrip revealed no significant differences in mRNA levels in the testes of *Setx*<sup>+/+</sup> and *Setx*<sup>-/-</sup> mice. Collectively, these data point to either a defect in translation or stability of these proteins.

Similar levels of total Chk1 protein were observed between the mice. Gapdh was used as a loading control to ensure equivalent protein loading. Western blotting for p-Chk1 and p-Rpa could not be achieved despite multiple attempts.

Altogether, these findings support the reduced Atr activity and subsequent signaling defects observed in *Setx*<sup>-/-</sup> spermatocytes.

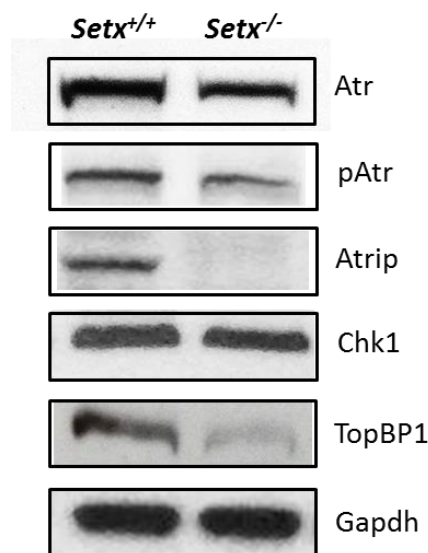


**Fig 4.14: DDR protein levels in *Setx*<sup>+/+</sup> and *Setx*<sup>-/-</sup> testes.** Western blotting for Atr, p-Atr, Atrip, Chk1 and TopBP1. A slight reduction in Atr and p-Atr protein levels was observed in *Setx*<sup>-/-</sup> as compared to *Setx*<sup>+/+</sup>. A lack of Atrip in *Setx*<sup>-/-</sup> spermatocytes was seen. Similar levels of Chk1 both *Setx*<sup>+/+</sup> and *Setx*<sup>-/-</sup> was observed. Gapdh was used as a loading control.

The inability to detect Atrip in total cell extracts from testes of *Setx*<sup>+/+</sup> and *Setx*<sup>-/-</sup> mice was particularly interesting. A recent report by Liu *et al.* 2013 showed that a protein member of the Never-in-Mitosis A (NIMA) related kinase family, Nek1, was important for the activity of the Atr-Atrip heterodimer<sup>229</sup>. Cells deficient in Nek1 failed to support autophosphorylation of Atr as well as the phosphorylation of several Atr substrates. They also showed that when Nek1 was knocked down using siRNA, Atrip protein levels were decreased but not that of Atr's, supporting the findings in Fig 4.17. Additionally, Nek1 is also highly expressed in meiotic germ cells<sup>230</sup>.

The localization of Nek1 was subsequently investigated via immunostaining on spermatocyte spreads. Results showed that Nek1 localized to the axial element of the autosomes, with a stronger signal on the XY chromosomes in *Setx*<sup>+/+</sup> spermatocytes. In contrast, Nek1 localized neither to the autosomes nor the XY chromosomes but formed a diffuse staining pattern throughout the nucleus in *Setx*<sup>-/-</sup> spermatocytes (Fig 4.15A). Western blotting for Nek1 protein from total cell extracts from testes of *Setx*<sup>+/+</sup> and *Setx*<sup>-/-</sup> mice revealed a decreased level in *Setx*<sup>-/-</sup> as compared to *Setx*<sup>+/+</sup> (Fig 4.15B). The decreased protein level of Nek1 as well as its mis-localization in *Setx*<sup>-/-</sup> spermatocytes suggests that senataxin may modulate the expression and/or localization of Nek1, and that a deficiency in Nek1 may account for the defect in Atr signaling observed in *Setx*<sup>-/-</sup> spermatocytes.

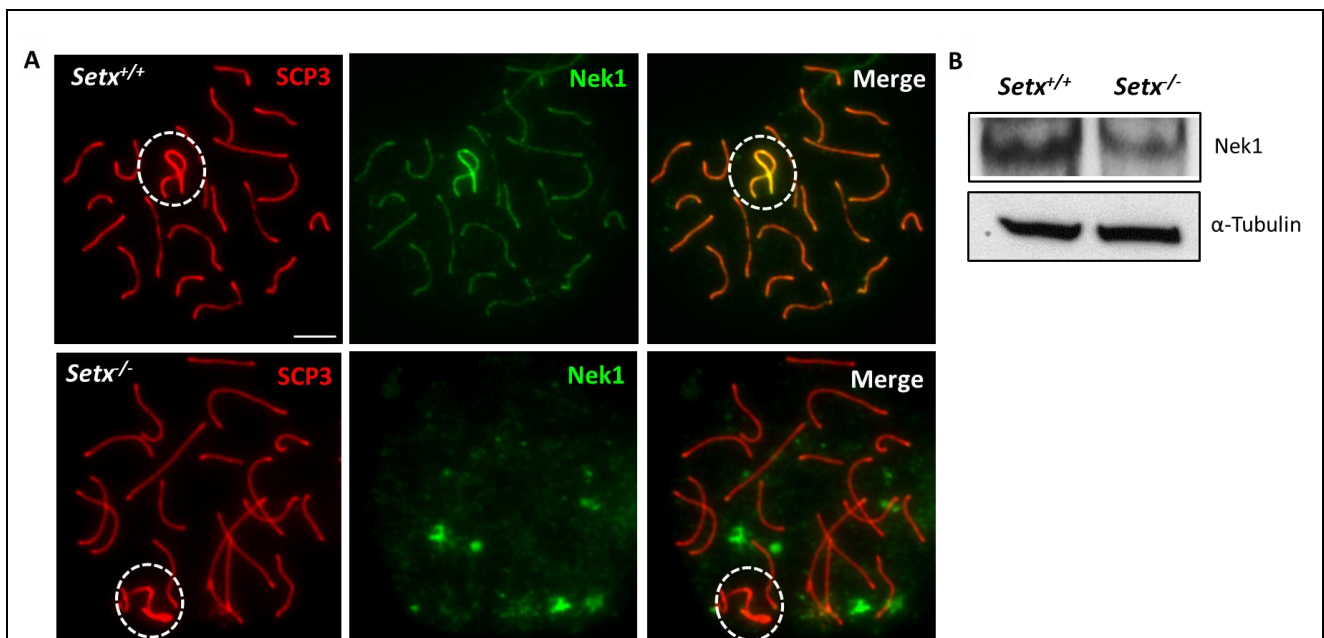


**Fig 4.15: Mis-localization of Nek1 in *Setx*<sup>-/-</sup> spermatocytes.** Nek1 was observed to localize specifically to the axial element of the autosomes with a stronger intensity on the XY chromosomes in *Setx*<sup>+/+</sup> spermatocytes whereas Nek1 in *Setx*<sup>-/-</sup> spermatocytes was granulated and scattered throughout the nucleus. Scale bar, 20  $\mu$ m. Dotted circle, XY chromosomes. **B.** Western blotting for Nek1 from total cell extracts from testes of *Setx*<sup>+/+</sup> and *Setx*<sup>-/-</sup> mice showed lower levels of Nek1 in

*Setx*<sup>-/-</sup> spermatocytes.  $\alpha$ -Tubulin was used as a loading control. Number of animals ( $n \geq 3$ ), a total of 50 cells per animal were analysed.

#### 4.2.6 Defect in XY heterochromatin formation in *Setx*<sup>-/-</sup> mice

MSCI triggers chromatin conformation changes via post-translational modification that leads to the transcriptional silencing of the XY body. One such modification is the ubiquitination of histone H2A (ubH2A), which has been shown to be associated with transcriptional silencing of XY chromatin regions<sup>231</sup>. Because of the continued presence of RNA Pol II on the XY chromosomes in *Setx*<sup>-/-</sup> spermatocytes as previously described in section 3.2.6 and the abnormal Atr localization and signaling, it was hypothesized that the ubiquitination of histone H2A would be defective in *Setx*<sup>-/-</sup> mice. The results in Fig 4.16 revealed the distinct accumulation of ubH2A as a diffuse cloud over the XY chromosomes in spermatocytes of *Setx*<sup>+/+</sup> mice, consistent with heterochromatin formation and transcriptional repression. In contrast, reduced labeling for ubH2A over the XY chromosomes of *Setx*<sup>-/-</sup> spermatocytes was observed, and unlike that in the spermatocytes of *Setx*<sup>+/+</sup> mice, ubH2A was also not localized to the XY chromosomes but distributed across the autosomes in *Setx*<sup>-/-</sup> mice as well.

The lack of ubH2A on the XY chromosomes is in agreement with the defective XY silencing observed in *Setx*<sup>-/-</sup> spermatocytes and suggests a differential conformation of chromatin, predominantly in the formation and distribution of heterochromatin. These findings indicate a major difference in ubH2A and heterochromatin distribution in *Setx*<sup>-/-</sup> spermatocytes, which may reflect a genome-wide abnormal transcriptional regulation in these cells. Indeed, this is supported by the observation of genome-wide differential gene expression following microarray analysis for *Setx*<sup>+/+</sup> and *Setx*<sup>-/-</sup> mouse testes (Dr Brent Fogel, Dr Olivier Becherel, unpublished data).

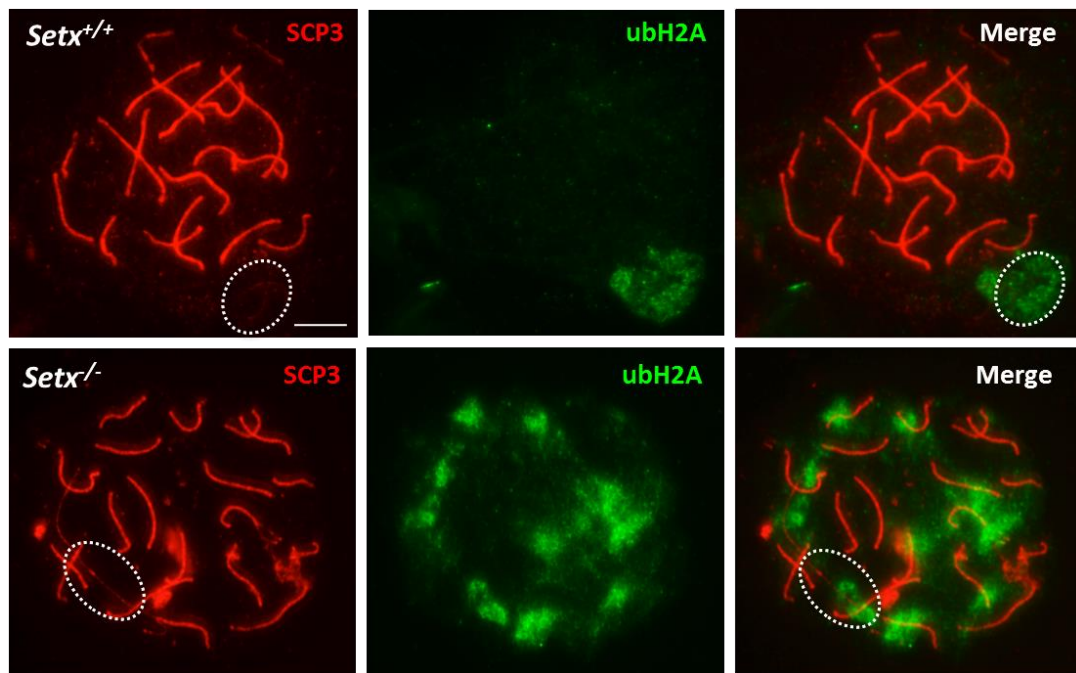


**Fig 4.16: Differential localization of ubH2A in *Setx*<sup>-/-</sup> spermatocytes.** Immunostaining against ubH2A revealed localized staining over the XY chromosomes as a diffused cloud in spermatocytes of *Setx*<sup>+/+</sup> mice. In contrast, ubH2A was observed to be distributed on the autosomes of *Setx*<sup>-/-</sup> spermatocytes, indicating a general defect in heterochromatin formation and transcription repression. Scale bar, 20  $\mu$ m. Dotted circle, XY chromosomes. Number of animals ( $n \geq 3$ ), a total of 50 cells per animal were analysed.

To provide additional evidence for a major difference in chromatin conformation in *Setx*<sup>-/-</sup> spermatocytes, another epigenetic marker believed to be associated with transcription repression, H3K4me1<sup>232</sup> was examined. Immunostaining against this marker revealed a strong signal over the XY chromosomes in *Setx*<sup>+/+</sup> spermatocytes, consistent with transcriptional repression. Some signal over the autosomes was also observed. In contrast, signal for H3K4me1 was not observed on the XY chromosomes of *Setx*<sup>-/-</sup> spermatocytes. A brighter signal on the autosomes of this marker was only observed, indicating a general defect in chromatin topology in *Setx*<sup>+/+</sup> mice that could possibly have contributed to the differences in transcription repression observed in these mice (Fig 4.17). Together with the presence of active RNA Polymerase II staining over the XY chromosomes and the increased expression of X- and Y-linked genes (Fig 3.15), these data provide substantial direct evidence for the lack of XY silencing.

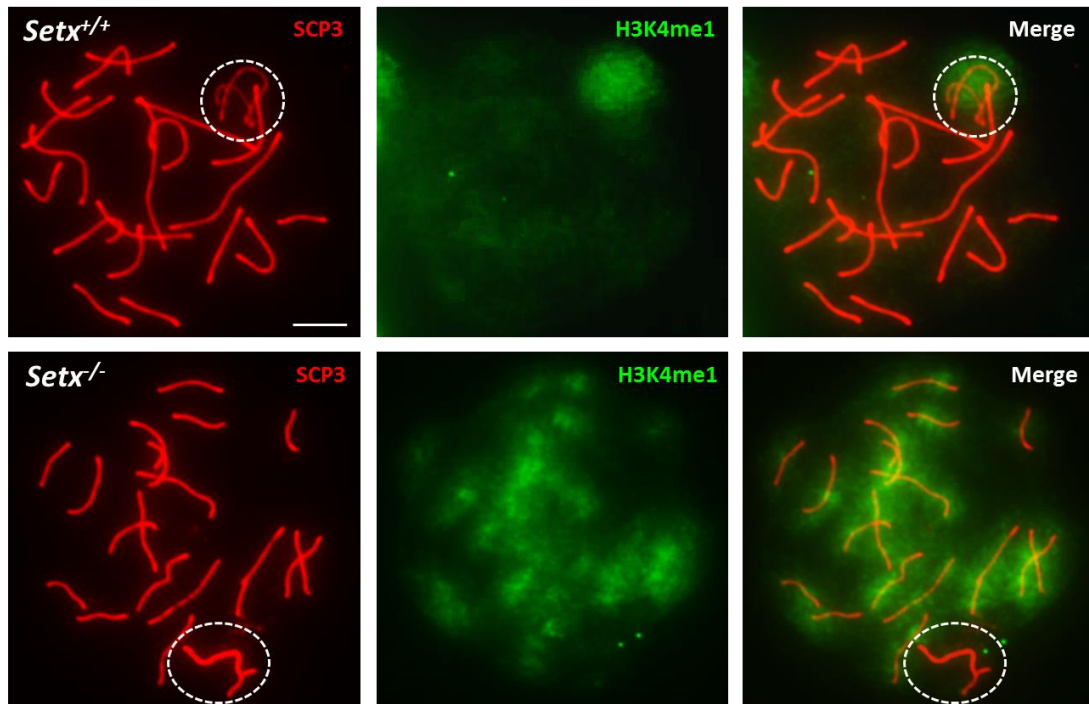


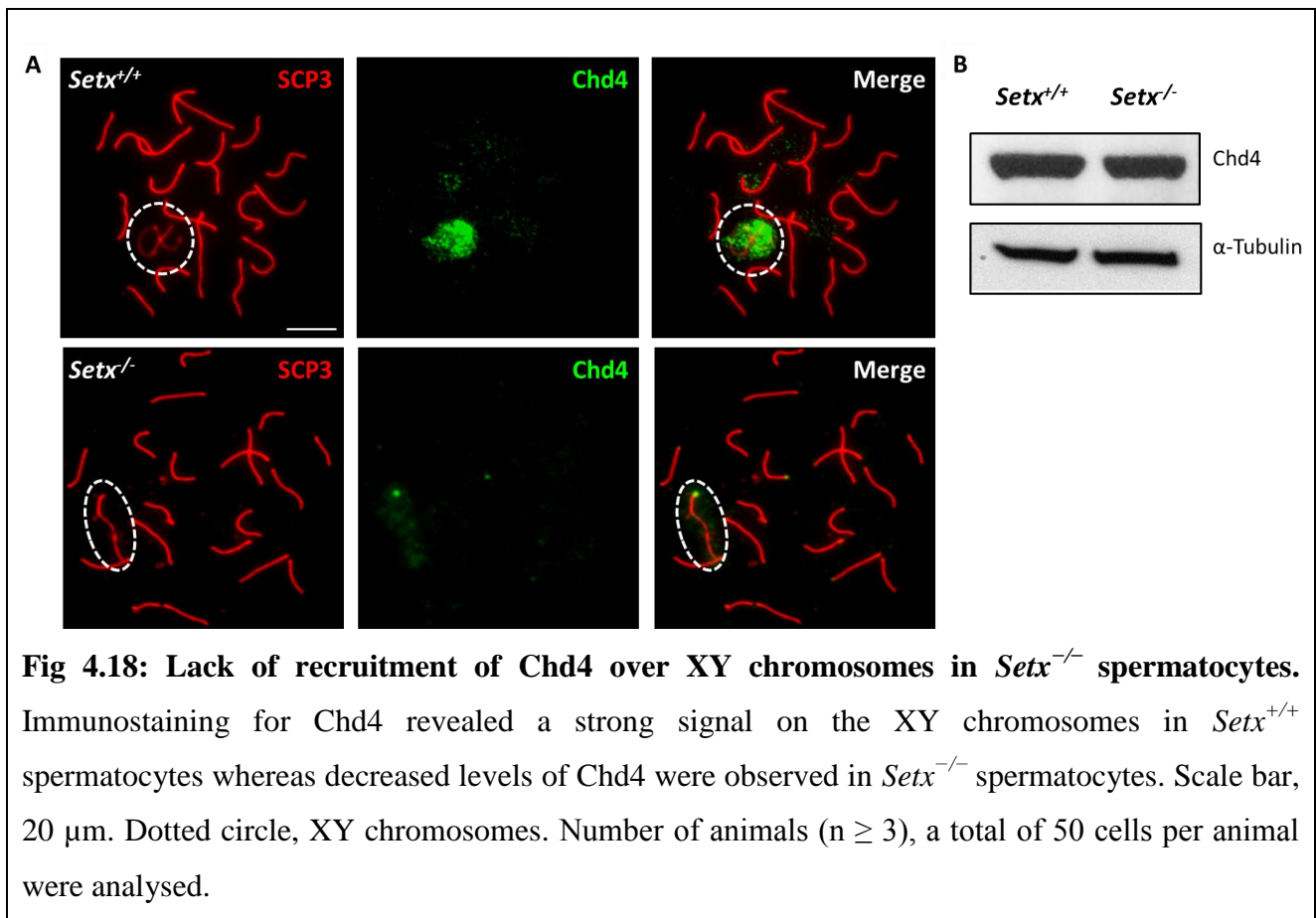
**Fig 4.17: Differential formation of heterochromatin of XY chromosomes in *Setx*<sup>-/-</sup> spermatocytes.** Immunostaining for the epigenetic marker H3K4me1 showed that suggesting a difference in chromatin topology between the mice. Scale bar, 20  $\mu$ m. Dotted circle, XY chromosomes. Number of animals ( $n \geq 3$ ), a total of 50 cells per animal were analysed.

Changes in the conformation of chromatin required for activation or silencing of transcription are dependent on chromatin remodelers. Through connectivity mapping of senataxin (Dr. Derek Richard, Queensland University of Technology, personal communication) as well as from previous findings by senataxin co-immunoprecipitation<sup>233</sup>, the chromodomain helicase binding DNA protein 4 (Chd4), a member of the nucleosome remodeling and deacetylase (NuRD) complex<sup>234</sup>, is thought to be an interacting partner of senataxin. Interestingly, Chd4 has also been reported to interact with Atr<sup>235</sup>, suggesting a link between Atr's role in mediating checkpoints induced by DNA damage and chromatin modulation via remodeling and deacetylation<sup>236</sup>. The abnormal Atr localization and defective downstream signaling together with the lack of XY silencing subsequently prompted us to investigate the status of Chd4 in *Setx*<sup>+/+</sup> and *Setx*<sup>-/-</sup> spermatocytes.

Immunostaining for Chd4 revealed similar localization to the pseudo-autosomal region (PAR) of the XY chromosomes in *Setx*<sup>+/+</sup> and *Setx*<sup>-/-</sup> spermatocytes, however, a much stronger signal was observed in *Setx*<sup>+/+</sup> spermatocytes (Fig 4.18A). To examine whether the faint Chd4 staining at the XY chromosomes in *Setx*<sup>-/-</sup> resulted from reduced protein levels, western blotting was performed on total protein extracts. Similar levels of Chd4 were observed in both *Setx*<sup>+/+</sup> and *Setx*<sup>-/-</sup> testes



extracts indicating that the faint Chd4 staining on the XY chromosomes in *Setx*<sup>-/-</sup> spermatocytes result from the lack of recruitment rather than reduced levels of the protein (Fig 4.18B). These data suggest that it is the mis-localization in the absence of senataxin, and not the lack of Chd4, which could possibly contribute to the defect in chromatin remodeling observed in *Setx*<sup>-/-</sup> spermatocytes.



While Chd4 was shown to interact with senataxin by co-immunoprecipitation in somatic cells<sup>233</sup>, it was important to determine whether senataxin and Chd4 interact *in vivo* in spermatocytes. PLA was performed between senataxin and Chd4 to assess for an *in situ* interaction between the two proteins. As shown in Fig. 4.19, an interaction between Chd4 and senataxin was observed at the XY chromosomes in *Setx*<sup>+/+</sup> spermatocytes. This interaction suggests that senataxin, together with Atr and Chd4 (and potentially as a part of the NuRD complex), are important for chromatin remodeling required for XY silencing. Furthermore, it is possible that absence of senataxin and/or Atr signaling prevents the recruitment of Chd4 to the XY chromosomes in *Setx*<sup>-/-</sup> spermatocytes.

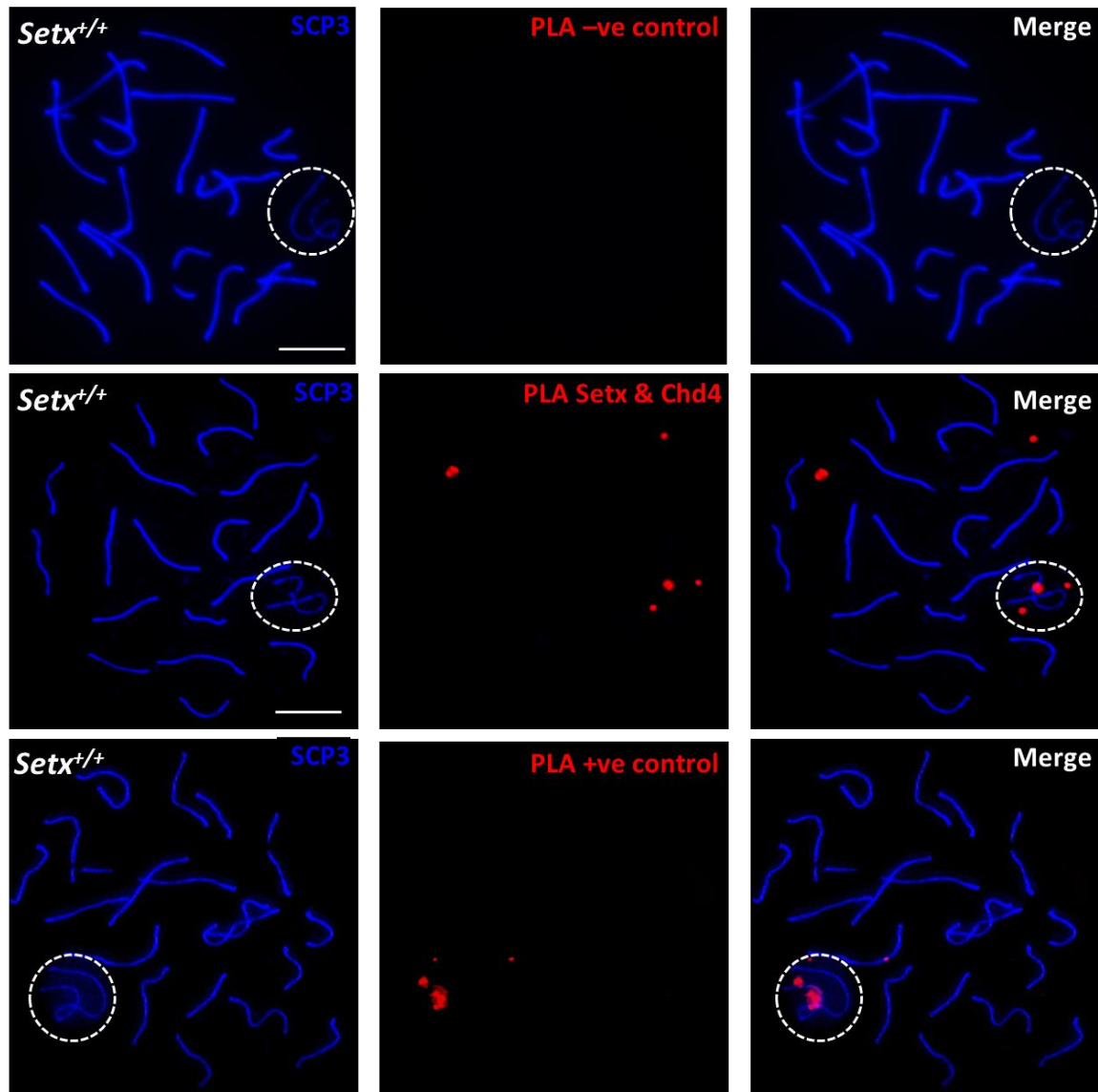


**Fig 4.19: *In situ* interaction of senataxin with Chd4 at the XY chromosomes during MSCI.** PLA between senataxin and Chd4 revealed an interaction between these proteins at the XY chromosomes in spermatocytes of *Setx*<sup>+/+</sup> mice (middle panels). An appropriate negative control containing no primary antibodies (top panels) as well as a positive control using antibodies against Brca1 and Atr, two proteins known to interact directly<sup>216</sup>, was used (bottom panels). Scale bar, 20  $\mu$ m. Dotted circle, XY chromosomes. Number of animals ( $n \geq 3$ ), a total of 50 cells per animal were analysed.

### **4.3 Discussion**

In this chapter the localisation of several key DDR factors involved in MSCI was investigated to better understand the molecular mechanism involved and to elucidate the defect in MSCI observed in *Setx*<sup>-/-</sup> mice.

Protein post-translational modifications (PTM) are important and participate in nearly all aspects of cellular physiology. Amongst PTMs such as glycosylation and phosphorylation, SUMOylation [small ubiquitin-like modifier (SUMO)] has emerged as a major regulator of nuclear functions; playing a key role in transcriptional regulation and in organising the trafficking of DDR proteins at sites of DNA damage<sup>237</sup>. As a consequence, SUMO modifications have been associated with many disease conditions, ranging from neurodegeneration to diabetes and inflammation<sup>238</sup>. Four major SUMO paralogues have been identified: SUMO-1, 2, 3 and 4, all being abundantly expressed in different tissues. SUMO-1 and SUMO-2/3 have been studied during mouse and human spermatogenesis, where they were shown to localize to different sub-domains of germ cells<sup>131,133,138</sup>. The differential localization patterns suggest multiple roles for SUMO during germ cell development. SUMO was found to localise to sites of DNA DSBs during spermatogenesis and is involved in the stress response<sup>239</sup>, in particular, the appearance of SUMO-1 was reported to precede the accumulation of  $\gamma$ H2AX on the XY chromosomes, indicating a specific role for SUMO-1 in initiating MSCI<sup>131</sup>. SUMO-1 localized only to the axial element of the XY chromosomes in *Setx*<sup>-/-</sup> spermatocytes as opposed to the diffused cloud pattern observed in *Setx*<sup>+/+</sup> spermatocytes, suggesting possible DDR protein trafficking disruption which could account for impaired MSCI observed in *Setx*<sup>-/-</sup>. Furthermore, it was shown in this Chapter that endogenous senataxin is SUMOylated, which is in agreement with previous reports<sup>215,240</sup> and that SUMOylated senataxin was present on the XY chromosomes. This is relevant given the recent findings from Richard *et al.* 2013 showing a SUMO-dependant interaction between senataxin and Rrp45, a subunit of the exosome at sites of transcription-related DNA damage<sup>240</sup>. The exosome complex 3'-5' exonuclease is an important multi-subunit component of the RNA processing machinery that monitors RNA turnover and quality<sup>241</sup>. Hence, it is possible that in *Setx*<sup>+/+</sup> pachytene-staged spermatocytes, SUMOylated senataxin interacts with this exosome complex on the XY chromosomes to ensure proper RNA processing and degradation, and to facilitate MSCI. In contrast, the absence of SUMOylated senataxin in *Setx*<sup>-/-</sup> spermatocytes could possibly disrupt this interaction and in turn impact on RNA processing and degradation, potentially leading to the expression of unstable RNA species, failure in MSCI and germ cell apoptosis. The ideal demonstration to confirm the SUMOylation of senataxin would be to mutate putative SUMOylation sites in senataxin to ablate

SUMOylation. However, our primary aim is to study the *in vivo* role of senataxin in meiosis and this by definition imposes certain limitations on the types of experiments that can be performed, in particular, the study of post-translational modifications. This includes the re-expression of senataxin constructs mutated in putative SUMO sites in germ cells.

Senataxin specifically localizes to the XY body in pachytene partially co-localizing with Brca1 and Atr, suggesting that it may have a role in MSCI. While Brca1 coats the unsynapsed axis of the XY chromosomes, senataxin appears as a more diffuse distribution on the XY chromatin. The diffuse staining pattern of senataxin over the XY body is reminiscent of other DNA repair proteins that include Atr, Mdc1 and TopBp1<sup>126,192,197</sup>. Prior to MSCI initiation, Brca1 is targeted to the unsynapsed axial elements of the X and Y chromosomes where it remains throughout spermatogenesis<sup>134</sup>. It subsequently recruits ATR to the axial elements where it phosphorylates histone H2AX. Atr localization to the XY chromosomes at the onset of MSCI was disrupted in mice with a mutant form of the tumour suppressor protein Brca1 (Brca1<sup>Δ11/Δ11</sup>). In the mutant pachytene cells, there is evidence of MSCI failure since Atr is mostly present at autosomal, non-XY sites, where it co-localizes with aberrant sites of H2AX phosphorylation. The meiotic phenotype observed in *Setx*<sup>-/-</sup> mice resembles that seen in *Brca1*<sup>Δ11/Δ11</sup> *p53*<sup>+/-</sup> mice where although chromosomal synapses occur normally and spermatocytes progress through to pachytene stage, no chiasmata were observed as well<sup>242</sup>. Similarly, DNA DSBs were not repaired in the correct temporal framework, as demonstrated by persistent γH2AX foci in *Brca1*<sup>Δ11/Δ11</sup> *p53*<sup>+/-</sup> spermatocytes<sup>242</sup>.

The failure to complete meiosis due to the persistence of unrepaired DSB, the lack of crossing-over and defective MSCI is common to the *Setx* and *Brca1* mutants and this prompted us to investigate whether the recruitment of senataxin to the XY chromosomes would depend on Brca1. It was observed that the recruitment of senataxin is indeed Brca1-dependent since senataxin was not recruited to the XY chromosomes in *Brca1*<sup>Δ11/Δ11</sup> *p53*<sup>+/-</sup> mutant mice even though the smaller Brca1 mutant protein lacking exon 11 still localized to the axes of these chromosomes<sup>243</sup>. Brca1-dependent senataxin recruitment to the XY body may be indirect since an *in situ* direct endogenous protein-protein interaction through a proximity-ligation assay (PLA) and co-immunoprecipitations of the endogenous proteins was not detected. How Brca1-dependent recruitment of senataxin to the XY body occurs remains unclear. In contrast to our findings, Hill *et al.* 2014 recently reported the interaction of senataxin with the C-terminus of BRCA1 using the yeast two-hybrid system and tandem-affinity purification followed by mass spectrometry identification (TAP-MS)<sup>244</sup>. The difference may result from overexpression employed as in the case of Hill *et al.* 2014 versus endogenous protein *in situ* interaction and co-immunoprecipitation.

Once Brca1 localizes to the axial elements of the XY chromosomes, it recruits Atr which in turn diffuses out into XY chromatin and phosphorylates histone H2AX, triggering MSCI<sup>120,134</sup>. Loss of senataxin does not change the overall distribution of Brca1 on the XY chromosomes however Atr is no longer diffusely distributed over the XY chromosomes but is instead retained on the axial element of the XY chromosomes, similar to that of Brca1 as visualized by immunostaining. The axial staining of Atr in *Setx*<sup>-/-</sup> mouse spermatocytes suggests that (i) meiosis proceeds only to early /mid pachytene in these mice and/or (ii) that Atr re-localization is dependent on senataxin. Given the key role of Atr in MSCI initiation, the localization of an active, phosphorylated form of Atr was determined. Several phosphorylated forms of Atr have been reported<sup>245</sup>. Nam *et al.* 2011 have shown that phosphorylation of Atr on threonine 1989 (p-Thr1989) is regulated by DNA damage, depends on Atr kinase activity, and appears concurrently with Atr-dependent phosphorylation of Chk1<sup>246</sup>. Phosphorylation of Thr1989 relies on Rpa, Atrip, and Atr kinase activity, but unexpectedly not on the Atr stimulator TopBp1<sup>245</sup>. Recruitment of Atr-Atrip to Rpa-ssDNA leads to congregation of Atr-Atrip complexes and promotes p-Thr1989 in trans. p-Thr1989 is directly recognized by TopBp1, enabling TopBp1 to engage Atr-Atrip, to stimulate the Atr kinase, and to facilitate Atr substrate recognition. Functionally, p-Thr1989 is not essential for the Atr-Chk1 signalling axis following replication stress but supports cellular viability<sup>246</sup>. Hence, p-Thr1989 may not be important for ATR function and the low conservation of Thr1989 even among vertebrate Atr orthologs and the lack of noticeable activation and signalling defects support this conclusion. Interestingly, Thr1989 is not a conserved residue in the mouse, thus preventing its monitoring during MSCI. .

The lack of conservation of this residue in the mouse suggests that another residue may possibly take up the function of Thr1989. Several other phosphorylation sites in human ATR protein include Ser428, 435, 436, 437<sup>245</sup>. Out of these sites, only Ser428 has been functionally characterized for Atr activation<sup>245,247,248</sup> and is conserved in the mouse sequence<sup>247</sup> (equivalent to murine S431). Therefore to determine Atr activation during MSCI, immunostaining with an anti-phospho Ser428 Atr (p-Ser428) antibody was performed. As expected, a similar pattern to that of un-phosphorylated Atr was seen in *Setx*<sup>+/+</sup> and *Setx*<sup>-/-</sup> spermatocytes, respectively. Relevant to MSCI and transcription regulation, recent evidence support a role for Atr/Chk1 signalling pathways in the alternative splicing of the TAF1 pre-mRNA<sup>249</sup>. Indeed, experiments with pharmacological inhibitors also indicate that Atr kinase activity is necessary to signal alternative splicing of the TAF1 pre-mRNA in response to camptothecin treatment<sup>249</sup>, highlighting a novel role for the Atr/Chk1 signalling pathway in regulating alternative splicing. More recently, Chandris *et al.* 2010 studied the

distribution and localization of active, p-Ser428-Atr in regards to the regulation of mRNA splicing and polyadenylation<sup>250</sup>. They reported a distinctive pattern of p-Ser428-Atr in the nucleus of senescent cells when mRNA splicing and polyadenylation was perturbed, implicating this phosphosite in mRNA processing<sup>250</sup>. Hence, the role of Atr in MSCI may not only be restricted to the phosphorylation of H2AX to initiate MSCI, but it may also play a role in the RNA processing of X- and Y-linked genes.

While a role for active p-Ser428 Atr in mRNA processing during MSCI remains unclear, its lack of diffusion in the XY chromatin domain suggest a possible defect in the Atr/Chk1 signalling pathway. Indeed, two substrates for phosphorylation by Atr, phospho-Rpa and phospho-Chk1 were observed to be restricted to the axes of the XY chromosomes in *Setx*<sup>-/-</sup> spermatocytes. This is in contrast to the expected, diffuse cloud seen in *Setx*<sup>+/+</sup> spermatocytes, thus indicating a defect in Atr signalling in *Setx*<sup>-/-</sup> spermatocytes during meiosis. In addition to the abnormal Atr localization pattern over the XY chromosomes in *Setx*<sup>-/-</sup> spermatocytes, a reduction in Atrip, the obligate partner of Atr, was shown. Although a very faint signal for Atrip was detected on the axes of the XY chromosomes by immunostaining, western blotting revealed an absence of the protein. It is important to note that western blotting was performed on whole testes extracts which contain multiple cell types such Sertoli cells, Leydig cells, spermatogonia and spermatocytes at various stages, hence a dilution of the signal can be expected and this may explain the absence of Atrip protein observed in *Setx*<sup>-/-</sup> testes extracts. While a reduction in Atrip was observed in *Setx*<sup>-/-</sup>, comparable levels of Atr protein to that in *Setx*<sup>+/+</sup> was detected. A similar observation regarding Atr and Atrip levels was found after the down-regulation of NIMA (never in mitosis gene a)-related kinase 1 (Nek1), a Ser/Thr kinase involved in cell cycle regulation<sup>229</sup>. Nek1 is involved in the DNA damage response and has been shown to associate with and stabilize the Atr-Atrip complex. Nek1 also promotes the activation of Atr with its kinase activity and is required for maintaining Atrip levels in cells<sup>229</sup>. Interestingly, Nek1 is highly expressed in germ cells, with a distribution consistent with a role in meiosis<sup>230</sup>. Evidence of Nek1 mis-localization as well as a reduction in its protein levels in *Setx*<sup>-/-</sup> spermatocytes was obtained via immunostaining and western blotting respectively, which may account for the reduction in Atrip protein levels and contribute to the defect in the Atr/Chk1 signalling pathway during MSCI. To demonstrate whether Nek1 is responsible for the defect in Atr signaling, the re-expression of Nek1 in germ cells would be expected rescue this phenotype. However, limitations exist on the types of experiments that can be performed to study this *in vivo*.

Another factor that could have contributed to the defect in the Atr/Chk1 signalling pathway in *Setx*<sup>-/-</sup> spermatocytes is the lack of SUMOylation on Atrip. It was recently reported that the

SUMOylation of Atrp was shown to enhance protein-protein interactions along the ATR pathway during DNA damage signalling<sup>221</sup>. Hence, having reduced levels of Atrp or even SUMOylated Atrp in *Setx*<sup>-/-</sup> spermatocytes is likely to affect the diffusion of DDR factors on the XY chromosomes in the Atr pathway during MSCI.

Several histone modifications that allow for changes in chromatin topology have been reported to occur over the XY chromosomes during MSCI and these include acetylation, methylation and ubiquitination<sup>232,251</sup>. Chromatin topology modification is important as it allows access of key binding sites to essential factors involved in meiotic-related processes such as recombination, DDR and MSCI<sup>252</sup>. One such modification associated with XY silencing during MSCI is the ubiquitination of histone H2A (ubH2A)<sup>253</sup>. In contrast to *Setx*<sup>+/+</sup> spermatocytes, a reduction of ubH2A over the XY chromosomes and the increase of ubH2A on the autosomes in *Setx*<sup>-/-</sup> spermatocytes indicate extensive anomalies in chromatin structure and transcriptional activity in the absence of senataxin in these cells. Another histone modification associated with transcriptional silencing of the XY chromosomes during MSCI is the mono-methylation of histone H3 on lysine 4 (H3K4me1). H3K4me1 has been reported to be evenly distributed over the entire nucleus of spermatocytes during the leptotene and zygotene stages, intensely labelling only the XY chromosomes during pachytene and diplotene stages<sup>232</sup>. In *Setx*<sup>-/-</sup> pachytene-staged spermatocytes, H3K4me1 labelling was not only more intense on the autosomes but was also excluded from the XY chromosomes, further supporting the evidence found with ubH2A. Additionally, genome-wide gene expression profiling using microarray has similarly confirmed a widespread transcription deregulation in spermatocytes of *Setx*<sup>-/-</sup> mice (Dr Brent Fogel, Dr Olivier J. Becherel, personal communication).

Several protein complexes also participate in chromatin remodelling via histone modifications and these include the Sin3a, SWI/SNF, and nucleosome remodelling deacetylase (NuRD) complexes<sup>254,255</sup>. The NuRD complex is associated with transcription regulation via chromatin remodelling, cell cycle progression and differentiation, as well as overall genomic stability<sup>255,256</sup>. The chromodomain helicase DNA binding protein 4 (Chd4) is the major catalytic subunit of the NuRD complex and is involved in epigenetic transcription silencing via deacetylation of histones as well as in DNA damage repair. Reports have shown that in the absence of Chd4, cells are hypersensitive to ionizing radiation and accumulate DNA DSBs<sup>257,258</sup>. It was also shown that Chd4 not only promotes DNA repair but also suppresses transcription at sites of damage<sup>257</sup>. Chd4 was recently reported to be SUMOylated<sup>259</sup>, and given that SUMOylation has been associated with DNA repair and heterochromatin formation<sup>238,239,260</sup>, the localization of Chd4 to the XY

chromosomes might suggest its role in modulating chromatin topology and XY silencing during meiosis. Interestingly, Chd4 was also reported to interact with Atr as well as with senataxin<sup>233,261</sup>. Chd4 as a phosphorylation target of the Atm/Atr kinase family could link the Atm/Atr pathways to chromatin remodelling, in particular heterochromatin and gene silencing. Hence, the defect in Atr/Chk1 signalling and the altered Chd4 distribution in *Setx*<sup>-/-</sup> spermatocytes are likely to be responsible for the defect in MSCI observed in these mice.

Altogether, the findings presented in this Chapter highlight the molecular mechanism and the different components that can contribute to the defect in MSCI observed in male *Setx*<sup>-/-</sup> mice, thereby providing evidence for a crucial role of senataxin in coordinating DNA damage repair, particularly through the Atr/Chk1 signalling pathway, chromatin remodelling and transcription silencing during MSCI (Fig 4.20).

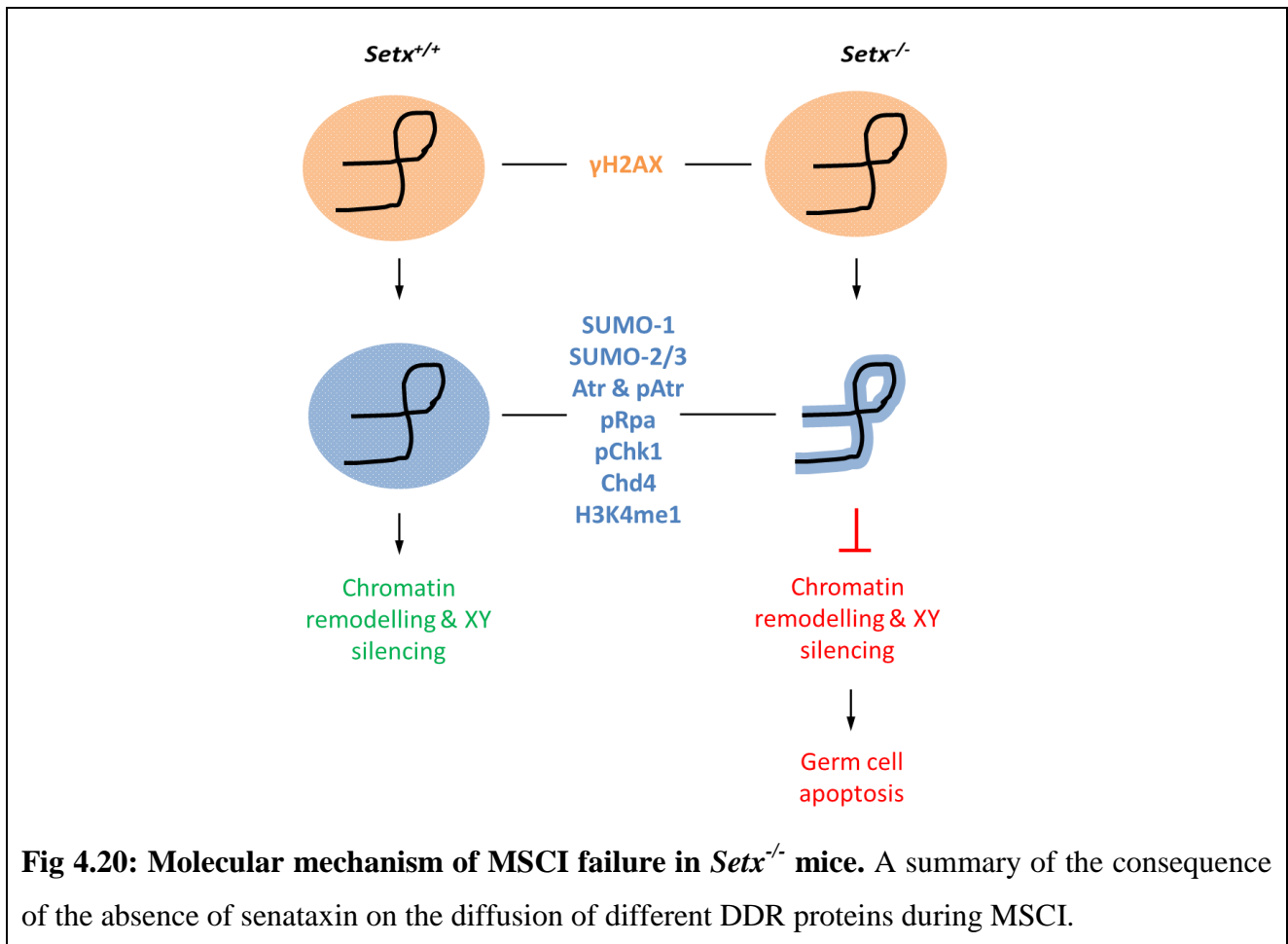


**Fig 4.20: Molecular mechanism of MSCI failure in *Setx*<sup>-/-</sup> mice.** A summary of the consequence of the absence of senataxin on the diffusion of different DDR proteins during MSCI.





## **CHAPTER 5: Senataxin & R-loop Resolution**

## **5.1 Introduction**

As previously mentioned in section 1.2.3, senataxin is a protein found to be involved in transcription regulation, several RNA processing activities such as in mRNA splicing and splice site selection, splicing efficiency, termination of transcription, and more recently, R-loop resolution<sup>63,71,73</sup>. A recent report by Yüce and West 2013 showed that senataxin forms distinctive foci in nuclei of HeLa and U2OS cells upon exposure to replication stress. They also showed the loss of these foci following transcription inhibition and R-loop resolution. Their results indicate that senataxin not only localizes to sites of collision between the replication and transcription machinery, but that it is also targeted to R-loops, where it plays an important role at the interface of transcription and the DNA damage response<sup>233</sup>.

R-loops are naturally occurring DNA/RNA hybrid structures that form behind elongating RNA polymerase by the interaction between the nascent mRNA and its ssDNA template from which it was transcribed, particularly over G-rich regions<sup>150,151,152</sup>. Although the exact function of these R-loop structures remains unclear, it has been hypothesized that they are required for efficient transcription initiation and termination and that they induce transcription-associated recombination and other mutagenic events such as immunoglobulin class-switch recombination and somatic hyper-recombination in B lymphocytes<sup>74,75</sup>.

Replication and transcription are fundamental features of DNA metabolism that can occur on the same DNA template strand<sup>262</sup>. It has been postulated that collisions between the DNA replication and transcription machinery can cause DNA SSBs/DSBs, chromosomal rearrangements, R-loop formation and consequently genomic instability<sup>233,262</sup>. Additionally, it was also suggested that conflicts between replication and transcription are not restricted to the physical interaction or collision between polymerases but that the transcription process itself can also hamper replication through the natural formation of R-loops at pause sites during transcription<sup>150,262</sup>. R-loops potentially stall RNA polymerase during transcription, thereby interfering with the progression of replication forks through the collision of these two processes<sup>165</sup>. To protect the genome from abortive replication-transcription encounters, various mechanisms exist within a cell that prevent this phenomenon and these include the activities of several helicases (e.g. Rrm3 and Dhx9) and DNA topoisomerases (e.g. Top1 and Top2)<sup>165,263</sup>.

Several other proteins involved in DNA damage repair (DDR), such as ataxia-telangiectasia mutated (ATM), aprataxin (APTX) and tyrosyl-DNA phosphodiesterase 1 (TDP1) in addition to

senataxin (SETX), have also been implicated in transcription processes<sup>260,264,265</sup>. ATM has been shown to be a regulator of two genes, *MCL1* and *Gadd45a*, in response to histone deacetylation (HDAC) inhibition<sup>266</sup>; nucleolar localization and function of APTX was shown to be dependent on rRNA transcription<sup>56</sup>; TDP1 is known to facilitate transcription by RNA Polymerase I in trypanosomes<sup>267</sup> and SETX, as discussed previously, is involved in RNA processing<sup>63,71</sup>. Mutations in the genes encoding these DDR proteins (ATM, APTX, TDP1 and SETX) also cause autosomal recessive cerebellar ataxias (ARCA) in humans and knockout mouse models for these disorders have been generated, providing further insight into the roles of these proteins in the DNA damage response. Given that unresolved R-loops can cause DNA breaks<sup>75,268</sup>, the absence of these key DDR proteins required for repairing DNA breaks may then lead to increased genomic instability.

To determine whether R-loops can contribute to the genomic instability observed in these ARCA models, whether R-loop formation is a general phenomenon across tissues, its accumulation and how it can lead to genomic instability and cell death were investigated. It was first hypothesized that the lack of gross neurological phenotype in the ARCA mouse models may be related to a threshold effect in the nervous tissue. It was therefore decided to expose these mice to topotecan hydrochloride (TPT), a DNA damaging agent that readily induces R-loop formation in cells<sup>269</sup>, to assess whether additional DNA damage can trigger the formation of R-loops in the nervous tissue of these mutant animals.

Section 5.2 is a publication that reports the findings from our study where it is shown for the first time, R-loops accumulate along candidate genes from *Setx*<sup>-/-</sup> mice using a DNA/RNA immunoprecipitation (DRIP) assay. These findings also show that treatment of ARCA mouse models with TPT (2mg/kg/day) induces the formation of R-loops structures only in proliferative tissues and not in post-mitotic tissues, further supporting a dependence of R-loop formation on the concomitant activity of replication and transcription. Hence, it is hypothesized that R-loops may represent a currently neglected widespread lesion and the presence of unresolved R-loops may contribute to overall genomic instability observed in DNA damage mouse models.

Additional data from this study that were not included in the publication are described in Section 5.3.

# R-Loops in Proliferating Cells but Not in the Brain: Implications for AOA2 and Other Autosomal Recessive Ataxias

Abrey J. Yeo<sup>1,2</sup>, Olivier J. Becherel<sup>1,3</sup>, John E. Luff<sup>1</sup>, Jason K. Cullen<sup>1</sup>, Thidathip Wongsurawat<sup>4,5</sup>, Piroon Jenjaroenpoon<sup>4</sup>, Vladimir A. Kuznetsov<sup>4,5</sup>, Peter J. McKinnon<sup>6</sup>, Martin F. Lavin<sup>1,2\*</sup>

**1** QIMR Berghofer Medical Research Institute, Radiation Biology and Oncology Laboratory, Brisbane, Queensland, Australia, **2** School of Medicine, University of Queensland, Herston, Queensland, Australia, **3** School of Chemistry and Molecular Biology, University of Queensland, St. Lucia, Queensland, Australia, **4** Department of Genome and Gene Expression Data Analysis, Bioinformatics Institute, Singapore, Singapore, **5** School of Computer Engineering, Nanyang Technological University, Singapore, Singapore, **6** Department of Genetics and Tumour Cell Biology, St. Jude Children's Research Hospital, Memphis, Tennessee, United States of America

## Abstract

Disruption of the *Setx* gene, defective in ataxia oculomotor apraxia type 2 (AOA2) leads to the accumulation of DNA/RNA hybrids (R-loops), failure of meiotic recombination and infertility in mice. We report here the presence of R-loops in the testes from other autosomal recessive ataxia mouse models, which correlate with fertility in these disorders. R-loops were coincident in cells showing high basal levels of DNA double strand breaks and in those cells undergoing apoptosis. Depletion of *Setx* led to high basal levels of R-loops and these were enhanced further by DNA damage both *in vitro* and *in vivo* in tissues with proliferating cells. There was no evidence for accumulation of R-loops in the brains of mice where *Setx*, *Atm*, *Tdp1* or *Aptx* genes were disrupted. These data provide further evidence for genome destabilisation as a consequence of disrupted transcription in the presence of DNA double strand breaks arising during DNA replication or recombination. They also suggest that R-loop accumulation does not contribute to the neurodegenerative phenotype in these autosomal recessive ataxias.

**Citation:** Yeo AJ, Becherel OJ, Luff JE, Cullen JK, Wongsurawat T, et al. (2014) R-Loops in Proliferating Cells but Not in the Brain: Implications for AOA2 and Other Autosomal Recessive Ataxias. PLoS ONE 9(3): e90219. doi:10.1371/journal.pone.0090219

**Editor:** Nuri Gueven, University of Tasmania, Australia

**Received:** November 8, 2013; **Accepted:** January 27, 2014; **Published:** March 17, 2014

**Copyright:** © 2014 Yeo et al. This is an open-access article distributed under the terms of the Creative Commons Attribution License, which permits unrestricted use, distribution, and reproduction in any medium, provided the original author and source are credited.

**Funding:** This work was supported by the Australian Research Council (ARC) and the BrAshA-T Foundation to MFL. AJY is a recipient of the International Postgraduate Research Scholarship (IPRS) awarded by the Department of Innovation, Australian Government, and the UQCentennial and UQAdvantage scholarships awarded by the University of Queensland, Australia. The funders had no role in study design, data collection and analysis, decision to publish, or preparation of the manuscript.

**Competing Interests:** The authors have declared that no competing interests exist.

\* E-mail: martin.lavin@qimrberghofer.edu.au

## Introduction

The autosomal recessive cerebellar ataxias (ARCAs) are a diverse group of disorders arising from defects in genes involved in the response to DNA damage; mitochondrial function and those controlling different levels of metabolic and other cellular processes [1,2]. These are a class of progressive neurodegenerative diseases that result from cerebellar atrophy and spinal tract dysfunction [3]. A subgroup of these are characterised by defects in proteins that recognise and/or repair various forms of damage to DNA [4,5]. The best characterised of these is ataxia-telangiectasia (A-T) which arises due to mutations in the ATM gene [6]. ATM is recruited to DNA double strand breaks (DSB) by the Mre11/Rad50/NBN (MRN) complex where it is activated to phosphorylate a multitude of proteins involved in the response to DNA damage [7]. Disorders arising due to mutations in members of the MRN complex are also characterised by defects in the response to DNA DSB [8]. Hypomorphic mutations in Mre11 give rise to A-T like disorder (ATLD), which overlaps in its clinical phenotype with A-T and also features radiosensitivity and cell cycle defects [9]. Nijmegen breakage syndrome (NBS) is caused by mutations in NBN and is characterised by microcephaly, cell cycle checkpoint defects and ionizing radiation sensitivity [10]. Muta-

tion in the third member of the MRN complex, Rad50, has been reported for a single patient who has an NBS-like disorder as well as a defect in the response to DNA DSB [11,12]. Failure to resolve DNA single strand breaks (SSB) is also associated with a number of cerebellar atrophies [13] and these include ataxia oculomotor apraxia type 1 (AOA1) and spinocerebellar ataxia with axonal neuropathy (SCAN1). AOA1 is an autosomal recessive cerebellar ataxia syndrome that lacks the extraneurological features of A-T and related disorders [14]. The protein defective in AOA1, aprataxin, resolves abortive DNA ligation intermediates as part of the process of repair of DNA SSB [15,16]. Mutations in another gene, tyrosyl DNA phosphodiesterase 1 (TDP1) gives rise to SCAN1. TDP1 removes the Topoisomerase (Topo1) complex from DNA termini primarily at DNA SSB that arise due to collision of the transcription machinery with Topo1 intermediates or due to oxidative stress [17]. Disruption of this gene in mice leads to age-dependent cerebral atrophy and neurons from *Tdp1*<sup>-/-</sup> cells fail to rapidly repair DNA SSB at Topo1 complexes [18]. Another member of this group, ataxia oculomotor apraxia type 2 (AOA2) is also characterised by sensitivity to DNA damaging agents [19,20]. However, the genomic instability that occurs in AOA2 cells appears to result from the accumulation of DNA/

RNA hybrids (R-loops) following collisions between the transcription apparatus and DNA replication forks [21]. In addition, evidence for a role in transcriptional regulation which could also impact on genomic stability has also been reported for senataxin [22]. Recently, we generated the first *Setx* knockout mouse model to investigate the physiological role of senataxin. *Setx*<sup>-/-</sup> mice are defective in spermatogenesis, meiotic recombination and meiotic sex chromosome inactivation [23]. DNA DSBs persist in *Setx*<sup>-/-</sup> spermatocytes as well as R-loops, which appear to collide with Holiday junctions, thus preventing crossing-over. Skourti-Stathaki et al 2011 demonstrated that senataxin resolves R-loops formed at transcriptional pause sites to enable transcription initiation and termination [24]. This is in agreement with previous data providing evidence for transcription readthrough and defects in RNA splicing in senataxin-depleted cells [22]. The yeast ortholog of senataxin, Sen1, has also been shown to resolve R-loops to protect the genome against transcription-associated instability [25–28]. R-loops constitute a novel trigger for genomic instability and the accumulation of these structures may represent an underlying and contributing mechanism in autosomal recessive ataxias characterised by defective responses to DNA damage. Accumulating evidences have shown correlations between transcription deregulation, defective RNA processing, genome instability and neurodegeneration [29,30]. Here, we investigated for the presence of R-loops in both proliferating and non-proliferating tissues in order to address the potential role of R-loops in the neuropathology in autosomal recessive cerebellar ataxias.

## Results

### Accumulation of R-loops in germ cells of ARCA mouse models correlates with infertility

Since infertility is frequently associated with these disorders, we initially examined the testes for evidence of these structures. Testes sections from four ARCA mouse models (*Atm*<sup>-/-</sup>, *Setx*<sup>-/-</sup>, *Aptx*<sup>-/-</sup>, *Tdp1*<sup>-/-</sup>) were screened for the presence of R-loops. Initial histological examination of testes sections revealed a severe disruption of the seminiferous tubules, vacuolation and absence of mature germ cells in both *Setx*<sup>-/-</sup> and *Atm*<sup>-/-</sup> testes (Figure 1A) which is expected given that these mice have been reported to be sterile [23,31]. On the other hand, tubules were grossly normal for both *Aptx*<sup>-/-</sup> and *Tdp1*<sup>-/-</sup> mice. Testes size was reduced in *Setx*<sup>-/-</sup> and *Atm*<sup>-/-</sup> mice but these were of normal size in the other two mutant animals (data not shown). Immunofluorescent labelling with an antibody (S9.6) specific for R-loops revealed high levels of staining in the testes sections of both *Setx*<sup>-/-</sup> and *Atm*<sup>-/-</sup> mice (Figure 1B). R-loops staining was distributed across the entire cell nucleus in agreement with previous report indicating the genome wide distribution of R-loops [25–28]. R-loops were also detected albeit at a lower level in both *Aptx*<sup>-/-</sup> and *Tdp1*<sup>-/-</sup> mice. To determine whether the accumulation of R-loops may impact on cell viability, co-staining with TUNEL (marker of apoptotic cells) was performed. It was observed that most cells positive for R-loops were also undergoing apoptosis (Figure 1B). Treatment of sections with RNase H prior to staining significantly reduced staining with S9.6 antibody, providing further evidence of the specificity of this antibody and that R-loops are being detected in this assay (Figure S1 A). Another characteristic of genomic instability and infertility results from a defective repair of programmed DNA DSB occurring during meiosis [23,31]. In addition to R-loop accumulation, we also stained for  $\gamma$ H2AX, a well-described marker for DNA DSBs [32]. DNA DSBs were detected in spermatocytes for all sections as part of the process of meiotic recombination (Figure 1C). However, the intensity of

staining for  $\gamma$ H2AX was higher in *Setx*<sup>-/-</sup>, *Atm*<sup>-/-</sup> and *Aptx*<sup>-/-</sup> sections. It is also evident that in the spermatocytes from *Atm*<sup>-/-</sup> and *Setx*<sup>-/-</sup> mice, the intense staining for DNA DSBs coincides with the appearance of marked TUNEL labelling (Figure 1C). These data provide evidence for the accumulation of R-loops in the presence of DNA DSBs arising as a consequence of absence of defects in proteins that are involved in the DNA damage response. Quantitative analysis demonstrated that a significantly higher number of tubules from all 4 mutant mice (~30–45%) contained R-loops as compared to control (~10%) (Figure 2A). This was also the case for apoptosis, with the highest levels of apoptosis observed in *Setx*<sup>-/-</sup> and *Atm*<sup>-/-</sup> mice, followed by *Aptx*<sup>-/-</sup> and *Tdp1*<sup>-/-</sup> mice (Figure 2B). It was also clear that in the case of the wildtype testes where there are only a few apoptotic cells, the great majority of these did not stain for R-loop. When tubules were differentiated based on the number of R-loop-containing spermatocytes per tubule, a clear distinction appeared. Only *Setx*<sup>-/-</sup> and *Atm*<sup>-/-</sup> mice scored in the high range with tubules containing >11 R-loop & TUNEL-positive cells per tubule (Figure 2C). Combining both high (>11 affected cells per tubule) and low (6–10 affected cells per tubule) categories, *Setx*<sup>-/-</sup> mice had an average of 40% R-loop-containing cells per tubule and *Atm*<sup>-/-</sup> mice had 30%. In the lower range, *Aptx*<sup>-/-</sup> mice had significantly greater numbers than wildtype mice whereas that of *Tdp1*<sup>-/-</sup> mice were less markedly elevated (Figure 2C). Interestingly, while *Atm*<sup>-/-</sup> mice showed the highest numbers of  $\gamma$ H2AX-positive cells, only ~25% of those stained for TUNEL (Figure 2D). This was also observed in *Tdp1*<sup>-/-</sup> mice (Figure 2D). In contrast, in *Setx*<sup>-/-</sup> and *Aptx*<sup>-/-</sup>, ~50% of the cells were positive for both  $\gamma$ H2AX and TUNEL. These data indicate that there is a higher proportion of germ cells containing DNA DSBs that undergo apoptosis in *Setx*<sup>-/-</sup> and *Aptx*<sup>-/-</sup> mice compared to *Atm*<sup>-/-</sup> and *Tdp1*<sup>-/-</sup>. The elevated levels of apoptosis in the spermatocytes of *Tdp1*<sup>-/-</sup>, *Aptx*<sup>-/-</sup>, *Setx*<sup>-/-</sup> and *Atm*<sup>-/-</sup> mice suggest that a significant amount of DNA DSBs are not processed/repared properly, thus triggering apoptosis. As expected in wildtype, there were low levels of apoptosis which is in agreement with the formation and then effective repair of programmed DNA DSBs that occur during meiosis [33].

### R-loops do not form in post-mitotic tissues

To date R-loops have been detected in cells/tissues where active transcription and replication occur [34,35]. However, the most debilitating aspect of autosomal recessive cerebellar ataxias is caused by the progressive loss of post-mitotic nerve cells, leading to cerebellar atrophy and peripheral neuropathy [5]. Post-mitotic neurons are metabolically highly active due to the synthesis of neurotransmitters to ensure proper function of the nervous system and therefore possess a high transcriptional activity [36]. Given that R-loops form normally during transcription at RNA Polymerase II pause sites and that post-mitotic neurons display high levels of transcription and RNA processing, it raises the question as to whether R-loops form or accumulate in the nervous tissues of disorders characterized by the defects in proteins involved in the DNA damage response. Given the role of senataxin in resolving these structures [24], we initially examined brain sections from *Setx*<sup>-/-</sup> mice for the presence of R-loops. However, we did not detect any R-loops in either whole brain or cerebellum sections from *Setx*<sup>-/-</sup> mice (Figure 3A & 3B). Furthermore, there was also no evidence of cells undergoing apoptosis in these tissues (Figure 3A & 3B). This is in agreement with the fact that no neurological anomalies or neurodegeneration were present in these animals [23]. Testes sections from *Setx*<sup>-/-</sup> animals were included as positive control for R-loop staining

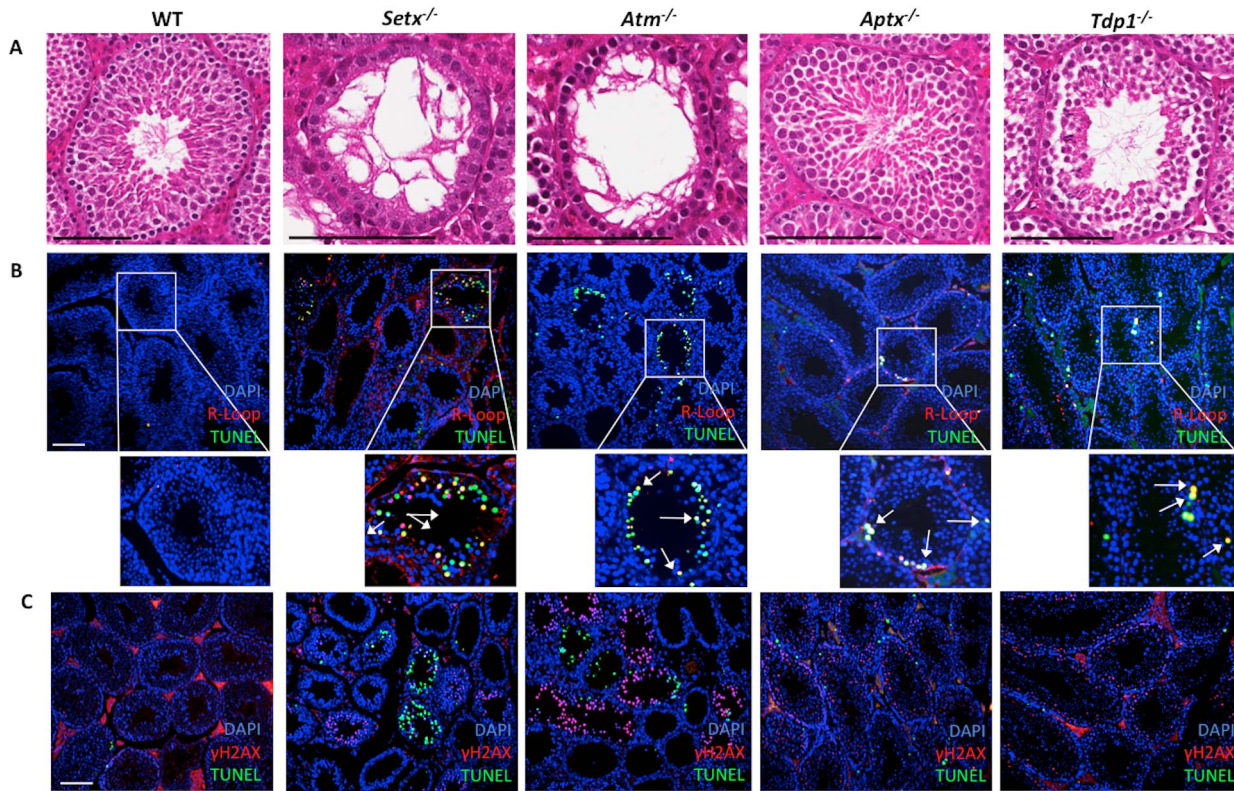


**Figure 1. Evidence of DNA/RNA hybrids (R-loops) accumulation in spermatocytes of ARCA mouse model.** **A.** Histological cross-sections of seminiferous tubules from ARCA mouse models *Setx*<sup>-/-</sup>, *Atm*<sup>-/-</sup>, *Aptx*<sup>-/-</sup>, *Tdp1*<sup>-/-</sup> and wildtype (WT) littermates. Sections were H & E stained. Scale bar, 100  $\mu$ m. **B.** Immunostaining of testes sections with R-loop (S9.6) antibody (red) and TUNEL (green). Nuclei were stained using Hoechst 33342 (blue). Scale bar, 100  $\mu$ m. Magnified views of the tubules are also shown. Representative spermatocytes staining positive for both R-loop and TUNEL are indicated by white arrows. **C.** Immunostaining of testes sections with  $\gamma$ H2AX (red), a marker of DNA DSBs, and TUNEL (green). Scale bar, 100  $\mu$ m.

doi:10.1371/journal.pone.0090219.g001

(Figure 3C). Accumulation of R-loops observed in *Setx*<sup>-/-</sup> germ cells and their absence in the brain and cerebella was supported using DRIP (DNA/RNA immunoprecipitation) assays for *Setx*<sup>+/+</sup> and *Setx*<sup>-/-</sup> testes, brain, and cerebella. In order to perform DRIP assays, we first searched for R-loop prediction using the R-loop forming sequence (RLFS) model to predict location of RLFSs on the mouse genome [37]. Given the role of R-loops in transcription termination [24], we selected candidate genes where RLFSs localized <500 bp downstream of the poly(A) signal(s) for further analyses. Among these genes, the HS44.2 locus, a region of recombination hot spot located on the chromosome 19 [38] was selected. The RLFS-containing region was located downstream the *Pkd2l1* gene located in the HS44.2 locus (Figure 4A). We observed similar background levels of R-loop formation in both *Setx*<sup>+/+</sup> and *Setx*<sup>-/-</sup> brain and cerebellum. However, a significant increase (>1.6-fold) in R-loop formation was observed in *Setx*<sup>-/-</sup> testes compared to wildtype supporting our immunofluorescence findings (Figure 2). In addition, given the meiotic sex chromosome inactivation (MSCI) defect previously observed in *Setx*<sup>-/-</sup> [23] we selected a second locus on the X chromosome to perform the DRIP analysis. We selected the *Foxo4* gene based on the same criteria. Similar results were obtained for *Foxo4*, confirming background levels of R-loops in brain and cerebellum and a significant increase of R-loop formation (>1.8 fold) in *Setx*<sup>-/-</sup> testes (Figure 4B). Figure 4C shows the Bioanalyzer Spectra of untreated, S1 Nuclease-treated, and RNase H-treated DRIP samples to confirm the specificity of the S9.6 antibody (R-loop) for

DNA/RNA hybrids as shown by the reduction of fluorescence intensity after RNase H treatment. Altogether, these data confirmed the specific accumulation of R-loops in *Setx*<sup>-/-</sup> germ cells and the presence similar normal background levels of R-loops in *Setx*<sup>+/+</sup> and *Setx*<sup>-/-</sup> brain and cerebellum, in agreement with the fact that no neurological anomalies or neurodegeneration were present in these animals [23]. Thus, S9.6 immunofluorescence staining represents a simple and reliable method to detect R-loop formation and screen for aberrant RNA metabolism in tissues.

To determine whether this was also the case in other ARCA models, we screened for R-loop accumulation in the brains and cerebella of *Atm*<sup>-/-</sup>, *Aptx*<sup>-/-</sup> and *Tdp1*<sup>-/-</sup> mice. Similar to that in *Setx*<sup>-/-</sup>, we did not detect these structures in these tissues (Figure S1 A and B). The lack of R-loops in the nervous tissues of these autosomal recessive cerebellar ataxias may not be entirely unexpected due to the lack of major neurological defects in these animals.

### DNA damage induces R-loops accumulation in proliferating cells not in post-mitotic cells

The accumulation of unrepaired DNA damage in post-mitotic neurons can lead to genome instability, abnormal transcriptional regulation and thus ultimately to neurodegeneration [30]. The lack of R-loop formation in the nervous tissues of these mutants under normal living conditions prompted us to investigate whether additional DNA damage exposure may trigger the formation of these structures. To address this, we first knocked down *SETX* in

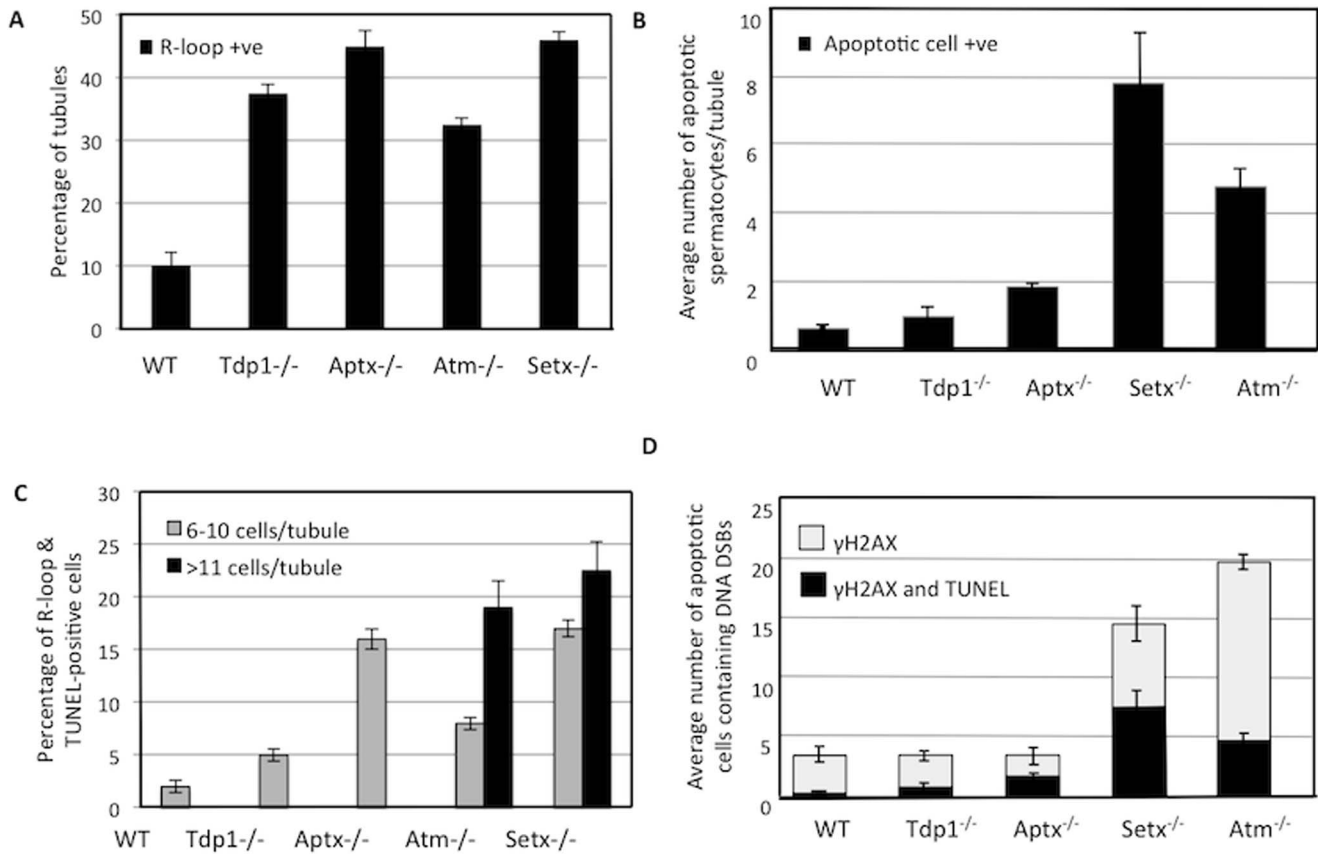


**Figure 2. R-loop formation, apoptosis, and DNA damage quantitation in ARCA mouse testes.** **A.** Percentage of seminiferous tubules containing R-loops. **B.** Average number of apoptotic spermatocytes per tubule in testes from ARCA mice. **C.** Percentage of R-loop & TUNEL-positive cells. **D.** Average number of apoptotic cells containing DNA DSBs ( $\gamma$ H2AX). For each panel, 200 tubules were examined per animal and cells were counted in each tubule ( $n=3$ ). Error bars represent SEM. doi:10.1371/journal.pone.0090219.g002

HeLa cells (Figure S2) and monitored R-loop formation in these cells. As shown in Figure 5A, R-loops were primarily detected in nucleoli. This is compatible with R-loop formation at highly transcribed and R-loop-prone ribosomal arrays as previously reported [39]. The major nucleolar R-loops staining observed here is consistent with the staining pattern found in previous studies that reported the genome wide distribution of R-loops using DRIP assays [40]. Ribosomal DNA transcription represents the vast majority of transcriptional activity in the cell thus explaining the strong R-loop signal observed in nucleoli. The detection of R-loops in nucleoli does not mean that R-loops only form in nucleoli but may reflect a difference in sensitivity between immunofluorescence and DRIP assays. As shown in Figure 4, we detected the formation of R-loops at non-rDNA loci on two different chromosomes using DRIP assays thus confirming that R-loops occur on a genome wide scale. Extra-nuclear staining for R-loops was also observed in agreement with the formation of R-loops during mitochondrial replication as previously reported [41,42]. These data confirm the role for senataxin in resolving R-loops as previously described [21,23,24]. Exposure of cells to the DNA damaging agent, camptothecin (CPT), a DNA topoisomerase I inhibitor, led to the appearance of R-loops in nucleoli in control cells and a further increased levels of R-loops in SETX knockdown cells, in keeping with the higher basal level in these cells (Figure 5A). The accumulation of positive supercoiling ahead of the transcription bubble resists opening of the DNA, which can

slow or impede transcription elongation by RNA Polymerase I [43], as seen following treatment with CPT [44]. In contrast, negative supercoiling behind the transcription bubble can lead to the unwinding of DNA. When this happens, the nascent RNA may hybridize to the transcribed strand, creating R-loops [44]. The additional increase in R-loop formation observed after CPT treatment supports previous findings, showing that the blocking of DNA topoisomerase I leads to R-loop-mediated transcriptional stalling during ribosomal RNA synthesis [39,40]. To confirm that R-loop formation requires active transcription, we employed the use of Actinomycin D (AD), a transcription inhibitor that binds DNA at the transcription initiation complex and prevents elongation of RNA by RNA polymerases [45]. Following AD treatment, R-loop levels decreased in both control siRNA- and SETX siRNA-treated cells (Figure 5A and 5B), confirming the involvement of active transcription in R-loop formation.

Having established that CPT-induced DNA damage can stimulate R-loop formation; we then treated wildtype, *Setx*<sup>-/-</sup> and *Tdp1*<sup>-/-</sup> mutant mice with topotecan (TPT), a water-soluble analogue of CPT [46]. Knockout mice of both models treated with this agent lost approximately 30% of body weight over a 10-day period (Figure 6). This may have resulted from damage to the mucosal tissue in the lower intestine, causing disruption to nutrient absorption. It has also been shown that TPT can cause gastrointestinal toxicity in mice [18,47]. However, no abnormal neurological behaviour was observed in TPT-treated animals as



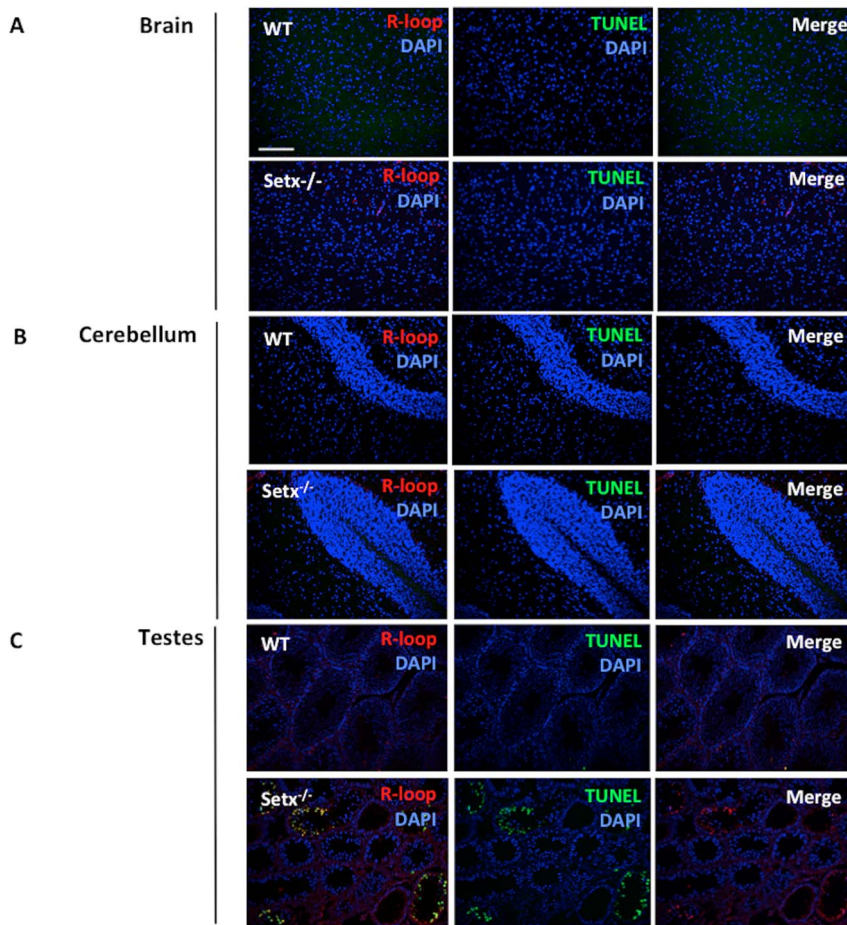


**Figure 3. Absence of R-loops in *Setx*<sup>-/-</sup> nervous tissues.** **A.** Whole brain sections from wildtype (*Setx*<sup>+/+</sup>) and *Setx*<sup>-/-</sup> were stained for R-loop (Red) and apoptosis (TUNEL, Green). Nuclei were labelled with DAPI. **B.** Wildtype and *Setx*<sup>-/-</sup> cerebellar sections staining with R-loops and TUNEL. DAPI stained nuclei. **C.** As a control for R-loop and TUNEL staining, both wildtype and *Setx*<sup>-/-</sup> testes sections are shown. Scale bar, 100  $\mu$ m. doi:10.1371/journal.pone.0090219.g003

compared to untreated controls over the treatment period. We then screened for the presence of R-loops in both proliferating and post-mitotic tissues of these mice using the R-loop-specific S9.6 antibody together with the Ki67 antibody, which was used as a marker of proliferation. As expected, in the testes of *Setx*<sup>-/-</sup> mice, coinciding R-loop and Ki67 signals were detected under untreated conditions [23] and this increased after TPT treatment (Figure 7). However, examination of the brain and cerebella tissues from both treated and untreated *Setx*<sup>-/-</sup> mice failed to reveal evidence of R-loop formation (Figure 7). Although TPT is able to readily cross the blood-brain barrier and has been demonstrated to be active in brain metastases from small cell lung cancer [48], it did not induce the formation of R-loops in these animals. Since increased R-loop levels were only observed in a proliferative tissue such as the testes, we then investigated for the presence of R-loops in other highly proliferative tissues such as the intestine and the spleen. Increased levels of coinciding R-loop and Ki67 signals were detected in these tissues after TPT treatment (Figure 8). Similar results were found in *Tdp1*<sup>-/-</sup> mice (Figure 9). Quantitation of the number of R-loop-, TUNEL- and R-loop & TUNEL-positive cells is shown in Figure 10. Only a very small number of R-loop positive cells (< 0.4% of cells) were detected in *Setx*<sup>+/+</sup> intestine, spleen and testes. Treatment of *Setx*<sup>+/+</sup> mice with TPT lead to a 2.7-fold, 1.5-fold, and 6.8-fold increase in the number of R-loop formation cells in intestine, spleen and testes, respectively (Figure 10A). As antic-

ipated, *Setx*<sup>-/-</sup> mice exhibited higher levels of R-loop formation in intestine, spleen and testes, with testes showing the highest number of R-loop-positive cells (6.9% of cells). Following TPT treatment, the number of R-loops-containing cells in *Setx*<sup>-/-</sup> mice drastically increased in all three tissues by a 17.3-fold in the intestine, 10.5-fold in the spleen, and 1.5-fold in the testes which remained the tissue containing the highest number of R-loops-positive cells (Figure 10B). Similar results were observed for *Tdp1*<sup>-/-</sup> mice (Figure 10C). Less than 0.5% of R-loops-positive cells were detected in *Tdp1*<sup>-/-</sup> mice under normal conditions. TPT treatment of *Tdp1*<sup>-/-</sup> mice lead to a drastic increase in the number of R-loops-positive cells with intestine and testes displaying a 19-fold and 34.4-fold increase, respectively (Figure 10C). As a consequence of the TPT-induced R-loop accumulation, the number of double-positive cells (R-loop & TUNEL) after TPT treatment dramatically increased in *Setx*<sup>+/+</sup>, *Setx*<sup>-/-</sup> and *Tdp1*<sup>-/-</sup> mice further supporting the effect of R-loop accumulation in genome stability. We next examined the levels of senataxin protein in these tissues using immunoblotting. We failed to detect senataxin protein using western blotting of wildtype total tissue extracts, suggesting very low levels of senataxin in these tissues and/or weak sensitivity of the senataxin antibody. We thus performed senataxin immunoprecipitation from wildtype and *Setx*<sup>-/-</sup> tissues extracts. As seen in Figure S4 A, a weak signal for senataxin was only detected in *Setx*<sup>+/+</sup> testes extracts. This is

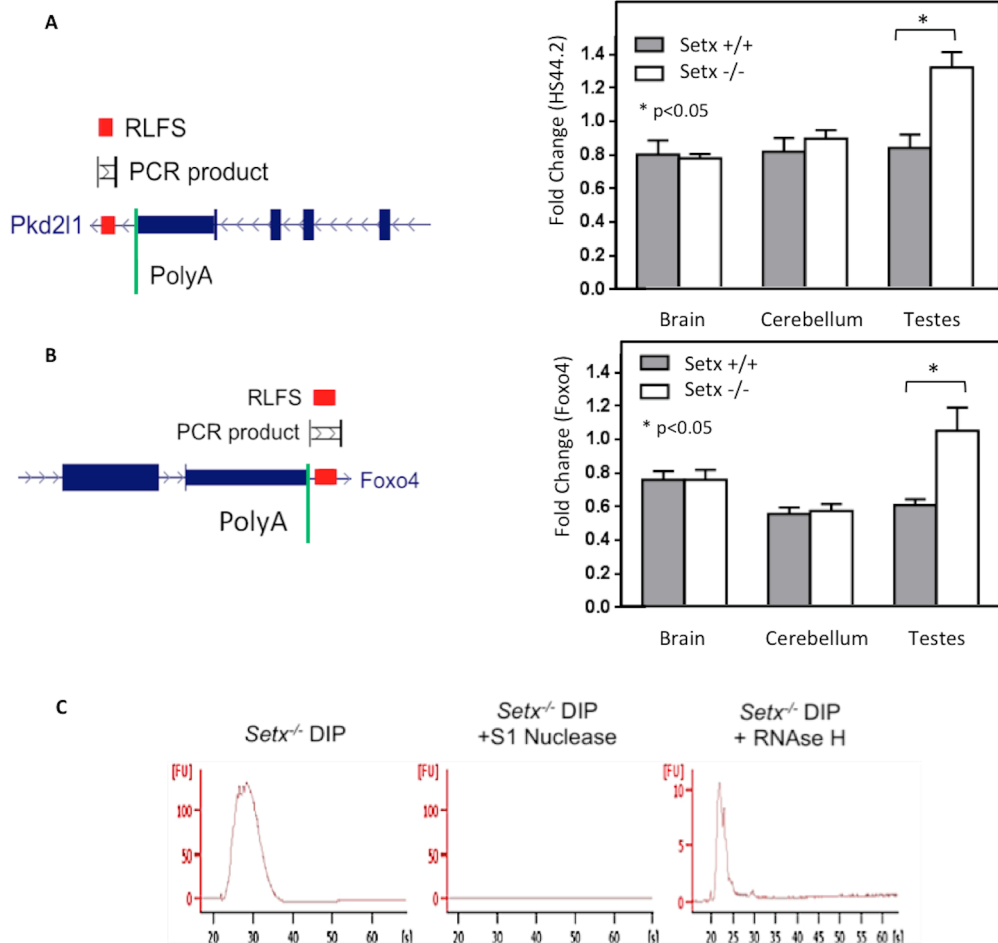


**Figure 4. R-loops forming sequences (RLFS) prediction and R-loops detection using DRIP assay.)** UCSC Genome browser shows chromosome mapping of RLFS and poly(A) signal location at 3' UTR of studied genes. RFLS (red box), and PCR products (black vertical lines connected by horizontal lines) are indicated on the diagram. **A.** RLFS prediction in the 3' UTR of the mouse *Pkd2l1* gene located in the HS44.2 locus on chromosome 19. See Figure S5 for sequence details. DRIP quantitation from *Setx*<sup>+/+</sup> and *Setx*<sup>-/-</sup> showed similar background levels of R-loops in brain and cerebellum. Only a significant increase in R-loop formation was observed in *Setx*<sup>-/-</sup> testes as compared to *Setx*<sup>+/+</sup> (Students t-test,  $p < 0.05$ ,  $n = 3$ ). **B.** RLFS prediction in the 3' UTR of the mouse *Foxo4* gene located on the X chromosome. DRIP quantitation from *Setx*<sup>+/+</sup> and *Setx*<sup>-/-</sup> showed similar background levels of R-loops in brain and cerebellum. Similarly, a significant increase in R-loop formation was only observed in *Setx*<sup>-/-</sup> testes (Students t-test,  $p < 0.05$ ,  $n = 3$ ). **C.** Treatment of *Setx*<sup>-/-</sup> DRIP samples with S1 Nuclease and RNase H confirmed the specificity of the S9.6 (R-loop) antibody towards DNA/RNA hybrids as shown by reduced fluorescence intensities on Bioanalyzer Spectra. doi:10.1371/journal.pone.0090219.g004

agreement with the GEO expression data, which showed the highest expression for senataxin in testes as compared to other tissues. Using RT-PCR, we confirmed the low levels of senataxin in brain, cerebellum, spleen and intestine compared to testes (Figure S4 B).

Altogether, these data indicate that R-loops form preferentially in replicating cells of proliferative tissues due to the collision of the replication fork and the transcription machinery [21,27], and not in post-mitotic cells such as the neurons in the brain and cerebellum even after DNA damage exposure.

Given that the loss of TDP1 leads to an age-dependant and progressive cerebellar atrophy, and that cerebellar neurons or primary astrocytes derived from *Tdp1*<sup>-/-</sup> mice display an inability to rapidly repair DNA SSBs associated with Top1-DNA complexes or oxidative damage [18], we generated *Setx*<sup>-/-</sup> *Tdp1*<sup>-/-</sup> double mutants to investigate whether the compounded defects would induce or exacerbate R-loop formation and trigger a neurological phenotype. However, while male sterility was observed in the double knockout, no neurological defects were

observed. Similar results to the single *Setx*<sup>-/-</sup> and *Tdp1*<sup>-/-</sup> knockout TPT-treated mice were observed in the double knockout, with similar levels of R-loop accumulation seen in the testes, spleen and intestine but not in the brain or cerebellum (data not shown).

## Discussion

Recent evidence suggests that senataxin plays a central role at the interface between transcription, DNA replication and genetic recombination in resolving R-loops to minimise the risk of genome instability [21,23,24]. In this report, we demonstrate that the disruption of a number of DNA damage response genes including *Setx* and *Tdp1* in mice led to the accumulation of R-loops in proliferating cells consistent with collision between transcription and DNA replication forks when DNA lesions were not repaired [21,27]. However, there was no evidence of the accumulation of R-loops in the nervous tissues of these gene-disrupted animals even when DNA damage was inflicted. These data suggest that in post-

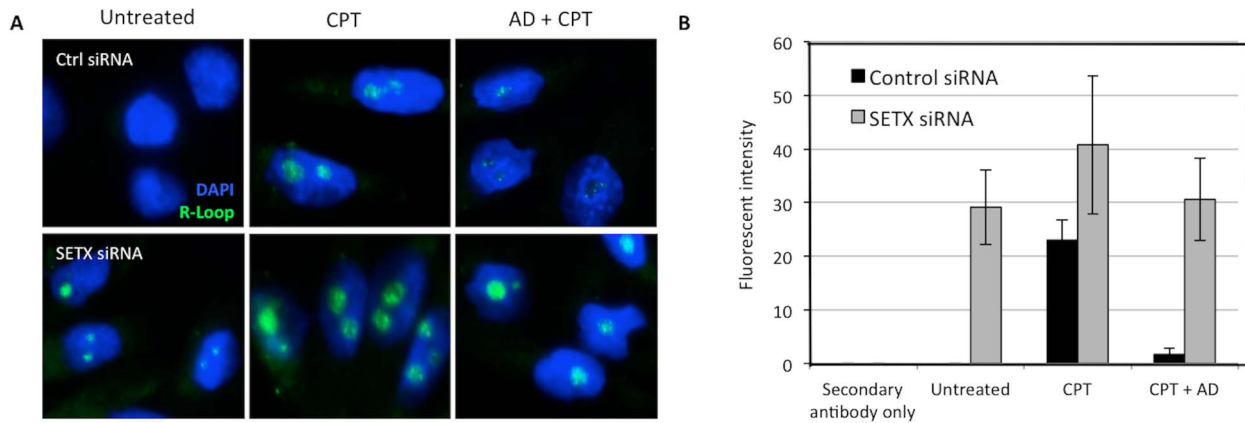


**Figure 5. Induction of R-loop after DNA damage exposure.** **A.** Knock down of senataxin in HeLa cells using short interfering RNA (siRNA) induced the accumulation of R-loops in nucleoli. Knock down efficiency for senataxin is shown in Figure S2. Treatment of these cells with 25  $\mu$ M of camptothecin (CPT) led to the accumulation of R-loops in control cells (Ctrl siRNA) and a further increase in senataxin knockdown cells (*SETX* siRNA). Pre-treatment of these with RNA polymerase inhibitor Actinomycin D (AD, 5  $\mu$ g/ml), ablated the CPT-induced formation of R-loop in both cell types. **B.** Quantitation of R-loops formation in control and senataxin knockdown cells. No R-loops were detected in ctrl siRNA-treated cells under normal growing conditions. CPT induced the formation of R-loops in both cell types and pre-treatment these cells with AD prevented the induction of R-loops following DNA damage exposure. Levels of R-loops returned to basal levels in *SETX* siRNA-treated cells after addition of AD. doi:10.1371/journal.pone.0090219.g005

mitotic cells, where transcription is highly active, only basal levels of R-loops exist and they do not accumulate even in the presence of DNA damage. Thus this is a phenomenon that appears to be restricted to proliferating cells. We have previously shown that the disruption of *Setx* in mice caused persistence of DNA DSB, a defect in Rad51 disassembly, accumulation of R-loops and a failure of

crossing-over in spermatocytes [23]. Here, we showed that R-loops accumulate in the testes even when other DNA damage response genes were disrupted. Mutations in the ATM gene give rise to ataxia-telangiectasia (A-T), which is characterised by immunodeficiency, cancer predisposition, neurodegeneration and also infertility [5]. *Atm*<sup>-/-</sup> spermatocytes halt development largely at

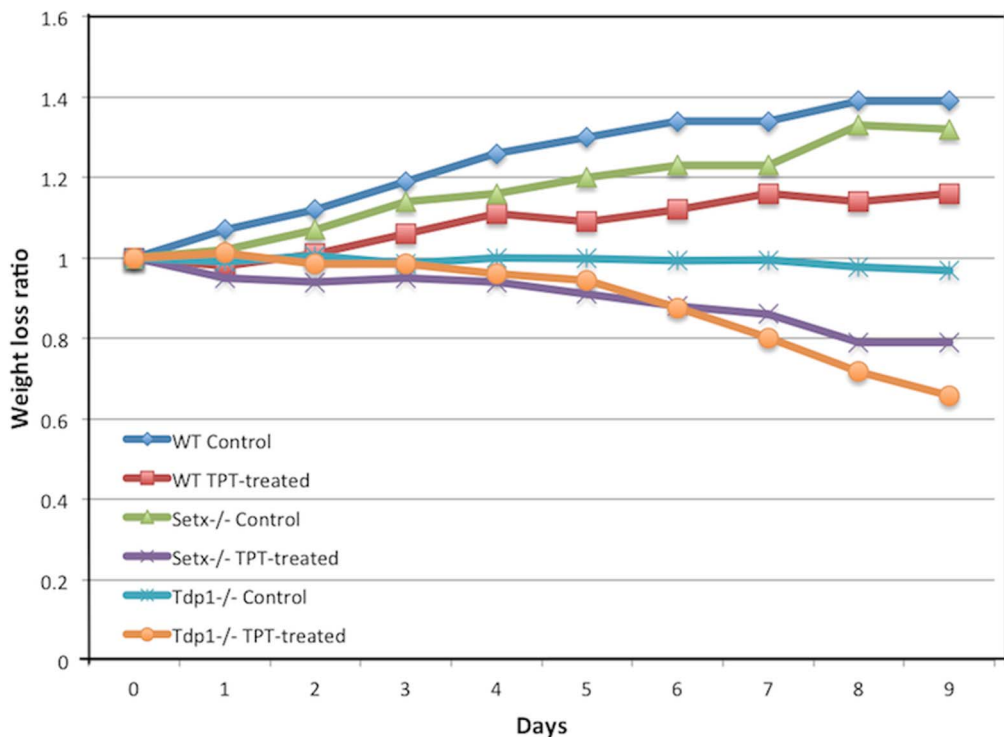


**Figure 6. Treatment of *Setx* and *Tdp1* mice with Topotecan induces severe weight loss.** Wiltype (WT), *Setx*<sup>-/-</sup> and *Tdp1*<sup>-/-</sup> mice were treated with a daily dose of topotecan (TPT, 2 mg/kg/day) over a period of 9 days in order to exacerbate the formation of R-loops in these mice. Mice of each genotype were injected daily with a dose of TPT (2 mg/kg/day) and weights were recorded daily (n=3). Controls were injected with an equivalent volume of purified water. doi:10.1371/journal.pone.0090219.g006

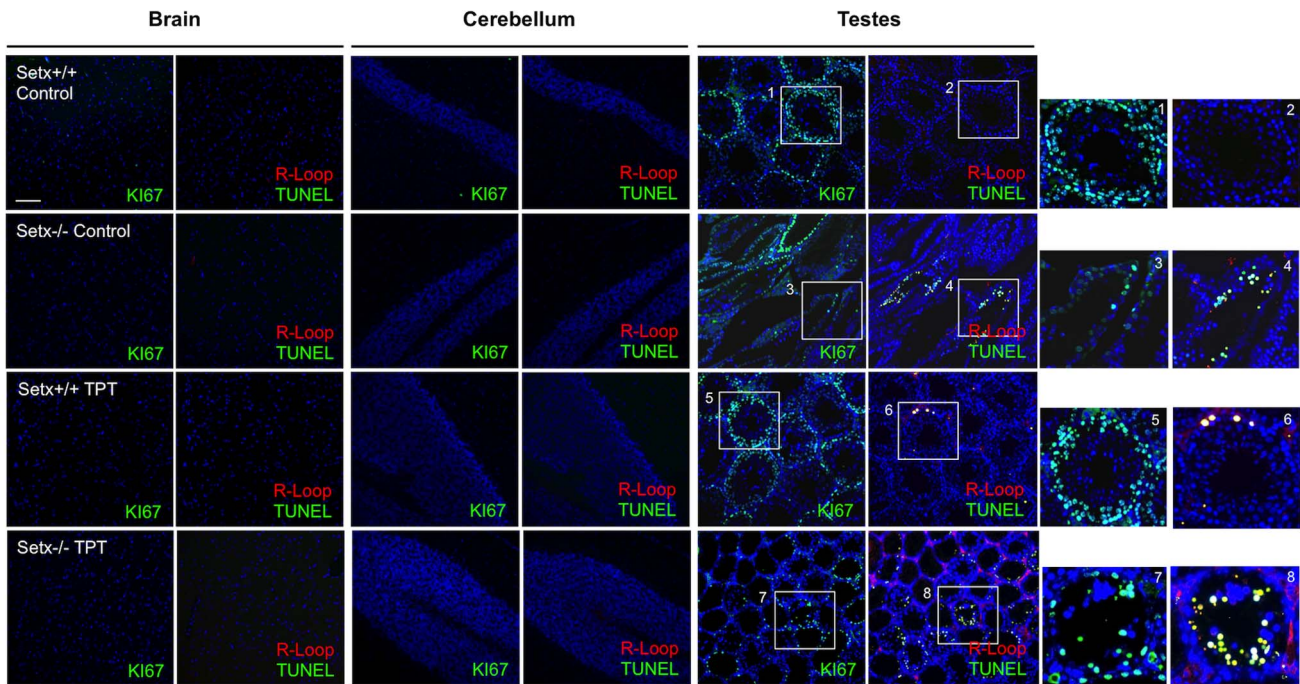


**Figure 7. Topotecan treatment does not induce R-loops formation in post-mitotic nervous tissues in *Setx*<sup>-/-</sup> mice.** Histological sections of brain, cerebellum, and testes were immunostained for R-loops (Red) and TUNEL (Green). No R-loops were detected in brain and cerebellum sections after TPT treatment. In contrast, an increase in the number of R-loop-containing cells was observed in wildtype and *Setx*<sup>-/-</sup> after TPT exposure suggesting that R-loop preferentially form in proliferating cells, most likely due to collision between the DNA replication machinery and the transcription apparatus. DAPI stained nuclei and Ki67 (Red) was used as a marker for proliferation. Scale bar, 100  $\mu$ m. doi:10.1371/journal.pone.0090219.g007

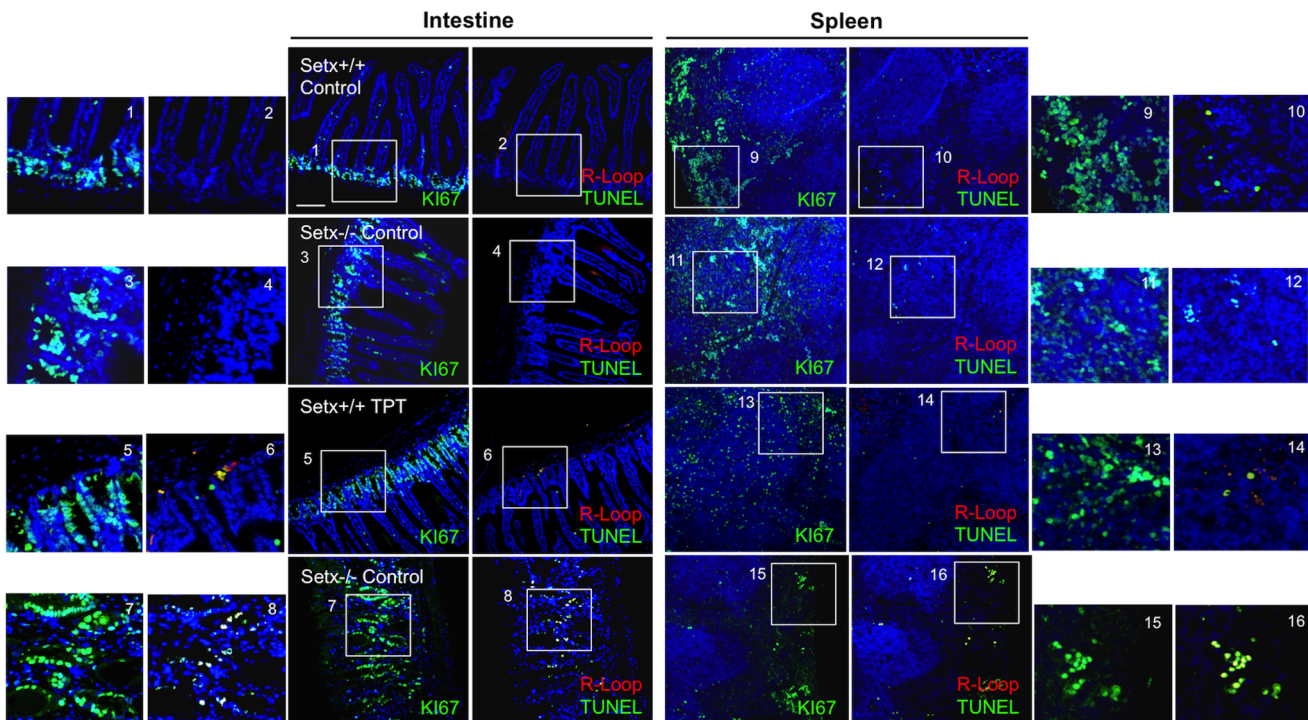


**Figure 8. Induction of R-loops in proliferating cells after topotecan treatment.** Wildtype and *Setx*<sup>-/-</sup> histological sections of intestine and spleen, two tissues with a high proliferative capacity, were stained for R-loops, TUNEL, and Ki67. TPT induced the formation of R-loops and apoptosis in both intestine and spleen. TPT disrupted the structure of the small intestine in *Setx*<sup>-/-</sup> animals supporting the severe weight loss observed in these mice. R-loop (red), TUNEL (green) and Ki67 (red). DAPI (blue) stained nuclei. Scale bar, 100  $\mu$ m. doi:10.1371/journal.pone.0090219.g008

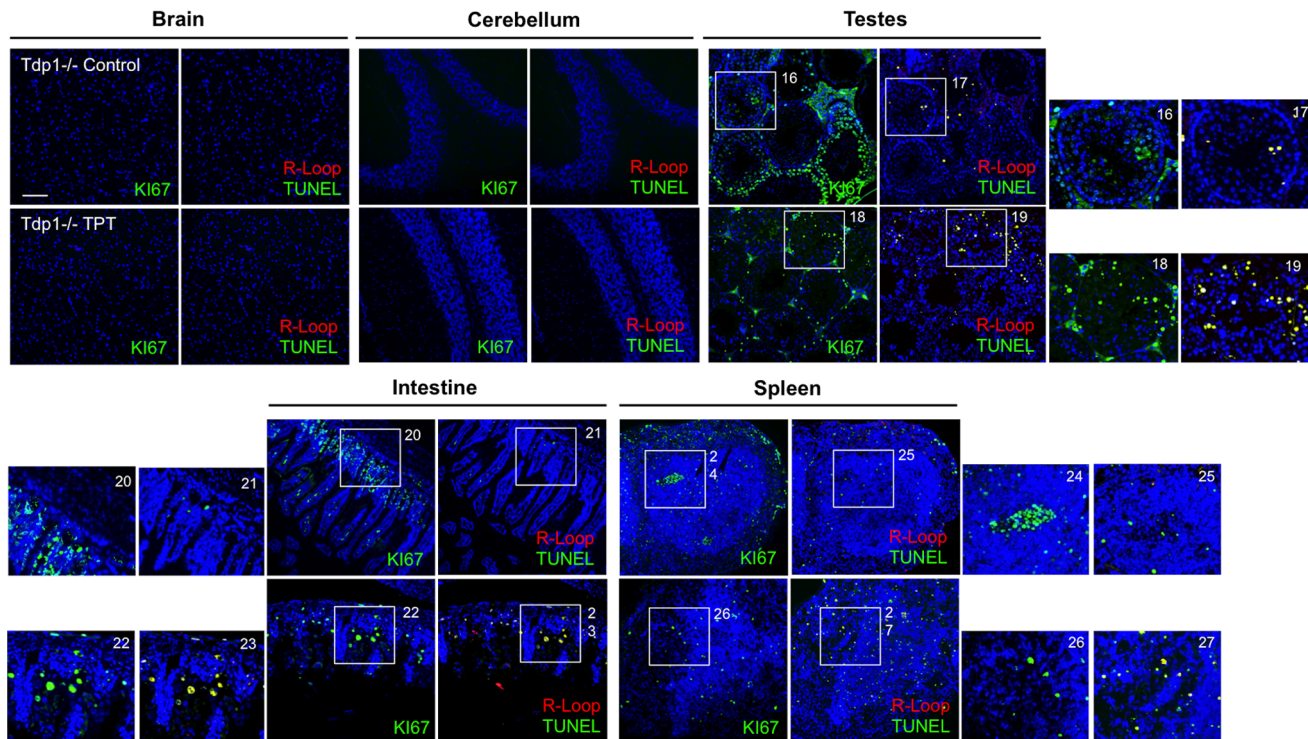


**Figure 9. Induction of R-loops only in proliferative tissues in *Tdp1*<sup>-/-</sup> after topotecan treatment.** Histological sections from *Tdp1*<sup>-/-</sup> mice were stained for R-loops, TUNEL and Ki67 after topotecan exposure. Similar to *Setx*<sup>-/-</sup>, TPT induced the formation of R-loops formation only in proliferative tissues testes, intestine and spleen). No R-loops were detected in post-mitotic tissues (brain and cerebellum). Scale bar, 100  $\mu$ m. doi:10.1371/journal.pone.0090219.g009

leptotene stage of meiotic prophase 1 and ovaries from females contain no primary oocytes or follicles [49]. The integrity of axial elements and synaptonemal complexes were disrupted and DNA DSB persisted in *Atm*<sup>-/-</sup> spermatocytes consistent with a role for ATM in monitoring DNA DSB during meiotic recombination in early leptotene. ATM responds to the presence of excess breaks by inducing apoptosis. In this study we detected excess DNA DSB in testes sections from *Atm*<sup>-/-</sup> mice and these co-localised with R-loops suggesting that a combination of blocked transcription together with unrepaired DNA DSBs is responsible for the disrupted spermatogenesis. It is also evident that the majority of R-loop-containing spermatocytes are undergoing apoptosis. Mutations in *TDPI* give rise to spinocerebellar ataxia with axonal neuropathy (SCAN1) [17]. Mice disrupted for this gene display an inability to rapidly repair SSB [18]. There is also a requirement for this enzyme in the removal of acutely elevated levels of Topo1-associated DNA strand breaks in intestinal and haematopoietic progenitor cells. Although *Tdp1*<sup>-/-</sup> mice are fertile and do not exhibit the same high level of R-loop accumulation and cell death in testes sections as *Setx*<sup>-/-</sup> and *Atm*<sup>-/-</sup> mice, we did detect levels of R-loops that were significantly higher than wildtype and there was concordance between these and apoptosis. This suggests that there is elevation in DNA breaks in *Tdp1*<sup>-/-</sup> mouse spermatocytes or increased DNA replication blockage that leads to R-loop accumulation. Mutations in the *APT*X gene lead to ataxia oculomotor apraxia type 1 (AOA1). *APT*X codes for aprataxin, which is an enzyme that catalyzes the removal of abortive DNA ligation intermediates and is important for DNA SSB repair [15,16]. The fourth mutant mouse model, *Aptx*<sup>-/-</sup> which also exhibits normal fertility, had elevated numbers of R-loops in the testes as compared to wildtype and similar to the *Tdp1*<sup>-/-</sup> mouse. However it was not to the same extent as that seen in the *Setx*<sup>-/-</sup>

and *Atm*<sup>-/-</sup> mice. These data indicate that in the absence of proteins involved in recognition and/or repair of DNA damage, R-loops occur in proliferating cells due the presence of unrepaired DNA lesion that can stall the transcription machinery. In addition, the extent of R-loop accumulation can exacerbate genomic instability, trigger apoptosis and is indicative of the fertility status.

All four mutants studied here correspond to autosomal recessive ataxias characterised by cerebellar atrophy and loss of Purkinje cells [50]. While the syndromes vary in the extent of extra-neuronal involvement, they are all characterised by neurodegeneration. Although the mouse models for the disorders described here do not recapitulate the neurodegeneration seen in human patients, some neurological abnormalities can be observed. For example, in the case of *Tdp1*<sup>-/-</sup> mice, there is an accumulation of Topo1-linked breaks in astrocytes and an age-dependent reduction in cerebellar size [18]. *Atm*<sup>-/-</sup> mice also exhibit cerebellar pathology, neuronal cell death *in vitro*, reduced synchronization persistence in neural networks, vascular abnormalities and degeneration of the nigro-striated pathway [51]. Neuronal cells are characterised by active transcription and high levels of metabolic activity [36]. As such, it seemed likely that in the presence of unrepaired DNA breaks, R-loops would accumulate in the brains of these mutant mice. Only background levels of R-loops were detected in either the brain as a whole or cerebellum using the more sensitive DRIP assay. However, treatment of any of these animals with TPT, which is a compound that readily crosses the blood-brain barrier and induces DNA damage, did not trigger accumulation of R-loops in post-mitotic tissues. This suggests that while R-loops occur normally at pause sites during transcription [52], their accumulation is only observed in cells where transcription collides with either DNA replication forks [21] or with DNA recombination intermediates during meiosis

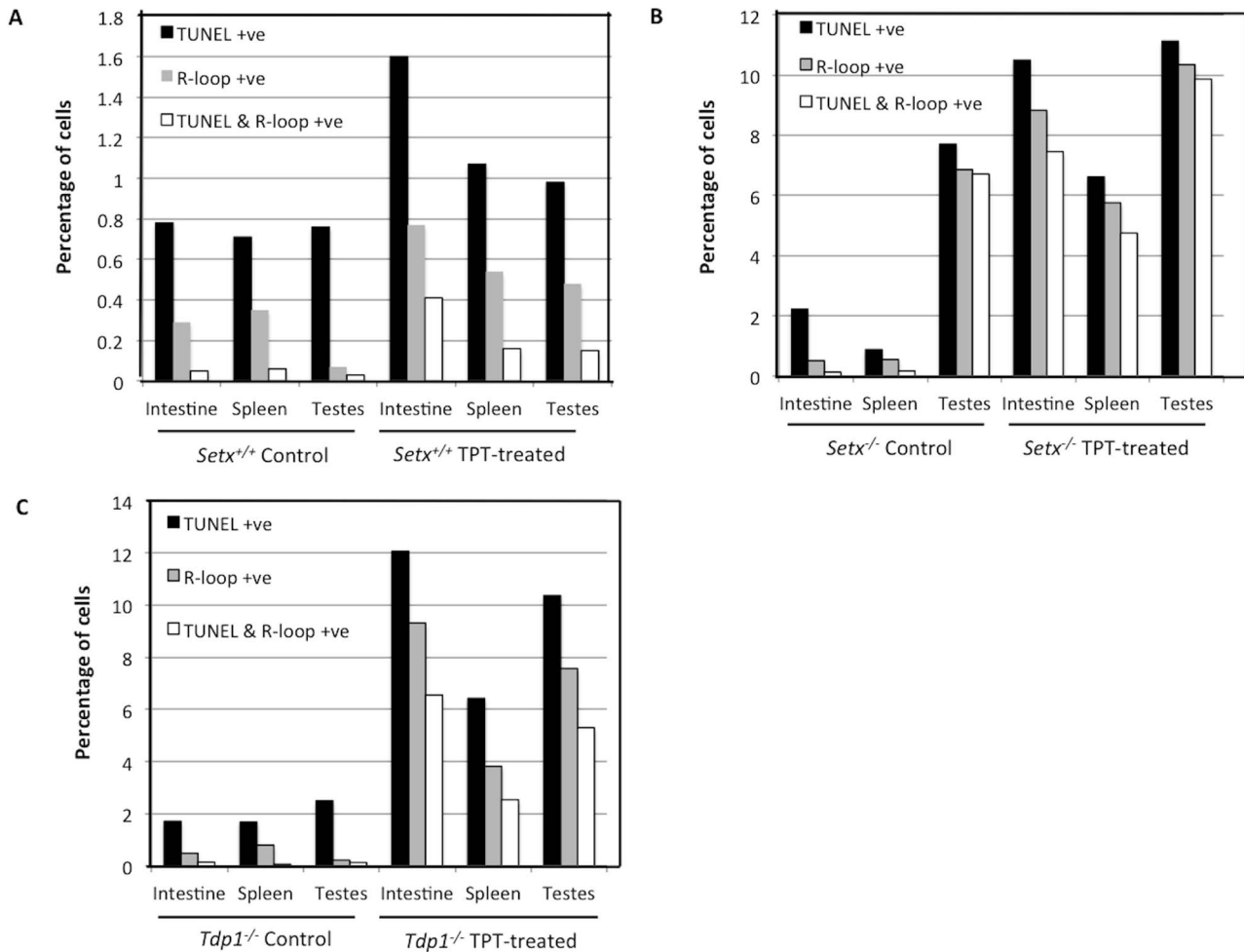


**Figure 10. Increased R-loop formation in TPT-treated knockout *Setx* and *Tdp1* mice.** Graphs show the percentage of apoptotic (TUNEL) cells only, cells containing R-loops only and apoptotic cells containing R-loops in the different tissues of *Setx* (A and B) and *Tdp1* mice (C). Counts were performed using 5 fields of view per tissue per animal (n=3). Higher levels of these three cell types were observed in TPT-treated knockout animals. doi:10.1371/journal.pone.0090219.g010

(Figure 11) [23]. Clearly neither of these events occur in post-mitotic neurons. While R-loops have been identified as a substrate for senataxin [24], it is possible there are other substrates which might be more important in post-mitotic cells. In this context, it has been shown that senataxin functions at different stages during transcription [22]. For instance, the binding of RNA polymerase II to candidate genes was significantly reduced in senataxin deficient cells and consequently the expression of these genes. Transcription termination was also abnormal as determined by transcript readthrough [22]. This was demonstrated in senataxin-depleted cells where an over-expression of RNase H resolved R-loops and caused transcriptional readthrough [24]. Suraweera et al 2009 also demonstrated that the splicing efficiency of specific mRNAs and alternate splice site selection were altered in senataxin-deficient cells [22]. The absence of R-loops in post-mitotic tissues may reflect a regulatory role for senataxin in transcription and/or RNA processing that does not involve the resolution of R-loops *per se*. Vantaggiato et al. 2011 reported a role for senataxin in neuronal differentiation through fibroblast growth factor 8 (FGF8) signalling where they found that an overexpression of senataxin was sufficient to trigger neuronal differentiation in primary hippocampal

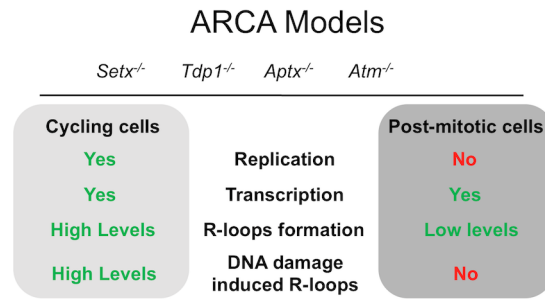


**Figure 11. R-loops preferentially form in cycling but not in post-mitotic cells.** Model depicting the requirements for R-loops formation in the various ARCA models. While transcription is implied in the formation of R-loops, active replication appears to be a necessary condition too. Thus R-loops accumulation does not appear to contribute to the neurodegenerative phenotype observed in autosomal recessive cerebellar ataxias. doi:10.1371/journal.pone.0090219.g011

neurons or in P19 cells treated with retinoic acid [53]. FGF8 is one of several growth factors that regulate neurogenesis, neuronal differentiation, survival and synaptic plasticity, both during development and in adulthood [53].

Cellular viability depends on the well-orchestrated functions carried out by numerous protein-coding and non-coding RNAs, as well as RNA-binding proteins. Mutations or abnormalities that disrupt RNA or protein components of RNP complexes can be deleterious to cells and cause disease states. During the last decade, it has become increasingly evident that abnormalities in RNA processing represent a common feature among many neurodegenerative diseases. For instance, some neurodegenerative diseases result from mutated coding and non-coding RNAs, and misregulation of long non-coding RNA transcription [54,55]. “RNAopathies” include diseases caused by non-coding repeat expansions and RNAs that exert toxicity via diverse mechanisms such as RNA foci formation, bidirectional transcription, and the production of toxic RNAs and proteins by repeat associated non-ATG translation [29]. Much work remains in order to elucidate the mechanisms underlying “RNA-binding proteinopathies”, such as amyotrophic lateral sclerosis (ALS) in which the RNA-binding protein TDP-43 plays a prominent role [54]. The absence of R-loops formation in post-mitotic neuronal cells as observed here in this study suggests that AOA2 may represent a novel “RNAopathy” in which defects in senataxin can affect the fidelity of the transcriptome. Further investigation of transcriptional regulation, RNA processing, and gene expression in AOA2 awaits the generation of an appropriate neuronal model for this disease.

## Materials and Methods

### Ethics Statement

All animal work and experiments have been approved by The QIMR Berghofer Medical Research Institute Animal Ethics Committee and all efforts were made to minimize suffering.

### Animal housing, husbandry and genotyping

The *Setx* (C57Bl6/129Sv), *Tdp1* (C57Bl6), *Aptx* (C57Bl6) and *Atm* (C57Bl6/129Sv) mouse strains were bred in house (QIMR Berghofer Medical Research Institute Animal House) and have previously been characterised and described [18,23,56,57]. Heterozygote mice for *Setx*<sup>+/-</sup> and *Atm*<sup>+/-</sup> were crossed to generate homozygote knockouts since both knockouts animals are sterile. *Tdp1*<sup>-/-</sup> and *Aptx*<sup>-/-</sup> were used for breeding since these animals are fertile. The mice were housed in a specific pathogen Free (SPF) PC2 facility in OptiMICE caging system (Opti-Polycarbonate cages) with artificial bedding material and subjected to a light/dark cycle of 12 h/12 h. Temperature of the animal facility was maintained constant (21°C–23°C) and the mice had permanent access to food and water (24 h/7days). Mice were housed with 2–5 companions per cage and had an enriched environment composed of shredded paper and toilet rolls. Welfare-related assessments were carried out prior to, during and after the experiment to ensure minimal suffering. The mice were ear clipped for identification at 10 days post-partum, genotyped, and weaned at 21 days post-partum. Genotyping was carried out by PCR on genomic DNA isolated from tail tips. Genotyping for the *Setx*, *Tdp1*, *Aptx* and *Atm* mice has been previously described [18,23,56,57]. Primer pairs are detailed in Figure S3. All experiments were carried out on adult (1 month-old) male animals. Tissue collection was performed after euthanasia (CO<sub>2</sub> gas) as instructed by Animal welfare guidelines. Animal colonies were regularly screened every 3 months for health and immune status.

### Histological analysis of ARCA mice testes

Testes from adult (1 month-old) male mice were collected and fixed in PBS buffered 10% formalin, embedded in paraffin block and sectioned at 4 μm. Sections were stained with Hematoxylin and Eosin (H&E). Slides were examined under light microscope and then scanned using Scanscope CS system (Aperio Technologies, Vista, USA). Images corresponding to ×10 and ×20 magnification were captured and assembled into Adobe Photoshop 7 (Adobe Systems Inc, USA).

### TUNEL assay for apoptosis

Paraffin sections from testes, brain, cerebellum, spleen and intestines were dewaxed and rehydrated with Shandon Varistain Gemini ES (Thermo Scientific, USA). Apoptotic cells were detected by Terminal deoxynucleotidyl transferase UTP Nick End Labelling (TUNEL) assay using the Fluorescence *in situ* Cell Death Detection Kit (Roche, Switzerland) following the manufacturer’s instructions. TUNEL is a method for detecting DNA fragmentation by labelling the terminal end of nucleic acids and a common method for detecting DNA fragmentation that results from apoptotic signalling cascades. DNA was stained with DAPI (1:10,000; Sigma-Aldrich) for 10 min at room temperature, and slides were mounted in Celvol 603 medium. Images were captured at room temperature using a digital camera (AxioCamMrm, Carl Zeiss Microimaging Inc., Germany) attached to a fluorescent microscope (Axioskop 2 mot plus, Carl Zeiss Microimaging Inc., Germany) and the AxioVision 4.8 software (Carl Zeiss, Microimaging Inc. Germany). The objectives employed were a Zeiss Plan Neofluar ×10/0.30 (mt10 magnification) or a 63× Zeiss Plan Aplanachromat 1,4 Oil DIC (Carl Zeiss, Germany). Images were subsequently assembled in Adobe Photoshop 7 (Adobe Systems Inc, USA), and contrast and brightness were adjusted on the whole image panel at the same time. For double staining, TUNEL was carried out first followed by immunostaining as described below.

### R-loop and DNA damage immunostaining on tissue sections

Slides with tissue sections were dewaxed and enzymatic antigen retrieval was performed by incubating the sections with 1:10 Trypsin dilution in PBS for 20 min at 37°C. Slides were washed 3 times for 5 min with PBS at room temperature for 5 min each. Tissues sections were blocked in (20% FCS, 2% BSA, 0.2% Triton X-100) for 1 h at room temperature. Slides were incubated with anti-R-loop (1:100, S9.6), anti-γH2AX (1:100, Y-P1016, Millipore) or anti-Ki67 (1:100, ab15580, Abcam) antibodies overnight at 4°C in a humidified chamber. Slides were washed 5 times with 1× PBS containing 0.5% Triton X-100 for 5 min each at room temperature. Alexa-Dye488 or Alexa-Dye594-conjugated secondary antibody (Molecular Probes, Life technologies) was added for 1 h at 37°C in a humidified chamber. Subsequently, slides were washed 3 times as before and DAPI (1:10,000; Sigma-Aldrich) was added for 10 min to staining nuclei. Slides were finally washed twice and glass coverslips were mounted in Celvol 603 medium for imaging. Imaging was performed as described above. Confirmation of R-loop specific staining was obtained by pre-treating *Setx*<sup>-/-</sup> testes sections with RNase H (New England Biolabs, USA) (Figure S1 A).

### siRNA transfection into HeLa cells and CPT treatment

HeLa cells (ATCC) were transfected with Stealth RNAi Negative Control LO GC (#12935200) (Invitrogen) and Stealth RNAi specific for the knock-down of *SETX* (Invitrogen): *SETX* 1 (CCAUCUAACUCUGUACAACUUGCUU) and *SETX* 3

(CCAAUUGCUCUUUCAGGUGUUUGA). Approximately  $2.5\text{--}10 \times 10^5$  cells were transiently transfected in a six-well plate with control/*SETX* RNAi oligoribonucleotide (5  $\mu\text{l}$  of a 20  $\mu\text{M}$  stock) using Lipofectamine 2000 (Invitrogen) as described by the manufacturer. Knock-down efficiency of *SETX* was determined 48 h post-transfection by immunoblotting of whole cell extracts and immunostaining using anti-senataxin (1:2000, Ab-1) antibody [20]. PARP-1 protein levels (1:1000, MCA1522G, Serotec) were used as the loading control. Control and *SETX* siRNA-transfected cells were treated with 25  $\mu\text{M}$  of camptothecin (CPT, Sigma-Aldrich) for 2 hours at 37°C/5% CO<sub>2</sub> to induce DNA damage and then fixed with 4% PFA and processed for immunostaining as previously described to detect R-loop formation [20,23]. Control and *SETX* siRNA-transfected cells were also treated with actinomycin D (5  $\mu\text{g}/\text{ml}$  for 2 hours at 37°C/5% CO<sub>2</sub>, Sigma-Aldrich) to transiently inhibit transcription prior to the addition of camptothecin to confirm the transcription-dependant formation of R-loops.

### Topotecan treatment of ARCA mouse models

In order to exacerbate the formation of R-loops and determine whether R-loop could form in post-mitotic tissues upon DNA damage accumulation, ARCA mouse models were treated with Topotecan (TPT) (Sigma-Aldrich), a water-soluble derivative of camptothecin for a period of 9 days. Topotecan was administered daily (approximately at 10:00 am) as an intraperitoneal injection following a brief anaesthesia using Isoflurane gas (2.5% at 3 L/min). Isoflurane is one of the safest methods recognised for rodents anaesthesia. For each genotype group, 3 mice were injected daily either with carrier solution (Sterile Injection Water BP, Pfizer) or TPT (2 mg/Kg/Day) and weight was monitored and recorded daily prior and 24 hours post injection. Animal weights were recorded prior, during, and after the treatment regimen. General health and behaviour of the mice was monitored daily until the end of the treatment when the animals were sacrificed to assess for R-loop formation, apoptosis levels and proliferation status.

### R-loop forming sequences (RLFS) prediction and DNA/RNA Immunoprecipitation (DRIP)

R-loop forming sequence (RLFS) model [37] was applied to predict the location of RLFSs in the mouse genome. RLFS region located downstream to the poly(A) signal (<500 bp) were selected for DRIP analysis (Figure S5). Two candidate genes, the *Pkd2l1* gene located in the HS44.2 locus on chromosome 19 and the *Foxo4* gene located on the X chromosome, were selected for DRIP analysis. Genomic DNA and RNA extraction from *Setx*<sup>+/+</sup> and *Setx*<sup>-/-</sup> mice testes, LCLs and HeLa cells were performed using the DNeasy Blood & Tissue Kit (Qiagen, USA) following the manufacturer's instructions. Extracts were sonicated (maximum voltage, constant output, microtip limit) for 3 min with 1 min incubation on ice within each min. 40  $\mu\text{l}$  of Protein G beads (50:50 slurry) (Millipore, Germany) was added to the extracts and pre-cleared. In a separate tube, 15  $\mu\text{g}$  of anti-R-loop antibody (S9.6) and 40  $\mu\text{l}$  of Protein G beads (50:50 slurry) (Millipore, Germany) were added together and incubated at 4°C overnight on a rotating wheel to allow binding of antibody to beads. Mouse anti-IgG antibody and 40  $\mu\text{l}$  of Protein G beads (50:50 slurry) (Millipore, Germany) were also added together to serve as a non-specific control for our experiment. The next day, the tubes were centrifuged at 5400 $\times$  g for 2 min to pellet the beads. The supernatant was then divided equally into 3 tubes- 1 was left untreated, 1 was treated with 200 U of S1 Nuclease (Promega, USA) and the other was treated with 10 U of RNase H (New

England BioLabs, USA). Extracts were incubated at 37°C for 2 h, heat inactivated for 20 min at 65°C then added on to the antibody-bound Protein G beads and incubated at 4°C overnight on a rotating wheel to allow binding of R-loops fragments to antibody-bound beads. The next day, the beads were pelleted at 5400 $\times$  g for 2 min and the supernatant was discarded. The beads were washed once with the IP Wash Buffer 1 (20 mM Tris-HCl pH 8.1, 2 mM EDTA, 50 mM NaCl, 1% Triton X-100, 0.1% SDS), twice with the High Salt Wash Buffer (20 mM Tris-HCl pH 8.1, 2 mM EDTA, 500 mM NaCl, 1% Triton X-100, 0.1% SDS), once with the IP Wash Buffer 2 (10 mM Tris-HCl pH 8.1, 1 mM EDTA, 0.25 M LiCl, 1% NP-40, 1% Deoxycholic Acid) and twice with TE Buffer (20 mM Tris-HCl pH 8.0, 1 mM EDTA). The immunoprecipitates were incubated at 4°C on a rocker for 3 min between each wash. The nucleic acids were then eluted twice with 100  $\mu\text{l}$  of Elution Buffer (100 mM NaHCO<sub>3</sub>, 1% SDS). 3  $\mu\text{l}$  of Proteinase K (20 mg/ml) was then added to each sample and incubated at 55°C. The samples were then diluted to 400  $\mu\text{l}$  with TE Buffer and 3  $\mu\text{l}$  of Glycogen (20 mg/ml) (Roche, Switzerland) was added. The nucleic acids were extracted using 400  $\mu\text{l}$  of Phenol Chloroform (1:1) and vortexed for 1 min. The samples were centrifuged at 16,000 $\times$  g for 5 min and the aqueous phase containing the nucleic acids were retained. These were extracted again using 400  $\mu\text{l}$  of Chloroform under the same conditions. 2.5 $\times$  of 100% EtOH was added to the samples and these were incubated at -80°C for 20 min. The samples were centrifuged at 16,000 $\times$  g for 20 min and the supernatant was decanted. The pellet was washed with 70% EtOH, centrifuged at 16,000 $\times$  g for 20 min and the supernatant was decanted. The pellet was air-dried and resuspended in EB Buffer (Qiagen, USA).

### PCR analyses from DRIP assay

Primers for the predicted RLFS of mouse HS44.2 region were mHS44.2 1F and mHS44.2 1R. Primers for the predicted RLFS of mouse *Foxo4* region were mFoxo4 F and mFoxo4 R. RLFS regions are detailed in Figure S5. PCR cycling conditions were as follows: 35 cycles, initial denaturation at 95°C for 3 min, denaturation at 95°C for 45 sec, annealing at 60°C for 45 sec, extension at 72°C for 1 min, with a final cycle and extension of 7 min at 72°C. The PCR product size for the HS44.2 and *Foxo4* regions were 226 bp and 357 bp respectively. See Figure S3 for list of primers.

### Senataxin immunoprecipitation

Immunoprecipitation of senataxin protein was performed as previously described [23].

### RT-PCR analysis for senataxin gene expression

Total RNA was isolated from 35-day-old wild type and knockout mice testes using the RNeasy mini kit (Qiagen, USA) according to the manufacturer's protocol. RNA concentrations were determined by UV spectrophotometry using a Nanodrop ND-2000 (Thermo scientific, USA) and cDNA was made from 1  $\mu\text{g}$  of purified RNA using Super Script III (Life technologies, USA) according to the manufacturer's protocol. Gene expression analysis was performed by PCR in a 2720 Thermal Cycler (Applied Biosystem, USA). Reactions (25  $\mu\text{l}$ ) contained 14.5  $\mu\text{l}$  of sterile water, 300 ng of cDNA template, 1 $\times$  PCR Buffer II (Roche, Switzerland), 2.5 mM MgCl<sub>2</sub> (Roche, Switzerland), 20  $\mu\text{M}$  dNTPs, 1  $\mu\text{M}$  of each primer, and 5  $\mu\text{l}$  of AmpliTaq Gold DNA Polymerase (Roche, Switzerland). The primer pairs used for gene expression analysis are described in Figure S3. Amplification was for 30 cycles and cycling conditions were as follows: denaturation for 5 min at 95°C for 30 sec, annealing at



65°C for 30 sec, elongation for 1 min at 72°C followed by a final extension step of 7 min at 72°C. PCR reactions were separated on 2% TAE agarose gels and visualised using Ethidium bromide and GelDoc system (Biorad, USA).

## Supporting Information

**Figure S1 Lack of R-loops formation in *Atm*<sup>-/-</sup>, *Aptx*<sup>-/-</sup> and *Tdp1*<sup>-/-</sup> brain and cerebellar sections.** **A.** Specificity of the R-loop (S9.6) antibody. Serial testes sections from *Setx*<sup>-/-</sup> animals were either pre-incubated with RNase H (1 hour at 37°C) or left untreated and subsequently immunostained for R-loops. As expected a reduction of R-loop fluorescence intensity is visible in RNase H-treated samples thus confirming the specificity of the R-loop antibody. **B.** Histological sections of brain and cerebellum were stained for R-loops (Red) and TUNEL (Green). DAPI stained nuclei. Scale bar, 100 µm. (TIFF)

**Figure S2 Knockdown of senataxin in HeLa cells using short interfering RNA (siRNA).** **A.** Following transfection of Control (Ctrl siRNA) and *SETX* siRNA, HeLa cells were immunostained for senataxin (SETX) and also processed for immunoblotting. As shown in panel A, a reduction in senataxin fluorescence signal was observed after *SETX* siRNA treatment. **B.** These data demonstrated the effective knock down of senataxin in HeLa cells via immunoblotting. **C.** Graph is plotted to show knockdown efficiency of *SETX*. (TIFF)

**Figure S3 Primer pairs used for the genotyping of *Atm*<sup>-/-</sup>, *Setx*<sup>-/-</sup>, *Aptx*<sup>-/-</sup>, *Tdp1*<sup>-/-</sup> mice, PCR analyses for HS44.2 and *Foxo4* regions from DRIP assay as well as RT-PCR.** (TIFF)

## References

- Anheim M, Monga B, Fleury M, Charles P, Barbot C, et al. (2009) Ataxia with oculomotor apraxia type 2: clinical, biological and genotype/phenotype correlation study of a cohort of 90 patients. *Brain* 132: 2688–2698.
- Sailer A, Houlden H (2012) Recent advances in the genetics of cerebellar ataxias. *Curr Neurol Neurosci Rep* 12: 227–236.
- Palau F, Espinos C (2006) Autosomal recessive cerebellar ataxias. *Orphanet J Rare Dis* 1: 47.
- Barzilai A, Biton S, Shiloh Y (2008) The role of the DNA damage response in neuronal development, organization and maintenance. *DNA Repair (Amst)* 7: 1010–1027.
- Lavin MF (2008) Ataxia-telangiectasia: from a rare disorder to a paradigm for cell signalling and cancer. *Nat Rev Mol Cell Biol* 9: 759–769.
- Savitsky K, Bar-Shira A, Gilad S, Rotman G, Ziv Y, et al. (1995) A single ataxia telangiectasia gene with a product similar to PI-3 kinase. *Science* 268: 1749–1753.
- Shiloh Y, Ziv Y (2013) The ATM protein kinase: regulating the cellular response to genotoxic stress, and more. *Nat Rev Mol Cell Biol* 14: 197–210.
- Schiller CB, Lammens K, Guerini I, Coordest B, Feldmann H, et al. (2012) Structure of Mre11-Nbs1 complex yields insights into ataxia-telangiectasia-like disease mutations and DNA damage signaling. *Nat Struct Mol Biol* 19: 693–700.
- Stewart GS, Maser RS, Stankovic T, Bressan DA, Kaplan MI, et al. (1999) The DNA double-strand break repair gene hMRE11 is mutated in individuals with an ataxia-telangiectasia-like disorder. *Cell* 99: 577–587.
- Carney JP, Maser RS, Olivares H, Davis EM, Le Beau M, et al. (1998) The hMre11/hRad50 protein complex and Nijmegen breakage syndrome: linkage of double-strand break repair to the cellular DNA damage response. *Cell* 93: 477–486.
- Barbi G, Scheres JM, Schindler D, Taalman RD, Rodens K, et al. (1991) Chromosome instability and X-ray hypersensitivity in a microcephalic and growth-retarded child. *Am J Med Genet* 40: 44–50.
- Walters R, Kalb R, Gatei M, Kijas AW, Stumm M, et al. (2009) Human RAD50 deficiency in a Nijmegen breakage syndrome-like disorder. *Am J Hum Genet* 84: 605–616.
- Caldecott KW (2008) Single-strand break repair and genetic disease. *Nat Rev Genet* 9: 619–631.
- Aicardi J, Barbosa C, Andermann E, Andermann F, Morcos R, et al. (1988) Ataxia-ocular motor apraxia: a syndrome mimicking ataxia-telangiectasia. *Ann Neurol* 24: 497–502.
- Ahel I, Rass U, El-Khamisy SF, Katyal S, Clements PM, et al. (2006) The neurodegenerative disease protein aprataxin resolves abortive DNA ligation intermediates. *Nature* 443: 713–716.
- Harris JL, Jakob B, Taucher-Scholz G, Dianov GL, Becherel OJ, et al. (2009) Aprataxin, poly-ADP ribose polymerase 1 (PARP-1) and apurinic endonuclease 1 (APE1) function together to protect the genome against oxidative damage. *Hum Mol Genet* 18: 4102–4117.
- Takashima H, Boerkoel CF, John J, Saifi GM, Salih MA, et al. (2002) Mutation of TDP1, encoding a topoisomerase I-dependent DNA damage repair enzyme, in spinocerebellar ataxia with axonal neuropathy. *Nat Genet* 32: 267–272.
- Katyal S, el-Khamisy SF, Russell HR, Li Y, Ju L, et al. (2007) TDP1 facilitates chromosomal single-strand break repair in neurons and is neuroprotective in vivo. *EMBO J* 26: 4720–4731.
- Moreira MC, Klur S, Watanabe M, Nemeth AH, Le Ber I, et al. (2004) Aprataxin, the ortholog of a yeast RNA helicase, is mutant in ataxia-ocular apraxia 2. *Nat Genet* 36: 225–227.
- Suraweera A, Becherel OJ, Chen P, Rundle N, Woods R, et al. (2007) Senataxin, defective in ataxia oculomotor apraxia type 2, is involved in the defense against oxidative DNA damage. *J Cell Biol* 177: 969–979.
- Yuce O, West SC (2013) Senataxin, defective in the neurodegenerative disorder ataxia with oculomotor apraxia 2, lies at the interface of transcription and the DNA damage response. *Mol Cell Biol* 33: 406–417.
- Suraweera A, Lim Y, Woods R, Birrell GW, Nasim T, et al. (2009) Functional role for senataxin, defective in ataxia oculomotor apraxia type 2, in transcriptional regulation. *Hum Mol Genet* 18: 3384–3396.
- Becherel OJ, Yeo AJ, Stellati A, Heng EY, Luff J, et al. (2013) Senataxin plays an essential role with DNA damage response proteins in meiotic recombination and gene silencing. *PLoS Genet* 9: e1003435.
- Skourtis-Stathaki K, Proudfoot NJ, Gromak N (2011) Human Senataxin Resolves RNA/DNA Hybrids Formed at Transcriptional Pause Sites to Promote Xrn2-Dependent Termination. *Mol Cell* 42: 794–805.

**Figure S4 Senataxin expression in mouse tissues.** **A.** Senataxin immunoprecipitations from testes, brain, cerebellum, spleen and intestine were carried out to detect senataxin protein levels. A faint signal corresponding to senataxin protein was only detected in *Setx*<sup>+/+</sup> testes indicating lower levels of senataxin in the others tissues and/or weak sensitivity of the senataxin (Ab-1) antibody. **B.** RT-PCR analysis from testes, brain, cerebellum, spleen and intestine confirmed the lower levels of senataxin expression in brain, cerebellum, spleen and intestine compared to testes. (TIFF)

**Figure S5 R-loop prediction and candidate genes selection.** **A.** An RLFS-containing region was found downstream of the *Pkd2l1* gene located in the HS44.2 locus. The predicted RLFS was found at the position Chr19: 44,221,689–44,221,838. **B.** In chromosome X, the RLFS located in *Foxo4* was found nearby a poly(A) signal. The predicted RLFS was found at the position ChrX: 98,456,266–98,456,499. For these genes, the predicted RLFS was located close to poly(A) signals (<500 bp) observed in mouse testes (by UCSC browser). Nucleotide sequence of the RLFS is in bold and primers are underlined. (TIFF)

## Acknowledgments

We thank QIMR Berghofer animal house staff for the maintenance of the mice.

## Author Contributions

Conceived and designed the experiments: AJY OJB MFL. Performed the experiments: AJY OJB JEL PJM TW PJ VK JKC. Analyzed the data: AJY OJB MFL. Wrote the paper: AJY OJB TW VAK MFL. In charge of the mouse-breeding program: JEL. Provided the *Tdp1* and *Aptx* mouse strains: PJM. Performed in silico RLFS prediction: TW PJ VK. Produced senataxin antibody: JKC.

25. Mischo HE, Gomez-Gonzalez B, Grzechnik P, Rondon AG, Wei W, et al. (2011) Yeast Sen1 helicase protects the genome from transcription-associated instability. *Mol Cell* 41: 21–32.
26. Hazelbaker DZ, Marquardt S, Wlotzka W, Buratowski S (2013) Kinetic competition between RNA Polymerase II and Sen1-dependent transcription termination. *Mol Cell* 49: 55–66.
27. Alzu A, Bermejo R, Begnis M, Lucca C, Piccini D, et al. (2012) Senataxin associates with replication forks to protect fork integrity across RNA-polymerase-II-transcribed genes. *Cell* 151: 835–846.
28. Richard P, Feng S, Manley JL (2013) A SUMO-dependent interaction between Senataxin and the exosome, disrupted in the neurodegenerative disease AOA2, targets the exosome to sites of transcription-induced DNA damage. *Genes Dev* 27: 2227–2232.
29. Belzil VV, Gendron TF, Petrucelli L (2013) RNA-mediated toxicity in neurodegenerative disease. *Mol Cell Neurosci* 56: 406–419.
30. Rulten SL, Caldecott KW (2013) DNA strand break repair and neurodegeneration. *DNA Repair (Amst)* 12: 558–567.
31. Barlow C, Liyanage M, Moens PB, Tarsounas M, Nagashima K, et al. (1998) Atm deficiency results in severe meiotic disruption as early as leptotema of prophase I. *Development* 125: 4007–4017.
32. Rogakou EP, Pilch DR, Orr AH, Ivanova VS, Bonner WM (1998) DNA double-stranded breaks induce histone H2AX phosphorylation on serine 139. *J Biol Chem* 273: 5858–5868.
33. Baudat F, Imai Y, de Massy B (2013) Meiotic recombination in mammals: localization and regulation. *Nat Rev Genet* 14: 794–806.
34. Wimberly H, Shee C, Thornton PC, Sivaramakrishnan P, Rosenberg SM, et al. (2013) R-loops and nicks initiate DNA breakage and genome instability in non-growing *Escherichia coli*. *Nat Commun* 4: 2115.
35. Gan W, Guan Z, Liu J, Gui T, Shen K, et al. (2011) R-loop-mediated genomic instability is caused by impairment of replication fork progression. *Genes Dev* 25: 2041–2056.
36. Ooi L, Wood IC (2008) Regulation of gene expression in the nervous system. *Biochem J* 414: 327–341.
37. Wongsurawat T, Jenjaroenpun P, Kwok CK, Kuznetsov V (2012) Quantitative model of R-loop forming structures reveals a novel level of RNA-DNA interactome complexity. *Nucleic Acids Res* 40: e16.
38. Wu ZK, Getun IV, Bois PR (2010) Anatomy of mouse recombination hot spots. *Nucleic Acids Res* 38: 2346–2354.
39. El Hage A, French SL, Beyer AL, Tollervey D (2010) Loss of Topoisomerase I leads to R-loop-mediated transcriptional blocks during ribosomal RNA synthesis. *Genes Dev* 24: 1546–1558.
40. Marinello J, Chillemi G, Bueno S, Manzo SG, Capranico G (2013) Antisense transcripts enhanced by camptothecin at divergent CpG-island promoters associated with bursts of topoisomerase I-DNA cleavage complex and R-loop formation. *Nucleic Acids Res*.
41. Kasiviswanathan R, Minko IG, Lloyd RS, Copeland WC (2013) Translesion synthesis past acrolein-derived DNA adducts by human mitochondrial DNA polymerase gamma. *J Biol Chem* 288: 14247–14255.
42. Falkenberg M, Larsson NG, Gustafsson CM (2007) DNA replication and transcription in mammalian mitochondria. *Annu Rev Biochem* 76: 679–699.
43. Zhang G, Darst SA (1998) Structure of the *Escherichia coli* RNA polymerase alpha subunit amino-terminal domain. *Science* 281: 262–266.
44. Koster DA, Palle K, Bot ES, Bjornsti MA, Dekker NH (2007) Antitumour drugs impede DNA uncoiling by topoisomerase I. *Nature* 448: 213–217.
45. Sobell HM (1985) Actinomycin and DNA transcription. *Proc Natl Acad Sci U S A* 82: 5328–5331.
46. Kollmannsberger C, Mross K, Jakob A, Kanz L, Bokemeyer C (1999) Topotecan - A novel topoisomerase I inhibitor: pharmacology and clinical experience. *Oncology* 56: 1–12.
47. Guichard S, Montazeri A, Chatelut E, Hennebelle I, Bugat R, et al. (2001) Schedule-dependent activity of topotecan in OVCAR-3 ovarian carcinoma xenograft: pharmacokinetic and pharmacodynamic evaluation. *Clin Cancer Res* 7: 3222–3228.
48. Wong ET, Berkenblit A (2004) The role of topotecan in the treatment of brain metastases. *Oncologist* 9: 68–79.
49. Xu Y, Ashley T, Brainerd EE, Bronson RT, Meyn MS, et al. (1996) Targeted disruption of ATM leads to growth retardation, chromosomal fragmentation during meiosis, immune defects, and thymic lymphoma. *Genes Dev* 10: 2411–2422.
50. Fogel BL, Perlman S (2007) Clinical features and molecular genetics of autosomal recessive cerebellar ataxias. *Lancet Neurol* 6: 245–257.
51. Lavin MF (2013) The appropriateness of the mouse model for ataxia-telangiectasia: neurological defects but no neurodegeneration. *DNA Repair (Amst)* 12: 612–619.
52. Gromak N, West S, Proudfoot NJ (2006) Pause sites promote transcriptional termination of mammalian RNA polymerase II. *Mol Cell Biol* 26: 3986–3996.
53. Vantaggiato C, Bondioni S, Airolti G, Bozzato A, Borsani G, et al. (2011) Senataxin modulates neurite growth through fibroblast growth factor 8 signalling. *Brain* 134: 1808–1828.
54. Hanson KA, Kim SH, Tibbetts RS (2012) RNA-binding proteins in neurodegenerative disease: TDP-43 and beyond. *Wiley Interdiscip Rev RNA* 3: 265–285.
55. Cirillo D, Agostini F, Klus P, Marchese D, Rodriguez S, et al. (2013) Neurodegenerative diseases: quantitative predictions of protein-RNA interactions. *RNA* 19: 129–140.
56. Barlow C, Hirotsune S, Paylor R, Liyanage M, Eckhaus M, et al. (1996) Atm-deficient mice: a paradigm of ataxia telangiectasia. *Cell* 86: 159–171.
57. El-Khamisy SF, Katyal S, Patel P, Ju L, McKinnon PJ, et al. (2009) Synergistic decrease of DNA single-strand break repair rates in mouse neural cells lacking both Tdp1 and aprataxin. *DNA Repair (Amst)* 8: 760–766.

**Figure S1**

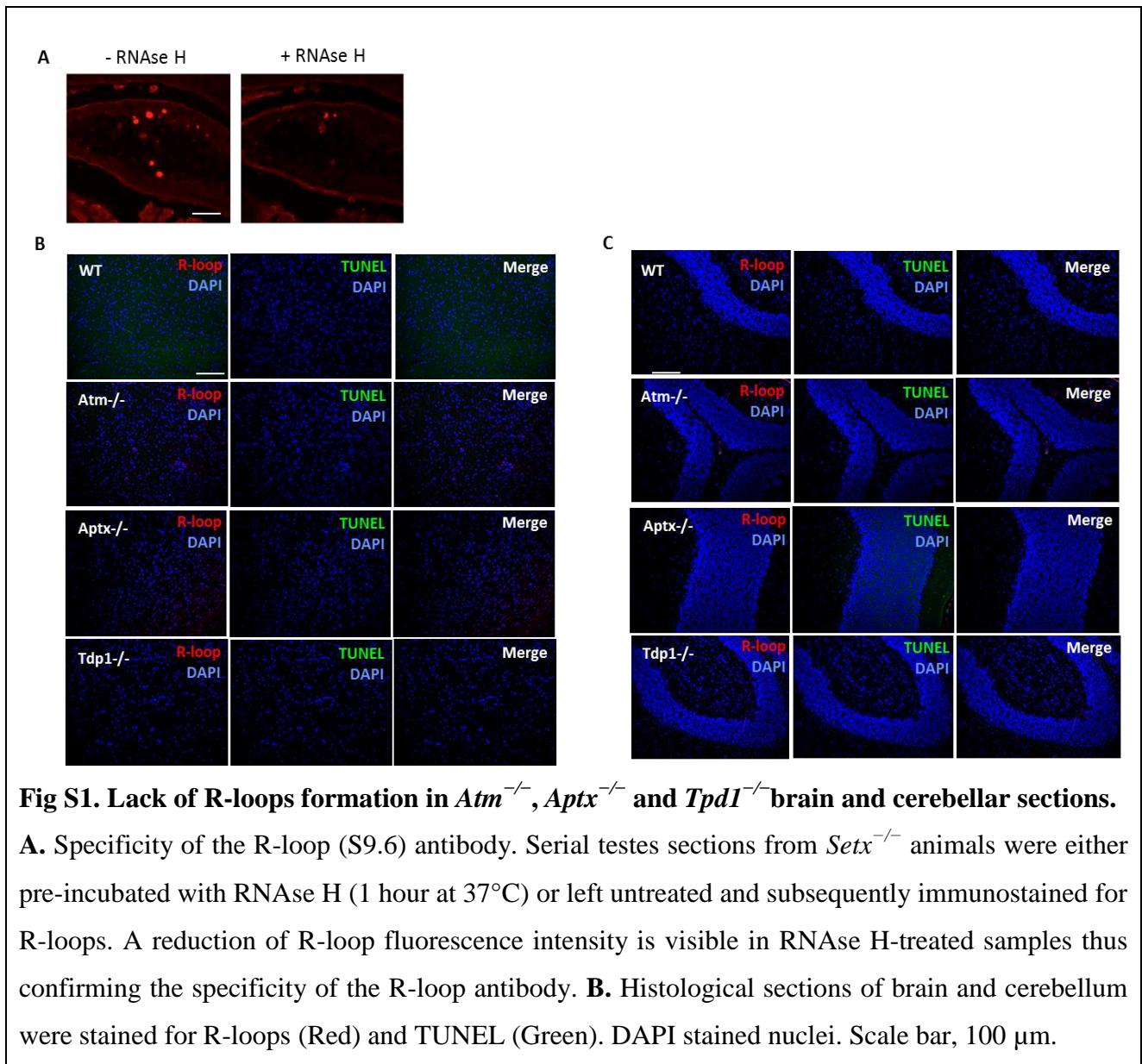


**Figure S2**

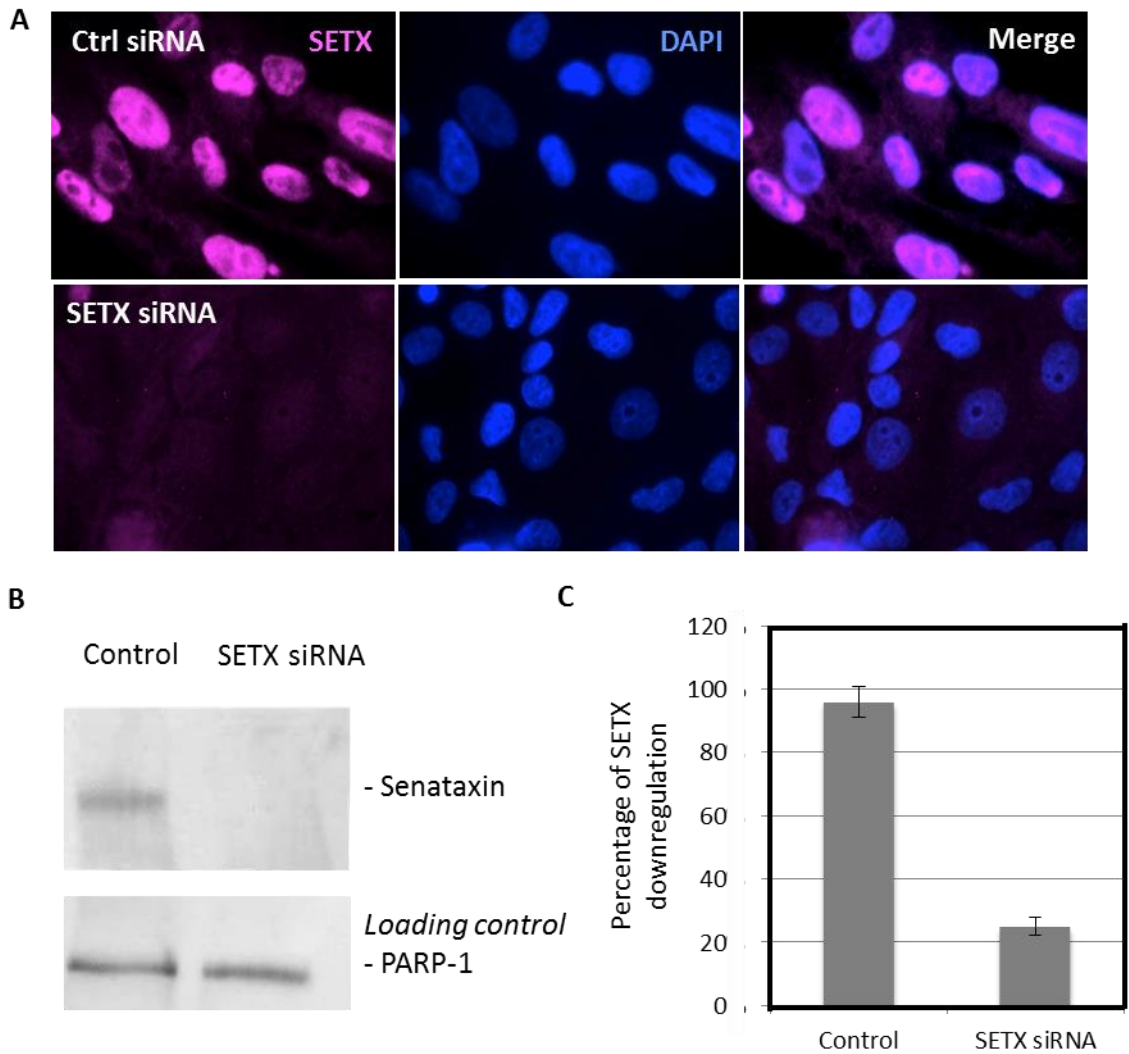


**Fig S2. Knockdown of senataxin in HeLa cells using short interfering RNA (siRNA).** **A.** Following transfection of Control (Ctrl siRNA) and *SETX* siRNA, HeLa cells were immunostained for senataxin (SETX) and also processed for immunoblotting. As shown in panel **A**, a reduction in senataxin fluorescence signal was observed after *SETX* siRNA treatment. **B.** Effective knockdown of senataxin in HeLa cells revealed by immunoblotting. **C.** Graph is plotted to show knockdown efficiency of *SETX*.

**Figure S3**

Gene	Primer name	Primer sequence
<i>Atm</i>	KO1F	5'-TGGTCAGTGTAACAGTCATTGTGC-3'
	KO1R	5'-AAGGTTGTAGATAGGTCAGCATTG-3'
	KO2R	5'AACGAGATCAGCAGCCTCTGTTC-3'
<i>Setx</i>	In3F	5'-TTTAAGGAACAGTGCTGC-3'
	In3R	5'-ATGAAGCAGGTAGGATT-3'
	LoxPR	5'-CGAAGTTATATTAAGGGT-3'
<i>Tdp1</i>	Tdp1F	5'-TCTTCCAGTTCTTAGCCTCCTCTGC-3'
	Tdp1R	5'-TGGCCTGGATCTCACTCTGGAGGC-3'
	Geor3	5'-GAGTTCCCAGGAGGAGCCAAGGC-3'
<i>Aptx</i>	Aptx1F	5'-TTCTCTCCATGACTGGTCATGGC-3'
	Aptx1R	5'-TATACTCAGAGCCGGCCT-3'
	Aptx2R	5'-TCCTCGTCGTTTACGGTATC-3'
<i>HS44.2</i>	mHS44.2 1F	5' AGCGGGTTTACGGAATGCTT-3'
	mHS44.2 1R	5'-AGTCTTCAGAGAGGAGATTAGAGGA-3'
<i>Foxo4</i>	mFoxo4 F	5'-GGTTTCTGGTTTCTGCTGCC-3'
	mFoxo4 R	5'-AGGGCTGGAGTGAACACTTG-3'
<i>SETX (cDNA)</i>	SETX2F	5'-CAGCCTCTTCATCCTCGGAC-3'
	SETX2R	5'-ACTGTCTAGCTTGCTGCTGG-3'
<i>GAPDH (cDNA)</i>	GAPDH1F	5'-TGGTGAAGCAGGCATCTGAG-3'
	GAPDH1R	5'-CCATGTAGCCATGAGGTCC-3'

**Fig S3. Primer pairs used for the genotyping of *Atm*<sup>-/-</sup>, *Setx*<sup>-/-</sup>, *Aptx*<sup>-/-</sup>, *Tdp1*<sup>-/-</sup> mice, PCR analyses for HS44.2 and Foxo4 RLFS regions and RT-PCR for *Setx* expression.**

**Figure S4**

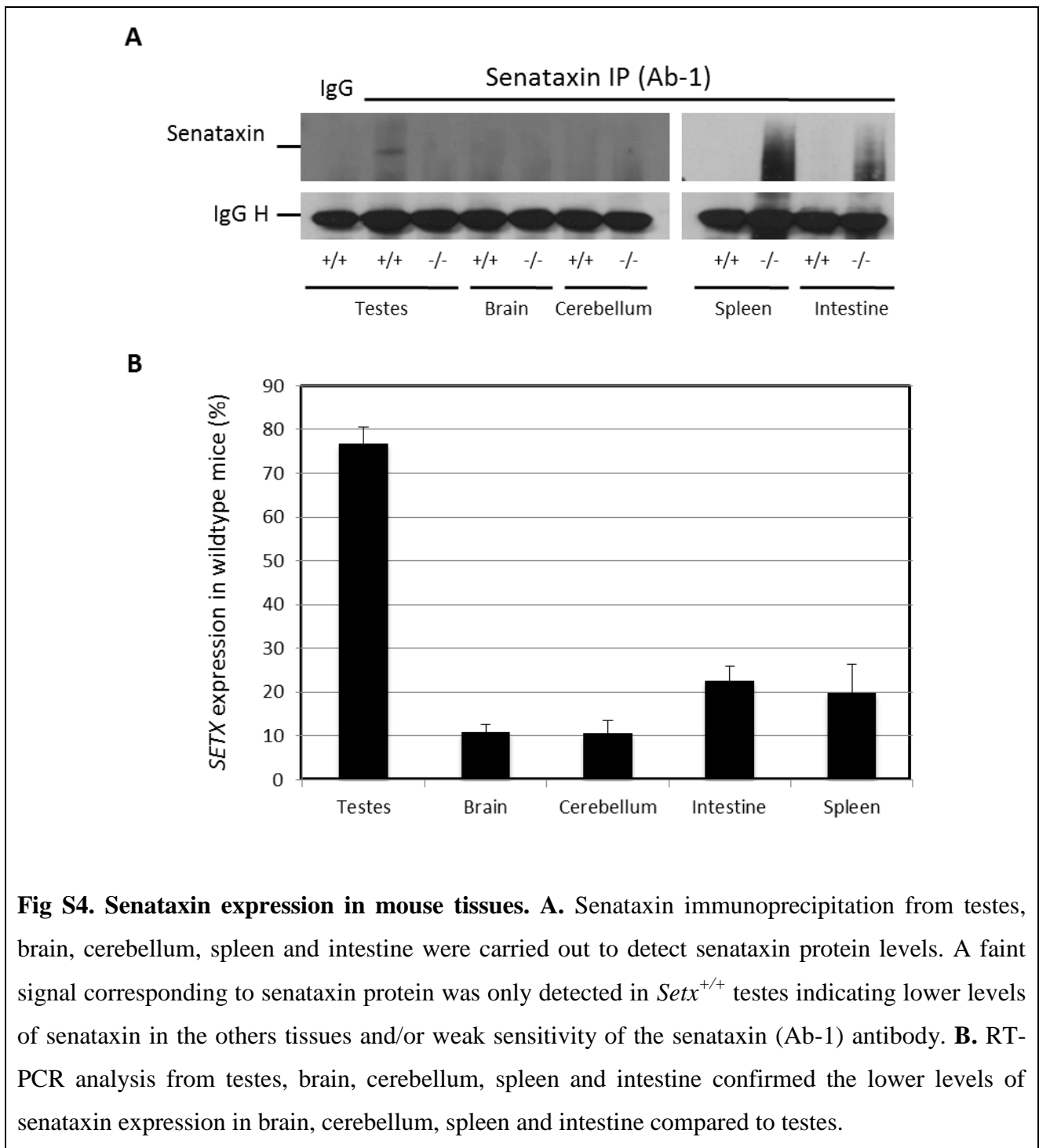


## Figure S5

**A**

5'AGCGGGTTTACGGAATGCTT**GGGGGAGGGGGTGGTGAGAACAGGTGGGGGTGACAGGGATGAATAGAA**  
**GGCTCAGTGTGAGGGAATGAGAGTCACTGGAGAGGGGGAAAGAGGTGTGTAAGGGTTTTTCAGGATGCAGG**  
**CTCCTGAGCATCCAAAATCTTAAGTGTAGAG**TTTTTACTAAGTTAACTTAGTCTTGGTTATCCCTCTAATCTCCT  
CTCTGAAGACT-3'

**B**

5'GGTTTCTGGTTTCTGCTGCCTTTGCTGCCCCCCCTCCCCGTCCAATAT**GGGGGAGGGAGGGAGGCCG**  
**AAAGGCGAAGGGCAGTTAGGCGAAGGGCTGGTGGGAGGGACTGCCCGCAGGCTGGGAGGTGGGGGAATT**  
**TCAGCCTGGGAGGTAATGGAGTGTGTTGGGGGAGGGACACCTAACCCAGCAGGAGTAGGCCGGCTGCAAG**  
**ATAGGCCTCCCCGAGGGGAGGTAGTCTGGTTTGAGAAGACCCACCCCTTCTCTGGCCCTCAAAGGCTTA**  
**TTGTACTAAAAGTCTAGCAAGTAGACTTCACAGTCTTTCCTCACCGCCCCCCCCCT**CAAGTGTTCACTCCAGC  
CCT-3'

**Figure S5. R-loop prediction and candidate gene selection.** **A.** An RLFS-containing region was found downstream of the *Pkd21l* gene located in the HS44.2 locus. The predicted RLFS was found at the position Chr19: 44,221,689–44,221,838. **B.** In chromosome X, the RLFS located in *Foxo4* was found nearby a poly (A) signal. The predicted RLFS was found at the position ChrX: 98,456,266–98,456,499. For these genes, the predicted RLFS was located close to poly(A) signals (<500 bp) observed in mouse testes (by UCSC browser). Nucleotide sequence of the RLFS is in bold and primers are underlined.

### 5.3 Results (continued)

The following section contains results of the TPT-treatment experiment performed on *Atm* and *Aptx* mice, and additional DRIP assays performed on *Setx*<sup>-/-</sup> mice.

#### 5.3.1 DNA damage induces R-loop accumulation in proliferative tissues in *Atm*<sup>-/-</sup> and *Aptx*<sup>-/-</sup> mice

Similar to that seen in *Setx*<sup>-/-</sup> and *Tdp1*<sup>-/-</sup> mice, *Atm*<sup>-/-</sup> and *Aptx*<sup>-/-</sup> mice treated with TPT (2mg/kg/day) for 9 days showed approximately 30% weight loss after a 9-day period as compared to WT mice (Fig 5.1).

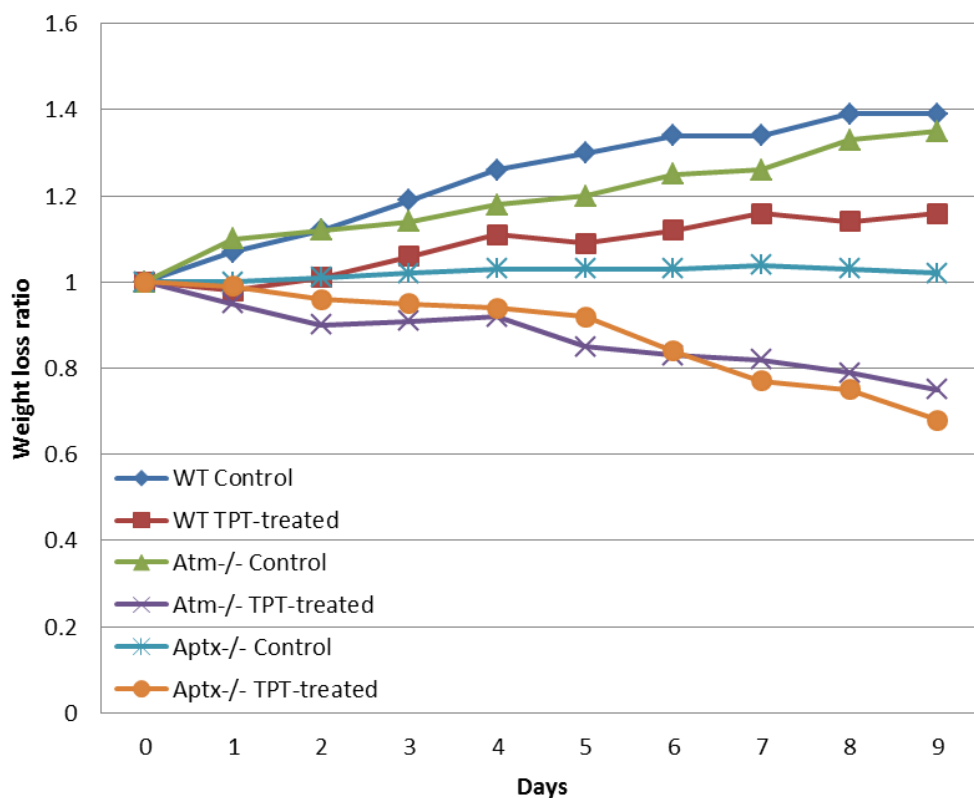


**Fig 5.1 Treatment of *Atm* and *Aptx* mice with topotecan hydrochloride induces severe weight loss.** Wild type (WT), *Atm*<sup>-/-</sup> and *Aptx*<sup>-/-</sup> mice were treated with topotecan hydrochloride (TPT, 2 mg/kg/day) over a period of 9 days. Mice of each genotype were injected daily with TPT and weights were recorded daily (n = 3). Controls were injected with an equivalent volume of purified water.



As previously reported, these mice do not display any gross neurological phenotype associated with the corresponding human disorders<sup>59,270</sup>. The presence of R-loops and cell death via TUNEL assay were assessed in both untreated and TPT-treated animals in highly proliferative tissue and post-mitotic tissue.

Following TPT treatment, R-loop accumulation was only observed in replicating cells of the intestine, spleen and testes [Fig 5.2 and Fig 5.3 (extreme right panels)] and not in post-mitotic cells of the brain and cerebellum [(Fig 5.3, extreme left and middle panels)]. Similar results were obtained in the *Aptx* mice.

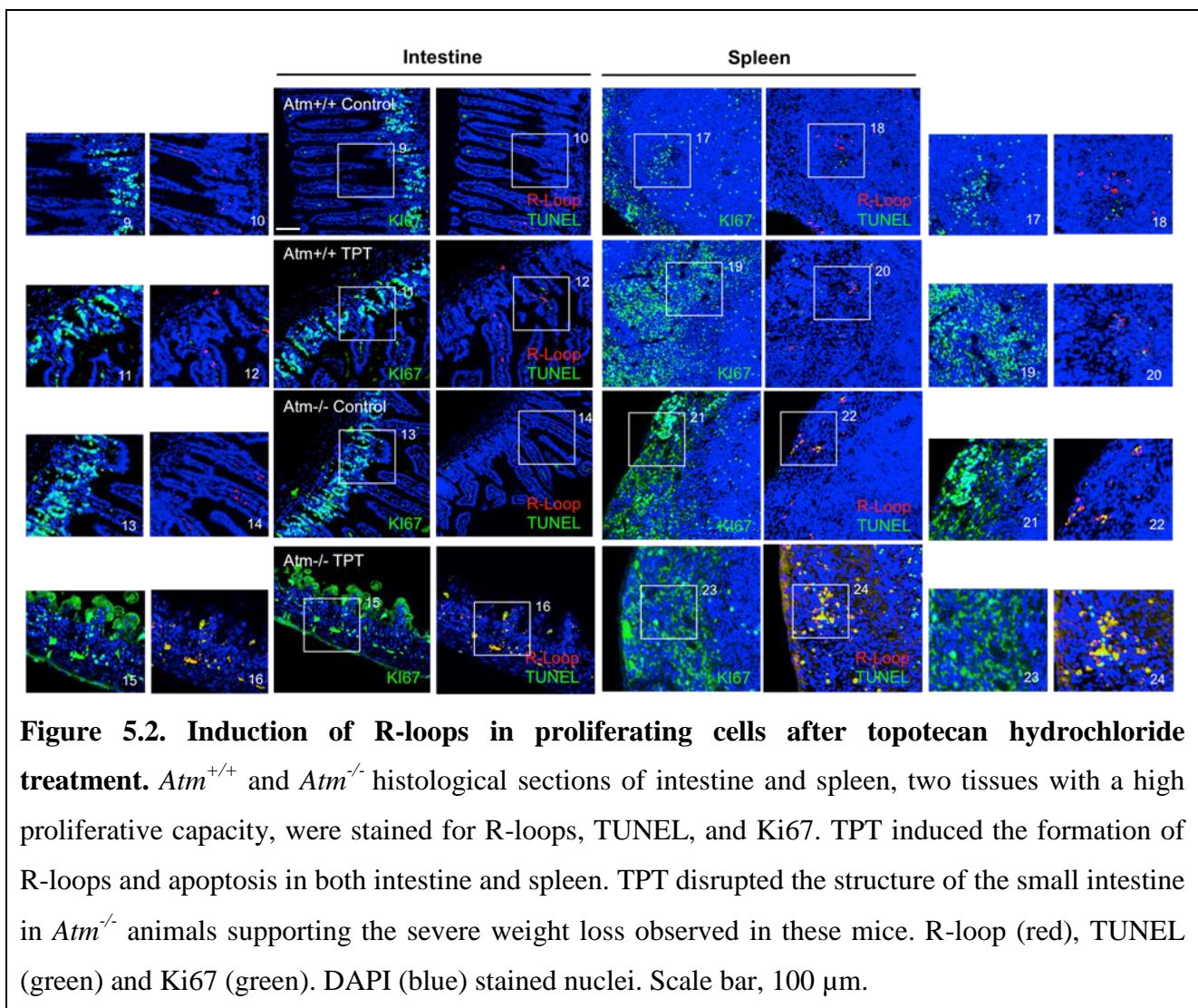


**Figure 5.2. Induction of R-loops in proliferating cells after topotecan hydrochloride treatment.** *Atm*<sup>+/+</sup> and *Atm*<sup>-/-</sup> histological sections of intestine and spleen, two tissues with a high proliferative capacity, were stained for R-loops, TUNEL, and Ki67. TPT induced the formation of R-loops and apoptosis in both intestine and spleen. TPT disrupted the structure of the small intestine in *Atm*<sup>-/-</sup> animals supporting the severe weight loss observed in these mice. R-loop (red), TUNEL (green) and Ki67 (green). DAPI (blue) stained nuclei. Scale bar, 100  $\mu$ m.

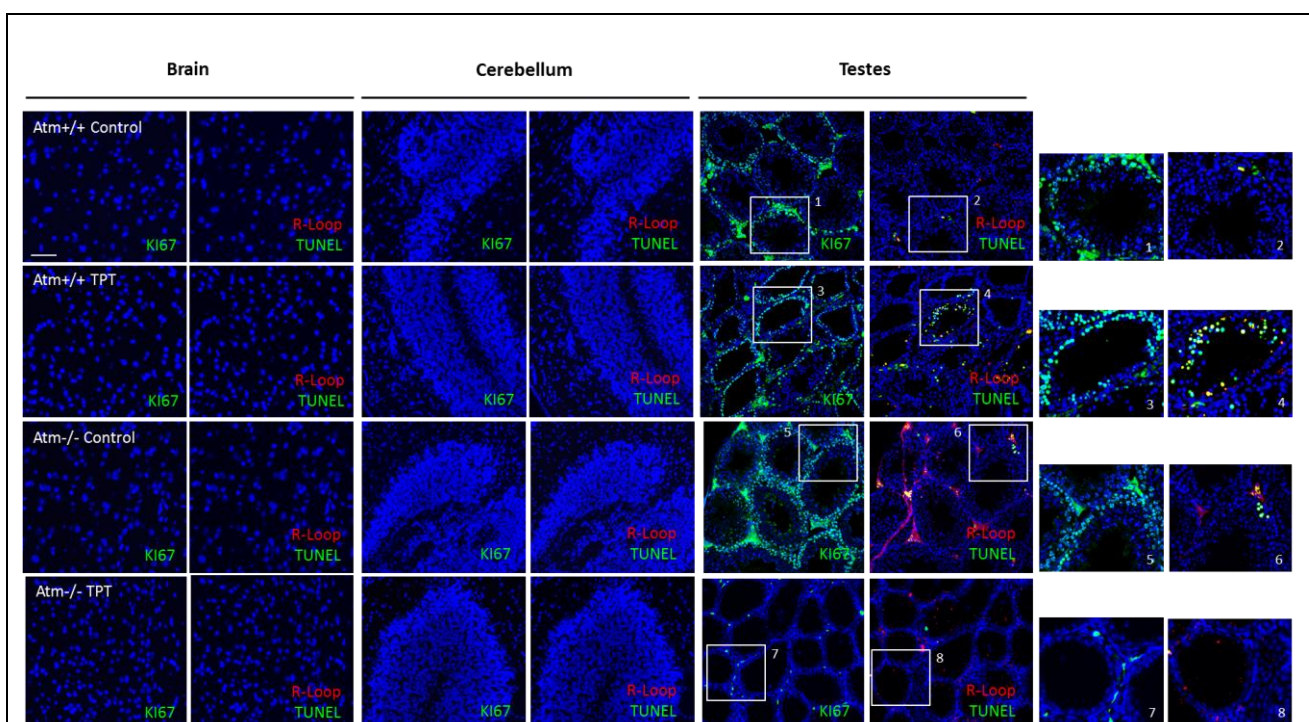
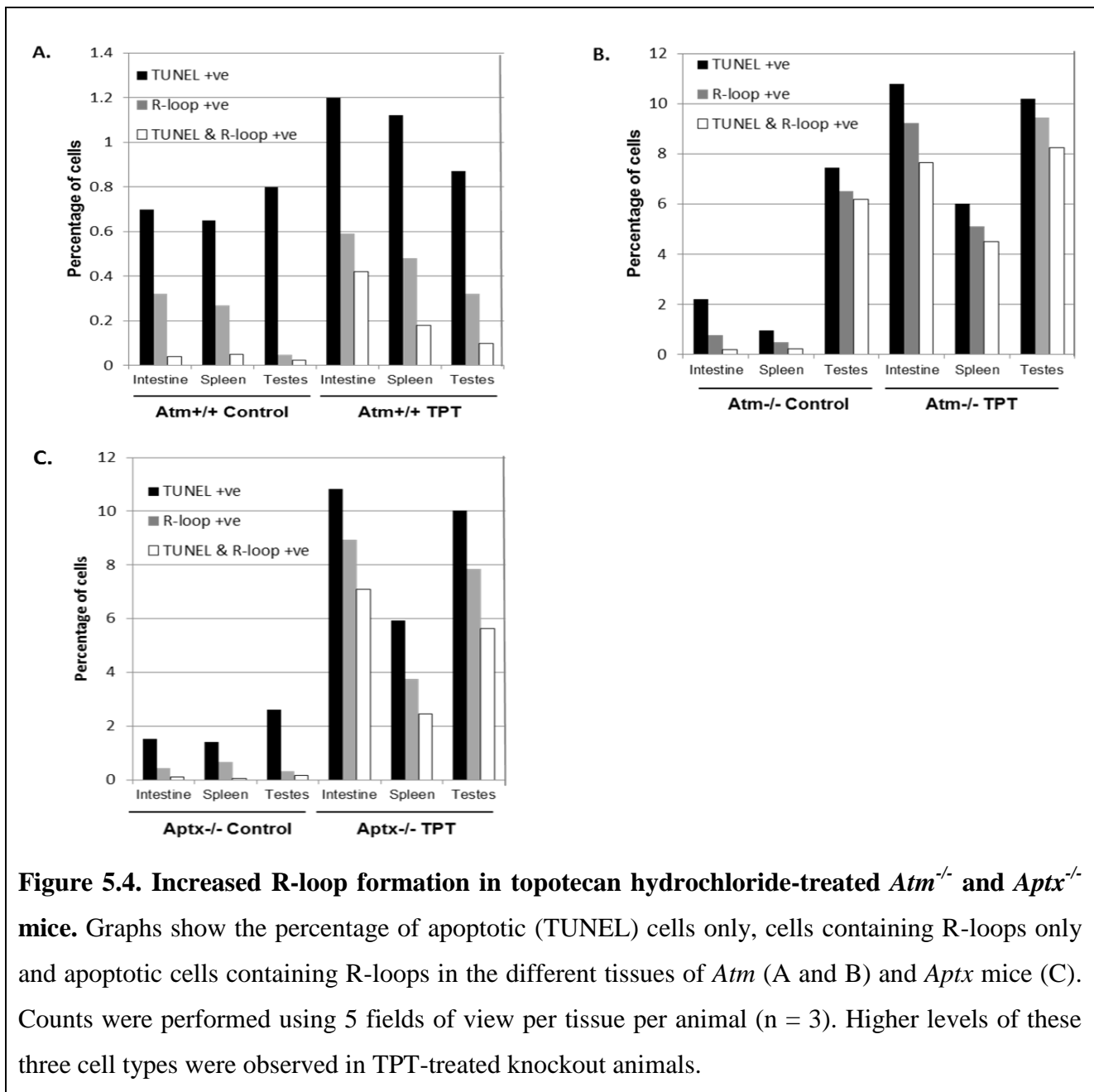


**Figure 5.3. Topotecan hydrochloride treatment does not induce R-loops formation in post-mitotic nervous tissues in *Atm*<sup>-/-</sup> mice.** Histological sections of brain, cerebellum, and testes were immunostained for R-loops (Red) and TUNEL (Green). No R-loops were detected in brain and cerebellum sections after TPT treatment. DAPI stained nuclei and Ki67 (green) was used as a marker for proliferation. Scale bar, 100  $\mu\text{m}$ .

The number of R-loops-containing cells in TPT-treated *Atm*<sup>-/-</sup> mice increased in all three highly proliferative tissues by an 11.83-fold in the intestine, 10.24-fold in the spleen, and 1.45-fold in the testes which remained the tissue containing the highest number of R-loops-positive cells (Fig 5.4A and B). This is in contrast to treated *Atm*<sup>+/+</sup> mice where only a 1.8 fold increase was observed in the intestine, a 1.7 fold in the spleen and a 6.4 fold in the testes.

Similar results were observed for *Aptx*<sup>-/-</sup> mice (Fig 5.4C). Less than 0.5% of R-loops-positive cells were detected in *Aptx*<sup>-/-</sup> mice under normal conditions. TPT treatment of *Aptx*<sup>-/-</sup> mice also lead to a significant increase in the number of R-loops-positive cells with intestine and testes displaying a 21.3-fold and 25.2-fold increase, respectively. As a consequence of the TPT-induced R-loop accumulation, the number of double-positive cells (R-loop & TUNEL) after TPT treatment also increased in *Atm*<sup>+/+</sup>, *Atm*<sup>-/-</sup>, and *Aptx*<sup>-/-</sup> mice further supporting the effect of R-loop accumulation in genome stability.



The lack of *Atm* and *Aptx*, two proteins involved in the DNA damage response and repair, led to the accumulation of R-loops in proliferative tissues after TPT treatment, indicating that besides protein involved directly in R-loops processing such as senataxin and RNase H, mutations in proteins associated with various DNA repair can also promote the formation of R-loops. These findings provide evidence for a broader, novel role for R-loops in genomic instability, and that perhaps the detection of R-loops may represent a useful diagnostic marker to assess for genome integrity.

### 5.3.2 R-loops accumulate along the mouse *WWOX* and *XY* genes in *Setx*<sup>-/-</sup> spermatocytes

Common fragile sites (CSFs) are specific chromosomal regions that have a higher propensity to form gaps or breaks under replication stress due to frequent replication fork stalling<sup>271,272</sup>. Such lesions can lead to genomic instability, and FRA16D in the *WWOX* gene is one such site in the human genome that is very prone to damage<sup>273</sup>. *WWOX* encodes the WW domain containing oxidoreductase that is known to be a tumor suppressor gene and is an example of a long gene that requires more than 1 cycle of replication to complete<sup>271,274</sup>. The FRA16D region encodes a 1.2 kb transcript but the gene itself covers over 1 mb in length. Interestingly, the downregulation of *WWOX* has been reported in neurological disorders such as Alzheimer's disease<sup>36</sup>, cerebellar ataxias<sup>275</sup> and microcephaly syndromes<sup>276</sup>.

Helmrich et al. 2011 showed that the collision between the replication and transcription machinery along the *WWOX* gene resulted in the formation of R-loops and led to genomic instability<sup>271</sup>. Therefore, whether or not a similar phenomenon occurs in the *Setx*<sup>-/-</sup> mouse model was investigated. FRA16D and its associated gene *WWOX* are highly conserved in the mouse at Fra8E1<sup>277</sup>; hence an R-loop forming site (RLFS) prediction on this region was performed based on the algorithm used by Wongsurawat et al. 2012<sup>278</sup> (Fig 5.5A). A DRIP assay (described in section 2.2) was subsequently performed from the testes, brain and cerebellum of WT and *Setx*<sup>-/-</sup> mice followed by PCR analysis along the predicted RLFS. A similar background level in the WT and *Setx*<sup>-/-</sup> brain and cerebellum was observed but there was a significantly higher level of R-loop formation in this region in the *Setx*<sup>-/-</sup> testes as compared to WT (Fig 5.5B).

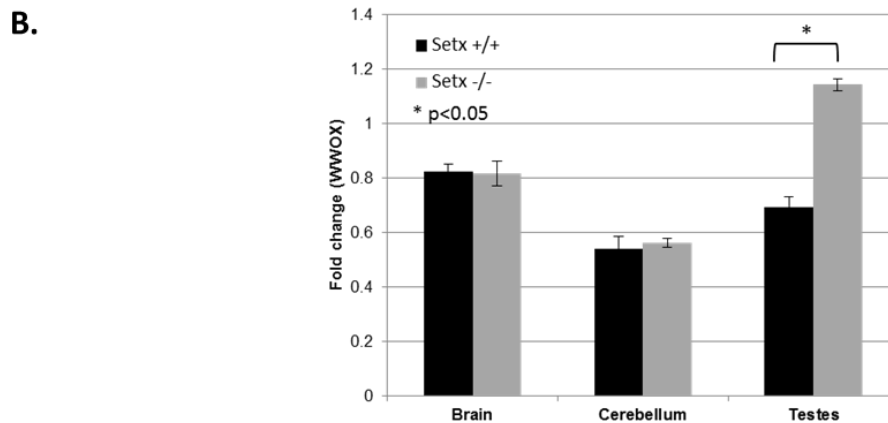
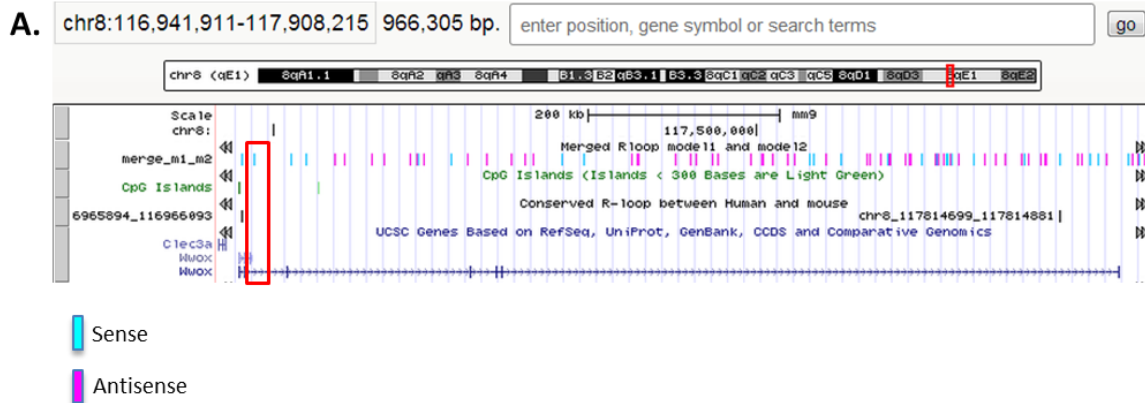


**Figure 5.5. Increased R-loop formation at Fra8E1 in testes of *Setx*<sup>-/-</sup> mice.** **A.** Predicted RLFS denoted in blue (sense) and pink (antisense) bars. Regions on the sense strand were selected for DRIP-PCR analysis and are indicated in red boxes. **B.** Graph shows the DRIP quantitation of various tissues taken from WT and *Setx*<sup>-/-</sup> mouse. Similar background levels of R-loops were observed in brain and cerebellum, with a significant increase observed in the testes of *Setx*<sup>-/-</sup> mice.

These data are comparable to those presented in Section 5.2 for the HS44.2 locus and the X chromosome *FOXO4* gene, where increased levels of R-loops were observed only in the testes. These data further support that hypothesis that both ongoing transcription and replication are necessary and that the collision between replication and transcription causes R-loop formation and can lead to genomic instability.

Spermatocytes from male *Setx*<sup>-/-</sup> mice show an accumulation of R-loops at the pachytene stage of meiosis and the failure of meiotic sex chromosome inactivation (MSCI) during spermatogenesis, which could contribute to the male sterility observed in *Setx*<sup>-/-</sup> mice. It was also shown in Chapter 3, via RT-PCR, that X- and Y-linked genes were being transcribed in the testes of *Setx*<sup>-/-</sup> mice instead of being repressed as in MSCI. Aberrant gene expression could be due to the lack of methylation along these genes as reported by Ginno et al. 2012, where it was shown that the methylation of CpG

island promoters was hampered by the formation of R-loops along these GC-rich regions<sup>170</sup>. Hence, R-loop accumulation along X- and Y-linked genes in *Setx*<sup>-/-</sup> spermatocytes was examined. Two XY genes that were found to be highly expressed in *Setx*<sup>-/-</sup> mouse testes (see Chapter 2), *Ube1y* and *Tktl1*, were selected for the DRIP analysis. In addition to the R-loop prediction described by Wongsurawat et al. 2012, RLFSS in these genes were also predicted using an online bioinformatics tool, QuadFinder (<http://miracle.igib.res.in/quadfinder/>), which predicts likely regions of R-loop formation based on G-quadruplexes-forming sequences. G-quadruplexes are non-canonical four-stranded nucleic acid structures formed by G-rich sequences. Although their physiological roles remain unclear, they have been implicated in transcription regulation and translation among other functions<sup>279,280</sup>. A region on each of the sense strands of *Ube1y1* and *Tktl1* were selected for the DRIP analysis (Fig 5.6).

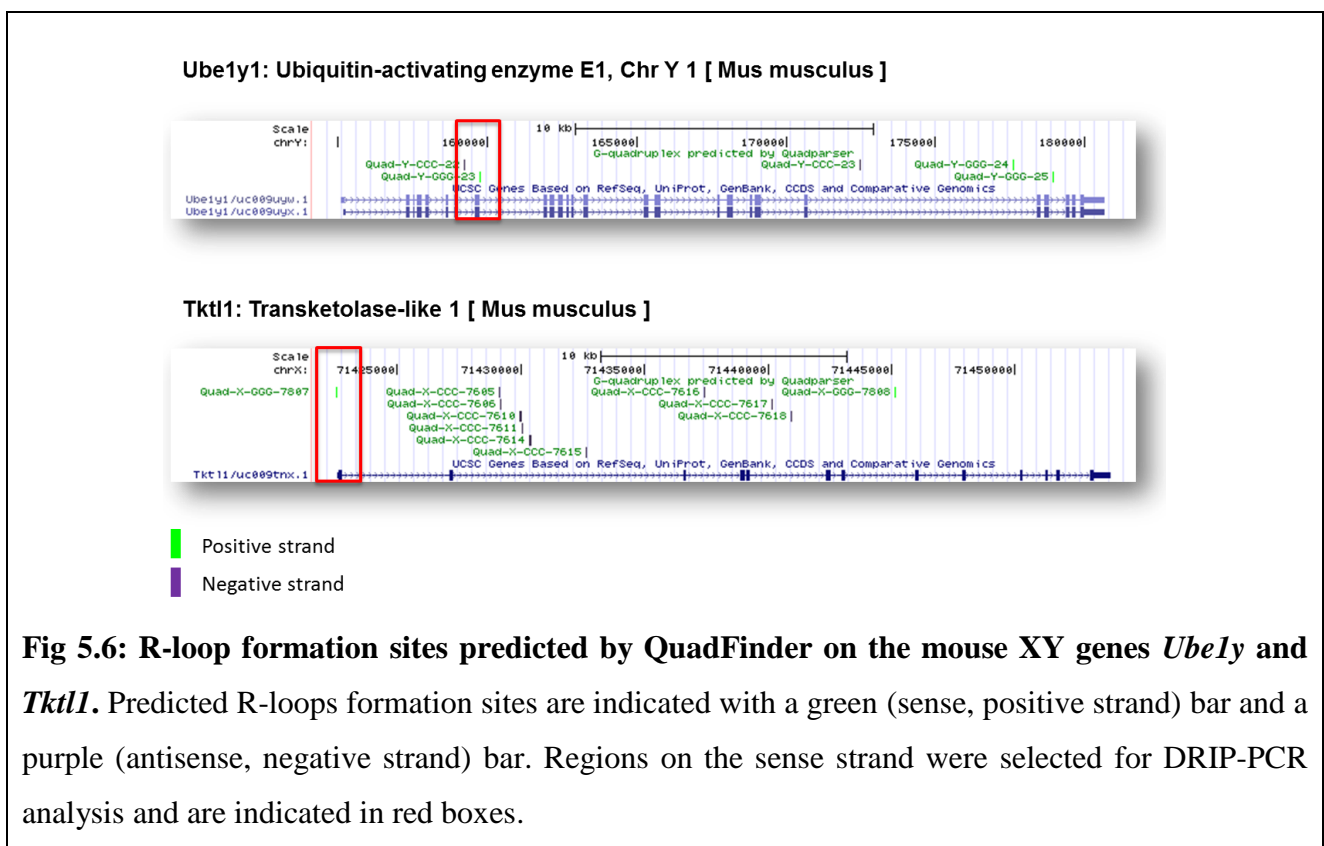


**Fig 5.6: R-loop formation sites predicted by QuadFinder on the mouse XY genes *Ube1y* and *Tktl1*.** Predicted R-loops formation sites are indicated with a green (sense, positive strand) bar and a purple (antisense, negative strand) bar. Regions on the sense strand were selected for DRIP-PCR analysis and are indicated in red boxes.

Subsequent PCR (primers described in Appendix B) performed for predicted RLFSS in both *Ube1y1* and *Tktl1* on mouse testes after the DRIP assay showed a significant increase in R-loop accumulation in *Setx*<sup>-/-</sup> as compared to WT (Fig 5.7). RNase H (RH) treatment prior to the DRIP assay was also performed as a quality control for the S9.6 (R-loops antibody) used in the assay. As expected, RH pre-treatment dramatically reduced the amount of DNA/RNA hybrids pulled down in the DRIP assay confirming the specificity of the R-loops antibody. These data showed that the

formation of R-loops can occur on the XY chromosomes which may also contribute to the defects in MSCI observed in *Setx*<sup>-/-</sup> mice.

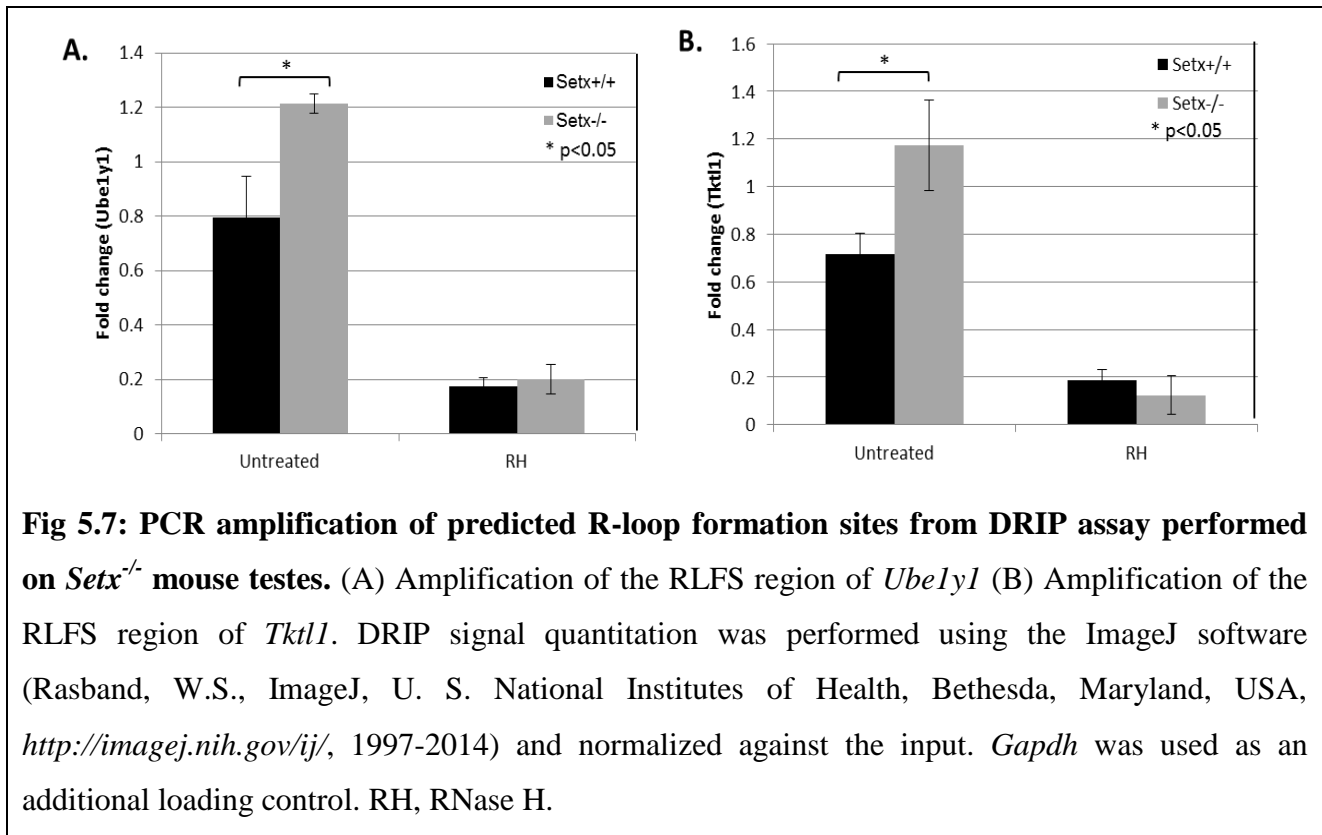


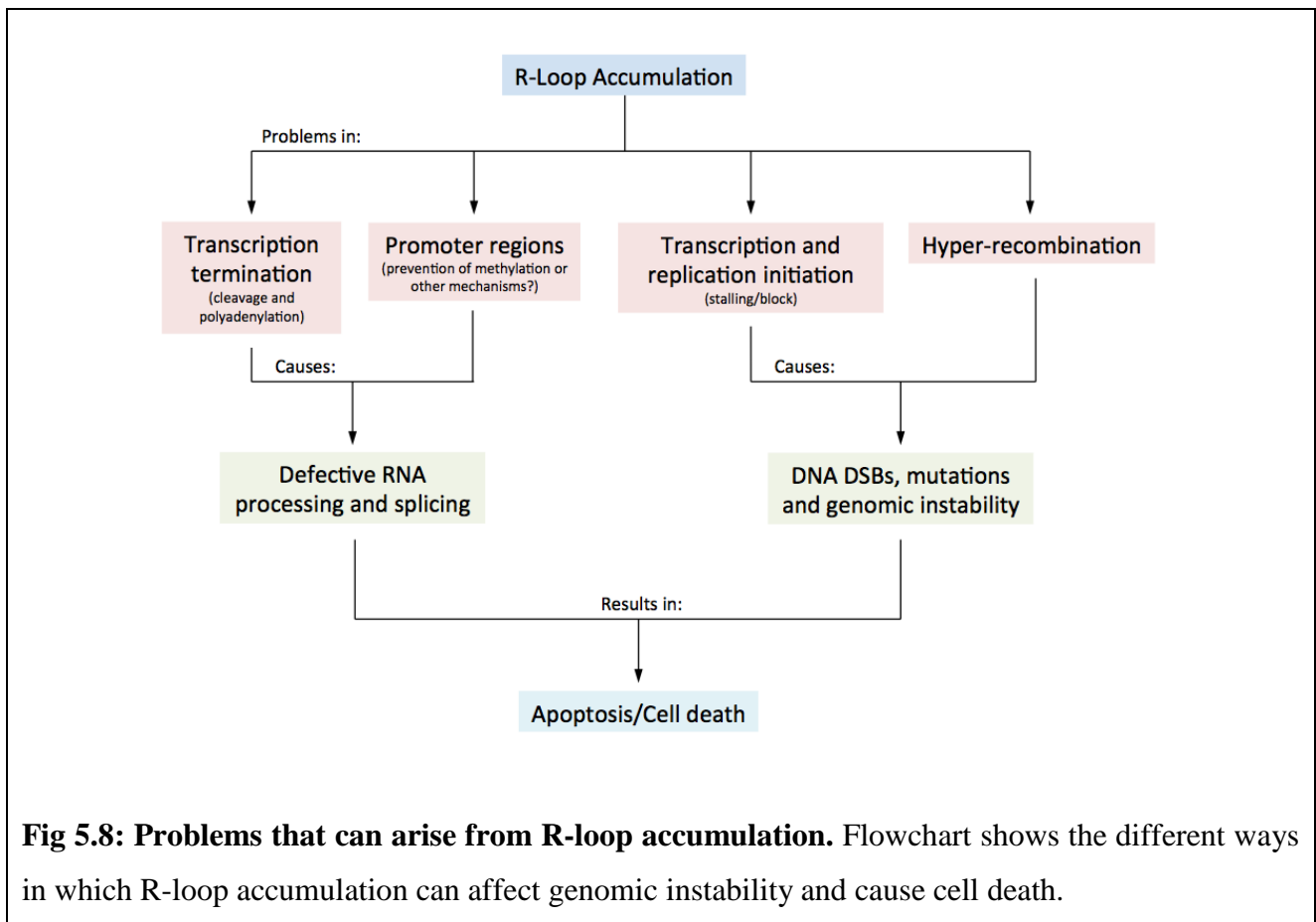
**Fig 5.7: PCR amplification of predicted R-loop formation sites from DRIP assay performed on *Setx*<sup>-/-</sup> mouse testes.** (A) Amplification of the RLFS region of *Ube1y1* (B) Amplification of the RLFS region of *Tkt11*. DRIP signal quantitation was performed using the ImageJ software (Rasband, W.S., ImageJ, U. S. National Institutes of Health, Bethesda, Maryland, USA, <http://imagej.nih.gov/ij/>, 1997-2014) and normalized against the input. *Gapdh* was used as an additional loading control. RH, RNase H.

## **5.4 Discussion**

Sen1, the yeast homolog of senataxin, restricts co-transcriptionally formed R-loops which accumulate in *sen1* mutant in a transcription-dependent manner<sup>76</sup>. Furthermore, Mischo *et al.* 2011 observed a genetic interaction between *sen1* and various factors involved in HR such as *rad50*, *mre11*, *sgs1* and *rad52* and concluded that *sen1* plays a pivotal role in preventing genomic instability by transcription-mediated recombination<sup>76</sup>. More recently, Skourti-Stathaki *et al* (2011) provided evidence that senataxin, like *sen1*, resolves DNA/RNA hybrid structures known as R-loops, which form naturally at transcriptional pause sites to ensure effective transcription initiation and/or termination. This Chapter has described the *in vivo* accumulation of R-loops in *Setx*<sup>-/-</sup> mouse seminiferous tubules and in pachytene-stage spermatocytes, supporting a role for senataxin in resolving such structures during meiosis. Furthermore, co-localization between R-loops and TUNEL staining in *Setx*<sup>-/-</sup> mouse germ cells indicates that accumulation of these structures may contribute to cell death and the sterility phenotype observed in *Setx*<sup>-/-</sup> male mice. It is possible that the phenotype observed results from a combination of different factors including but not limited to R-loop formation. An experiment that would provide stronger evidence for the causal role of R-loop accumulation in sterility/cell death would be to overexpress RNase H1, which digests R-loops, in germ cells of *Setx*<sup>-/-</sup> animals to rescue the phenotype, however such an experiment is not currently feasible *in vivo*.

Following its transcription from DNA, RNA undergoes a series of complex processing events that can affect its stability and function, and a deregulation in any of these processes can compromise genomic integrity. An accumulation of R-loops can cause problems in transcription regulation. Efficient transcription initiation and termination depends on the resolution of R-loops, which are potentially harmful if left unresolved, as they can stall transcription and/or cause DNA breaks<sup>74,150</sup>. Gene expression can also be affected as R-loops have been shown to prevent the methylation of CpG island promoters<sup>170,172</sup>. Transcriptional R-loop formation in eukaryotes is also highly correlated with DNA recombination and is capable of inducing hyper-recombination<sup>160,281</sup>, leading to mutations and genomic instability. R-loop accumulation can also cause DNA damage by impeding transcription elongation and termination<sup>74,160,282</sup>, in turn resulting in cell death (Fig 5.8). Thus, R-loop formation can be an intrinsic threat to genomic integrity throughout evolution and species have evolved a variety of co-transcriptional processes to prevent the formation of these structures<sup>159</sup>.





Senataxin represents a novel factor that minimizes the impact of R-loops that arise as part of normal transcription processes<sup>73</sup> and/or DNA-damage-induced transcription stalling<sup>282</sup>. In the case of *Setx*<sup>-/-</sup> spermatocytes, accumulation of R-loops occur throughout leptotene and zygotene which are the stages where DNA DSBs are being repaired by crossing over and/or other mechanisms. R-loop staining was observed on autosomes at all stages and persisted up to pachytene stage indicating a widespread genomic distribution. Consequently, it is likely that R-loops may form in the vicinity of meiotic recombination hotspots and collide with Holliday Junctions, thus interfering with the resolution of DNA DSBs and in turn, meiotic recombination. This Chapter has provided evidence of R-loop formation at a recombination hotspot, the H44.2 locus located on chromosome 19<sup>283</sup>. Additionally, the accumulation of R-loops throughout the chromatin would also affect the repair of DNA DSBs that are repaired through non-crossover mechanisms. The accumulation of R-loops observed in *Setx*<sup>-/-</sup> germ cell further supports their role as a trigger of genome instability. Furthermore, an increase in the formation of R-loops at the loci of two XY genes (*Ube1y1* and *Tktl1*) found to be abnormally expressed in *Setx*<sup>-/-</sup> mouse testes, was reported here. In addition, the formation of R-loops in GC-rich promoter regions have previously been shown to prevent the methylation of CpG islands and disrupt transcriptional repression<sup>171</sup>, thus the formation of R-loops

on the XY chromosomes may affect the methylation status of XY genes promoter regions and hinder their silencing, thereby contributing to the defective MSCI observed in *Setx*<sup>-/-</sup> spermatocytes.

Interestingly, accumulation of R-loops was neither detected in the brain nor cerebellum of *Setx*<sup>-/-</sup> mice and other ARCA models, indicating that R-loop formation preferentially occur in transcriptionally active replicating cells. Indeed, increased R-loop formation was also detected in spleen and intestine, in addition to the testes, which are all highly proliferative tissues. Using DRIP analysis, a more sensitive assay to detect R-loop formation, a similar background level of R-loops in nervous tissues of *Setx*<sup>+/+</sup> and *Setx*<sup>-/-</sup> mice was observed and this confirmed the significant accumulation of R-loops in *Setx*<sup>-/-</sup> testes. This hypothesis was supported by showing that R-loop accumulation was present only in highly proliferative tissue of mice treated with the DNA-damaging agent, topotecan hydrochloride, and not in post-mitotic tissues. It was also shown that cells treated with DNA damaging agents such a camptothecin, a DNA Topoisomerase I inhibitor, led to the formation of R-loops mostly visible in the nucleolus indicating that R-loops formation preferentially occur at highly transcribed genes, such as rDNA. This is in agreement with the nucleolar localization of DNA Topoisomerase I and the presence of GC-rich regions on the rDNA which are pre-requisite for R-loop formation<sup>265</sup>.

The difference observed between the detection of R-loops using immunostaining and DRIP highlighted a difference in sensitivity for both assays with a greater sensitivity for the DRIP. However, with greater sensitivity, a greater background was also observed (as seen in levels of R-loops in *Setx*<sup>+/+</sup> and *Setx*<sup>-/-</sup> brain and cerebellum) which dramatically reduced the signal/noise ratio. Although immunostaining for R-loops is a less sensitive assay, it provides a quicker and better discrimination and thus may represent a valuable tool for screening samples for potential transcription deregulation and/or genomic instability.

The formation of R-loops at the fragile site of a long gene, *WWOX*, where replication forks tend to stall frequently given the length of the gene, was also shown. These data are in agreement with a role for senataxin in resolving R-loop structures and that replication is necessary for the formation of these structures.

Given that R-loops require the concomitant activities of both replication and transcription, the lack of R-loops in the nervous tissue may not be surprising since these are post-mitotic cells devoid of replication activity. In this Chapter, strong evidence has been provided for the lack of R-loop formation in TPT-treated of untreated *Setx*<sup>-/-</sup> post-mitotic nervous tissues, which prompts the

question as to whether R-loop accumulation may actually be involved in the neuropathology of human AOA2 patients. Given the lack of nervous tissue sample availability for AOA2 patients and based on our findings, R-loops may not be the cause of the neurodegenerative phenotype observed in AOA2 patients. These findings point to the current limitations to decipher the neuropathology of AOA2 and indicate the necessity to develop a more relevant human neuronal model system.

The absence of a neurodegenerative phenotype in *Setx*<sup>-/-</sup> mice suggest that either (i) the mouse nervous system does not mimic the human nervous system due to significant evolutionary structural and functional differences, (ii) existing redundant pathways help resolve R-loop structures in the mouse nervous system, or (iii) that there is an alternative function for senataxin in the nervous tissue of these mice. There exists a plethora of R-loop resolving mechanisms that include the RNase H enzyme and other DNA/RNA helicases<sup>284, 285</sup>. Senataxin has previously been shown to be involved in RNA metabolism and splice site selection<sup>71</sup> therefore, it may be that abnormal splice site selection and/or transcriptional read-through of genes giving rise to abnormal transcripts is occurring instead, which would be reflected at the transcriptome level. Indeed, a recent study by Fogel et al. 2014 identified an AOA2-specific transcriptional signature<sup>286</sup>. Weighted gene co-expression network analysis (WGCNA) identified two gene modules highly enriched for this transcriptional signature that were disease-specific and preserved in patient peripheral blood, patient fibroblasts and in the cerebellum of *Setx*<sup>-/-</sup> mice, demonstrating conservation across species and cell types, including neurons. This study identified novel genes and cellular pathways related to senataxin function in normal and disease states, and implicate alterations in gene expression as underlying the phenotypic differences between AOA2 and ALS4, which is the autosomal dominant form of the disorder caused by mutant senataxin<sup>286</sup>.

Further investigation of the role of senataxin in RNA metabolism and gene regulation in the nervous tissues of *Setx*<sup>-/-</sup> mice is currently under way as part of a collaboration with Dr Brent Fogel (UCLA, USA) through the in-depth analysis of the *Setx*<sup>-/-</sup> transcriptome via RNA-seq on RNA isolated from nervous tissues, to study the nature of the transcripts and alternative splice variants.

Altogether, these findings reveal a complex and coordinated network between transcription, DNA replication and repair pathways, thus supporting the emerging importance of RNA processing factors, such as senataxin, in the DNA damage response. Furthermore, they also highlight a more prominent role than previously suspected for RNA secondary structures such as R-loops in contributing to genomic instability and tissue degeneration.

## **CHAPTER 6: General Discussion & Future Directions**

## **6.1 General discussion**

Autosomal recessive cerebellar ataxias (ARCA) are a class of neurodegenerative disorders that result from cerebellar atrophy and spinal cord dysfunction<sup>1,4</sup>. Ataxia oculomotor apraxia type II (AOA2) is one such ARCA and is characterized by cerebellar atrophy, oculomotor apraxia and axonal neuropathy with an onset during the 2<sup>nd</sup> decade of life<sup>67,69,190</sup>. The gene mutated in AOA2 is *SETX*, which encodes for a 2,677 amino-acid protein called senataxin<sup>60</sup>. Senataxin is a putative DNA/RNA helicase that is involved in the protection against oxidative DNA damage and in transcription regulation such as mRNA splicing and DNA:RNA (R-loop) resolution<sup>63,71,73</sup>.

This work reports the characterization of the first *Setx*<sup>-/-</sup> mouse model which revealed male sterility due to a disruption of spermatogenesis. *Setx*<sup>-/-</sup> mice unfortunately do not recapitulate the neuropathology seen in human AOA2 patients that include clinical hallmarks such as cerebellar atrophy, gait ataxia and loss of Purkinje cells in the cerebellum<sup>61,69,184</sup>. The absence of a neurological phenotype in ARCA mouse models is not uncommon, and it has been observed for several other models including those of *Atm*, *Aptx*, and *Tdp1*<sup>20,59</sup>. This raises the question as to whether the *Mus musculus* is an appropriate model to mimic neurodegenerative disorders in humans such as ARCAs. Rat models on the other hand, have been shown to mimic human disease more accurately, and these diseases include diabetes, cardiovascular disorders and neurological conditions such as Parkinson's<sup>287</sup>. It has also been reported that rat models are phylogenetically and physiologically more similar to humans, and have become the standardized toxicological model of choice, especially in the pharmaceutical industry<sup>287,288</sup>.

Another parameter that is important to consider is that the onset of AOA2 is during the second decade of life. The difference in the life span of humans and mice may also affect the development of the progressive neurological phenotype. The progressive onset of neurodegeneration suggests that it results from a temporal accumulation of various lesions (e.g. DNA lesions) over time as in most cases the symptoms worsen as the patients' age. Indeed, evidence of accumulated DNA damage in the nervous system has been observed in human patients and may thus account for the neurological phenotype. However, an accumulation of DNA damage was not observed in both young and old-aged *Setx*<sup>-/-</sup> mice, in agreement with the lack of neurological phenotype in these animals.

Although, no neurodegenerative phenotype was observed in the *Setx*<sup>-/-</sup> animals, this model has provided valuable mechanistic insights into the role of senataxin in DNA damage repair (DDR) and

transcription regulation. Indeed, many proteins involved in DDR have also been found to be essential for meiosis where sterility due to a disruption in various stages of meiosis is a fairly common phenotype observed in several other DDR mouse models such as the *Atm*<sup>-/-</sup>, *Brca1*<sup>Δ11/Δ11</sup> and the *Mlh1*<sup>-/-</sup> mice<sup>20,204,242,289</sup>. We have shown that senataxin is essential for male germ cell maturation during spermatogenesis, acting during meiosis prophase I to ensure efficient meiotic recombination and meiotic sex chromosome inactivation (MSCI). The absence of senataxin results in an increase of unrepaired DNA breaks at pachytene stage which in turn prevents meiotic recombination and the exchange of genetic material between sister chromatids. Senataxin also localizes to the XY chromosomes during the pachytene stage, suggesting a potential role for senataxin during MSCI. Comparative analysis of the MSCI process between *Setx*<sup>+/+</sup> and *Setx*<sup>-/-</sup> implicate senataxin as a novel, indispensable player in the silencing of XY chromosomes through the Atr signaling pathway. Atr and its downstream phosphorylation target, Chk1 are activated during DNA replication stress which can lead to the formation of ssDNA regions. These ssDNA are promptly coated by Rpa which then recruits Atr through Atrip. The formation of this complex, in addition to the SUMOylation of Atrip, subsequently drives the activation or phosphorylation of Chk1 and other downstream signalling partners that are crucial for coordinating cellular responses to DNA damage<sup>221,290</sup>. The lack of diffusion of these key DDR proteins to the XY chromatin domain and a defect in the Atr/Chk1 signaling pathway were observed in *Setx*<sup>-/-</sup> mice, which may have contributed to aberrant X- and Y-linked gene expression.

The abnormal chromatin topology observed in *Setx*<sup>-/-</sup> spermatocytes could be due to the lack of an interaction with Chd4, a member of the nucleosome remodeling histone deacetylase (NuRD) complex, in the absence of senataxin. An interaction between senataxin and Chd4 via co-immunoprecipitation in somatic cells was recently reported<sup>233</sup>. Indeed, senataxin was found to interact *in vivo* with Chd4 via PLA over the XY chromosomes in *Setx*<sup>+/+</sup> spermatocytes and appeared to be necessary for its recruitment to the XY chromosomes, supporting a role for senataxin in heterochromatin formation. In addition, given that Atr has been reported to interact with Chd4, it could be that the compounding effects from the defect in Atr signaling as well as the lack of interaction between Chd4 and senataxin led to the defect in MSCI observed in the *Setx*<sup>-/-</sup> mouse. Interestingly, Chd4 conditional knockout in rodents was reported to cause defects in the synaptogenesis of granule neuron parallel fiber/Purkinje cells and neurotransmission in the cerebellar cortex of these animals due to the NuRD-dependent promoter decommissioning<sup>291</sup>. These findings implicate the NuRD-dependent developmentally regulated mechanism in post-mitotic neurons as a driver of synaptic connectivity. While an *in vivo* interaction between senataxin and Chd4 has been reported here in the context of male meiosis, it remains unclear whether a functional

interaction is also taking place in the human nervous system that may account for the neurodegenerative cerebellar atrophy and Purkinje cell loss observed in AOA2 patients. To date, most studies on AOA2 have relied on proliferating patient-derived cells lines such as B-lymphoblastoid cells (LCLs) or fibroblasts<sup>63,71</sup>. In order to investigate the functional significance of the senataxin-Chd4 interaction in developmental gene expression regulation in the pathophysiology of AOA2, an appropriate human neural human system must be developed. Two such models could include patient-derived induced pluripotent stem cell (iPSC) models or patient-derived olfactory neural stem cell (ONSC) models, as reported for the ARCA, ataxia-telangiectasia (A-T)<sup>292,293</sup>. Both iPSC and ONSC have the capacity to differentiate into functional neurons which can then provide ideal models to delineate the neurological defect in AOA2 patients<sup>292,293</sup>.

Despite the fact that the *Setx*<sup>-/-</sup> mouse model did not recapitulate the AOA2 neurodegenerative phenotype, they provided evidence for genome-wide differential gene regulation in *Setx*<sup>-/-</sup> and for a conserved AOA2-disease transcriptional signature<sup>286</sup>. There is increasing evidence linking the epigenetic machinery and chromatin modifications with neurologic dysfunction<sup>294</sup>. Indeed, chromatin-modifying drugs have emerged as potential therapeutic tools for neurodegeneration caused by a CAG-repeat expansion in *ATXN7*, a gene encoding ataxin-7, an essential component of the SPT3-TAF9-ADA-GCN5 (STAGA) acetyltransferase chromatin remodelling complex<sup>295</sup>. Recently, Duncan et al. 2013 have reported that histone deacetylase 3 (HDAC3) physically interacts with and stabilizes ataxin-7, in turn increasing modification of the protein<sup>296</sup>. Robust HDAC3 expression in neurons and glia of the cerebellum and an increase in the levels of HDAC3 were observed in SCA7 mice<sup>296</sup>. Altered lysine acetylation levels and deacetylase activity in the brains of SCA7 transgenic mice indicate that SCA7 that may be treated by HDAC inhibitors. Additional evidence for the importance of histone acetylation in neurological disorders comes from the dysregulation of histone 4 lysine 16 (H4K16) acetylation in the mouse brain which has been linked to aging phenotypes and DDR deficiency<sup>297,298</sup>. One, two, or three- methyl groups can be added to or removed from lysine residues and differences in these processes can affect chromatin structure and gene expression<sup>299</sup>. Down-regulation of genes due to alterations in epigenetics lead to cognitive deficiencies associated with a range of neurological disorders such as Alzheimer's disease, Huntington's disease, Rett's syndrome and other psychiatric disorders<sup>294</sup>. Thus it is possible that in AOA2, the absence of senataxin, which normally interacts with Chd4, may affect the NuRD complex distribution and/or activity, in turn leading to genome-wide alteration of chromatin modification. Given the high levels of transcription that occurs in neurons, this can consequently result in aberrant gene expression and subsequent neuronal cell death.

The *Setx*<sup>-/-</sup> mouse model also provided the first *in vivo* evidence of R-loop accumulation in germ cells in the absence of senataxin. Although R-loop formation occurs naturally during transcription through the interaction of nascent RNA and the DNA strand from which it was transcribed from, its accumulation can cause the stalling of transcription, abnormal gene expression, aberrant splicing/termination of transcription, genomic instability and the subsequent collapse of the cell<sup>74,150,159,164</sup>. Our preliminary findings suggest that R-loops provide a novel level of DNA-RNA interactome complexity, playing key roles in gene expression controls, mutagenesis, recombination, chromosomal rearrangement, alternative splicing, DNA-editing and epigenetic modifications. An accumulation of R-loops was observed to be a common feature in several ARCA (*Atm*<sup>-/-</sup>, *Aptx*<sup>-/-</sup>, *Setx*<sup>-/-</sup>, *Tdp1*<sup>-/-</sup>) mouse models, although only *Atm*<sup>-/-</sup> and *Setx*<sup>-/-</sup> mice are sterile. While there are other elements contributing to the sterility observed in *Atm*<sup>-/-</sup> and *Setx*<sup>-/-</sup> mice such as defective DDR and meiotic recombination, the extent of R-loop accumulation in the seminiferous tubules in these mouse models is also likely to contribute to the difference between fertility and sterility observed in these models. These data also suggest that there may also be a threshold of R-loop accumulation in germ cells which when reached leads to apoptosis induction, loss of germ cells and consequently sterility. Indeed, the accumulation of R-loops can trigger genomic instability and altered gene expression and changes in chromatin condensation<sup>74,150,164</sup>, which are all very tightly regulated during spermatogenesis. Any adverse changes in these processes may then present a threat to the proper development and maturation of germ cells.

The formation and accumulation of R-loops depend on several parameters, these include (i) the primary DNA sequence which can affect their location within the genome, (ii) the levels of transcription in the loci where R-loops can form, (iii) their frequency of occurrence within the genome with their effect on gene expression and (iv) transcription termination. In germ cells for instance, accumulation of R-loops may affect regions where Spo11-programmed DNA DSBs occur as well as at meiotic recombination hot spots, thus potentially impairing the meiotic recombination process and in turn the formation of crossing overs. The defect in meiotic recombination observed in *Setx*<sup>-/-</sup> mice supports this argument and evidence in this Report has shown an accumulation of R-loops in the recombination hotspot 44.2 on chromosome 19. Additionally, R-loops may also affect regions containing genes important for spermatogenesis or contribute to the induction of DNA breaks. Using *in silico* R-loop formation site (RLFS) prediction programs and candidate gene approaches in combination with DNA/RNA immunoprecipitation (DRIP) assays, the presence of R-loops has indeed been demonstrated on the autosomes at common fragile sites of long genes, recombination hotspots and in XY genes of *Setx*<sup>-/-</sup> spermatocytes.



In order to investigate whether a neurological phenotype in these ARCA models can be induced by an increased accumulation of DNA damage, cross breeding of several models (*Atm x Setx*, *Setx x Tdp1*, *Setx x Aptx*) to generate double knockouts were carried out. Preliminary data showed that *Atm* and *Setx* double knockouts were very rare events, occurring only at a very low frequency of ~1/250 live births, these mice die quickly as well. Only a couple of *Atm*<sup>-/-</sup> *Setx*<sup>-/-</sup> mice have been obtained and these have not shown any signs of neurodegeneration or abnormal neurological behavior either. The very low frequency of these double knockout mice suggests that many may die *in utero*. From the few *Atm* and *Setx* double knockout mice that survived, infertility due to defects in spermatogenesis was observed as well. For *Tdp1 Setx* double knockouts, similar observations were made. These double knockouts also occurred at a very low frequency of ~1/150 and no signs of neurodegeneration or abnormal neurological behavior were observed. Similarly, histological analyses of testes sections from these mice revealed male sterility, indicating that the *Setx*<sup>-/-</sup> phenotype exerts dominance over the *Tdp1*<sup>-/-</sup> phenotype.

Camptothecin and its water-soluble analogue topotecan hydrochloride, are DNA Topoisomerase I inhibitors that are potent DNA damaging and transcription-blocking agents. These chemicals are also capable of inducing the formation of R-loops in cellular models<sup>269,300</sup>. Given R-loop accumulation was detected in the testes of ARCA mouse models, topotecan hydrochloride was administered to artificially increase R-loop formation in these models. It was observed that R-loop accumulation only occurred in proliferating tissues of the spleen, testes and intestines, and not in post-mitotic tissues of the nervous system such as the brain and cerebellum. These data are in agreement with previous reports of R-loop formation occurring preferentially under both the concomitant activities of replication and transcription<sup>151,233,284</sup>. The lack of R-loop accumulation in these post-mitotic tissues could also be due to a redundancy in R-loop resolution mechanisms that may exist in the nervous tissues of mice. Indeed, several pathways have evolved to resolve R-loops that include RNase H, DHX9 RNA helicase, NPH-II helicase, and splicing factor ASF-SF2<sup>168,301</sup>. Whether or not these are highly active in the nervous system of mice remains unclear. Furthermore, R-loops may not readily form in post-mitotic tissues due to the lack of concomitant transcription and replication activities. Determining whether R-loops form and/or accumulate in the cerebellum of AOA2 patients and contribute to the loss of Purkinje cells will require the availability of human AOA2 cerebellar biopsies, which to date have not been available.

In conclusion, the formation of R-loops in proliferative cells may result from the collision of the transcription apparatus with the replication machinery, with stalled replication forks and/or Holliday junctions that form during DNA damage repair. Once these accumulate due to the absence of

senataxin, they are likely to contribute to aberrant gene expression, mRNA splicing, abnormal transcriptional read-through, and formation of DNA breaks, thus leading to genomic instability and cell death. On the other hand, in non-replicative, post-mitotic highly-transcribed cells such as those from the nervous tissues of the brain and cerebellum, the absence of senataxin may affect splice site selection, transcriptional read-through and/or gene expression through chromatin modification and the binding of the transcription machinery. These may then contribute to the neuronal degeneration observed in AOA2/ALS4 patients. A model summarizing the findings of this work and the proposed role for senataxin in the neuropathology of AOA2 is shown in Figure 6.1.

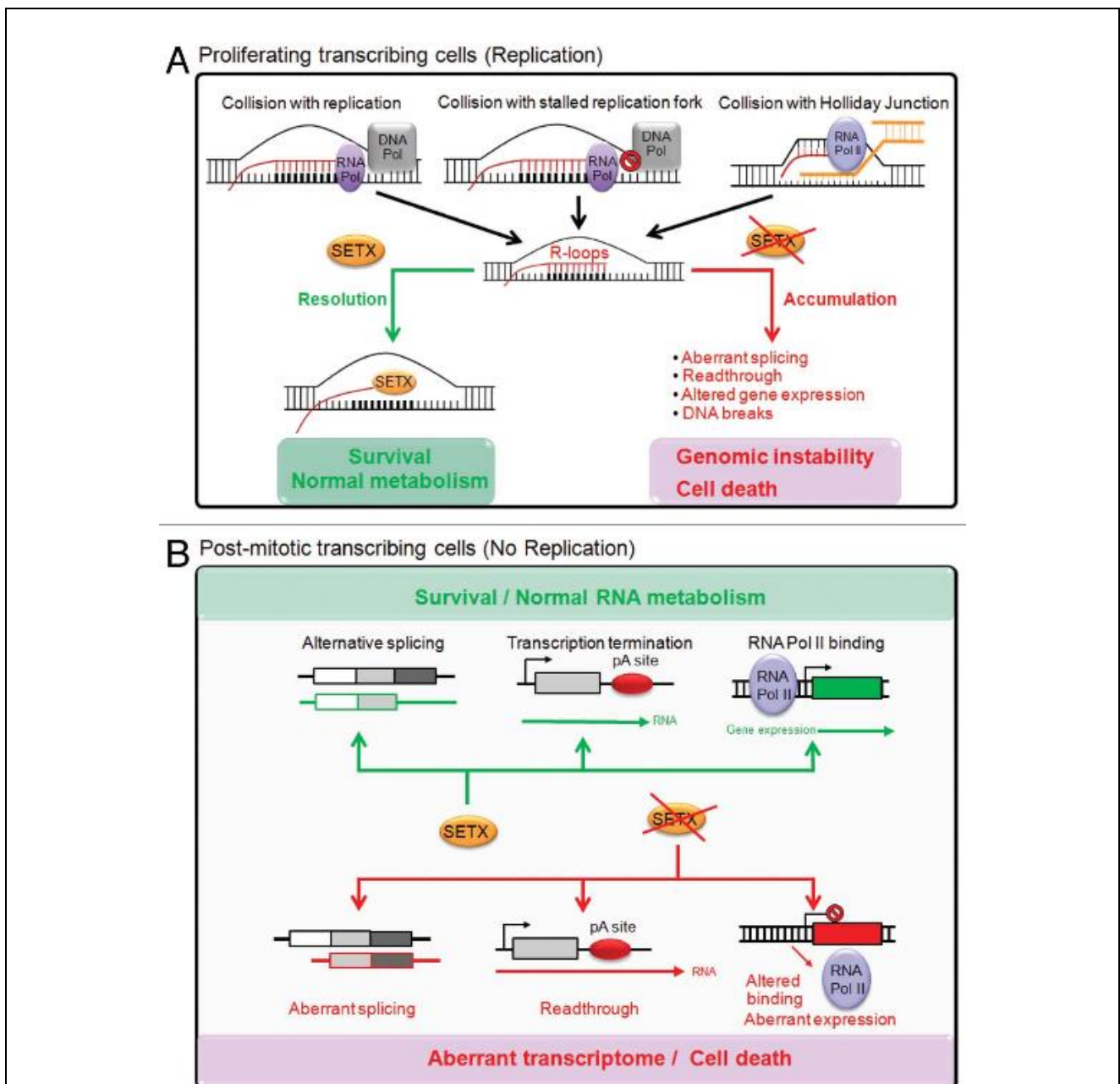


**Fig 6.1: Senataxin in proliferating and post-mitotic cells.** A. In proliferating cells, the absence of senataxin can cause R-loop formation through the collision of the transcription machinery with

replication, stalled replication forks and Holliday junctions, leading to aberrant gene expression and mRNA splicing, transcriptional read-through and DNA damage, resulting in genomic instability and cellular collapse. **B.** In non-proliferating, post-mitotic cells, it is hypothesized that the absence of senataxin may cause defects in transcription termination and splice site selection, leading to aberrant gene expression and subsequent genomic instability and cell death. *Image taken from Lavin et al 2013.*

## **6.2 Future directions**

Given that several roles for senataxin in transcription regulation have been described here, future work should aim to further dissect the mechanistic role of senataxin in germ cell development and chromatin remodeling. Future experiments will include:

1) The investigation of senataxin as a DNA/RNA helicase.

Senataxin is a putative DNA/RNA helicase that has a predicted C-terminal domain belonging to the superfamily I of helicases<sup>68</sup>. These helicases are motor proteins that are driven by ATP hydrolysis, translocating along and unwinding both DNA and RNA strands. The formation of single-stranded intermediates from the unwinding of these nucleic acids is essential for several aspects of cellular metabolism such as replication, repair and recombination<sup>68,185</sup>. To date, no direct evidence for senataxin's helicase activity has yet been reported. Given that senataxin was recently shown to be required for the resolution of R-loops<sup>73,233,302</sup>, it may be worthwhile investigating whether its helicase domain is responsible for the unwinding of these R-loops. This can be performed by a classical helicase assay that entails the addition of purified senataxin protein to radiolabeled RNA oligonucleotide annealed to a ssDNA template<sup>303</sup>.

2) Gene expression profiling of *Setx*<sup>+/+</sup> and *Setx*<sup>-/-</sup> testes.

Recent gene expression profiling via RNA-Seq and microarray performed on senataxin-defective (both AOA2 and ALS4) fibroblasts as well as on brain and cerebellar tissue from *Setx*<sup>+/+</sup> and *Setx*<sup>-/-</sup> mice revealed the altered expression of several genes implicated in neurogenesis<sup>286</sup>. Using the weighted gene co-expression network analysis (WGCNA), the associations of several networks with the clinical symptoms of AOA2 and ALS4 patients were also revealed<sup>286</sup>. These findings are essential in gaining a better understanding of the mechanism behind the neurodegeneration observed in AOA2/ALS4 patients. Using similar approaches, initial gene expression profiling is currently being performed on the testes of *Setx*<sup>+/+</sup> and *Setx*<sup>-/-</sup> mice to further identify the genes involved in meiotic recombination and XY silencing that are affected in the absence of senataxin.

3) The functional characterization of the Setx-Chd4 interaction.

Chd4 is a component of the nucleosome remodeling and deacetylation (NuRD) complex that is associated with heterochromatin formation and gene silencing. Given its *in situ* interaction with senataxin over the XY chromosomes as shown in this Report, it would be worthwhile to examine the histone acetylation status of the XY chromosomes. Several other markers associated with histone acetylation include H3K9 and H4K12, and this can be investigated using antibodies against these histone marks on spermatocytes spreads made from *Setx*<sup>+/+</sup> and *Setx*<sup>-/-</sup> mice. In addition, given the observation of the SUMOylation of senataxin in addition to the recent report of the SUMOylation of Chd4<sup>259</sup>, it would be interesting to map these interaction sites and determine whether this interaction is dependent on SUMO modification.

4) The investigation of the association between Nek1 and Atrp in Atr/Chk1 signaling

A relationship between Nek1 and Atrp was recently reported by Liu *et al.* 2013. They showed that Nek1 was essential for the stabilization of Atrp and that the association between these two proteins was required for the amplification of Atr/Chk1 signaling following DNA damage<sup>229</sup>. In this Report, significantly reduced levels of Atrp protein was observed in *Setx*<sup>-/-</sup> spermatocytes. This was coupled with reduced levels and mis-localization of Nek1, suggesting that senataxin may be important for the expression, stability as well as recruitment of Nek1. A deregulation in the association of Nek1 and Atrp in the absence of senataxin may be responsible for the defect in Atr/Chk1 signaling that was observed in *Setx*<sup>-/-</sup> spermatocytes. Further examination is needed to investigate this phenomenon.

5) Genome-wide mapping of R-loop forming sites and histone modifications

Identifying sites of R-loop formation within a genome can potentially lead to the uncovering of novel target sites for drug therapy. It was recently reported by Skourti-Stathaki *et al.* 2014 that the formation of R-loops could induce marks of chromatin repression, more specifically H3K9me2, at sites of protein-coding gene termination regions<sup>304</sup>. They proposed that the formation of these R-loop structures was required for the stalling of RNA Polymerase II, thereby allowing for the efficient termination of transcription<sup>304</sup>. Interestingly, preliminary data from immunostaining using an antibody against H3K9me2 in *Setx* spermatocytes revealed higher levels of this histone modification in *Setx*<sup>-/-</sup> as compared to *Setx*<sup>+/+</sup>, in

agreement with the report by Skourti-Stathaki *et al.* 2014. Given the increased accumulation of R-loops coupled with abnormal heterochromatin formation observed in the spermatocytes of *Setx*<sup>-/-</sup> mice, the extending and refining of these sites to recombination hot spots, fragile sites, and/or genes involved in meiosis and DNA damage repair will be performed using chromatin immunoprecipitation (ChIP) assays against H3K4me1 or H3K9me2 and S9.6 (R-loop antibody) DNA:RNA immunoprecipitation assays (DRIP) from testes of *Setx*<sup>-/-</sup> mice followed by next generation sequencing (DNA-Seq).

While the *Setx*<sup>-/-</sup> mouse model has provided us with valuable insight into the role of senataxin in DNA repair and transcription regulation, it does not recapitulate the neurological phenotype that is observed in human AOA2 patients. Hence, a more appropriate human neurological model is required to better understand the mechanism of neurodegeneration that occurs due to mutant senataxin in both in AOA2 and ALS4 patients. AOA2 patient-derived induced pluripotent stem cells (iPSC) have been generated and are currently under phenotypic characterization (unpublished data).

## **REFERENCES**

1. Di Donato S, Gellera C, Mariotti C. The complex clinical and genetic classification of inherited ataxias. II. Autosomal recessive ataxias. *Neurol Sci* 2001;22:219-28.
2. Lavin MF. Ataxia-telangiectasia: from a rare disorder to a paradigm for cell signalling and cancer. *Nature reviews Molecular cell biology* 2008;9:759-69.
3. Gensler HL, Bernstein H. DNA damage as the primary cause of aging. *Q Rev Biol* 1981;56:279-303.
4. Palau F, Espinos C. Autosomal recessive cerebellar ataxias. *Orphanet J Rare Dis* 2006;1:47.
5. Katyal S, el-Khamisy SF, Russell HR, et al. TDP1 facilitates chromosomal single-strand break repair in neurons and is neuroprotective in vivo. *EMBO J* 2007;26:4720-31.
6. Gueven N, Chen P, Nakamura J, et al. A subgroup of spinocerebellar ataxias defective in DNA damage responses. *Neuroscience* 2007;145:1418-25.
7. Xu Y, Ashley T, Brainerd EE, Bronson RT, Meyn MS, Baltimore D. Targeted disruption of ATM leads to growth retardation, chromosomal fragmentation during meiosis, immune defects, and thymic lymphoma. *Genes Dev* 1996;10:2411-22.
8. Boder E. Ataxia-telangiectasia: an overview. *Kroc Found Ser* 1985;19:1-63.
9. Lavin MF, Kozlov S. DNA damage-induced signalling in ataxia-telangiectasia and related syndromes. *Radiother Oncol* 2007;83:231-7.
10. Chun HH, Gatti RA. Ataxia-telangiectasia, an evolving phenotype. *DNA Repair (Amst)* 2004;3:1187-96.
11. Chen H. *Atlas of Genetic Diagnosis and Counselling*. New Jersey, USA: Humana Press; 2006.
12. Lefton-Greif MA, Crawford TO, Winkelstein JA, et al. Oropharyngeal dysphagia and aspiration in patients with ataxia-telangiectasia. *J Pediatr* 2000;136:225-31.
13. McKinnon PJ. ATM and ataxia telangiectasia. *EMBO Rep* 2004;5:772-6.
14. Lakin ND, Weber P, Stankovic T, Rottinghaus ST, Taylor AM, Jackson SP. Analysis of the ATM protein in wild-type and ataxia telangiectasia cells. *Oncogene* 1996;13:2707-16.
15. Stewart GS, Last JI, Stankovic T, et al. Residual ataxia telangiectasia mutated protein function in cells from ataxia telangiectasia patients, with 5762ins137 and 7271T-->G mutations, showing a less severe phenotype. *J Biol Chem* 2001;276:30133-41.
16. Bakkenist CJ, Kastan MB. DNA damage activates ATM through intermolecular autophosphorylation and dimer dissociation. *Nature* 2003;421:499-506.
17. Shiloh Y. ATM and related protein kinases: safeguarding genome integrity. *Nat Rev Cancer* 2003;3:155-68.



18. Kurz EU, Lees-Miller SP. DNA damage-induced activation of ATM and ATM-dependent signaling pathways. *DNA Repair (Amst)* 2004;3:889-900.
19. Beamish H, Williams R, Chen P, Lavin MF. Defect in multiple cell cycle checkpoints in ataxia-telangiectasia postirradiation. *J Biol Chem* 1996;271:20486-93.
20. Barlow C, Hirotsune S, Paylor R, et al. Atm-deficient mice: a paradigm of ataxia telangiectasia. *Cell* 1996;86:159-71.
21. Kanaar R, Wyman C. DNA repair by the MRN complex: break it to make it. *Cell* 2008;135:14-6.
22. Waltes R, Kalb R, Gatei M, et al. Human RAD50 deficiency in a Nijmegen breakage syndrome-like disorder. *Am J Hum Genet* 2009;84:605-16.
23. Herzog KH, Chong MJ, Kapsetaki M, Morgan JI, McKinnon PJ. Requirement for Atm in ionizing radiation-induced cell death in the developing central nervous system. *Science* 1998;280:1089-91.
24. Spring K, Ahangari F, Scott SP, et al. Mice heterozygous for mutation in Atm, the gene involved in ataxia-telangiectasia, have heightened susceptibility to cancer. *Nat Genet* 2002;32:185-90.
25. Chiesa N, Barlow C, Wynshaw-Boris A, Strata P, Tempia F. Atm-deficient mice Purkinje cells show age-dependent defects in calcium spike bursts and calcium currents. *Neuroscience* 2000;96:575-83.
26. Stracker TH, Theunissen JW, Morales M, Petrini JH. The Mre11 complex and the metabolism of chromosome breaks: the importance of communicating and holding things together. *DNA Repair (Amst)* 2004;3:845-54.
27. Taylor AM, Groom A, Byrd PJ. Ataxia-telangiectasia-like disorder (ATLD)-its clinical presentation and molecular basis. *DNA Repair (Amst)* 2004;3:1219-25.
28. Buis J, Wu Y, Deng Y, et al. Mre11 nuclease activity has essential roles in DNA repair and genomic stability distinct from ATM activation. *Cell* 2008;135:85-96.
29. Dinkelmann M, Spehalski E, Stoneham T, et al. Multiple functions of MRN in end-joining pathways during isotype class switching. *Nat Struct Mol Biol* 2009;16:808-13.
30. Shiloh Y. Ataxia-telangiectasia and the Nijmegen breakage syndrome: related disorders but genes apart. *Annu Rev Genet* 1997;31:635-62.
31. Carney JP, Maser RS, Olivares H, et al. The hMre11/hRad50 protein complex and Nijmegen breakage syndrome: linkage of double-strand break repair to the cellular DNA damage response. *Cell* 1998;93:477-86.
32. Williams BR, Mirzoeva OK, Morgan WF, Lin J, Dunnick W, Petrini JH. A murine model of Nijmegen breakage syndrome. *Curr Biol* 2002;12:648-53.

33. Shull ER, Lee Y, Nakane H, et al. Differential DNA damage signaling accounts for distinct neural apoptotic responses in ATLD and NBS. *Genes Dev* 2009;23:171-80.
34. Stracker TH, Morales M, Couto SS, Hussein H, Petrini JH. The carboxy terminus of NBS1 is required for induction of apoptosis by the MRE11 complex. *Nature* 2007;447:218-21.
35. Reina-San-Martin B, Nussenzweig MC, Nussenzweig A, Difilippantonio S. Genomic instability, endoreduplication, and diminished Ig class-switch recombination in B cells lacking Nbs1. *Proc Natl Acad Sci U S A* 2005;102:1590-5.
36. Sze CI, Su M, Pugazhenth S, et al. Down-regulation of WW domain-containing oxidoreductase induces Tau phosphorylation in vitro. A potential role in Alzheimer's disease. *J Biol Chem* 2004;279:30498-506.
37. Luo G, Yao MS, Bender CF, et al. Disruption of mRad50 causes embryonic stem cell lethality, abnormal embryonic development, and sensitivity to ionizing radiation. *Proc Natl Acad Sci U S A* 1999;96:7376-81.
38. Bender CF, Sikes ML, Sullivan R, et al. Cancer predisposition and hematopoietic failure in Rad50(S/S) mice. *Gene Dev* 2002;16:2237-51.
39. Stracker TH, Petrini JH. The MRE11 complex: starting from the ends. *Nat Rev Mol Cell Biol* 2011;12:90-103.
40. Walton C, Interthal H, Hirano R, Salih MA, Takashima H, Boerkoel CF. Spinocerebellar ataxia with axonal neuropathy. *Adv Exp Med Biol* 2010;685:75-83.
41. Takashima H, Boerkoel CF, John J, et al. Mutation of TDP1, encoding a topoisomerase I-dependent DNA damage repair enzyme, in spinocerebellar ataxia with axonal neuropathy. *Nat Genet* 2002;32:267-72.
42. El-Khamisy SF, Caldecott KW. TDP1-dependent DNA single-strand break repair and neurodegeneration. *Mutagenesis* 2006;21:219-24.
43. Pommier Y, Redon C, Rao VA, et al. Repair of and checkpoint response to topoisomerase I-mediated DNA damage. *Mutat Res* 2003;532:173-203.
44. Rass U, Ahel I, West SC. Defective DNA repair and neurodegenerative disease. *Cell* 2007;130:991-1004.
45. Hawkins AJ, Subler MA, Akopiants K, et al. In vitro complementation of Tdp1 deficiency indicates a stabilized enzyme-DNA adduct from tyrosyl but not glycolate lesions as a consequence of the SCAN1 mutation. *DNA Repair (Amst)* 2009;8:654-63.
46. Hirano R, Interthal H, Huang C, et al. Spinocerebellar ataxia with axonal neuropathy: consequence of a Tdp1 recessive neomorphic mutation? *EMBO J* 2007;26:4732-43.

47. Gorodetsky E, Calkins S, Ahn J, Brooks PJ. ATM, the Mre11/Rad50/Nbs1 complex, and topoisomerase I are concentrated in the nucleus of Purkinje neurons in the juvenile human brain. *DNA Repair (Amst)* 2007;6:1698-707.
48. Shimazaki H, Takiyama Y, Sakoe K, et al. Early-onset ataxia with ocular motor apraxia and hypoalbuminemia: the aprataxin gene mutations. *Neurology* 2002;59:590-5.
49. Criscuolo C, Mancini P, Sacca F, et al. Ataxia with oculomotor apraxia type 1 in Southern Italy: late onset and variable phenotype. *Neurology* 2004;63:2173-5.
50. McKinnon PJ, Caldecott KW. DNA strand break repair and human genetic disease. *Annu Rev Genomics Hum Genet* 2007;8:37-55.
51. D'Arrigo S, Riva D, Bulgheroni S, et al. Ataxia with oculomotor apraxia type 1 (AOA1): clinical and neuropsychological features in 2 new patients and differential diagnosis. *J Child Neurol* 2008;23:895-900.
52. Clements PM, Breslin C, Deeks ED, et al. The ataxia-oculomotor apraxia 1 gene product has a role distinct from ATM and interacts with the DNA strand break repair proteins XRCC1 and XRCC4. *DNA Repair (Amst)* 2004;3:1493-502.
53. Takahashi T, Tada M, Igarashi S, et al. Aprataxin, causative gene product for EAOH/AOA1, repairs DNA single-strand breaks with damaged 3'-phosphate and 3'-phosphoglycolate ends. *Nucleic Acids Res* 2007;35:3797-809.
54. Ahel I, Rass U, El-Khamisy SF, et al. The neurodegenerative disease protein aprataxin resolves abortive DNA ligation intermediates. *Nature* 2006;443:713-6.
55. Zhou W, Reines D, Doetsch PW. T7 RNA polymerase bypass of large gaps on the template strand reveals a critical role of the nontemplate strand in elongation. *Cell* 1995;82:577-85.
56. Becherel OJ, Gueven N, Birrell GW, et al. Nucleolar localization of aprataxin is dependent on interaction with nucleolin and on active ribosomal DNA transcription. *Hum Mol Genet* 2006;15:2239-49.
57. Mosesso P, Piane M, Palitti F, Pepe G, Penna S, Chessa L. The novel human gene aprataxin is directly involved in DNA single-strand-break repair. *Cell Mol Life Sci* 2005;62:485-91.
58. Gueven N, Becherel OJ, Kijas AW, et al. Aprataxin, a novel protein that protects against genotoxic stress. *Hum Mol Genet* 2004;13:1081-93.
59. El-Khamisy SF, Katyal S, Patel P, Ju L, McKinnon PJ, Caldecott KW. Synergistic decrease of DNA single-strand break repair rates in mouse neural cells lacking both Tdp1 and aprataxin. *DNA Repair (Amst)* 2009;8:760-6.
60. Chen YZ, Hashemi SH, Anderson SK, et al. Senataxin, the yeast Sen1p orthologue: characterization of a unique protein in which recessive mutations cause ataxia and dominant mutations cause motor neuron disease. *Neurobiology of disease* 2006;23:97-108.

61. Moreira MC, Klur S, Watanabe M, et al. Senataxin, the ortholog of a yeast RNA helicase, is mutant in ataxia-ocular apraxia 2. *Nature genetics* 2004;36:225-7.
62. Le Ber I, Bouslam N, Rivaud-Pechoux S, et al. Frequency and phenotypic spectrum of ataxia with oculomotor apraxia 2: a clinical and genetic study in 18 patients. *Brain : a journal of neurology* 2004;127:759-67.
63. Suraweera A, Becherel OJ, Chen P, et al. Senataxin, defective in ataxia oculomotor apraxia type 2, is involved in the defense against oxidative DNA damage. *The Journal of cell biology* 2007;177:969-79.
64. Weng Y, Czaplinski K, Peltz SW. Genetic and biochemical characterization of mutations in the ATPase and helicase regions of the Upf1 protein. *Mol Cell Biol* 1996;16:5477-90.
65. Grohmann K, Schuelke M, Diers A, et al. Mutations in the gene encoding immunoglobulin mu-binding protein 2 cause spinal muscular atrophy with respiratory distress type 1. *Nat Genet* 2001;29:75-7.
66. Lynch DR, Braastad CD, Nagan N. Ovarian failure in ataxia with oculomotor apraxia type 2. *Am J Med Genet A* 2007;143A:1775-7.
67. Criscuolo C, Chessa L, Di Giandomenico S, et al. Ataxia with oculomotor apraxia type 2: a clinical, pathologic, and genetic study. *Neurology* 2006;66:1207-10.
68. Chen YZ, Bennett CL, Huynh HM, et al. DNA/RNA helicase gene mutations in a form of juvenile amyotrophic lateral sclerosis (ALS4). *American journal of human genetics* 2004;74:1128-35.
69. Anheim M, Monga B, Fleury M, et al. Ataxia with oculomotor apraxia type 2: clinical, biological and genotype/phenotype correlation study of a cohort of 90 patients. *Brain : a journal of neurology* 2009;132:2688-98.
70. Ursic D, Chinchilla K, Finkel JS, Culbertson MR. Multiple protein/protein and protein/RNA interactions suggest roles for yeast DNA/RNA helicase Sen1p in transcription, transcription-coupled DNA repair and RNA processing. *Nucleic Acids Res* 2004;32:2441-52.
71. Suraweera A, Lim Y, Woods R, et al. Functional role for senataxin, defective in ataxia oculomotor apraxia type 2, in transcriptional regulation. *Human molecular genetics* 2009;18:3384-96.
72. Steinmetz EJ, Warren CL, Kuehner JN, Panbehi B, Ansari AZ, Brow DA. Genome-wide distribution of yeast RNA polymerase II and its control by Sen1 helicase. *Molecular cell* 2006;24:735-46.
73. Skourti-Stathaki K, Proudfoot NJ, Gromak N. Human senataxin resolves RNA/DNA hybrids formed at transcriptional pause sites to promote Xrn2-dependent termination. *Molecular cell* 2011;42:794-805.

74. Aguilera A, Gomez-Gonzalez B. Genome instability: a mechanistic view of its causes and consequences. *Nature reviews Genetics* 2008;9:204-17.
75. Li X, Manley JL. Inactivation of the SR protein splicing factor ASF/SF2 results in genomic instability. *Cell* 2005;122:365-78.
76. Mischo HE, Gomez-Gonzalez B, Grzechnik P, et al. Yeast Sen1 helicase protects the genome from transcription-associated instability. *Molecular cell* 2011;41:21-32.
77. Andersen JK. Oxidative stress in neurodegeneration: cause or consequence? *Nat Med* 2004;10 Suppl:S18-25.
78. Klein JA, Ackerman SL. Oxidative stress, cell cycle, and neurodegeneration. *J Clin Invest* 2003;111:785-93.
79. Sayre LM, Smith MA, Perry G. Chemistry and biochemistry of oxidative stress in neurodegenerative disease. *Curr Med Chem* 2001;8:721-38.
80. Hirano M, Yamamoto A, Mori T, et al. DNA single-strand break repair is impaired in aprataxin-related ataxia. *Ann Neurol* 2007;61:162-74.
81. Guo Z, Deshpande R, Paull TT. ATM activation in the presence of oxidative stress. *Cell Cycle* 2010;9:4805-11.
82. Scandalios JG. Oxidative stress: molecular perception and transduction of signals triggering antioxidant gene defenses. *Braz J Med Biol Res* 2005;38:995-1014.
83. Halliwell B. Oxidative stress and neurodegeneration: where are we now? *J Neurochem* 2006;97:1634-58.
84. El-Khamisy SF, Saifi GM, Weinfeld M, et al. Defective DNA single-strand break repair in spinocerebellar ataxia with axonal neuropathy-1. *Nature* 2005;434:108-13.
85. Lee Y, Barnes DE, Lindahl T, McKinnon PJ. Defective neurogenesis resulting from DNA ligase IV deficiency requires Atm. *Genes Dev* 2000;14:2576-80.
86. Sekiguchi J, Ferguson DO, Chen HT, et al. Genetic interactions between ATM and the nonhomologous end-joining factors in genomic stability and development. *Proc Natl Acad Sci U S A* 2001;98:3243-8.
87. Katyal S, McKinnon PJ. DNA repair deficiency and neurodegeneration. *Cell Cycle* 2007;6:2360-5.
88. Lindahl T. Instability and decay of the primary structure of DNA. *Nature* 1993;362:709-15.
89. Wilson DM, 3rd, Bohr VA, McKinnon PJ. DNA damage, DNA repair, ageing and age-related disease. *Mech Ageing Dev* 2008;129:349-52.
90. Hakem R. DNA-damage repair; the good, the bad, and the ugly. *EMBO J* 2008;27:589-605.
91. Rich T, Allen RL, Wyllie AH. Defying death after DNA damage. *Nature* 2000;407:777-83.

92. Woodhouse BC, Dianova, II, Parsons JL, Dianov GL. Poly(ADP-ribose) polymerase-1 modulates DNA repair capacity and prevents formation of DNA double strand breaks. *DNA Repair (Amst)* 2008;7:932-40.
93. McKinnon PJ. DNA repair deficiency and neurological disease. *Nat Rev Neurosci* 2009;10:100-12.
94. Kolodner RD, Marsischky GT. Eukaryotic DNA mismatch repair. *Curr Opin Genet Dev* 1999;9:89-96.
95. Pellegrini L, Yu DS, Lo T, et al. Insights into DNA recombination from the structure of a RAD51-BRCA2 complex. *Nature* 2002;420:287-93.
96. Takata M, Sasaki MS, Sonoda E, et al. Homologous recombination and non-homologous end-joining pathways of DNA double-strand break repair have overlapping roles in the maintenance of chromosomal integrity in vertebrate cells. *EMBO J* 1998;17:5497-508.
97. Hoeijmakers JH. Genome maintenance mechanisms for preventing cancer. *Nature* 2001;411:366-74.
98. Lees-Miller SP, Meek K. Repair of DNA double strand breaks by non-homologous end joining. *Biochimie* 2003;85:1161-73.
99. Li B, Comai L. Functional interaction between Ku and the werner syndrome protein in DNA end processing. *J Biol Chem* 2000;275:39800.
100. Barzilai A. The contribution of the DNA damage response to neuronal viability. *Antioxid Redox Signal* 2007;9:211-8.
101. Staeva-Vieira E, Yoo S, Lehmann R. An essential role of DmRad51/SpnA in DNA repair and meiotic checkpoint control. *Embo Journal* 2003;22:5863-74.
102. Tarsounas M, Moens PB. Checkpoint and DNA-repair proteins are associated with the cores of mammalian meiotic chromosomes. *Current Topics in Developmental Biology, Vol 51* 2001;51:109-34.
103. Eddy EM. Male germ cell gene expression. *Recent progress in hormone research* 2002;57:103-28.
104. Griswold MD. The central role of Sertoli cells in spermatogenesis. *Seminars in cell & developmental biology* 1998;9:411-6.
105. Jan SZ, Hamer G, Repping S, de Rooij DG, van Pelt AM, Vormer TL. Molecular control of rodent spermatogenesis. *Biochimica et biophysica acta* 2012;1822:1838-50.
106. Clermont Y, Trott M. Duration of the cycle of the seminiferous epithelium in the mouse and hamster determined by means of 3H-thymidine and radioautography. *Fertility and sterility* 1969;20:805-17.

107. Yu Z, Guo R, Ge Y, et al. Gene expression profiles in different stages of mouse spermatogenic cells during spermatogenesis. *Biology of reproduction* 2003;69:37-47.
108. Chi YH, Cheng LI, Myers T, et al. Requirement for Sun1 in the expression of meiotic reproductive genes and piRNA. *Development* 2009;136:965-73.
109. Cole F, Keeney S, Jasin M. Evolutionary conservation of meiotic DSB proteins: more than just Spo11. *Genes Dev* 2010;24:1201-7.
110. Baudat F, Manova K, Yuen JP, Jasin M, Keeney S. Chromosome synapsis defects and sexually dimorphic meiotic progression in mice lacking Spo11. *Molecular cell* 2000;6:989-98.
111. Page SL, Hawley RS. The genetics and molecular biology of the synaptonemal complex. *Annual review of cell and developmental biology* 2004;20:525-58.
112. Di Carlo A, Travia G, De Felici M. The meiotic specific synaptonemal complex protein SCP3 is expressed by female and male primordial germ cells of the mouse embryo. *Int J Dev Biol* 2000;44:241-4.
113. Qiao HY, Chen JK, Reynolds A, Hoog C, Paddy M, Hunter N. Interplay between Synaptonemal Complex, Homologous Recombination, and Centromeres during Mammalian Meiosis. *Plos Genet* 2012;8.
114. Keeney S. Mechanism and control of meiotic recombination initiation. *Current topics in developmental biology* 2001;52:1-53.
115. Fernandez-Capetillo O, Mahadevaiah SK, Celeste A, et al. H2AX is required for chromatin remodeling and inactivation of sex chromosomes in male mouse meiosis. *Developmental cell* 2003;4:497-508.
116. Kinner A, Wu W, Staudt C, Iliakis G. Gamma-H2AX in recognition and signaling of DNA double-strand breaks in the context of chromatin. *Nucleic Acids Res* 2008;36:5678-94.
117. Redon C, Pilch D, Rogakou E, Sedelnikova O, Newrock K, Bonner W. Histone H2A variants H2AX and H2AZ. *Curr Opin Genet Dev* 2002;12:162-9.
118. Lobrich M, Shibata A, Beucher A, et al. gammaH2AX foci analysis for monitoring DNA double-strand break repair: strengths, limitations and optimization. *Cell Cycle* 2010;9:662-9.
119. Inagaki A, Sleddens-Linkels E, Wassenaar E, et al. Meiotic functions of RAD18. *Journal of cell science* 2011;124:2837-50.
120. Bellani MA, Romanienko PJ, Cairatti DA, Camerini-Otero RD. SPO11 is required for sex-body formation, and Spo11 heterozygosity rescues the prophase arrest of *Atm*<sup>-/-</sup> spermatocytes. *Journal of cell science* 2005;118:3233-45.
121. Handel MA, Schimenti JC. Genetics of mammalian meiosis: regulation, dynamics and impact on fertility. *Nat Rev Genet* 2010;11:124-36.

122. Mahadevaiah SK, Turner JM, Baudat F, et al. Recombinational DNA double-strand breaks in mice precede synapsis. *Nat Genet* 2001;27:271-6.
123. Oliver-Bonet M, Turek PJ, Sun F, Ko E, Martin RH. Temporal progression of recombination in human males. *Molecular human reproduction* 2005;11:517-22.
124. Plug AW, Peters AH, Keegan KS, Hoekstra MF, de Boer P, Ashley T. Changes in protein composition of meiotic nodules during mammalian meiosis. *Journal of cell science* 1998;111 ( Pt 4):413-23.
125. Cohen PE, Pollard JW. Regulation of meiotic recombination and prophase I progression in mammals. *BioEssays : news and reviews in molecular, cellular and developmental biology* 2001;23:996-1009.
126. Turner JM. Meiotic sex chromosome inactivation. *Development* 2007;134:1823-31.
127. Solari AJ. The behavior of the XY pair in mammals. *International review of cytology* 1974;38:273-317.
128. McKee BD, Handel MA. Sex chromosomes, recombination, and chromatin conformation. *Chromosoma* 1993;102:71-80.
129. Cloutier JM, Turner JM. Meiotic sex chromosome inactivation. *Curr Biol* 2010;20:R962-3.
130. Huynh KD, Lee JT. X-chromosome inactivation: a hypothesis linking ontogeny and phylogeny. *Nat Rev Genet* 2005;6:410-8.
131. Vigodner M. Sumoylation precedes accumulation of phosphorylated H2AX on sex chromosomes during their meiotic inactivation. *Chromosome research : an international journal on the molecular, supramolecular and evolutionary aspects of chromosome biology* 2009;17:37-45.
132. Handel MA. The XY body: a specialized meiotic chromatin domain. *Experimental cell research* 2004;296:57-63.
133. Rogers RS, Inselman A, Handel MA, Matunis MJ. SUMO modified proteins localize to the XY body of pachytene spermatocytes. *Chromosoma* 2004;113:233-43.
134. Turner JM, Aprelikova O, Xu X, et al. BRCA1, histone H2AX phosphorylation, and male meiotic sex chromosome inactivation. *Curr Biol* 2004;14:2135-42.
135. Gill G. SUMO and ubiquitin in the nucleus: different functions, similar mechanisms? *Genes Dev* 2004;18:2046-59.
136. Johnson ES. Protein modification by SUMO. *Annual review of biochemistry* 2004;73:355-82.
137. Da Silva-Ferrada E, Lopitz-Otsoa F, Lang V, Rodriguez MS, Matthiesen R. Strategies to Identify Recognition Signals and Targets of SUMOylation. *Biochemistry research international* 2012;2012:875148.



138. Vigodner M, Morris PL. Testicular expression of small ubiquitin-related modifier-1 (SUMO-1) supports multiple roles in spermatogenesis: silencing of sex chromosomes in spermatocytes, spermatid microtubule nucleation, and nuclear reshaping. *Developmental biology* 2005;282:480-92.
139. Anthony K, Gallo JM. Aberrant RNA processing events in neurological disorders. *Brain Res* 2010;1338:67-77.
140. Dredge BK, Polydorides AD, Darnell RB. The splice of life: alternative splicing and neurological disease. *Nat Rev Neurosci* 2001;2:43-50.
141. Zheng S, Black DL. Alternative pre-mRNA splicing in neurons: growing up and extending its reach. *Trends in genetics : TIG* 2013;29:442-8.
142. Yap K, Makeyev EV. Regulation of gene expression in mammalian nervous system through alternative pre-mRNA splicing coupled with RNA quality control mechanisms. *Mol Cell Neurosci* 2013;56:420-8.
143. Hamilton G, Gillingwater TH. Spinal muscular atrophy: going beyond the motor neuron. *Trends Mol Med* 2013;19:40-50.
144. Frugier T, Nicole S, Cifuentes-Diaz C, Melki J. The molecular bases of spinal muscular atrophy. *Curr Opin Genet Dev* 2002;12:294-8.
145. Haramati S, Chapnik E, Sztainberg Y, et al. miRNA malfunction causes spinal motor neuron disease. *Proc Natl Acad Sci U S A* 2010;107:13111-6.
146. Ule J, Ule A, Spencer J, et al. Nova regulates brain-specific splicing to shape the synapse. *Nat Genet* 2005;37:844-52.
147. Gallo JM, Jin P, Thornton CA, et al. The role of RNA and RNA processing in neurodegeneration. *J Neurosci* 2005;25:10372-5.
148. Kosik KS, Krichevsky AM. The Elegance of the MicroRNAs: A Neuronal Perspective. *Neuron* 2005;47:779-82.
149. Iacoangeli A, Bianchi R, Tiedge H. Regulatory RNAs in brain function and disorders. *Brain Res* 2010;1338:36-47.
150. Aguilera A, Garcia-Muse T. R loops: from transcription byproducts to threats to genome stability. *Molecular cell* 2012;46:115-24.
151. Camps M, Loeb LA. Critical role of R-loops in processing replication blocks. *Front Biosci* 2005;10:689-98.
152. Gottipati P, Helleday T. Transcription-associated recombination in eukaryotes: link between transcription, replication and recombination. *Mutagenesis* 2009;24:203-10.
153. Wahba L, Gore SK, Koshland D. The homologous recombination machinery modulates the formation of RNA-DNA hybrids and associated chromosome instability. *eLife* 2013;2:e00505.

154. Roy D, Lieber MR. G clustering is important for the initiation of transcription-induced R-loops in vitro, whereas high G density without clustering is sufficient thereafter. *Mol Cell Biol* 2009;29:3124-33.
155. Wongsurawat T, Jenjaroenpun P, Kwoh CK, Kuznetsov V. Quantitative model of R-loop forming structures reveals a novel level of RNA-DNA interactome complexity. *Nucleic Acids Res* 2012;40:e16.
156. Reddy K, Tam M, Bowater RP, et al. Determinants of R-loop formation at convergent bidirectionally transcribed trinucleotide repeats. *Nucleic Acids Research* 2011;39:1749-62.
157. Lin Y, Dent SY, Wilson JH, Wells RD, Napierala M. R loops stimulate genetic instability of CTG.CAG repeats. *Proc Natl Acad Sci U S A* 2010;107:692-7.
158. McIvor EI, Polak U, Napierala M. New insights into repeat instability Role of RNA.DNA hybrids. *Rna Biol* 2010;7:551-8.
159. Li X, Manley JL. Cotranscriptional processes and their influence on genome stability. *Genes Dev* 2006;20:1838-47.
160. Huertas P, Aguilera A. Cotranscriptionally formed DNA:RNA hybrids mediate transcription elongation impairment and transcription-associated recombination. *Molecular cell* 2003;12:711-21.
161. Arakawa H, Iwasato T, Hayashida H, Shimizu A, Honjo T, Yamagishi H. The complete murine immunoglobulin class switch region of the alpha heavy chain gene-hierarchical repetitive structure and recombination breakpoints. *J Biol Chem* 1993;268:4651-5.
162. Lin WQ, Sampathi S, Dai HF, et al. Mammalian DNA2 helicase/nuclease cleaves G-quadruplex DNA and is required for telomere integrity. *Embo Journal* 2013;32:1425-39.
163. Sun H, Yabuki A, Maizels N. A human nuclease specific for G4 DNA. *P Natl Acad Sci USA* 2001;98:12444-9.
164. Aguilera A. The connection between transcription and genomic instability. *EMBO J* 2002;21:195-201.
165. Hamperl S, Cimprich KA. The contribution of co-transcriptional RNA:DNA hybrid structures to DNA damage and genome instability. *DNA Repair* 2014;19:84-94.
166. Santos-Pereira JM, Herrero AB, Garcia-Rubio ML, Marin A, Moreno S, Aguilera A. The Npl3 hnRNP prevents R-loop-mediated transcription-replication conflicts and genome instability. *Genes Dev* 2013;27:2445-58.
167. Umate P, Tuteja N, Tuteja R. Genome-wide comprehensive analysis of human helicases. *Commun Integr Biol* 2011;4:118-37.
168. Chakraborty P, Grosse F. Human DHX9 helicase preferentially unwinds RNA-containing displacement loops (R-loops) and G-quadruplexes. *DNA Repair (Amst)* 2011;10:654-65.

169. Lin Y, Wilson JH. Nucleotide excision repair, mismatch repair, and R-loops modulate convergent transcription-induced cell death and repeat instability. *PloS one* 2012;7:e46807.
170. Ginno PA, Lott PL, Christensen HC, Korf I, Chedin F. R-loop formation is a distinctive characteristic of unmethylated human CpG island promoters. *Molecular cell* 2012;45:814-25.
171. Deaton AM, Bird A. CpG islands and the regulation of transcription. *Genes Dev* 2011;25:1010-22.
172. Vertino PM, Wade PA. R loops: lassoing DNA methylation at CpGi. *Molecular cell* 2012;45:708-9.
173. Sen D, Gilbert W. Formation of parallel four-stranded complexes by guanine-rich motifs in DNA and its implications for meiosis. *Nature* 1988;334:364-6.
174. Gilbert DE, Feigon J. Multistranded DNA structures. *Curr Opin Struct Biol* 1999;9:305-14.
175. Lam EYN, Beraldi D, Tannahill D, Balasubramanian S. G-quadruplex structures are stable and detectable in human genomic DNA. *Nat Commun* 2013;4.
176. Zheng KW, Xiao S, Liu JQ, Zhang JY, Hao YH, Tan Z. Co-transcriptional formation of DNA:RNA hybrid G-quadruplex and potential function as constitutional cis element for transcription control. *Nucleic Acids Research* 2013;41:5533-41.
177. Murat P, Balasubramanian S. Existence and consequences of G-quadruplex structures in DNA. *Current Opinion in Genetics & Development* 2014;25:22-9.
178. Duquette ML, Handa P, Vincent JA, Taylor AF, Maizels N. Intracellular transcription of G-rich DNAs induces formation of G-loops, novel structures containing G4 DNA. *Genes Dev* 2004;18:1618-29.
179. Neidle S, Parkinson GN. The structure of telomeric DNA. *Curr Opin Struct Biol* 2003;13:275-83.
180. Grozdanov P, Georgiev O, Karagoyozov L. Complete sequence of the 45-kb mouse ribosomal DNA repeat: analysis of the intergenic spacer. *Genomics* 2003;82:637-43.
181. Hanakahi LA, Sun H, Maizels N. High affinity interactions of nucleolin with G-G-paired rDNA. *J Biol Chem* 1999;274:15908-12.
182. Wong Z, Wilson V, Patel I, Povey S, Jeffreys AJ. Characterization of a panel of highly variable minisatellites cloned from human DNA. *Ann Hum Genet* 1987;51:269-88.
183. Buroker N, Bestwick R, Haight G, Magenis RE, Litt M. A hypervariable repeated sequence on human chromosome 1p36. *Hum Genet* 1987;77:175-81.
184. Frismand S, Salem H, Panouilleres M, et al. MRI findings in AOA2: Cerebellar atrophy and abnormal iron detection in dentate nucleus. *NeuroImage Clinical* 2013;2:542-8.
185. Gilhooly NS, Gwynn EJ, Dillingham MS. Superfamily 1 helicases. *Frontiers in bioscience* 2013;5:206-16.

186. Chan W, Costantino N, Li R, et al. A recombineering based approach for high-throughput conditional knockout targeting vector construction. *Nucleic Acids Res* 2007;35:e64.
187. Guyenet SJ, Furrer SA, Damian VM, Baughan TD, La Spada AR, Garden GA. A simple composite phenotype scoring system for evaluating mouse models of cerebellar ataxia. *Journal of visualized experiments : JoVE* 2010.
188. Thomas PS, Jr., Fraley GS, Damian V, et al. Loss of endogenous androgen receptor protein accelerates motor neuron degeneration and accentuates androgen insensitivity in a mouse model of X-linked spinal and bulbar muscular atrophy. *Hum Mol Genet* 2006;15:2225-38.
189. Chou AH, Yeh TH, Ouyang P, Chen YL, Chen SY, Wang HL. Polyglutamine-expanded ataxin-3 causes cerebellar dysfunction of SCA3 transgenic mice by inducing transcriptional dysregulation. *Neurobiol Dis* 2008;31:89-101.
190. Gazulla J, Benavente I, Lopez-Fraile IP, Modrego P, Koenig M. Sensorimotor Neuronopathy in Ataxia with Oculomotor Apraxia Type 2. *Muscle Nerve* 2009;40:481-5.
191. Kuznetsov S, Pellegrini M, Shuda K, et al. RAD51C deficiency in mice results in early prophase I arrest in males and sister chromatid separation at metaphase II in females. *J Cell Biol* 2007;176:581-92.
192. Turner JM, Mahadevaiah SK, Fernandez-Capetillo O, et al. Silencing of unsynapsed meiotic chromosomes in the mouse. *Nat Genet* 2005;37:41-7.
193. Baudat F, de Massy B. Regulating double-stranded DNA break repair towards crossover or non-crossover during mammalian meiosis. *Chromosome research : an international journal on the molecular, supramolecular and evolutionary aspects of chromosome biology* 2007;15:565-77.
194. Kolas NK, Svetlanov A, Lenzi ML, et al. Localization of MMR proteins on meiotic chromosomes in mice indicates distinct functions during prophase I. *Journal of Cell Biology* 2005;171:447-58.
195. Vibranovski MD. Meiotic sex chromosome inactivation in *Drosophila*. *Journal of genomics* 2014;2:104-17.
196. Mahadevaiah SK, Bourc'his D, de Rooij DG, Bestor TH, Turner JM, Burgoyne PS. Extensive meiotic asynapsis in mice antagonises meiotic silencing of unsynapsed chromatin and consequently disrupts meiotic sex chromosome inactivation. *J Cell Biol* 2008;182:263-76.
197. Turner JM, Mahadevaiah SK, Ellis PJ, Mitchell MJ, Burgoyne PS. Pachytene asynapsis drives meiotic sex chromosome inactivation and leads to substantial postmeiotic repression in spermatids. *Developmental cell* 2006;10:521-9.
198. Namekawa SH, Park PJ, Zhang LF, et al. Postmeiotic sex chromatin in the male germline of mice. *Current Biology* 2006;16:660-7.

199. de Vries M, Vosters S, Merkx G, et al. Human Male Meiotic Sex Chromosome Inactivation. *PloS one* 2012;7.
200. Wang PJ, Page DC, McCarrey JR. Differential expression of sex-linked and autosomal germ-cell-specific genes during spermatogenesis in the mouse. *Human Molecular Genetics* 2005;14:2911-8.
201. Heard E, Turner J. Function of the sex chromosomes in mammalian fertility. *Cold Spring Harbor perspectives in biology* 2011;3:a002675.
202. Romanienko PJ, Camerini-Otero RD. The mouse Spo11 gene is required for meiotic chromosome synapsis. *Molecular cell* 2000;6:975-87.
203. Pittman DL, Cobb J, Schimenti KJ, et al. Meiotic prophase arrest with failure of chromosome synapsis in mice deficient for Dmc1, a germline-specific RecA homolog. *Molecular cell* 1998;1:697-705.
204. Bannister LA, Pezza RJ, Donaldson JR, et al. A dominant, recombination-defective allele of Dmc1 causing male-specific sterility. *PLoS Biol* 2007;5:e105.
205. Cressman VL, Backlund DC, Avrutskaya AV, Leadon SA, Godfrey V, Koller BH. Growth retardation, DNA repair defects, and lack of spermatogenesis in BRCA1-deficient mice. *Mol Cell Biol* 1999;19:7061-75.
206. Edelmann W, Cohen PE, Kneitz B, et al. Mammalian MutS homologue 5 is required for chromosome pairing in meiosis. *Nat Genet* 1999;21:123-7.
207. Kneitz B, Cohen PE, Avdievich E, et al. MutS homolog 4 localization to meiotic chromosomes is required for chromosome pairing during meiosis in male and female mice. *Genes Dev* 2000;14:1085-97.
208. Kolas NK, Svetlanov A, Lenzi ML, et al. Localization of MMR proteins on meiotic chromosomes in mice indicates distinct functions during prophase I. *J Cell Biol* 2005;171:447-58.
209. Lynch DR, Braastad CD, Nagan N. Ovarian failure in ataxia with oculomotor apraxia type 2. *American Journal of Medical Genetics Part A* 2007;143A:1775-7.
210. Fogel BL, Cho E, Wahnich A, et al. Mutation of senataxin alters disease-specific transcriptional networks in patients with ataxia with oculomotor apraxia type 2. *Hum Mol Genet* 2014;23:4758-69.
211. Burgoyne PS, Mahadevaiah SK, Turner JM. The consequences of asynapsis for mammalian meiosis. *Nat Rev Genet* 2009;10:207-16.
212. Kouznetsova A, Wang H, Bellani M, Camerini-Otero RD, Jessberger R, Hoog C. BRCA1-mediated chromatin silencing is limited to oocytes with a small number of asynapsed chromosomes. *Journal of cell science* 2009;122:2446-52.

213. Ichijima Y, Ichijima M, Lou ZK, et al. MDC1 directs chromosome-wide silencing of the sex chromosomes in male germ cells. *Gene Dev* 2011;25:959-71.
214. Zhao Q, Xie YB, Zheng YY, et al. GPS-SUMO: a tool for the prediction of sumoylation sites and SUMO-interaction motifs. *Nucleic Acids Research* 2014;42:W325-W30.
215. Hecker CM, Rabiller M, Haglund K, Bayer P, Dikic I. Specification of SUMO1- and SUMO2-interacting motifs. *Journal of Biological Chemistry* 2006;281:16117-27.
216. Tibbetts RS, Cortez D, Brumbaugh KM, et al. Functional interactions between BRCA1 and the checkpoint kinase ATR during genotoxic stress. *Gene Dev* 2000;14:2989-3002.
217. Searle BC. Scaffold: a bioinformatic tool for validating MS/MS-based proteomic studies. *Proteomics* 2010;10:1265-9.
218. Cortez D, Guntuku S, Qin J, Elledge SJ. ATR and ATRIP: Partners in checkpoint signaling. *Science* 2001;294:1713-6.
219. Choi JH, Lindsey-Boltz LA, Kemp M, Mason AC, Wold MS, Sancar A. Reconstitution of RPA-covered single-stranded DNA-activated ATR-Chk1 signaling. *P Natl Acad Sci USA* 2010;107:13660-5.
220. Kumagai A, Lee J, Yoo HY, Dunphy WG. TopBP1 activates the ATR-ATRIP complex. *Cell* 2006;124:943-55.
221. Wu CS, Ouyang J, Mori E, et al. SUMOylation of ATRIP potentiates DNA damage signaling by boosting multiple protein interactions in the ATR pathway. *Gene Dev* 2014;28:1472-84.
222. Xu XL, Qiao WH, Linke SP, et al. Genetic interactions between tumor suppressors Brca1 and p53 in apoptosis, cell cycle and tumorigenesis. *Nature Genetics* 2001;28:266-71.
223. Perera D, Perez-Hidalgo L, Moens PB, et al. TopBP1 and ATR colocalization at meiotic chromosomes: Role of TopBP1/Cut5 in the meiotic recombination checkpoint. *Mol Biol Cell* 2004;15:1568-79.
224. Daniel K, Lange J, Hached K, et al. Meiotic homologue alignment and its quality surveillance are controlled by mouse HORMAD1. *Nature Cell Biology* 2011;13:599-U232.
225. Yilmaz S, Sancar A, Kemp MG. Multiple ATR-Chk1 Pathway Proteins Preferentially Associate with Checkpoint-Inducing DNA Substrates. *PloS one* 2011;6.
226. Liu SQ, Opiyo SO, Manthey K, et al. Distinct roles for DNA-PK, ATM and ATR in RPA phosphorylation and checkpoint activation in response to replication stress. *Nucleic Acids Research* 2012;40:10780-94.
227. Sorensen CS, Syljuasen RG. Safeguarding genome integrity: the checkpoint kinases ATR, CHK1 and WEE1 restrain CDK activity during normal DNA replication. *Nucleic Acids Research* 2012;40:477-86.

228. Cha RS, Kleckner N. ATR homolog Mec1 promotes fork progression, thus averting breaks in replication slow zones. *Science* 2002;297:602-6.
229. Liu S, Ho CK, Ouyang J, Zou L. Nek1 kinase associates with ATR-ATRIP and primes ATR for efficient DNA damage signaling. *Proc Natl Acad Sci U S A* 2013;110:2175-80.
230. Letwin K, Mizzen L, Motro B, Bendavid Y, Bernstein A, Pawson T. A Mammalian Dual Specificity Protein-Kinase, Nek1, Is Related to the Nima Cell-Cycle Regulator and Highly Expressed in Meiotic Germ-Cells. *Embo Journal* 1992;11:3521-31.
231. Baarends WM, Wassenaar E, van der Laan R, et al. Silencing of unpaired chromatin and histone H2A ubiquitination in mammalian meiosis. *Mol Cell Biol* 2005;25:1041-53.
232. Page J, de la Fuente R, Manterola M, et al. Inactivation or non-reactivation: what accounts better for the silence of sex chromosomes during mammalian male meiosis? *Chromosoma* 2012;121:307-26.
233. Yuce O, West SC. Senataxin, Defective in the Neurodegenerative Disorder Ataxia with Oculomotor Apraxia 2, Lies at the Interface of Transcription and the DNA Damage Response. *Molecular and Cellular Biology* 2013;33:406-17.
234. Xue YT, Wong JM, Moreno GT, Young MK, Cote J, Wang WD. NURD, a novel complex with both ATP-dependent chromatin-remodeling and histone deacetylase activities. *Molecular cell* 1998;2:851-61.
235. Larsen DH, Poinsignon C, Gudjonsson T, et al. The chromatin-remodeling factor CHD4 coordinates signaling and repair after DNA damage. *Journal of Cell Biology* 2010;190:731-40.
236. Urquhart AJ, Gatei M, Richard DJ, Khanna KK. ATM mediated phosphorylation of CHD4 contributes to genome maintenance. *Genome integrity* 2011;2:1.
237. Muller S, Ledl A, Schmidt D. SUMO: a regulator of gene expression and genome integrity. *Oncogene* 2004;23:1998-2008.
238. Hay RT. SUMO: A history of modification. *Molecular cell* 2005;18:1-12.
239. Shrivastava V, Pekar M, Grosser E, Im J, Vigodner M. SUMO proteins are involved in the stress response during spermatogenesis and are localized to DNA double-strand breaks in germ cells. *Reproduction* 2010;139:999-1010.
240. Richard P, Feng S, Manley JL. A SUMO-dependent interaction between Senataxin and the exosome, disrupted in the neurodegenerative disease AOA2, targets the exosome to sites of transcription-induced DNA damage. *Gene Dev* 2013;27:2227-32.
241. Houseley J, LaCava J, Tollervey D. RNA-quality control by the exosome. *Nat Rev Mol Cell Bio* 2006;7:529-39.

242. Xu X, Aprelikova O, Moens P, Deng CX, Furth PA. Impaired meiotic DNA-damage repair and lack of crossing-over during spermatogenesis in BRCA1 full-length isoform deficient mice. *Development* 2003;130:2001-12.
243. Becherel OJ, Yeo AJ, Stellati A, et al. Senataxin plays an essential role with DNA damage response proteins in meiotic recombination and gene silencing. *Plos Genet* 2013;9:e1003435.
244. Hill SJ, Rolland T, Adelmant G, et al. Systematic screening reveals a role for BRCA1 in the response to transcription-associated DNA damage. *Gene Dev* 2014;28:1957-75.
245. Liu SZ, Shiotani B, Lahiri M, et al. ATR Autophosphorylation as a Molecular Switch for Checkpoint Activation. *Molecular cell* 2011;43:192-202.
246. Nam EA, Zhao RX, Glick GG, Bansbach CE, Friedman DB, Cortez D. Thr-1989 Phosphorylation Is a Marker of Active Ataxia Telangiectasia-mutated and Rad3-related (ATR) Kinase. *Journal of Biological Chemistry* 2011;286:28707-14.
247. Wang X, Zeng L, Wang J, et al. A positive role for c-Abl in Atm and Atr activation in DNA damage response. *Cell Death Differ* 2011;18:5-15.
248. Chen YM, Chen CF, Riley DJ, Chen PL. Nek1 kinase functions in DNA damage response and checkpoint control through a pathway independent of ATM and ATR. *Cell Cycle* 2011;10:655-63.
249. Katzenberger RJ, Marengo MS, Wassarman DA. ATM and ATR pathways signal alternative splicing of Drosophila TAF1 pre-mRNA in response to DNA damage. *Molecular and Cellular Biology* 2006;26:9256-67.
250. Chandris P, Giannouli CC, Panayotou G, Kleitsas D. Compromise in mRNA processing machinery in senescent human fibroblasts: implications for a novel potential role of Phospho-ATR (ser428). *Biogerontology* 2010;11:421-36.
251. Khalil AM, Wahlestedt C. Epigenetic mechanisms of gene regulation during mammalian spermatogenesis. *Epigenetics-U S* 2008;3:21-7.
252. Sheng K, Liang XT, Huang SZ, Xu WM. The Role of Histone Ubiquitination during Spermatogenesis. *Biomed Res Int* 2014.
253. Lu LY, Wu JX, Ye L, Gavrulina GB, Saunders TL, Yu XC. RNF8-Dependent Histone Modifications Regulate Nucleosome Removal during Spermatogenesis. *Developmental cell* 2010;18:371-84.
254. Hung H, Kohnken R, Svaren J. The Nucleosome Remodeling and Deacetylase Chromatin Remodeling (NuRD) Complex Is Required for Peripheral Nerve Myelination. *Journal of Neuroscience* 2012;32:1517-27.
255. Lai AY, Wade PA. Cancer biology and NuRD: a multifaceted chromatin remodelling complex. *Nature Reviews Cancer* 2011;11:588-96.



256. Yoshida T, Hazan I, Zhang J, et al. The role of the chromatin remodeler Mi-2 beta in hematopoietic stem cell self-renewal and multilineage differentiation. *Gene Dev* 2008;22:1174-89.
257. Chou DM, Adamson B, Dephoure NE, et al. A chromatin localization screen reveals poly (ADP ribose)-regulated recruitment of the repressive polycomb and NuRD complexes to sites of DNA damage. *P Natl Acad Sci USA* 2010;107:18475-80.
258. Polo SE, Kaidi A, Baskcomb L, Galanty Y, Jackson SP. Regulation of DNA-damage responses and cell-cycle progression by the chromatin remodelling factor CHD4. *Embo Journal* 2010;29:3130-9.
259. Hendriks IA, D'Souza RC, Yang B, Verlaan-de Vries M, Mann M, Vertegaal AC. Uncovering global SUMOylation signaling networks in a site-specific manner. *Nat Struct Mol Biol* 2014;21:927-36.
260. Hudson JJR, Chiang SC, Wells OS, Rookyard C, El-Khamisy SF. SUMO modification of the neuroprotective protein TDP1 facilitates chromosomal single-strand break repair. *Nat Commun* 2012;3.
261. Schmidt DR, Schreiber SL. Molecular association between ATR and two components of the nucleosome remodeling and deacetylating complex, HDAC2 and CHD4. *Biochemistry-US* 1999;38:14711-7.
262. Lin YL, Pasero P. Interference Between DNA Replication and Transcription as a Cause of Genomic Instability. *Curr Genomics* 2012;13:65-73.
263. Helmrich A, Ballarino M, Nudler E, Tora L. Transcription-replication encounters, consequences and genomic instability. *Nat Struct Mol Biol* 2013;20:412-8.
264. Shanbhag NM, Rafalska-Metcalf IU, Balane-Bolivar C, Janicki SM, Greenberg RA. ATM-Dependent Chromatin Changes Silence Transcription In cis to DNA Double-Strand Breaks. *Cell* 2010;141:970-81.
265. Tuduri S, Crabbe L, Conti C, et al. Topoisomerase I suppresses genomic instability by preventing interference between replication and transcription. *Nat Cell Biol* 2009;11:1315-24.
266. Jang ER, Choi JD, Park MA, Jeong G, Cho H, Lee JS. ATM modulates transcription in response to histone deacetylase inhibition as part of its DNA damage response. *Exp Mol Med* 2010;42:195-204.
267. Narayanan MS, Rudenko G. TDP1 is an HMG chromatin protein facilitating RNA polymerase I transcription in African trypanosomes. *Nucleic Acids Research* 2013;41:2981-92.
268. Sordet O, Redon CE, Guirouilh-Barbat J, et al. Ataxia telangiectasia mutated activation by transcription- and topoisomerase I-induced DNA double-strand breaks. *EMBO Rep* 2009;10:887-93.

269. El Hage A, French SL, Beyer AL, Tollervey D. Loss of Topoisomerase I leads to R-loop-mediated transcriptional blocks during ribosomal RNA synthesis. *Gene Dev* 2010;24:1546-58.
270. Lavin MF. The appropriateness of the mouse model for ataxia-telangiectasia: Neurological defects but no neurodegeneration. *DNA Repair* 2013;12:612-9.
271. Helmrich A, Ballarino M, Tora L. Collisions between Replication and Transcription Complexes Cause Common Fragile Site Instability at the Longest Human Genes. *Molecular cell* 2011;44:966-77.
272. Schwartz M, Zlotorynski E, Kerem B. The molecular basis of common and rare fragile sites. *Cancer letters* 2006;232:13-26.
273. Ma K, Qiu L, Mrasek K, et al. Common fragile sites: genomic hotspots of DNA damage and carcinogenesis. *International journal of molecular sciences* 2012;13:11974-99.
274. Bednarek AK, Laflin KJ, Daniel RL, Liao Q, Hawkins KA, Aldaz CM. WWOX, a novel WW domain-containing protein mapping to human chromosome 16q23.3-24.1, a region frequently affected in breast cancer. *Cancer research* 2000;60:2140-5.
275. Mallaret M, Synofzik M, Lee J, et al. The tumour suppressor gene WWOX is mutated in autosomal recessive cerebellar ataxia with epilepsy and mental retardation. *Brain* 2014;137:411-9.
276. Abdel-Salam G, Thoenes M, Afifi HH, Korber F, Swan D, Bolz HJ. The supposed tumor suppressor gene WWOX is mutated in an early lethal microcephaly syndrome with epilepsy, growth retardation and retinal degeneration. *Orphanet Journal of Rare Diseases* 2014;9.
277. Krummel KA, Denison SR, Calhoun E, Phillips LA, Smith DI. The common fragile site FRA16D and its associated gene WWOX are highly conserved in the mouse at Fra8E1. *Gene Chromosome Canc* 2002;34:154-67.
278. Wongsurawat T, Jenjaroenpun P, Kwoh CK, Kuznetsov V. Quantitative model of R-loop forming structures reveals a novel level of RNA-DNA interactome complexity. *Nucleic Acids Research* 2012;40.
279. Millevoi S, Moine H, Vagner S. G-quadruplexes in RNA biology. *Wiley interdisciplinary reviews RNA* 2012.
280. Wong HM, Stegle O, Rodgers S, Huppert JL. A toolbox for predicting g-quadruplex formation and stability. *Journal of nucleic acids* 2010;2010.
281. Aguilera A. mRNA processing and genomic instability. *Nat Struct Mol Biol* 2005;12:737-8.
282. Sordet O, Nakamura AJ, Redon CE, Pommier Y. DNA double-strand breaks and ATM activation by transcription-blocking DNA lesions. *Cell Cycle* 2010;9:274-8.
283. Wu ZK, Getun IV, Bois PR. Anatomy of mouse recombination hot spots. *Nucleic Acids Res* 2010;38:2346-54.

284. Gan WJ, Guan ZS, Liu J, et al. R-loop-mediated genomic instability is caused by impairment of replication fork progression. *Gene Dev* 2011;25:2041-56.
285. Loomis EW, Sanz LA, Chedin F, Hagerman PJ. Transcription-Associated R-Loop Formation across the Human FMR1 CGG-Repeat Region. *Plos Genet* 2014;10.
286. Fogel BL, Cho E, Wahnich A, et al. Mutation of senataxin alters disease-specific transcriptional networks in patients with ataxia with oculomotor apraxia type 2. *Hum Mol Genet* 2014.
287. Iannaccone PM, Jacob HJ. Rats! *Dis Model Mech* 2009;2:206-10.
288. Aitman TJ, Critser JK, Cuppen E, et al. Progress and prospects in rat genetics: a community view. *Nature Genetics* 2008;40:516-22.
289. Marcon E, Moens PB. The evolution of meiosis: recruitment and modification of somatic DNA-repair proteins. *BioEssays : news and reviews in molecular, cellular and developmental biology* 2005;27:795-808.
290. Zuazua-Villar P, Rodriguez R, Gagou ME, Eyers PA, Meuth M. DNA replication stress in CHK1-depleted tumour cells triggers premature (S-phase) mitosis through inappropriate activation of Aurora kinase B. *Cell Death Dis* 2014;5.
291. Yamada T, Yang Y, Hemberg M, et al. Promoter Decommissioning by the NuRD Chromatin Remodeling Complex Triggers Synaptic Connectivity in the Mammalian Brain. *Neuron* 2014;83:122-34.
292. Nayler S, Gatei M, Kozlov S, et al. Induced Pluripotent Stem Cells from Ataxia-Telangiectasia Recapitulate the Cellular Phenotype. *Stem Cell Transl Med* 2012;1:523-35.
293. Stewart R, Kozlov S, Matigian N, et al. A patient-derived olfactory stem cell disease model for ataxia-telangiectasia. *Human Molecular Genetics* 2013;22:2495-509.
294. Urduingio RG, Sanchez-Mut JV, Esteller M. Epigenetic mechanisms in neurological diseases: genes, syndromes, and therapies. *Lancet Neurol* 2009;8:1056-72.
295. Palhan VB, Chen SM, Peng GH, et al. Polyglutamine-expanded ataxin-7 inhibits STAGA histone acetyltransferase activity to produce retinal degeneration. *P Natl Acad Sci USA* 2005;102:8472-7.
296. Duncan CE, An MC, Papanikolaou T, Rugani C, Vitelli C, Ellerby LM. Histone deacetylase-3 interacts with ataxin-7 and is altered in a spinocerebellar ataxia type 7 mouse model. *Mol Neurodegener* 2013;8.
297. Krishnan V, Chow MZY, Wang ZM, et al. Histone H4 lysine 16 hypoacetylation is associated with defective DNA repair and premature senescence in Zmpste24-deficient mice. *P Natl Acad Sci USA* 2011;108:12325-30.

298. Peleg S, Sananbenesi F, Zovoilis A, et al. Altered Histone Acetylation Is Associated with Age-Dependent Memory Impairment in Mice. *Science* 2010;328:753-6.
299. Pattaroni C, Jacob C. Histone Methylation in the Nervous System: Functions and Dysfunctions. *Mol Neurobiol* 2013;47:740-56.
300. Yeo AJ, Becherel OJ, Luff JE, Cullen JK, Wongsurawat T, Jenjaroenpun P. R-Loops in Proliferating Cells but Not in the Brain: Implications for AOA2 and Other Autosomal Recessive Ataxias (vol 9, e90219, 2014). *PloS one* 2014;9.
301. Ranji A, Boris-Lawrie K. RNA helicases: emerging roles in viral replication and the host innate response. *Rna Biol* 2010;7:775-87.
302. Groh M, Gromak N. Out of balance: R-loops in human disease. *Plos Genet* 2014;10:e1004630.
303. Kim JH, Seo YS. In vitro assays for studying helicase activities. *Methods in molecular biology* 2009;521:361-79.
304. Skourti-Stathaki K, Kamieniarz-Gdula K, Proudfoot NJ. R-loops induce repressive chromatin marks over mammalian gene terminators. *Nature* 2014.

# **APPENDIX**

# **APPENDIX I**

# Senataxin Plays an Essential Role with DNA Damage Response Proteins in Meiotic Recombination and Gene Silencing

Olivier J. Becherel<sup>1,2</sup>, Abrey J. Yeo<sup>1,3</sup>, Alissa Stellati<sup>1,2</sup>, Evelyn Y. H. Heng<sup>1</sup>, John Luff<sup>1</sup>, Amila M. Suraweera<sup>1</sup>, Rick Woods<sup>1</sup>, Jean Fleming<sup>4</sup>, Dianne Carrie<sup>5</sup>, Kristine McKinney<sup>6</sup>, Xiaoling Xu<sup>7</sup>, Chuxia Deng<sup>7</sup>, Martin F. Lavin<sup>1,8\*</sup>

**1** Radiation Biology and Oncology Laboratory, Queensland Institute of Medical Research, Brisbane, Australia, **2** School of Chemistry and Molecular Biosciences, University of Queensland, St. Lucia, Australia, **3** School of Medicine, University of Queensland, Brisbane, Australia, **4** University of Otago, Dunedin, New Zealand, **5** QCF Transgenics Laboratory, Queensland Institute of Medical Research, Brisbane, Australia, **6** Dana Farber Cancer Institute, Harvard University, Boston, Massachusetts, United States of America, **7** Mammalian Genetics Section, National Institute of Diabetes and Digestive and Kidney Diseases, National Institutes of Health, Bethesda, Maryland, United States of America, **8** University of Queensland Centre for Clinical Research, University of Queensland, Brisbane, Australia

## Abstract

Senataxin, mutated in the human genetic disorder ataxia with oculomotor apraxia type 2 (AOA2), plays an important role in maintaining genome integrity by coordination of transcription, DNA replication, and the DNA damage response. We demonstrate that senataxin is essential for spermatogenesis and that it functions at two stages in meiosis during crossing-over in homologous recombination and in meiotic sex chromosome inactivation (MSCI). Disruption of the *Setx* gene caused persistence of DNA double-strand breaks, a defect in disassembly of Rad51 filaments, accumulation of DNA:RNA hybrids (R-loops), and ultimately a failure of crossing-over. Senataxin localised to the XY body in a Brca1-dependent manner, and in its absence there was incomplete localisation of DNA damage response proteins to the XY chromosomes and ATR was retained on the axial elements of these chromosomes, failing to diffuse out into chromatin. Furthermore persistence of RNA polymerase II activity, altered ubH2A distribution, and abnormal XY-linked gene expression in *Setx*<sup>-/-</sup> revealed an essential role for senataxin in MSCI. These data support key roles for senataxin in coordinating meiotic crossing-over with transcription and in gene silencing to protect the integrity of the genome.

**Citation:** Becherel OJ, Yeo AJ, Stellati A, Heng EYH, Luff J, et al. (2013) Senataxin Plays an Essential Role with DNA Damage Response Proteins in Meiotic Recombination and Gene Silencing. *PLoS Genet* 9(4): e1003435. doi:10.1371/journal.pgen.1003435

**Editor:** Peter J. McKinnon, St. Jude Children's Research Hospital, United States of America

**Received:** January 3, 2013; **Accepted:** February 12, 2013; **Published:** April 11, 2013

This is an open-access article, free of all copyright, and may be freely reproduced, distributed, transmitted, modified, built upon, or otherwise used by anyone for any lawful purpose. The work is made available under the Creative Commons CC0 public domain dedication.

**Funding:** Funding was obtained from the Australian National Health and Medical Research Council. The funders had no role in study design, data collection and analysis, decision to publish, or preparation of the manuscript.

**Competing Interests:** The authors have declared that no competing interests exist.

\* E-mail: Martin.Lavin@qimr.edu.au

## Introduction

Ataxia oculomotor apraxia type 2 (AOA2), a severe form of autosomal recessive cerebellar ataxia (ARCA) is characterised by progressive cerebellar atrophy and peripheral neuropathy, oculomotor apraxia and elevated  $\alpha$ -fetoprotein [1,2]. The gene defective in AOA2, *SETX*, is also associated with amyotrophic lateral sclerosis 4 (ALS4), an autosomal dominant juvenile-onset form of ALS [3]. Senataxin shares extensive homology in its putative helicase domain with the yeast, *Saccharomyces cerevisiae* splicing endonuclease 1 protein (Sen1p) which possesses helicase activity and is involved in RNA processing, transcription and transcription-coupled DNA repair [4]. A role for senataxin in DNA repair is supported by the observation that AOA2 patient cells display sensitivity to DNA damaging agents such as H<sub>2</sub>O<sub>2</sub>, camptothecin and mitomycin C and have elevated levels of oxidative DNA damage [5].

Senataxin also plays a role in transcription regulation by its ability to modulate RNA Polymerase II (Pol II) binding to chromatin and through its interaction with proteins involved in transcription [6]. mRNA splicing efficiency, splice site selection,

and transcription termination were all defective in senataxin-deficient cells [6]. A recent study has described an additional role for senataxin in transcription elongation and termination [7]. Cells deficient in senataxin displayed an increase in RNA read-through and Pol II density downstream of the Poly(A) site and also exhibited increased levels of R-loops (RNA:DNA hybrids that form over transcription pause sites) formation [8,9]. The yeast ortholog of senataxin, Sen1p, has also been shown to protect its heavily transcribed genome from R-loop-mediated DNA damage [10]. More recently, a role for senataxin has been described at the interface between transcription and the DNA damage response [11]. They revealed that senataxin forms nuclear foci in S/G2 phase cells and these foci increased in response to DNA damage and impaired DNA replication. These foci disappeared upon resolution of R-loops or after inhibition of transcription. Evidence has also been provided for the association of the yeast ortholog of senataxin, Sen1, with DNA replication forks across RNA polymerase II transcribed genes [12]. These data demonstrate a co-ordinating role for Sen1 between replication and transcription.

We generated a *Setx* knockout mouse model to investigate further the role of senataxin. Our data revealed that this protein is

## Author Summary

Ataxia with oculomotor apraxia type 2 (AOA2) caused by a defect in the gene *Setx* (coding for senataxin) is part of a subgroup of autosomal recessive ataxias characterized by defects in genes responsible for the recognition and/or repair of damage in DNA. Cells from these patients are characterized by oxidative stress and are defective in RNA processing and termination of transcription. Recent data suggest that senataxin is involved in coordinating events between DNA replication forks and ongoing transcription. To further understand the role of senataxin, we disrupted the *Setx* gene in mice and demonstrated its essential role in spermatogenesis during meiotic recombination and in meiotic sex chromosome inactivation (MSCI). In the absence of senataxin, DNA double-strand breaks persist, RNA:DNA hybrids (R-loops) accumulate, and homologous recombination is disrupted. Senataxin localised to the XY chromosomes during pachytene. This was dependent on *Brc1*, which functions early in MSCI to recruit DNA damage response proteins to the XY body. In the absence of senataxin, there was incomplete accumulation of DNA damage response proteins on the XY chromosomes and no MDC1-dependent diffusion of ATR to the broader XY chromatin. The end result was a defect in MSCI, apoptosis, and a failure to complete meiosis.

essential for male meiosis, acting at the interface of transcription and meiotic recombination, and also in the process of meiotic sex chromosome inactivation (MSCI).

## Results

### Disruption of the mouse *Setx* gene

*Setx*<sup>-/-</sup> mice were produced using a Cre-LoxP system to delete exon 4 as outlined in Figure 1A. Crosses between *Setx* heterozygotes produced all 3 genotypes (Wild type, heterozygotes and homozygote knockouts) as expected (Figure 1B) and a Mendelian inheritance pattern was observed (Wild type 25%; heterozygote 54%; knockout 21%; n=87). Inactivation of the *Setx* gene was confirmed by RT-PCR and the absence of *Setx* mRNA in the knockout mouse as compared to the wild type (Figure 1C). Immunoprecipitation (IP) with anti-senataxin antibodies from testes extracts confirmed the presence of the protein in *Setx*<sup>+/+</sup> mice but senataxin was not immunoprecipitated from *Setx*<sup>-/-</sup> extracts (Figure 1D). While progressive cerebellar degeneration is characteristic of senataxin-defective AOA2 patients [1,2] we failed to detect either structural alterations, general cerebellar degeneration, or specific loss of Purkinje cells in *Setx*<sup>-/-</sup> mice (data not shown). Using a simple phenotypic scoring system that has been employed to evaluate mouse models of cerebellar ataxia [13], we failed to reveal any significant neurological/behavioural difference and ataxia between *Setx*<sup>+/+</sup> and *Setx*<sup>-/-</sup> animals (Figure S1).

### Senataxin is essential for germ cell development and fertility

Multiple attempts to breed *Setx*<sup>-/-</sup> mice with each other or with wild type mice were unsuccessful. Male mutant mice had normal development of secondary sexual characteristics, and were capable of the mechanics of mating, but were infertile. Histological examination of *Setx*<sup>-/-</sup> female ovaries at various ages (from 35 days to 8 months of age) revealed no overt phenotypic difference from their wild type littermates, with normal structure and presence of follicles at all stages and an ability to ovulate (Figure S2). However, the yield of viable embryos at 0.5 dpc was very low

suggesting that *Setx*<sup>-/-</sup> females are less fertile than their wild type littermates. The fertility of an individual female is a reflection of the number of eggs ovulated and their competence. To investigate the fertility of *Setx*<sup>-/-</sup> female mice, we carried out superovulation and time mating to harvest one-cell stage (0.5 dpc, fertilised egg) embryos in order to compare their viability. A greater than 3.5-fold reduction in the yield of 0.5 dpc for *Setx*<sup>-/-</sup> was observed compared to wildtype animals (10–20 0.5 dpc embryos for *Setx*<sup>-/-</sup> compared to 50–70 for wild types). In addition, only 23% of viable embryos were obtained at 0.5 dpc for *Setx*<sup>-/-</sup> and most of the viable ones did not survive in culture, indicating that *Setx*<sup>-/-</sup> females have a reduced fertility.

Since oligospermia and testicular abnormalities are a frequent finding of ARCA patients and the corresponding mouse models [14,15], we compared the development of testes and seminiferous tubules from *Setx*<sup>-/-</sup> with those from wild type mice. *Setx*<sup>-/-</sup> testes were smaller in size (50–60% reduction in size) than wild-type littermates (Figure 2A) and histological examination of testes from 35 day-old *Setx*<sup>-/-</sup> males revealed a severe disruption of the seminiferous tubules and the absence of germ cells compared to *Setx*<sup>+/+</sup> males (Figure 2B–2G). Morphologically, spermatocytes in *Setx*<sup>-/-</sup> mice appear to have halted development at pachytene stage of meiotic prophase (Figure 2E), suggesting that meiotic arrest in *Setx*<sup>-/-</sup> mice occurs during prophase I. Overall the seminiferous epithelium from an 8-month *Setx*<sup>+/+</sup> mouse testis appears normal but there is evidence of some disruption in places, with few round or elongated spermatids and debris in the lumen (Figure S3). Histological examination of the epididymis from *Setx*<sup>-/-</sup> mice revealed the total absence of mature sperm (Figure 2F–2G) thus confirming the infertility of *Setx*<sup>-/-</sup> males mice. Elevated levels of apoptosis were detected in some tubules of *Setx*<sup>-/-</sup> mice following TUNEL staining (Figure 2H–2I), suggesting that arrested cells are eliminated via this pathway.

To monitor the development of spermatocytes we counted the number of spermatocytes in all stages of meiotic prophase I (Figure 2J). Synaptogenesis appeared to be grossly normal in *Setx*<sup>-/-</sup> mice as determined by staining for synaptonemal complex protein 3 (SCP3) [16] but while the earlier stages of meiosis were represented we failed to detect diplotene stage spermatocytes for *Setx*<sup>-/-</sup>, indicating a block at the pachytene-diplotene transition (Figure 2J). Further analysis of the first meiotic division of prophase I revealed a significant reduction of pachytene spermatocytes from day 16 to day 22 in *Setx*<sup>-/-</sup> (Figure 2K) in line with the lack of diplotene spermatocytes in *Setx*<sup>-/-</sup>. Fragmentation of the synaptonemal complex (SC) at pachytene stage in *Setx*<sup>-/-</sup> was also observed. To investigate the cause of the meiotic defect in more detail, we also determined the expression of spermatogenesis stage-specific markers (Figure S4A) [17,18]. Expression levels of spermatogonial and early spermatocyte markers *Dmc1*, *Calnegin*, and *A-myb* were similar in both *Setx*<sup>-/-</sup> and *Setx*<sup>+/+</sup>. *Pgk2*, a marker expressed from the beginning (pre-leptotene) and throughout meiosis (leptotene, zygotene, pachytene, diplotene) up to the round spermatid stage showed only a small reduction in expression in *Setx*<sup>-/-</sup> as compared to *Setx*<sup>+/+</sup>. Markers for haploid mature germ cells *Pml1*, *Pml2* and *Tup1* showed markedly reduced expression in *Setx*<sup>-/-</sup> compared to *Setx*<sup>+/+</sup> (Figure S4B). Together, these data indicate that male germ cells proceed normally from spermatogonia up to the meiotic pachytene stage in *Setx*<sup>-/-</sup> but fail to enter into spermiogenesis and form mature spermatids. Thus, both gene expression of meiosis stage-specific markers and spermatocyte spread analysis confirmed the blockage of meiosis in *Setx*<sup>-/-</sup> male germ cells and indicate that senataxin plays an essential role in the development and maturation of germ cells.



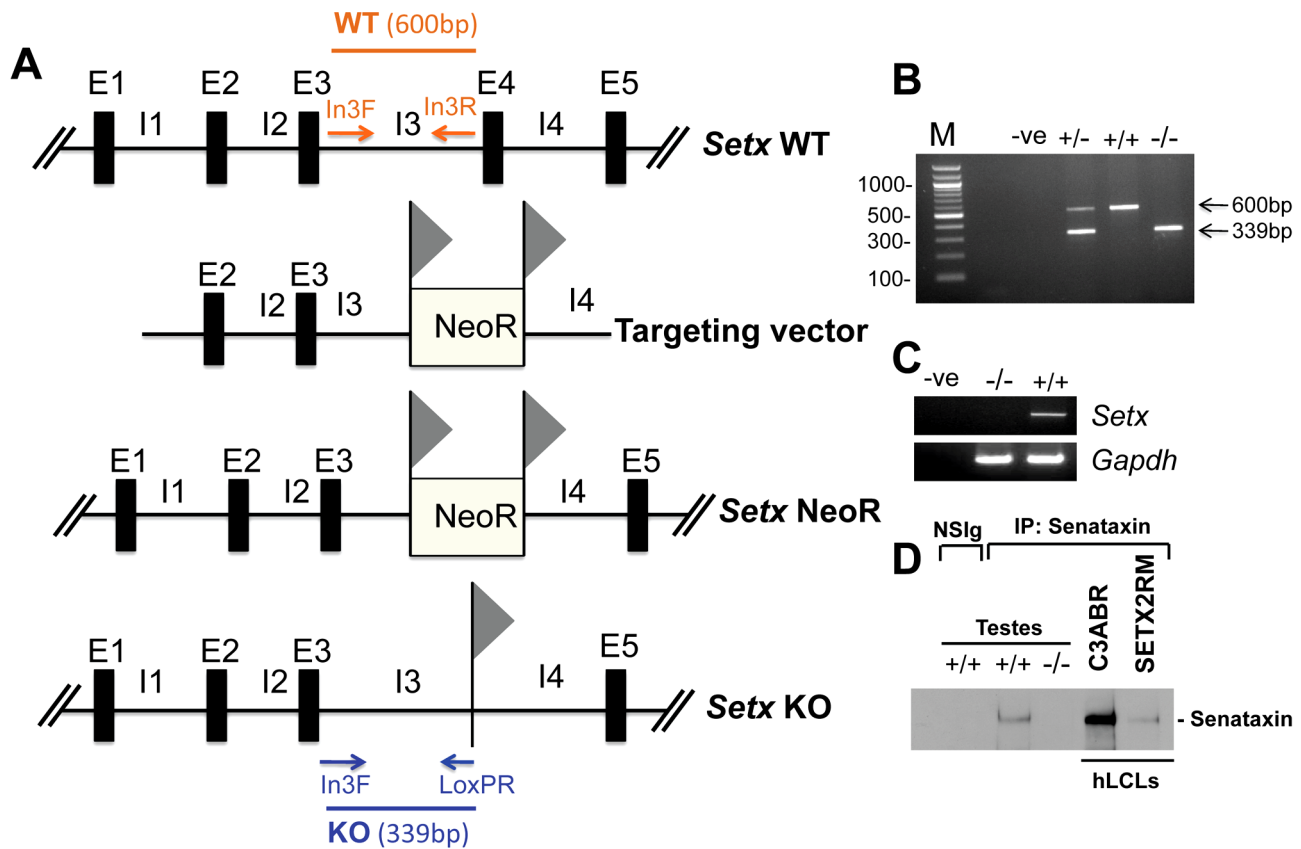


**Figure 1. Targeted disruption of the mouse *Setx* gene.** A. Diagram of the *Setx* wild type allele (WT), targeting vector, and mutant alleles (neo- and KO). Primers used for PCR genotyping (In3F, In3R, LoxPR) and the length of the PCR fragments obtained for WT (In3F and In3R yielding a 600 bp product) and KO (In3F and LoxPR yielding a 339 bp product) are indicated. E, exon; I, intron. NeoR represents the neomycin cassette, and triangles the *loxP* sites. B. Representative image of PCR genotyping using In3F, In3R and LoxPR primers. Wild type (+/+), heterozygotes (+/-) and knockout (-/-) alleles generate PCR products of 600 bp, 600 bp and 339 bp, respectively. A negative control for the PCR reaction (-ve) is also shown. M, 100 bp marker. C. RT-PCR of 35 day-old mice testes samples using primers specific to *Setx* cDNA indicates the absence of *Setx* expression in KO testes. GAPDH was used as an internal standard. D. Immunoprecipitation of senataxin using anti-human senataxin antibodies (Ab-1/Ab-3) from 35 day-old mouse testes extracts confirmed the absence of the protein in the *Setx*<sup>-/-</sup>. Immunoprecipitation of senataxin from human lymphoblastoid cell extracts from normal (C3ABR) and an AOA2 patient (SETX2RM) confirmed the similar size of senataxin in both species. A species-matched non-specific serum (NSIg) was used as a negative control in for the IP experiments. As expected, no senataxin protein was brought down from *Setx*<sup>+/+</sup> testes following the IP with the non-specific serum (NSIg). doi:10.1371/journal.pgen.1003435.g001

### DNA DSB persist and meiotic crossing-over is defective in *Setx*<sup>-/-</sup>

Meiotic recombination is initiated by the formation of DNA double strand breaks (DSB) catalysed by a type II topoisomerase-like protein Spo11 [19]. These breaks trigger phosphorylation of histone H2AX at ser139 ( $\gamma$ H2AX) on large domains of chromatin in the vicinity of the break [20]. As meiosis proceeds to the pachytene stage,  $\gamma$ H2AX disappears from synapsed chromosomes and is restricted to the largely unsynapsed sex chromosomes in the sex body [21,22]. Successful generation of DNA DSB and initiation of repair was observed in *Setx*<sup>-/-</sup> (Figure 3A). At pachytene stage, DSBs disappeared from the autosomes in *Setx*<sup>+/+</sup> mice and only the sex chromosomes stained positive for  $\gamma$ H2AX as expected [23,24]. On the other hand,  $\gamma$ H2AX foci remained on apparently synapsed autosomes at pachytene stage in *Setx*<sup>-/-</sup>, indicating the persistence of unrepaired DSBs. Both *Setx*<sup>-/-</sup> and *Setx*<sup>+/+</sup> displayed  $\gamma$ H2AX staining at the sex chromosomes at pachytene stage (Figure 3A). Staining of *Setx*<sup>-/-</sup> testes sections for  $\gamma$ H2AX confirmed the greater intensity of labelling (Figure S5).

The repair of meiotic DNA DSB occurs via homologous recombination (HR) and involves the participation of various

DNA repair factors including RPA, Dmc1 and Rad51 [16]. Both Rad51 and Dmc1 play key roles in the initial steps of HR by mediating strand invasion and homologous pairing. These proteins are normally observed as multiple foci decorating the chromosomes, first appearing at leptotene and sharply decreasing at pachytene [25]. This was the case for Rad51 in *Setx*<sup>+/+</sup> with few foci labelling pachytene chromosomes (Figure 3B). In contrast, multiple Rad51 foci persisted at pachytene stage in *Setx*<sup>-/-</sup> (Figure 3B, Figure S6A), pointing to a defect in Rad51 filament disassembly as a consequence of unrepaired DNA DSB and likely to interfere with HR progression in *Setx*<sup>-/-</sup>. Indeed, quantitation of the number of Rad51 foci at pachytene stage revealed a 6-fold increase of these foci in *Setx*<sup>-/-</sup> compared to *Setx*<sup>+/+</sup> (Figure 3C). This was not due to an over expression of *Rad51* since comparable mRNA levels are observed in both types of mice (Figure S7A). In contrast, immunoblotting of testes protein extracts revealed reduced levels of Rad51 protein in *Setx*<sup>-/-</sup> testes as compared to *Setx*<sup>+/+</sup> indicating that the absence of senataxin is affecting the translation or stability of Rad51 protein (Figure S7B). A similar abnormal pattern of retention at pachytene stage was found for Dmc1 with a 10-fold increase in *Setx*<sup>-/-</sup> compared to *Setx*<sup>+/+</sup>

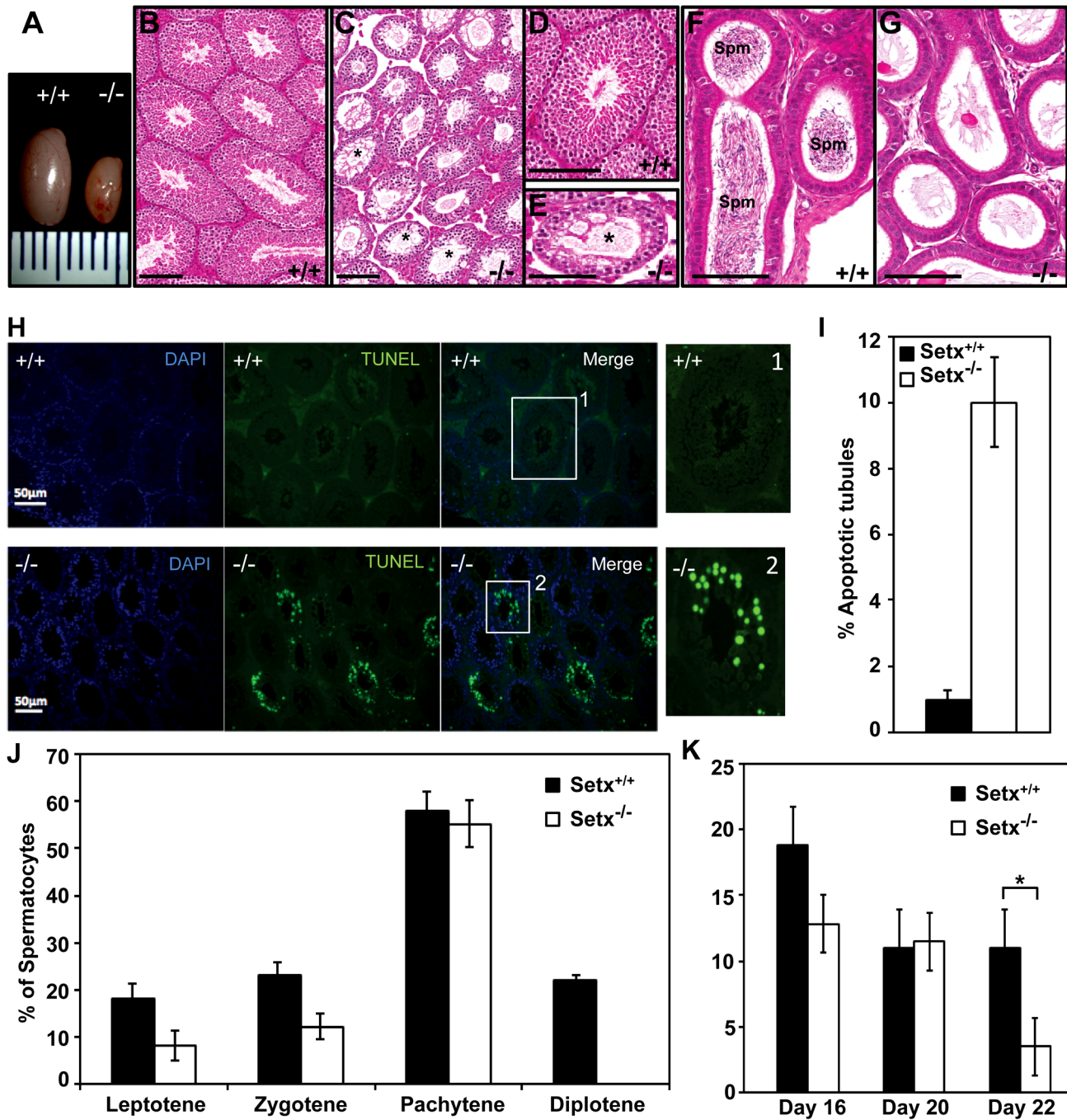


**Figure 2. Spermatogenesis is disrupted in *Setx*<sup>-/-</sup> mice.** A. Testes from 35-day-old *Setx*<sup>+/+</sup> and *Setx*<sup>-/-</sup> mice. B–C. Hematoxylin and eosin (H&E)-stained sections of testes from adults. Scale bar, 100  $\mu$ m. D–E. Enlarged images of regions in (B) and (C). Asterisks in (C) and (E) show vacuolated seminiferous tubules in which both spermatozoa and spermatids are absent. Scale bar, 100  $\mu$ m. F–G. H&E sections of epididymis from *Setx*<sup>+/+</sup> and *Setx*<sup>-/-</sup> adult mice. While there are numerous spermatozooids (Spm) in *Setx*<sup>+/+</sup> epididymis, no sperm is present in *Setx*<sup>-/-</sup>. Scale bar, 100  $\mu$ m. H. TUNEL-stained sections of testes from adult *Setx*<sup>+/+</sup> and *Setx*<sup>-/-</sup> mice. Many TUNEL-positive cells are observed in *Setx*<sup>-/-</sup> testes. Scale bar, 50  $\mu$ m. (1) and (2) are magnifications of a seminiferous tubule. I. Increased number of apoptotic tubules in *Setx*<sup>-/-</sup> (Tubules with  $\geq 8$  TUNEL-positive cells per tubule). Data is plotted as the mean  $\pm$  standard deviation,  $n = 1330$ . J. Block of meiosis at pachytene stage in *Setx*<sup>-/-</sup> mice. Meiotic stage distribution (leptotene, zygotene, pachytene, diplotene) in *Setx*<sup>+/+</sup> and *Setx*<sup>-/-</sup>. While a similar number of leptotene, zygotene and pachytene stage spermatocytes were found in both testes, no diplotene stage spermatocytes were found in *Setx*<sup>-/-</sup> testes indicating a block at pachytene in KO animals. Data plotted as the mean  $\pm$  standard deviation obtained from 3 mice, 2000 spermatocytes were counted in total for both *Setx*<sup>+/+</sup> and *Setx*<sup>-/-</sup>. K. Severe reduction in the number of pachytene spermatocytes in *Setx*<sup>-/-</sup> compared to *Setx*<sup>+/+</sup> during the first meiotic division. No significant change in the percentage of pachytene cells was observed in *Setx*<sup>+/+</sup> from day 16 to 22. However, a significant reduction in the percentage of pachytene spermatocytes was observed at day 22 in *Setx*<sup>-/-</sup> compared to *Setx*<sup>+/+</sup> (Student's *t*-test,  $p < 0.01$ ). \* indicates  $p < 0.01$ .

doi:10.1371/journal.pgen.1003435.g002

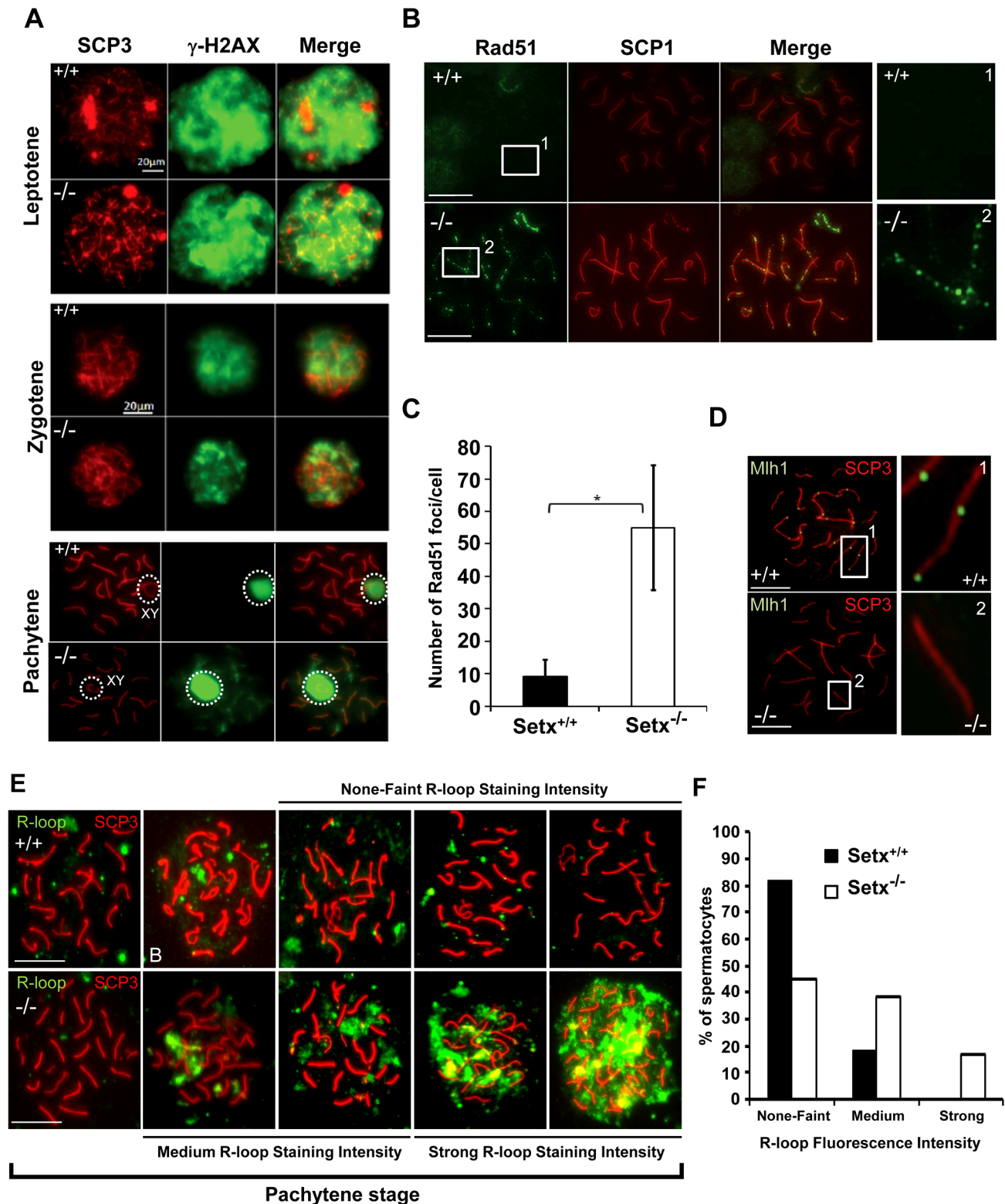


**Figure 3. Defective meiotic recombination and crossover formation in infertile *Setx*<sup>-/-</sup> males.** A. Initiation and repair of programmed DNA DSB as shown by  $\gamma$ H2AX staining of spermatocytes spreads of *Setx*<sup>+/+</sup> and *Setx*<sup>-/-</sup> adult mice. At pachytene,  $\gamma$ H2AX staining is restricted to the XY chromosomes (circle) in *Setx*<sup>+/+</sup> spermatocytes, whereas some  $\gamma$ H2AX foci remained on asynapsed autosomes indicating persistence of unrepaired DSB in *Setx*<sup>-/-</sup>. Normal  $\gamma$ H2AX staining of the XY chromosomes (circle) was observed in both *Setx*<sup>+/+</sup> and *Setx*<sup>-/-</sup> pachytene stage spermatocytes. Scale bar, 20  $\mu$ m. XY, sex chromosomes. B. Persistence of Rad51 foci at pachytene stage in *Setx*<sup>-/-</sup> spermatocytes indicating the presence of unrepaired DSBs (compare 1 and 2). Scale bar, 20  $\mu$ m. C. Quantitation of Rad51 foci revealed a 6-fold increase in the number of Rad51 foci at pachytene stage in *Setx*<sup>-/-</sup> as compared to *Setx*<sup>+/+</sup> (Student's t-test, n=50), \* indicates p<0.05. D. Formation of chiasmata at pachytene stage in *Setx*<sup>+/+</sup> spermatocytes as marked by Mlh1 staining. No Mlh1 foci were detected in *Setx*<sup>-/-</sup> pachytene cells indicating that crossovers do not occur in

*Setx*<sup>-/-</sup>. 1 and 2 represent magnification of autosomes. Scale bar, 20  $\mu$ m. SCP3 or SCP1 were used to identify the meiotic stages. E. Defect in senataxin leads to R-loop structures accumulation in germ cells. Staining with S9.6 antibody (R-loops) on adult spermatocytes revealed an increased formation of R-loops in *Setx*<sup>-/-</sup> germ cells. Scale bar, 20  $\mu$ m. F. Number of pachytene spermatocytes showing none-faint, medium, and strong R-loop staining intensities for *Setx*<sup>+/+</sup> and *Setx*<sup>-/-</sup>. doi:10.1371/journal.pgen.1003435.g003

(Figure S6B–S6C). Similar to *Rad51*, comparable levels of *Dmc1* mRNA levels were observed in both mice (Figure S7C). However, we were not able to determine the levels of Dmc1 protein in testes.

To assess whether meiotic recombination is completed in *Setx*<sup>-/-</sup>, we examined the distribution of the mismatch repair protein Mlh1, which normally forms foci and marks the location of chiasmata [26,27]. We observed an average of 22 Mlh1 foci per pachytene-stage spermatocyte in *Setx*<sup>+/+</sup> (Figure 3D), where up to 78% of spermatocytes SC contain one Mlh1 focus, 19.2% contain 2 foci, 0.5% contain 3 foci and 2.5% had no foci at all, in agreement with previous report [28]. In contrast, no foci were observed in *Setx*<sup>-/-</sup> pachytene-stage spermatocytes (Figure 3D), indicating the absence of crossovers. The lack of Mlh1 foci in *Setx*<sup>-/-</sup> spermatocytes was not due to a defective expression of *Mlh1* gene, as similar levels of the *Mlh1* mRNAs were detected in both *Setx*<sup>+/+</sup> and *Setx*<sup>-/-</sup> testes (Figure S7D). In contrast to *Rad51*, similar levels of Mlh1 protein in both *Setx*<sup>+/+</sup> and *Setx*<sup>-/-</sup> were shown by Mlh1 immunoblotting of testes protein extracts (Figure S7E). These results confirmed an essential role for senataxin in meiosis.

### Lack of senataxin leads to germ cell accumulation of R-loops and apoptosis

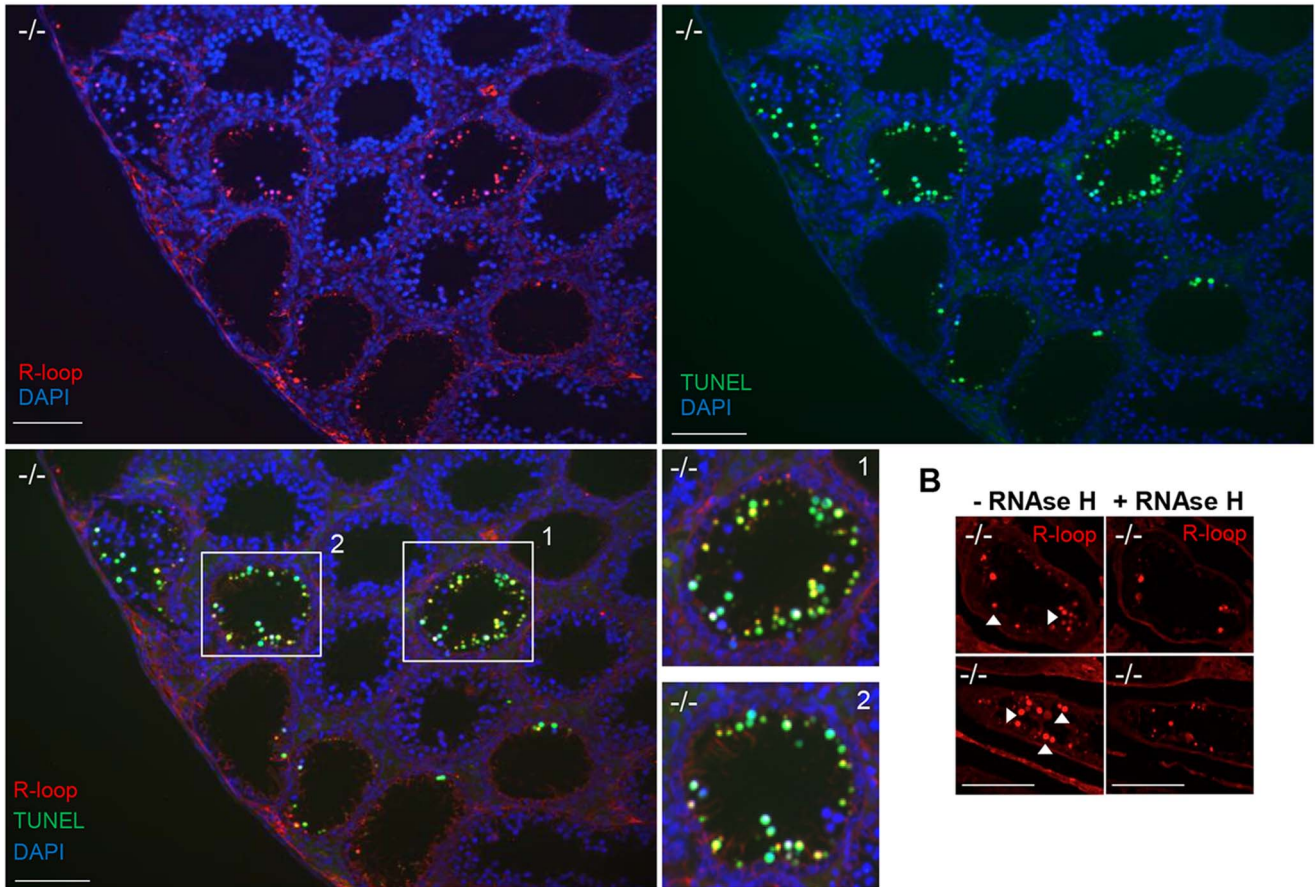
Sen1p, the yeast homolog of senataxin was recently found to restrict the occurrence of RNA:DNA hybrids, also known as R-loop structures, that form naturally during transcription, and can trigger genomic instability if left unresolved [10]. Furthermore the same group showed that senataxin resolves R-loop structures to facilitate transcriptional termination in mammalian cells [7]. We reasoned that the defective meiosis in *Setx*<sup>-/-</sup> testes and the consequent apoptosis at pachytene stage might be due to R-loop accumulation as a consequence of transcriptional abnormalities in the absence of senataxin. As shown in Figure 3E, a collection of pachytene-stage spermatocytes from *Setx*<sup>-/-</sup> mice showed a marked accumulation of R-loops compared to *Setx*<sup>+/+</sup>. There was some variation in the R-loop-specific (S9.6) antibody [29,30] staining intensity between individual pachytene-stage spermatocytes of *Setx*<sup>-/-</sup>, indicating heterogeneity in R-loop accumulation (Figure 3E–3F). The fluorescence intensity of individual pachytene-stage spermatocytes detected by the R-loop-specific antibody was classified into three categories: faint-none, medium and strong as indicated in Figure 3E. No pachytene spermatocytes with strong R-loop staining intensity were observed in *Setx*<sup>+/+</sup> (Figure 3E). This was confirmed with *Setx*<sup>-/-</sup> testes sections which again showed very intense R-loop staining which was variable in different spermatocytes (Figure 4A). Pre-treatment of testes sections with RNase H prior to immunostaining reduced dramatically the staining intensity in *Setx*<sup>-/-</sup> confirming that these were indeed R-loops (Figure 4B). Co-staining with TUNEL revealed that most cells with accumulated R-loops also undergo apoptosis (Figure 4A, 4E). Although occasionally present in *Setx*<sup>+/+</sup>, R-loop accumulation was dramatically increased in *Setx*<sup>-/-</sup> seminiferous tubules as shown by an increase in the number of R-loop positive cells per tubules (Figure 4C–4D). Co-staining with TUNEL revealed that most cells undergoing apoptosis in *Setx*<sup>-/-</sup> had accumulation of R-loops (Figure 4E). These data suggest that failure to resolve R-loops is responsible for the accumulation of DNA DSB and disruption of meiosis in *Setx*<sup>-/-</sup>.

### Senataxin localises with DNA damage response proteins to the sex chromosomes

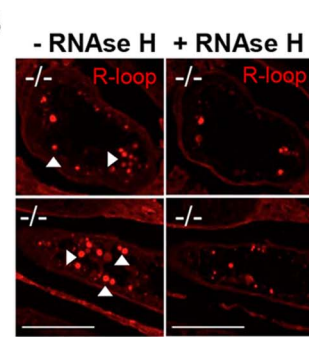
To investigate in more detail the role of senataxin in meiosis, we studied its localization by performing immunostaining on *Setx*<sup>+/-</sup> spermatocyte spreads. As shown in Figure 5A–5B, senataxin localised mostly to the sex chromosomes at pachytene stage. Some background staining was also observed over the autosomes (Figure 5A) in line with its effect on meiotic recombination and R-loop resolution. As expected there was no senataxin labelling in *Setx*<sup>-/-</sup> spreads (Figure 5A). Partial co-localisation between senataxin and Brca1 was observed albeit there was a more diffuse distribution of senataxin in the XY body (Figure 5C). Brca1 labels the axis of unsynapsed sex chromosomes at pachytene stage to where it is recruited to initiate (MSCI) meiotic sex chromosome inactivation [22]. While Brca1 localised to the axis of the sex chromosomes in *Setx*<sup>-/-</sup> this was incomplete since it was excluded from part of the chromosome (Figure 5D). It appears that this corresponds to the Y chromosome based on the structural morphology [31]. We also determined whether there was a dependence on Brca1 for localisation of senataxin to the sex chromosomes using a *Brca1* <sup>$\Delta 11/\Delta 11$</sup>  *p53*<sup>+/-</sup> mutant mouse. The results in Figure 5E show that while senataxin localises to XY chromosomes in wild-type mice it fails to do so in Brca1 mutant mice. The Brca1 <sup>$\Delta 11/\Delta 11$</sup>  mutant protein still localises to the sex chromosome but is unable to recruit senataxin (Figure 5F). We next determined whether senataxin and Brca1 interacted using Brca1 and senataxin co-immunoprecipitations from testes extracts. We failed to co-immunoprecipitate endogenous senataxin and Brca1 from mouse testes extracts (data not shown). In addition, Proximity Ligation Assay (PLA) which allows for the *in situ* detection of endogenous protein-protein interactions failed to reveal a direct interaction between these two proteins (Figure 5G). In contrast, we confirmed the previously reported endogenous Brca1 and ataxia-telangiectasia and Rad3 related (ATR) interaction [22] using PLA *in situ* over the XY body (Figure 5H). A specific PLA signal for the Brca1/ATR interaction is observed on/around the axis of the unsynapsed XY chromosomes in *Setx*<sup>+/+</sup> pachytene spermatocytes in agreement with the Brca1 and ATR distribution patterns over the sex chromosomes.

At pachytene stage, ATR kinase, another marker of XY chromosomes, is recruited to the unsynapsed axis of the XY chromosomes through an interaction with Brca1 and then diffuses to XY chromatin where it phosphorylates serine 139 of histone H2AX to trigger chromosomal condensation and transcriptional silencing [22,32]. The results in Figure 6A show a diffuse staining pattern for ATR in *Setx*<sup>+/+</sup> on the XY body. On the other hand, ATR decorates only part of the XY chromosome in *Setx*<sup>-/-</sup> and does not diffuse out into chromatin (Figure 6A and Figure S8). The mediator of DNA damage 1 (MDC1) protein also plays a key role at this stage in MSCI [33]. Recognition of unsynapsed axis of the XY chromosomes by Brca1, ATR and TopBP1 is independent of MDC1 but the chromosome wide spreading of these proteins is dependent on MDC1. We observed that MDC1 labelled the X chromosome but as with Brca1 and ATR failed to decorate the complete XY chromosome (Figure 6B). However,  $\gamma$ H2AX labelling was localised to XY chromatin (Figure 6C). As spermatocytes progress from early to mid pachytene the X chromosome appears elongated and sickle shaped prior to loop

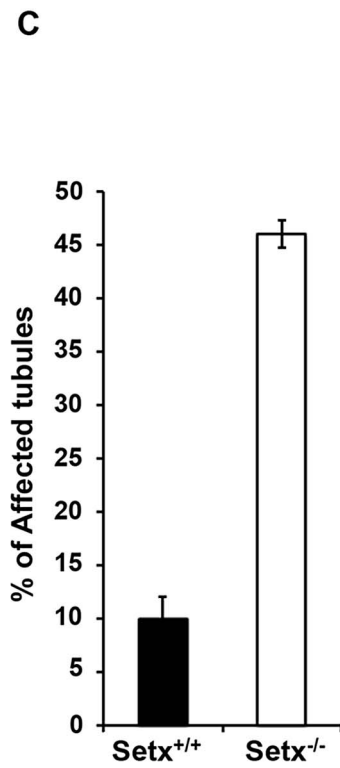
**A**



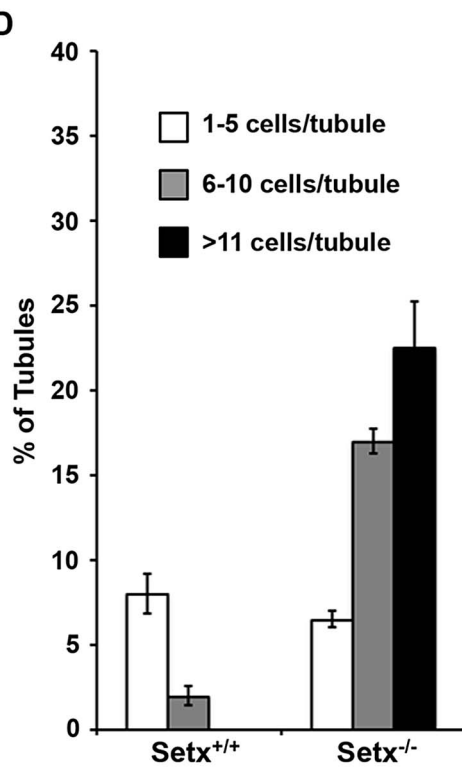
**B**



**C**



**D**



**E**

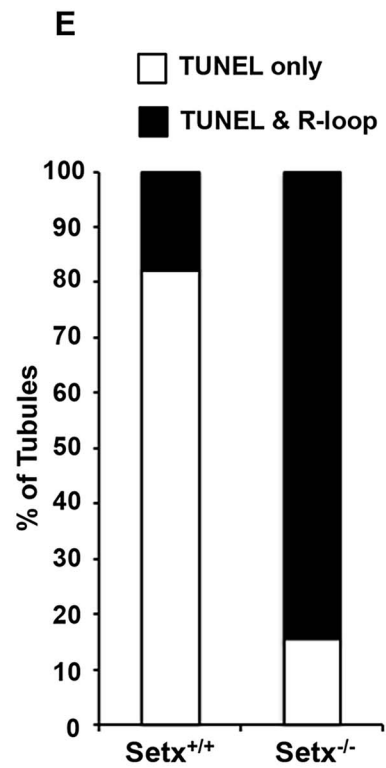


**Figure 4. Accumulation of R-loops correlates with apoptosis.** A. R-loop and TUNEL co-staining of histological cross-sections of adult *Setx*<sup>-/-</sup> mice revealed apoptosis in germ cells containing R-loops. Hoechst 33342 was used to stain for DNA. Scale bar, 50  $\mu$ m. B. Pre-treatment of consecutive testes sections from the same animal with RNase H dramatically reduced R-loop signal intensity in *Setx*<sup>-/-</sup>. Similar results were obtained for consecutive sections from different *Setx*<sup>-/-</sup> animals (data not shown). C. Quantitation of R-loop positive tubules in *Setx*<sup>+/+</sup> and *Setx*<sup>-/-</sup>. The Y-axis represents the % of tubules containing at least one R-loop positive cell within the tubule. D. Higher number of R-loops positive germ cells per tubule (1–5 R-loop-positive cells/tubule, 6–10 R-loop-positive cells/tubule, and more than 11 R-loop-positive cells/tubules) in *Setx*<sup>-/-</sup> compared *Setx*<sup>+/+</sup> confirming the role of senataxin in resolving R-loops *in vivo*. E. Correlation of apoptosis (TUNEL) with R-loop accumulation in *Setx*<sup>-/-</sup> seminiferous tubules uncovers an essential role for senataxin to resolve R-loops and prevent germ cell apoptosis. Graphic representation of the number of tubules that contain TUNEL-only positive germ cells (white) and TUNEL and R-loop co-stained germ cells (black). doi:10.1371/journal.pgen.1003435.g004

“curled bundle” formation in late pachytene [31]. These looped XY structures were observed in *Setx*<sup>+/+</sup> but sickle shaped chromosomes appeared mostly in *Setx*<sup>-/-</sup> indicative of arrest in mid pachytene (Figure 6D). Distinguishable “curled bundle” sex chromosomes in *Setx*<sup>-/-</sup> pachytene spermatocytes were seen only in half the percentage of wildtype (Figure 6E). Thus, the absence of senataxin also affects XY body formation/structure and reveals a defect in the recognition and distribution of DNA damage response proteins on the sex chromosomes and thus results in MSCI failure.

### Defective meiotic sex chromosome inactivation (MSCI) in *Setx*<sup>-/-</sup> spermatocytes

In mammalian spermatogenesis, the sex chromosomes are transcriptionally-silenced during the pachytene stage of meiotic prophase I, forming a condensed chromatin domain termed the sex body [31,34]. In the majority of *Brc1* mutant pachytene cells sex bodies do not form and transcription is maintained, demonstrating a failure in MSCI [22]. To determine whether the absence of senataxin had a similar effect on MSCI, we analysed the expression of sex-linked genes in *Setx*<sup>-/-</sup> mice using RT-PCR as previously described [35,36]. As shown in Figure 7A, an increase in the expression of the X-linked *Usp26* (2.44 fold), *Fthl17* (1.4 fold), *Tktl1* (1.36 fold) and *Ube1x* (1.65 fold) genes was observed for *Setx*<sup>-/-</sup> mice compared to *Setx*<sup>+/+</sup> mice. This was also true for several Y-linked genes that include *Ube1y* (2 fold) and *Rbmy* (2.14 fold) indicating that MSCI is defective in *Setx*<sup>-/-</sup>. Normal expression for autosomal genes *Actinb*, *Dazl*, and *Gapdh* was also observed, confirming the specific nature of MSCI (Figure 7A). In order to confirm that MSCI was induced, staining for the activated form (Phospho-S2) of RNA polymerase II (Pol II), which is engaged in transcriptional elongation, revealed a lack of staining at the XY body in *Setx*<sup>+/+</sup>, confirming transcriptional silencing (Figure 7B). In contrast, Pol II staining was visible over XY chromosomes in *Setx*<sup>-/-</sup> (Figure 7B). Ubiquitination of histone H2A has been shown to be associated with transcriptional silencing of large unravelled chromatin regions of the XY chromosomes [37]. Because of the continued presence of RNA Pol II on the sex chromosomes in *Setx*<sup>-/-</sup> we predicted that ubiquitination of H2A would be defective in *Setx*<sup>-/-</sup>. The results in Figure 7C revealed marked localisation of ubi-H2A to the XY body in *Setx*<sup>+/+</sup> spermatocytes. On the other hand the extent of ubi-H2A on the XY body of *Setx*<sup>-/-</sup> was much reduced but ubi-H2A was also distributed across the autosomes. These data suggest that senataxin plays a key role in the initial *Brc1*-dependent stage in MSCI.

### Discussion

This study provides compelling evidence for an essential role for senataxin in spermatogenesis. We showed that senataxin removes R-loops to maintain the integrity of the genome during meiotic recombination and it is also required for effective MSCI. In *Setx*<sup>-/-</sup> mutant mice, spermatogenesis was arrested in pachytene stage

where R-loop accumulation in cells coincided with apoptosis, resulting in male infertility. Testicular atrophy, depletion of germ cells and sterility are common features of animal models with defects in meiotic proteins such as Spo11 [38], strand exchange protein Dmcl [39], *Brc1* [40] and mismatch repair proteins Msh4, Msh5, Mlh3 and Mhl1 [41–43]. The phenotype in *Setx*<sup>-/-</sup> male mice overlaps with but is distinct from that described for these mutant mice. Unlike that for *Setx*<sup>+/+</sup>, where breaks were confined to the XY body in pachytene, breaks were still present in the autosomes as well as the XY body in *Setx*<sup>-/-</sup> mice indicating a defect in repair of DNA DSB and consequently a defect in meiotic recombination. This was confirmed by persistence of Rad51 and Dmcl on autosomes and a failure to detect chiasmata at late meiotic nodules in *Setx*<sup>-/-</sup> pachytene cells. Failure to remove Rad51, as seen in *Setx*<sup>-/-</sup>, prevents the completion of meiotic DSB repair. The meiotic phenotype of *Setx*<sup>-/-</sup> mice resembles that seen in *Brc1*<sup>A11/A11</sup>*p53*<sup>+/-</sup> mice [44]. In that model, chromosome synapsis occurred normally and cells progressed through to pachytene, however no chiasmata were observed [44]. Furthermore, DSBs were not repaired in the correct temporal framework, as demonstrated by persistent  $\gamma$ H2AX foci. While the failure to complete meiosis due to persistence of unrepaired DSB and lack of cross-overs is common to the *Setx*<sup>-/-</sup> and *Brc1* mutants, one obvious difference is diminished numbers of Rad51 foci and normal localisation of Dmcl in the *Brc1* mutant [44]. This could be accounted for by the interaction of Rad51 with *Brc1* which would be disrupted in the *Brc1* mutant.

Sen1, the yeast homolog of senataxin, restricts co-transcriptionally formed R-loops which accumulate in *sen1-1* mutant in a transcription-dependent manner [10]. Furthermore, Mischo *et al* [10] observed a genetic interaction between *sen1* and various factors involved in HR such as *rad50*, *mre11*, *sgs1* and *rad52* and concluded that *sen1* plays a pivotal role in preventing genomic instability by transcription-mediated recombination [10]. More recently, Skourti-Stathaki *et al* [7] provided evidence that senataxin, like *sen1*, resolves R-loop structures formed at transcriptional pause sites to ensure effective transcription termination. *In vivo* accumulation of R-loops was evident in *Setx*<sup>-/-</sup> seminiferous tubules and in pachytene stage spermatocytes, supporting a role for senataxin in resolving such structures. Furthermore, partial co-localisation between R-loops and TUNEL staining in *Setx*<sup>-/-</sup> germ cells indicates that this accumulation may contribute to cell death (Figure 4A–4E). Transcriptional R-loop formation in eukaryotes is highly correlated with DNA recombination and/or impairment of genome stability, indicating an inherent impact of R-looping on the integrity of the genome [9,45]. R-loop formation is capable of inducing hyper-recombination and/or hypermutation phenotypes in eukaryotes [8,4]. Recently, THO mutants from *S. cerevisiae* and *C. elegans* showed defective meiosis and an impairment of premeiotic replication as well as DNA-damage accumulation [46]. Gan *et al.* [47] have shown that R-loop formation impairs DNA replication which is responsible for the deleterious effects of those structures on genome stability. More recently, Alzu *et al.* [12] provided evidence

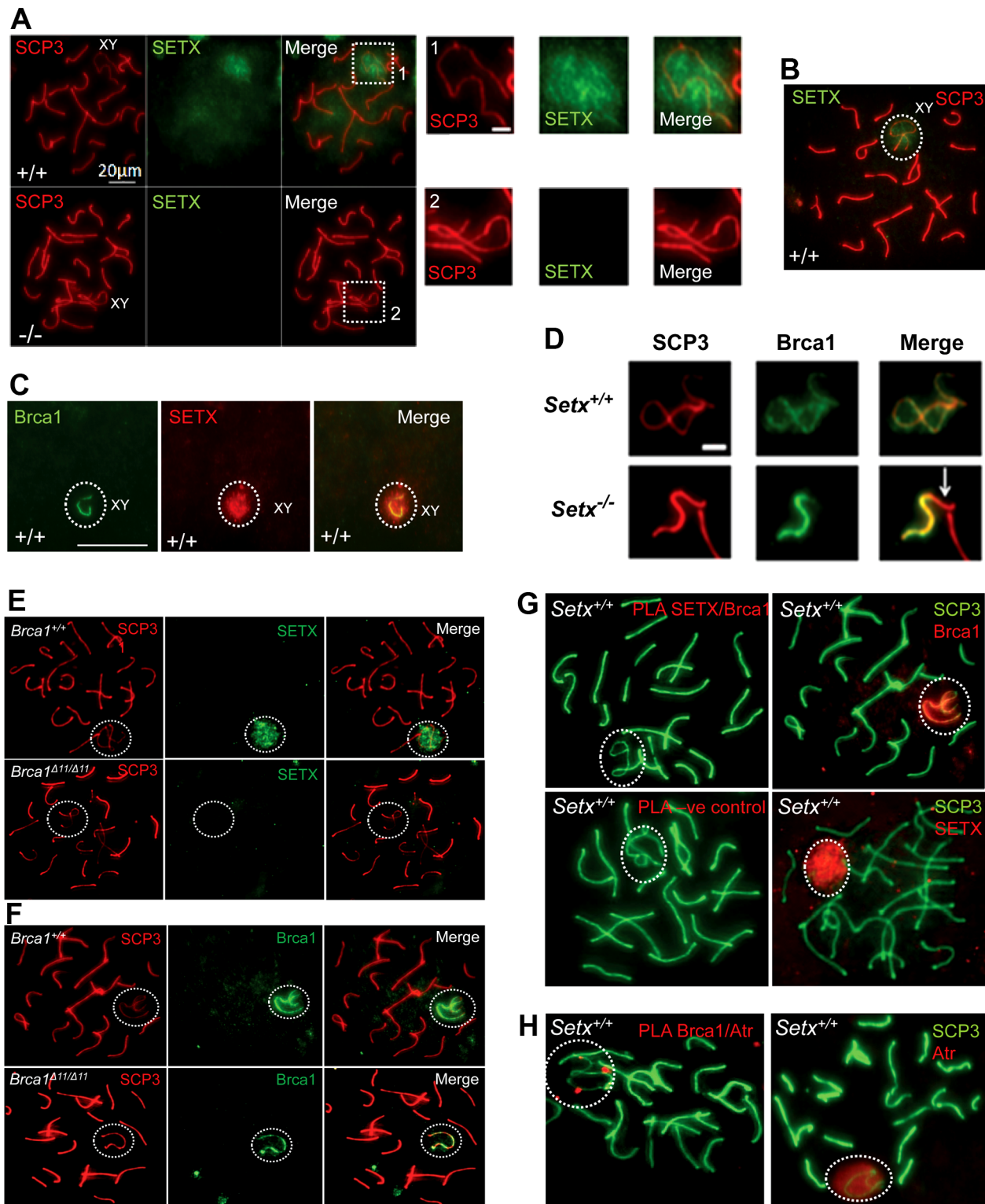


**Figure 5. Senataxin localises to the sex chromosomes during meiosis.** A. Staining of spermatocyte spreads with an anti-senataxin antibody (Ab-1) revealed that senataxin localised in majority to the XY chromosomes (1) at pachytene stage in *Setx*<sup>+/+</sup>. Some background staining was also observed on the autosomes. No senataxin was detected in *Setx*<sup>-/-</sup> spermatocytes confirming the specificity of our senataxin antibody. (1) and (2) are magnification of the XY chromosomes. B. Double staining of *Setx*<sup>+/+</sup> pachytene spermatocytes with senataxin (Ab-1) and SCP3 revealed a diffuse localisation of senataxin to the XY body. Scale bar, 20  $\mu$ m. C. Partial co-localisation of senataxin with the XY chromosome marker Brca1. While Brca1 stains exclusively the unsynapsed axis of the XY chromosomes, senataxin staining is more diffuse. D. Brca1 staining of the XY chromosomes in *Setx*<sup>+/+</sup> and *Setx*<sup>-/-</sup> pachytene spermatocytes (day 20). In *Setx*<sup>+/+</sup>, the unsynapsed axis of the XY chromosomes is entirely stained with Brca1 while an incomplete covering (white arrow) of the XY chromosomes is observed in *Setx*<sup>-/-</sup>. Scale bar, 5  $\mu$ m. E. Lack of senataxin recruitment to XY chromosomes in *Brca1* <sup>$\Delta$ 11/ $\Delta$ 11</sup> *p53*<sup>+/-</sup> as compared to *Brca1*<sup>+/+</sup> *p53*<sup>+/-</sup>. F. Brca1 localised to only part of the unsynapsed axis of the XY chromosomes in *Brca1* <sup>$\Delta$ 11/ $\Delta$ 11</sup> *p53*<sup>+/-</sup> spermatocytes. G. PLA analysis of SETX/Brca1 and SETX/SCP3 interactions. H. PLA analysis of Brca1/Atr interactions.

*Brca1*<sup>A11/A11</sup> *p53*<sup>+/-</sup> while Brca1 coated the entire unsynapsed axis of the XY chromosomes in *Brca1*<sup>+/+</sup> *p53*<sup>+/-</sup>. G. Lack of evidence for an *in situ* direct endogenous interaction between senataxin and Brca1 on the XY chromosomes as revealed by negative Proximity Ligation Assay (PLA) results on pachytene spermatocyte spreads. Immunostaining of *Setx*<sup>+/+</sup> pachytene spermatocytes with Brca1 and Setx individually with SCP3 is also shown. H. Endogenous interaction between ATR and Brca1 was confirmed by PLA. Here, we reveal for the first time a direct endogenous interaction between Brca1 and ATR *in situ* over the XY chromosomes.  
doi:10.1371/journal.pgen.1003435.g005

that when transcription and replication collide Sen1 displaces R-loops to counter recombinogenic events. Thus, R-loop formation may be an intrinsic threat to genome integrity throughout evolution and species have evolved a variety of co-transcriptional processes to prevent the formation of these structures [46]. Senataxin represents a novel factor that minimizes the impact of R-loops that arise as part of normal transcription processes [7,11] and/or DNA-damage-induced transcription stalling [48]. In the case of *Setx*<sup>-/-</sup> spermatocytes, accumulation of R-loops occurs throughout leptotene and zygotene at a time when DNA DSB are being repaired by crossing over and other mechanisms. Consequently it is likely that R-loops collide with Holiday junctions and interfere with resolution of DNA DSB and thus meiotic recombination. Furthermore, the accumulation of R-loops throughout the chromatin would also affect the repair of DNA DSB that are repaired through non crossover mechanisms.

Senataxin specifically localises to the XY body in pachytene stage partially co-localising with Brca1, MDC1 and ATR suggesting that it might have a role in MSC1. While Brca1 lines the unsynapsed axes of the XY chromosomes, senataxin is associated with these chromosomes but also has a more diffused distribution on chromatin. Prior to MSC1 initiation, Brca1 is targeted to the unsynapsed axial elements of the X and Y chromosomes where it remains [22]. It subsequently recruits ATR to the axial elements where it phosphorylates H2AX. In agreement with these findings we provided additional evidence for a direct endogenous interaction between Brca1 and ATR *in situ* over the XY body (Figure 5H). It seems likely that recruitment of senataxin is Brca1-dependent since senataxin did not localize to the XY chromosome in *Brca1*<sup>A11/A11</sup> *p53*<sup>+/-</sup> mutant mice even though the smaller protein mutant Brca1 (lacking exon 11) lined the axes of these chromosomes. We did not detect a direct endogenous interaction between senataxin and Brca1, suggesting

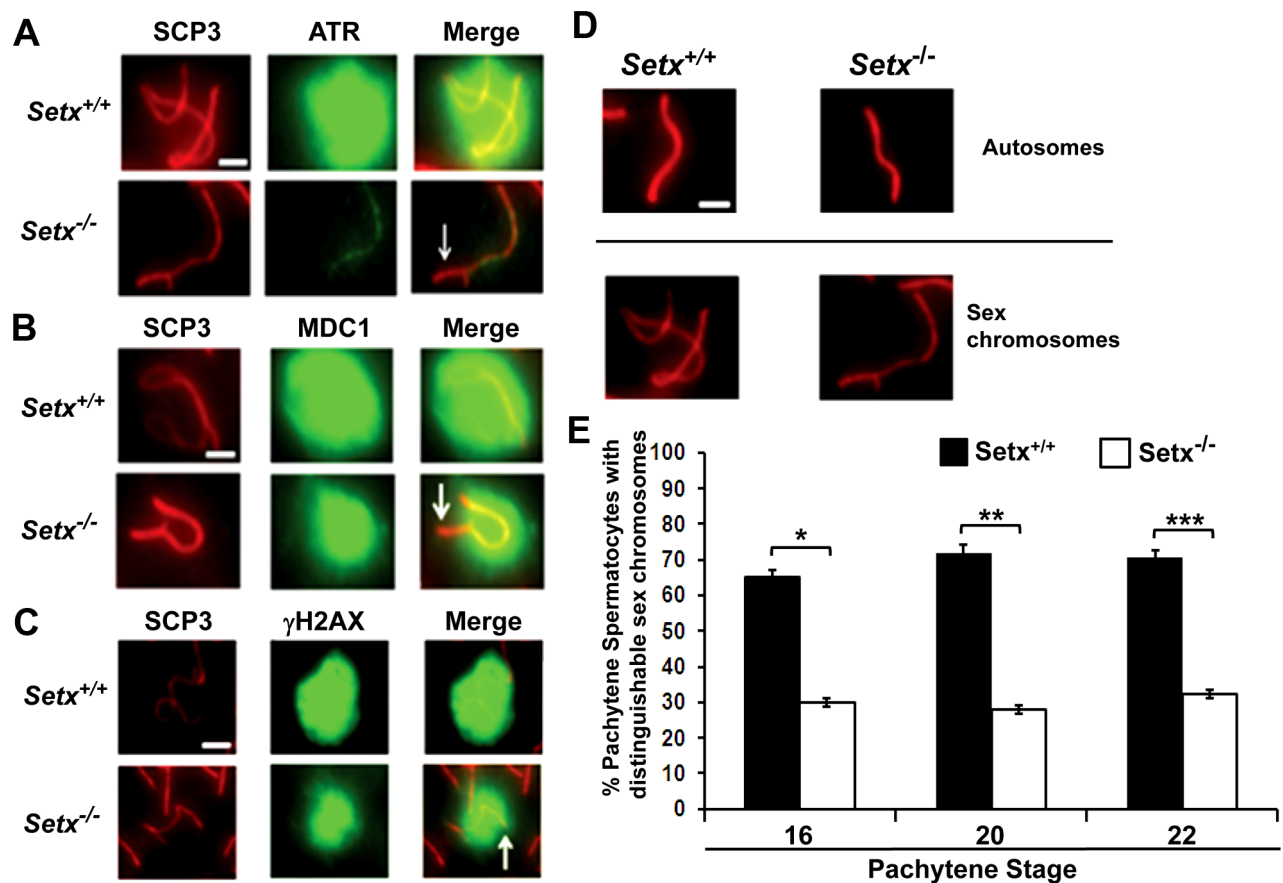


**Figure 6. Defective localisation and diffusion of DNA damage response proteins in *Setx*<sup>-/-</sup>.** A. Absence of ATR diffusion over the XY chromatin domain in *Setx*<sup>-/-</sup> compared to *Setx*<sup>+/+</sup>. Scale bar, 5  $\mu$ m. B. Incomplete diffusion of MDC1 over the XY chromatin domain in *Setx*<sup>-/-</sup>, as indicated by the white arrow. Scale bar, 5  $\mu$ m. C. Reduced intensity and diffusion of  $\gamma$ H2AX staining on the XY chromosomes in *Setx*<sup>-/-</sup> compared to *Setx*<sup>+/+</sup>. D. Altered XY chromosomes structure and formation in *Setx*<sup>-/-</sup> as shown by SCP3 staining. Scale bar 5  $\mu$ m. E. Percentage of *Setx*<sup>+/+</sup> and *Setx*<sup>-/-</sup> pachytene spermatocytes at days 16, 20 and 22 with clearly distinguishable XY chromosomes. At every time point, a significant higher percentage of distinguishable XY chromosomes was observed in *Setx*<sup>+/+</sup> ( $p < 0.01$  according to Student's t-test,  $n = 3600$ ). \*\*\*,\*\*\* indicates  $p < 0.01$ .  
doi:10.1371/journal.pgen.1003435.g006



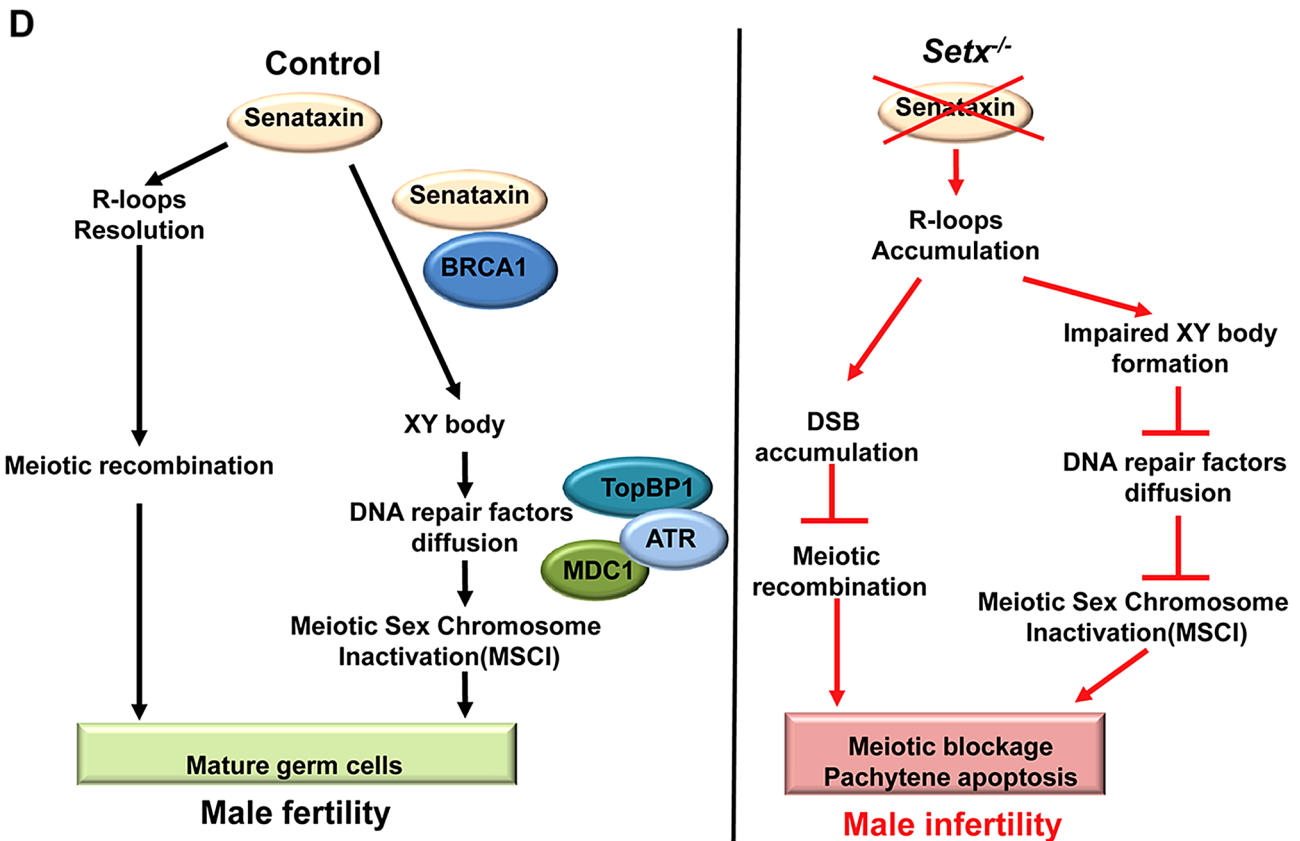
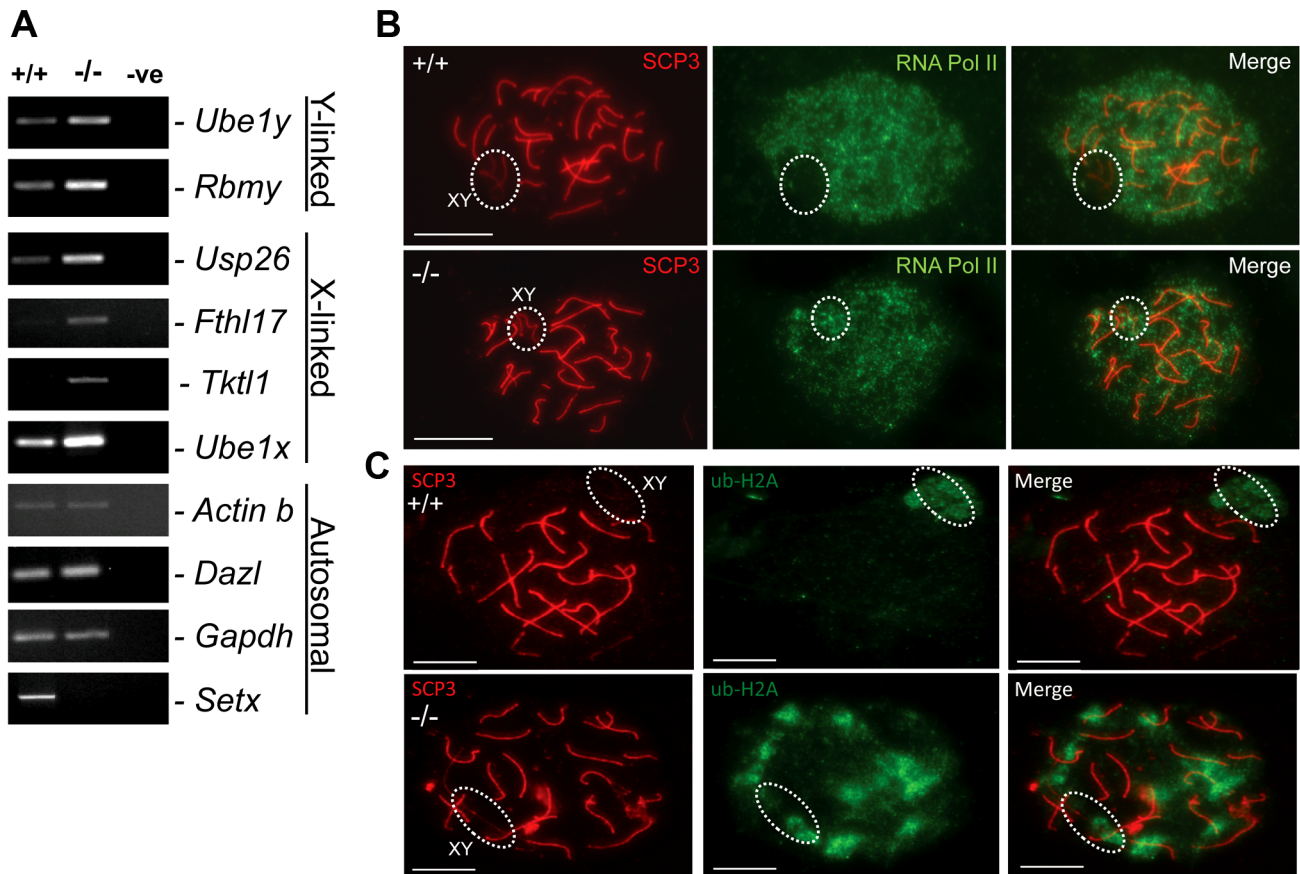


**Figure 7. Aberrant meiotic sex chromosome inactivation in *Setx*<sup>-/-</sup> mice.** A. Relative levels of transcript of XY-linked germ cell specific genes from *Setx*<sup>+/+</sup> and *Setx*<sup>-/-</sup> testes was determined by RT-PCR to assess MSCI as previously described [35]. Levels of *Actb* and *Gapdh* mRNA were used as positive controls for ubiquitous gene expression. Levels of *Dazl* transcripts were determined as a positive control for previously documented autosomal meiotic expression [35]. Levels of *Ube1x* and *Ube1y* transcripts were included as positive controls for previously documented X- and Y-linked gene expression during spermatogenesis, respectively [35]. X-linked *Usp26*, *Fthl17* and *Tktl1*, and Y-linked *Rbmy* genes have previously shown evidence of MSCI [35]. RT-PCR control without template is also shown. B. Immunostaining for the transcriptionally-active form of RNA Pol II (phospho-S2) revealed active transcription of the XY chromosomes in *Setx*<sup>-/-</sup> spermatocytes (circle). In contrast, no signal for active Pol II was visible over the XY chromosomes in *Setx*<sup>+/+</sup> spermatocytes (circle) confirming the silencing of the XY chromosomes. Scale bar, 20 μm. C. Immunostaining for ubiquitinated histone H2A (ubi-H2A) in *Setx*<sup>+/+</sup> and *Setx*<sup>-/-</sup> spermatocytes reveals a specific staining on the XY chromosomes (circle) in *Setx*<sup>+/+</sup>. In contrast, while ubi-H2A staining was still present on the XY chromosomes in *Setx*<sup>-/-</sup> (circle), it was also distributed on the autosomes. Scale bar, 20 μm. D. Model depicting the consequences of senataxin disruption on spermatogenesis. In wild type spermatocytes, senataxin resolves R-loops structures that may form during pachytene following the resumption of transcriptional activity, thus allowing effective meiotic recombination to proceed and spermatogenesis to be completed. Senataxin also localizes to the XY chromosomes in a Brca1-dependant manner thus enabling the localization of DNA damage response proteins MDC1, ATR and TopBP1 to the entire XY chromatin domain. This ensures that MSCI takes place and germ cells develop and mature properly. On the other hand, in *Setx*<sup>-/-</sup> spermatocytes, R-loops accumulates at pachytene stage interfering with meiotic recombination and the repair of DNA DSB. This leads to the absence of crossing-over, the arrest of meiosis at pachytene stage and the elimination of *Setx*<sup>-/-</sup> spermatocytes by apoptosis. The absence of senataxin also results in impaired XY body formation, defective localization of DNA damage response proteins on XY chromatin and failure to undergo MSCI. The combined defects of aborted meiotic recombination and MSCI failure are responsible for the infertility observed in *Setx*<sup>-/-</sup> males. doi:10.1371/journal.pgen.1003435.g007

that the Brca1-dependent localisation of senataxin to the XY chromosome may be indirect and mediated by other DNA damage response proteins involved in MSCI. On the other hand, Brca1 still localised to the sex chromosomes in *Setx*<sup>-/-</sup> mutant mice. However, this was incomplete since it was excluded from part of the XY structure in pachytene. This is consistent with a recent report that the X and Y chromosomes have different patterns of incorporation and release of recombination/repair and MSCI-related factors during different stages of meiosis [31]. In that study, they provided evidence that some MSCI steps are triggered much later on the Y chromosome than the X chromosome. Comparison with these results suggests that Brca1 has not localised to the Y chromosome in *Setx*<sup>-/-</sup> spermatocytes due to a block earlier in pachytene.

Once Brca1 localises to the axial elements of the sex chromosomes it recruits ATR which phosphorylates H2AX and it subsequently diffuses out into XY chromatin to trigger MSCI [22]. In Brca1 mutant cells, these proteins do not localise to the surrounding chromatin [44]. Loss of senataxin did not change the overall distribution of Brca1 on the XY chromosomes but ATR is no longer diffusely distributed and is instead retained on the axial elements of the XY chromosomes, similar to Brca1. The pattern of ATR staining in *Setx*<sup>-/-</sup> suggests that meiosis only proceeds from early to mid pachytene in these mice and that ATR re-localisation is dependent on senataxin (Figure 7D). Recent data show that in the absence of MDC1, the diffusion of ATR,  $\gamma$ H2AX and TopBP1 into XY chromatin is defective [33]. In the absence of senataxin the failure of ATR to diffuse from the axial elements to XY chromatin might be explained by defective MDC1 function. Our observation that MDC1 fails to localize fully to the XY body is consistent with this.

During leptotene and zygotene, the sex chromosomes are transcriptionally active [49]. However, at pachytene stage when meiotic synapsis is complete, the sex chromosomes are rapidly silenced and compartmentalized into a peripheral nuclear subdomain, the sex body [50]. MSCI then persists throughout the rest of pachytene and diplotene [49]. The second wave of phosphorylation only occurs on the chromatin of the sex chromosomes and is absolutely essential for MSCI [24,50]. This second wave of H2AX phosphorylation occurs in *Setx*<sup>-/-</sup> but breaks were still evident in the autosomes. This, together with failure to form chiasmata points to regions of asynapsis in *Setx*<sup>-/-</sup> autosomes. Extensive asynapsis has been shown to result in MSCI failure and pachytene stage IV apoptosis [51,52]. Expression analysis of X- and Y-linked genes revealed defective MSCI in *Setx*<sup>-/-</sup>. Furthermore, in contrast to that for *Setx*<sup>+/+</sup> mice RNA Pol

II staining was still visible on sex chromosomes in *Setx*<sup>-/-</sup>, consistent with continuing transcription. A reduction in ubi-H2A on the XY body of *Setx*<sup>-/-</sup> is also consistent with a failure of MSCI. While no ubi-H2A was observed associated with autosomes in *Setx*<sup>+/+</sup>, in keeping with transcriptional reactivation at pachytene stage, significant staining is seen on *Setx*<sup>-/-</sup> autosomes pointing to widespread abnormalities in transcriptional activity in these cells. This is in agreement with the increased R-loop staining observed at pachytene stage in *Setx*<sup>-/-</sup> cells. Recent results show that Brca1 preferentially mono-ubiquitinates H2A at satellite DNA regions and Brca1 deficiency impairs the integrity of constitutive heterochromatin causing disruption of gene silencing very likely through loss of ubi-H2A [53].

The evidence presented here suggests that R-loops accumulate in *Setx* deficient, actively transcribing cells in the presence of unrepaired DNA DSB. This supports a role for senataxin in resolving R-loops (Figure 7D). However, we previously showed that senataxin has a broader role in RNA processing since splicing efficiency, alternate splicing and transcription termination are abnormal in AOA2 cells [6]. It is unlikely that the extent of R-loops accumulation in actively transcribing/replicating spermatocytes will be duplicated in post-mitotic cells, such as Purkinje Cells. Neither DNA replication nor recombination is taking place in neuronal cells thus avoiding collisions with the transcriptional apparatus. Indeed, we were not able to detect R-loops in the cerebellum and brain of *Setx*<sup>-/-</sup> mice (unpublished data). These data suggest that the major clinical neurodegenerative phenotype seen in AOA2 patients is more likely to be due to a more general defect in RNA processing leading to reduced transcription fidelity rather than a failure to resolve R-loops. Altogether, these findings reveal a complex and coordinated network between transcription, RNA processing, and DNA repair pathways (Figure 7D), and support the emerging importance of RNA processing factors such as senataxin in the DNA damage response.

## Materials and Methods

### Ethics statement

All animal work and experiments have been approved by The Queensland Institute of Medical Research Animal Ethics Committee

### Targeted inactivation of mouse *Setx* gene

To disrupt the *Setx* gene a highly-effective recombineering approach was employed [54]. Briefly, two cassettes, a loxP-F3-

PGK-EM7-Neo-F3 (Neo) cassette was inserted into a BAC clone (RP23-389D11), Children's Hospital Oakland Research Institute corresponding to mouse chromosome 2 and covering the *Setx* genomic sequence. The Neo cassette which provides positive selection in ES cells was flanked by a 5' homology arm of 6.8 kb and a 3' homology arm of 3 kb. ES cells were then transfected with the linearized targeting vector and selected with 150 µg/ml of G418. Successful recombinant ES clones were determined by Southern blotting with a specific probe and PCR genotyping, and targeted cells (+neo) were subsequently micro-injected into C57BL6/129Sv mice blastocysts to generate chimeras. Excision of the Neo cassette was obtained by crossing the chimeras with a *Cre* deleter strain to generate *Setx*<sup>-/-</sup> mice containing only a *LoxP* site.

### Animal husbandry and genotyping

The mice were weaned at 21 days post-partum and ear clipped for identification. Genotyping was carried out by PCR on genomic DNA isolated from tail tips. Tail tips were lysed in directPCR Lysis eagent (Qiagen, USA) as recommended by the manufacturer. The primers used were In3F: 5'-TTTAAGGAACAGTGCTGC-3', In3R: 5'-ATGAAGCAGGTAGGATT-3' and LoxPR: 5'-CGAAGTTATATTAAGGGT-3'. PCR Cycling conditions were as follows: 35 cycles, denaturation at 95°C for 30 sec, annealing at 49°C for 30 sec, extension at 72°C for 1 min, with a final cycle and extension of 7 min at 72°C. Two PCR products were generated, a wild-type PCR product of 600 bp, and the targeted PCR product of 339 bp. PCR products were electrophoresed at 100 V for 30 min on 2% TAE Agarose (Boehringer Mannheim, Amresco, Lewes, UK) stained with Ethidium bromide and visualised with UV transillumination using a GelDoc XR (Biorad Laboratories Inc, UK).

### Histological analysis of *Setx* mice testes and ovaries

Testes from adult (35-day-old), 4 months, 8 months and 12 month-old mice were collected and fixed in PBS buffered 10% formalin, embedded in paraffin block and sectioned at 4 µm. Sections were stained with Hematoxylin and Eosin (H&E) and Toluidine blue. Slides were examined under light microscope and then scanned using Scanscope CS system (Aperio Technologies, Vista, USA). Images corresponding to ×10 and ×20 magnification were captured and assembled into Adobe Photoshop 7 (Adobe Systems Inc, USA).

### RT-PCR reactions and gene expression analysis

Total RNA was isolated from 35-day-old wild type and knockout mice testes using the RNeasy mini kit (Qiagen, USA) according to the manufacturer's protocol. RNA concentrations were determined by UV spectrophotometry using a Nanodrop ND-1000 (Thermo scientific, USA). cDNA was made from 5 µg of purified RNA. Briefly, RNA was mixed with 1 µl of random hexamer primers (Bio-Rad Laboratories Inc, USA), 1 µl of 10 mM dNTP mix and DEPC-treated water up to a 14 µl volume. The mixture was heat-denatured at 65°C for 5 min. 4 µl of First Strand buffer (Invitrogen, USA), 1 µl of 1 mM DTT, 1 µl of RNAaseIN (Promega, USA), and 1 µl of SuperScriptIII reverse transcriptase enzyme (Invitrogen, USA) was added to the mixture, and incubated for 10 min at 25°C, then 60 min at 50°C, 15 min at 70°C, and chilled on ice. 1 µl of RNAse H was subsequently added to each tube and incubated for 20 min at 37°C, followed by heat inactivation for 20 min at 65°C. The resulting cDNA were stored at -20°C prior to use. Gene expression analysis was performed by PCR in a 2720 Thermal Cycler (Applied Biosystem, USA). Reactions (25 µl) contained 14.5 µl of sterile water, 50 ng of

cDNA template, 1× PCR Buffer II (Roche, Switzerland), 2.5 mM MgCl<sub>2</sub> (Roche, Switzerland), 20 µM dNTPs, 1 µM of each primer, and 5 µl of AmpliTaq Gold DNA Polymerase (Roche, Switzerland). The primer pairs used for gene expression analysis are described in Table S1. Amplification was for 30 cycles and cycling conditions were as follows: denaturation for 5 min at 95°C for 30 sec, annealing at 55°C for 30 sec, elongation for 1 min at 72°C followed by a final extension step of 7 min at 72°C. PCR reactions were separated on 2% TAE agarose gels and visualised as above.

### Cell extracts and senataxin immunoprecipitation

Testes from 35 day-old mice were collected and ground with a pestle to disrupt their structure and lysed for 1 h at 4°C on a rotating wheel with lysis buffer (50 mM Tris-HCl pH 7.5, 50 mM β-glycerophosphate, 150 mM NaCl, 10% glycerol, 1% Tween 20, 1 mM PMSF, 5 mM DTT and 1× EDTA-free Complete Protease inhibitor (Roche, Switzerland). Cellular debris were pelleted by centrifugation at 16,100×g at 4°C for 10 min, and protein concentration was determined using Lowry Assay (Bio-Rad Laboratories, Inc, USA). 2 mg of total cell extract were pre-cleared with 50 µl of a mixture of 1:30 protein G+A beads (Millipore, Germany) for 3 hours at 4°C on a rotating wheel. Extract were centrifuged for 5 min at 2000×g, beads were removed, and 20 µg of anti-human senataxin antibody (Ab1/Ab-3) was added to the extract. Extracts and antibody were incubated overnight at 4°C on a rotating wheel to allow binding of the antibody to mouse senataxin. The next day, 50 µl of protein G+A beads were added to the extract and incubated for 1 h at 4°C on a rotating wheel. The immunoprecipitate was subsequently washed 3 times with lysis buffer and the beads were resuspended in gel loading buffer and separated on 5% SDS-PAGE at constant current (20 mA per gel) for 1.5 h. Once separated, proteins were transferred onto a nitrocellulose membrane (Hybond C, Amersham) for 1 h at 4°C with constant voltage (100 Volts). Immunoblotting with anti-senataxin (Ab-1) antibody was performed using standard procedure as previously described [5].

### Spermatocytes spreads, immunostaining, and imaging

All spreads were made from testes collected from adult 35-day-old mice or at day 16, 20 and 22 post partum. Briefly, testes were decapsulated, finely chopped and rinsed in GIBCO DME medium (Invitrogen, USA). Large clumps were removed by centrifugation at 6780×g for 5 min at room temperature. The remaining supernatant was centrifuged to pellet the cell suspension and mixed with 0.1M sucrose and spread onto glass slides pre-wetted with 1% paraformaldehyde and 0.1% Triton X-100 in PBS. Cells were fixed on the glass slides for 2 h at room temperature. The slides were subsequently washed with PBS and air-dried in the presence of a wetting agent, 1:250 Kodak Photo-Flo 200 (Kodak professional, USA). Once dried, spreads were stored at -80°C. For immunostaining, slides, were rehydrated in dH<sub>2</sub>O, and blocked in blocking buffer (0.2% BSA, 0.2% gelatine in PBS) for 30 min at room temperature. Spreads were incubated with primary antibodies overnight at 4°C in a humidified chamber. Primary antibodies used included anti-SCP3 (1:100, NB300-230, Novus Biologicals), anti-SCP1-Dye-Light conjugated (1:100, NB300-2201R, Novus Biologicals), anti-γH2AX (1:100, Y-P1016, Millipore), anti-Rad51 (1:100, SC-33626, Santa Cruz Biotechnology), anti-Dmcl (1:50, 2H12/4, Sapphire Bioscience), anti-Mlh1 (1:10, G168-15, Sapphire Bioscience), anti-ATR (1:100, SC-1887, Santa Cruz Biotechnology), anti-senataxin (1:100, Ab-1, [5]), anti-R-loop (1:100, S9.6), anti-RNA Pol II (phospho S2) (1:100, H5, ab24758,

Abcam), anti-mouse Brca1 (1:300, David Livingstone), anti-ubiquitin H2A (1:100, Clone E6C5, Millipore). Slides were subsequently washed 4 times for 3 min each in PBS on a rocker, and probed with the appropriate Alexa-Dye488 or Alexa-Dye594-conjugated secondary antibodies (1:250, Invitrogen, Molecular Probes, USA). Slides were washed again 4 times for 3 min each in PBS. DNA was stained with Hoechst 33342 (1:10,000) for 10 min at room temperature, and slides were mounted in Celvol 603 medium. Images were captured at room temperature using a digital camera (AxioCam Mrm, Carl Zeiss Microimaging Inc., Germany) attached to a fluorescent microscope (Axioskop 2 mot plus, Carl Zeiss Microimaging Inc., Germany) and the AxioVision 4.8 software (Carl Zeiss, Microimaging Inc. Germany). The objective employed was a 63× Zeiss Plan Aplanachromat 1,4 Oil DIC (Carl Zeiss, Germany). Images were subsequently assembled in Adobe Photoshop 7 (Adobe Systems Inc, USA), and contrast and brightness were adjusted on the whole image panel at the same time.

### TUNEL assay for apoptosis

Terminal deoxynucleotidyl transferase dUTP nick end labeling (TUNEL) is a method for detecting DNA fragmentation by labeling the terminal end of nucleic acids. TUNEL is a common method for detecting DNA fragmentation that results from apoptotic signaling cascades. The assay relies on the presence of nicks in the DNA which can be identified by terminal deoxynucleotidyl transferase (TdT), an enzyme that will catalyze the addition of Fluorescein-labeled dUTP. Paraffin sections were dewaxed and rehydrated with Shandon Varistain Gemini ES (Thermo Scientific, USA). TUNEL assay was performed using the Fluorescence *in situ* Cell Death Detection Kit (Roche, Switzerland) following the manufacturer's instructions. Slides were visualised under a fluorescent microscope and images were captured as previously described. The objective employed was a Zeiss Plan Neofluar ×10/0.30 (×10 magnification). For double staining, TUNEL was carried out first followed by immunostaining as described below.

### R-loop and DNA damage immunostaining on tissue sections

Slides with tissue sections were dewaxed and enzymatic antigen retrieval was performed by incubating the sections with 1:10 Trypsin dilution in PBS for 20 min at 37°C. Slides were washed 3 times for 5 min with PBS at room temperature for 5 min each. Tissues sections were blocked in (20% FCS, 2% BSA, 0.2% Triton X-100) for 1 h at room temperature. Slides were incubated with anti-R-loop (1:100, S9.6) [29] or anti-γH2AX (1:100, Y-P1016, Millipore) antibody overnight at 4°C in a humidified chamber. Slides were washed 5 times with 1× PBS containing 0.5% Triton X-100 for 5 min each at room temperature. Alexa-Dye488 or Alexa-Dye594-conjugated secondary antibody was added for 1 h at 37°C in a humidified chamber. Subsequently, slides were washed 3 times as before and Hoechst 33342 was added for 10 min to staining nuclei. Slides were finally washed twice and glass coverslips were mounted for imaging. Imaging was performed as described above. Confirmation of R-loop specific staining was obtained by pre-treating *Setx*<sup>-/-</sup> testes sections with RNase H (New England Biolabs, USA).

### Proximity Ligation Assay and endogenous *in situ* interaction

To investigate a possible interaction between Brca1, ATR and senataxin we employed *in situ* Proximity Ligation Assay (PLA)

(Duolink, Olink Bioscience, Uppsala, Sweden) on wild type (*Setx*<sup>+/+</sup>) spermatocytes spreads. PLA allows the monitoring of protein interactions and modifications with high specificity and sensitivity. Protein targets can be readily detected and localized with single molecule resolution and objectively quantified in unmodified cells and tissues. Utilizing only a few cells, sub-cellular events, such as transient or weak interactions are revealed *in situ*. Two primary antibodies raised in different species recognize the target antigens of interest. Species-specific secondary antibodies, called PLA probes, each with a unique short DNA strand attached to it, bind to the primary antibodies. When the PLA probes are in close proximity, the DNA strands can interact through a subsequent addition of two other circle-forming DNA oligonucleotides. After joining of the two added oligonucleotides by enzymatic ligation, they are amplified via rolling circle amplification using a polymerase. After the amplification reaction, several-hundredfold replication of the DNA circle has occurred, labeled complementary oligonucleotide probes highlight the product. The resulting high concentration of fluorescence in each single-molecule amplification product is visible as a distinct bright spot when viewed with a fluorescence microscope. The assay was performed according to the manufacturer's protocol using rabbit anti-mouse Brca1 (1:200, David Livingstone), sheep anti-senataxin (1:200, Ab-1) and goat anti-ATR antibody (1:100, SC-1887, Santa Cruz Biotechnology) antibodies and the corresponding anti-goat PLA Probe MINUS and anti-rabbit PLA probe PLUS. Identification of pachytene stage spermatocytes was determined by counterstaining with SCP3 antibody. PLA was also carried out on *Setx*<sup>-/-</sup> spermatocytes spreads as a negative control. Slide mounting and imaging was performed as described above.

### Supporting Information

**Figure S1** Absence of neurological phenotype and ataxia in *Setx*<sup>-/-</sup> mice. Neurological phenotype and ataxia were examined according to the phenotypic scoring system developed by Guyenet et al. 2010 [13]. No gross abnormal behaviour and ataxic phenotype progression was observed over a period of 3 to 17 months. Briefly, this scoring system combines phenotypic assessments that have been previously employed to assess various models of neurological disease including spinocerebellar ataxia, Huntington's disease and spinobulbar muscular atrophy [55–57]. Measures include hindlimb claspings, ledge test, gait and kyphosis. Each measure was recorded on a scale of 0–3 (0 representing the absence of the relevant phenotype and 3 the most severe manifestation) with a combined total of 0–12 for all four measures. Ledge test is a direct measure of coordination, the most directly comparable to human signs of cerebellar ataxia, which is impaired in cerebellar ataxias and many other neurodegenerative disorders. Hindlimb claspings is a marker of disease progression in many mouse models of neurodegeneration and certain ataxias [55]. Gait is a measure of coordination and muscle function and kyphosis is a characteristic dorsal curvature of the spine that is commonly observed in mouse models of neurodegenerative diseases [56,57]. Mice were assessed on a 0–3 scale each for ledge test, claspings, gait and kyphosis. Average composite score for *Setx*<sup>+/+</sup> and *Setx*<sup>-/-</sup> at each age was calculated. (TIF)

**Figure S2** Normal ovary structure in *Setx*<sup>-/-</sup> mice. We examined the histology of *Setx*<sup>-/-</sup> ovaries at 8 months of age to determine whether they exhibited similar signs as in the human patients [1,2]. A–D: Haematoxylin and eosin-stained 4 μm sections of four 8-month old *Setx*<sup>-/-</sup> mouse ovaries. Pre-antral and antral follicles (F) are present in all sections and many follicles

contain oocytes (asterisks). All sections also contain corpora lutea (CL), suggesting ovulation has occurred and the hypothalamic-pituitary-gonadal endocrine axis is intact in these mice. (Arrowheads denote the position of the bursal membrane enclosing the mouse ovary.) Scale bar, 200  $\mu$ m.

(TIF)

**Figure S3** Testis histology of *Setx*-deficient mice. A. Testis of a 35-day old *Setx*<sup>+/+</sup> mouse showing normal testis histology. Scale bar, 200  $\mu$ m. B. Testis of a 35-day-old *Setx*<sup>+/+</sup> mouse. Scale bar, 100  $\mu$ m. Interstitial (Leydig) cells lie between the seminiferous tubules (LD). C. Seminiferous tubule from a *Setx*<sup>+/+</sup> mouse at higher magnification. The tubule contains primary spermatocytes undergoing mitosis (short arrow), and elongated spermatids (asterisks) towards the lumen of the tubule, in which few sperm tails (T) can be seen. LD cells lie between the tubules. Sertoli cell nuclei (SCN) are present on the basement membrane of the tubule. D. Testis of a 35-day-old *Setx*<sup>-/-</sup> mouse showing seminiferous tubules with smaller diameter and disrupted spermatogenesis. Scale bar, 200  $\mu$ m. E. Testis of a 35-day-old *Setx*<sup>-/-</sup> mouse, showing tubules at different stages of the seminiferous epithelial cycle. In some stages, spermatocytes (asterisks) are abundant. In other stages of the seminiferous cycle spermatogonia and some spermatocytes (Sp) line an almost empty tubule. Scale bar, 100  $\mu$ m. F. Seminiferous tubule of a 35-day-old *Setx*<sup>-/-</sup> mouse testis, showing spermatogonia (Spn) and Sertoli cell nuclei (SCN) lining the basement membrane of the tubule. The lumen appears to contain remnants of Sertoli cell cytoplasm. Elongated spermatids and spermatozoa are completely absent. G–J. Male *Setx*<sup>+/-</sup> mice exhibit signs of reduced fertility at 8 months of age. G. Seminiferous tubules contain few mature spermatozoa and large inclusions (arrowheads), suggesting increased apoptosis of spermatogenic cells. The seminiferous epithelium contains post-meiotic round and elongating spermatids. Scale bar, 200  $\mu$ m. H. Seminiferous tubule from an 8-month *Setx*<sup>+/-</sup> mouse testis; Scale bar, 100  $\mu$ m. The seminiferous epithelium contains all stages of spermatogenesis, including round (R) and elongating spermatids (asterisks) and there are sperm tails (T) in the lumen. I. Seminiferous tubule from an 8-month *Setx*<sup>+/-</sup> mouse testis. Scale bar, 100  $\mu$ m. The seminiferous epithelium appears disrupted in places (arrow), with few round or elongating spermatids and debris in the lumen. J. In this seminiferous tubule from 8-month *Setx*<sup>+/-</sup> mouse testis there are few round (R) or elongating spermatids (asterisks) present and the lumen contains cell debris (arrow). Scale bar, 100  $\mu$ m.

(TIF)

**Figure S4** Abortion of meiosis following a block at pachytene stage in *Setx*<sup>-/-</sup> mice. A. Schematic representation of the various stages of spermatogenesis and the temporal expression of stage-specific makers as previously reported [58]. B. Semi-quantitative RT-PCR analysis of spermatogenesis stage-specific markers in *Setx*<sup>+/+</sup> and *Setx*<sup>-/-</sup> testes. Similar levels of expression for mitosis and meiosis-specific markers (*Dmc1*, *Calmegin*, *A-myb*) were observed in both *Setx*<sup>+/+</sup> and *Setx*<sup>-/-</sup> testes. A reduction of *Pgk2* is noticeable in *Setx*<sup>-/-</sup>. A marked reduction in expression for post-meiotic germ cells (*Pmm1*, *Pmm2* and *Tnp1*) is observed in *Setx*<sup>-/-</sup> testes in agreement the absence of these cells in *Setx*<sup>-/-</sup> seminiferous tubules as shown in Figure 2. These data suggest that *Setx*<sup>-/-</sup> spermatocytes do not proceed past meiosis. *Gapdh* was used as an internal standard. Cal, *Calmegin*.

(TIF)

**Figure S5** Elevated levels of DSBs in adult *Setx*<sup>-/-</sup> testes sections.  $\gamma$ H2AX staining of adult testes histological sections highlight the extensive amount of DNA DSB breaks in *Setx*<sup>-/-</sup> seminiferous tubules.

(TIF)

**Figure S6** Persistence of Rad51 and Dmc1 foci at pachytene stage in *Setx*<sup>-/-</sup> and *Brcal*<sup>A11/A11</sup>*p53*<sup>+/-</sup> spermatocytes. A. Persistence of DSB repair intermediates in pachytene cells of *Setx*<sup>-/-</sup> mice. Normal Rad51 foci formation occurred at leptotene and zygotene stage in *Setx*<sup>+/+</sup> and *Setx*<sup>-/-</sup> mice, there was persistence of Rad51 foci at pachytene stage in *Setx*<sup>-/-</sup> spermatocytes indicating the presence of unrepaired DSBs. Scale bar, 20  $\mu$ m. B. Persistence of DSB repair intermediates in pachytene cells of *Setx*<sup>-/-</sup> mice. Normal Dmc1 foci formation occurred at leptotene and zygotene stage in *Setx*<sup>+/+</sup> and *Setx*<sup>-/-</sup> mice, there was persistence of Dmc1 foci at pachytene stage in *Setx*<sup>-/-</sup> spermatocytes indicating the presence of unrepaired DSBs (compare 1 and 2). Scale bar, 20  $\mu$ m. C. Quantitation of Dmc1 foci at pachytene stage in *Setx*<sup>+/+</sup> and *Setx*<sup>-/-</sup> mice. A 10-fold increase of Dmc1 foci was observed in *Setx*<sup>-/-</sup>. (Student's t-test, n = 50) \* indicates p < 0.05. D. Rad51 foci in *Brcal*<sup>+/+</sup>*p53*<sup>+/-</sup> and *Brcal*<sup>A11/A11</sup>*p53*<sup>+/-</sup>. Normal Rad51 foci formation occurred at leptotene and zygotene stage in *Setx*<sup>+/+</sup> and *Setx*<sup>-/-</sup> mice, there was persistence of Rad51 foci at pachytene stage in *Brcal*<sup>A11/A11</sup>*p53*<sup>+/-</sup> spermatocytes indicating the presence of unrepaired DSBs. Scale bar, 20  $\mu$ m. E. Quantitation Rad51 foci at pachytene stage in *Brcal*<sup>+/+</sup>*p53*<sup>+/-</sup> and *Brcal*<sup>A11/A11</sup>*p53*<sup>+/-</sup> spermatocytes. A 2.5-fold increase in the numbers of Rad51 foci was observed in *Brcal*<sup>A11/A11</sup>*p53*<sup>+/-</sup> (Student's t-test, n = 50). \* indicates p < 0.05.

(TIF)

**Figure S7** Expression levels of recombination factors. A. RT-PCR analysis of *Rad51* expression revealed that the increased number of Rad51 foci in *Setx*<sup>-/-</sup> is not due to an increased expression of *Rad51* gene since similar levels of *Rad51* mRNA levels were detected in *Setx*<sup>+/+</sup> and *Setx*<sup>-/-</sup> testes. B. Immunoblotting of *Setx*<sup>+/+</sup> and *Setx*<sup>-/-</sup> testes protein extracts with anti-Rad51 antibody shows reduced levels of Rad51 protein in *Setx*<sup>-/-</sup>. Anti-GAPDH was used as a loading control. C. RT-PCR analysis of *Dmc1* expression revealed that the increased number of Dmc1 foci in *Setx*<sup>-/-</sup> is not due to an increased expression of *Dmc1* gene since similar levels of *Dmc1* mRNA levels were detected in *Setx*<sup>+/+</sup> and *Setx*<sup>-/-</sup> testes. D. RT-PCR analysis of *Mlh1* expression revealed that the absence of Mlh1 foci in *Setx*<sup>-/-</sup> is not due to a lack of expression of *Mlh1* gene since similar levels of *Mlh1* mRNA levels were detected in *Setx*<sup>+/+</sup> and *Setx*<sup>-/-</sup> testes. E. Immunoblotting of *Setx*<sup>+/+</sup> and *Setx*<sup>-/-</sup> testes protein extracts with anti-Mlh1 antibody shows similar levels of Mlh1 protein. Anti-GAPDH was used as a loading control.

(TIF)

**Figure S8** Abnormal localisation of ATR in *Setx*<sup>-/-</sup> pachytene spermatocytes. ATR foci formation occurred at leptotene and zygotene stages in *Setx*<sup>+/+</sup> and *Setx*<sup>-/-</sup> spermatocytes, however, ATR failed to spread to XY chromatin domain in *Setx*<sup>-/-</sup> at pachytene stage. Scale bar, 20  $\mu$ m.

(TIF)

**Table S1** Sequences of primers used for the gene expression analysis. Sequences of the primers used for the spermatogenesis stage specific markers and X- and Y-linked gene expression analysis. (PDF)

## Acknowledgments

The authors acknowledge Professor Helen Nicholson (University of Otago) with testes histology. We thank QIMR animal house staff for the maintenance of the mice.

## Author Contributions

Conceived and designed the experiments: OJB MFL. Performed the experiments: OJB AJY AS EYHH. Analyzed the data: OJB AJY AS

EYHH MFL. Contributed reagents/materials/analysis tools: KM XX CD. Wrote the paper: OJB MFL. Produced the senataxin antibodies: AMS. Designed and prepared KO targeting vector: RW. Provided expertise in

spermatogenesis and meiosis: JF. Provided assistance with breeding, maintenance, and genotyping of mice: JL. Provided assistance and expertise with mice superovulation and embryo collection: DC.

## References

- Moreira MC, Klur S, Watanabe M, Nemeth AH, Le Ber I, et al. (2004) Senataxin, the ortholog of a yeast RNA helicase, is mutant in ataxia-ocular apraxia 2. *Nat Genet* 36: 225–227.
- Anheim M, Monga B, Fleury M, Charles P, Barbot C, et al. (2009) Ataxia with oculomotor apraxia type 2: clinical, biological and genotype/phenotype correlation study of a cohort of 90 patients. *Brain* 132(Pt 10): 2688–2698.
- Chen YZ, Bennett CL, Huynh HM, Blair IP, Puls I, et al. (2004) DNA/RNA helicase gene mutations in a form of juvenile amyotrophic lateral sclerosis (ALS4). *Am J Hum Genet* 74: 1128–1135.
- Ursic D, Chinchilla K, Finkel JS, Culbertson MR (2004) Multiple protein/protein and protein/RNA interactions suggest roles for yeast DNA/RNA helicase Sen1p in transcription, transcription-coupled DNA repair and RNA processing. *Nucleic Acids Res* 32: 2441–2452.
- Suraweera A, Becherel OJ, Chen P, Rundle N, Woods R, et al. (2007) Senataxin, defective in ataxia oculomotor apraxia type 2, is involved in the defense against oxidative DNA damage. *J Cell Biol* 177: 969–979.
- Suraweera A, Lim Y, Woods R, Birrell GW, Nasim T, et al. (2009) Functional role for senataxin, defective in ataxia oculomotor apraxia type 2, in transcriptional regulation. *Hum Mol Genet* 18: 3384–3396.
- Skourtis-Stathaki K, Proudfoot NJ, Gromak N (2011) Human Senataxin Resolves RNA/DNA Hybrids Formed at Transcriptional Pause Sites to Promote Xrn2-Dependent Termination. *Mol Cell* 42: 794–805.
- Huertas P, Aguilera A (2003) Cotranscriptionally formed DNA:RNA hybrids mediate transcription elongation impairment and transcription-associated recombination. *Mol Cell* 12: 711–721.
- Li X, Manley JL (2005) Inactivation of the SR protein splicing factor ASF/SF2 results in genomic instability. *Cell* 122: 365–378.
- Mischo H E, Gomez-Gonzalez B, Grzechnik P, Rondon AG, Wei W, et al. (2011) Yeast Sen1 helicase protects the genome from transcription-associated instability. *Mol Cell* 41: 21–32.
- Yüce-Petronczki O, West SC (2012) Senataxin, defective in the neurodegenerative disorder AOA-2, lies at the interface of transcription and the DNA damage response. *Mol Cell Biol* doi:10.1128/MCB.01195-12.
- Alzu A, Bermejo R, Begnis M, Lucca C, Piccini D, et al. (2012) Senataxin Associates with Replication Forks to Protect Fork Integrity across RNA-Polymerase-II-Transcribed Genes. *Cell* 151:835–46.
- Guyenet SJ, Furrer SA, Damian VM, Baughan TD, La Spada AR, et al. (2010) A simple composite phenotype scoring system for evaluating mouse models of cerebellar ataxia. *J Vis Exp* 21 doi:pii: 1787. 10.3791/1787.
- Barlow C, Hirotsune S, Paylor R, Liyanage M, Eckhaus M, et al. (1996) Atm-deficient mice: a paradigm of ataxia telangiectasia. *Cell* 86: 159–171.
- Xu Y, Ashley T, Brainerd EE, Bronson RT, Meyn MS, et al. (1996) Targeted disruption of ATM leads to growth retardation, chromosomal fragmentation during meiosis, immune defects, and thymic lymphoma. *Genes Dev* 10: 2411–2422.
- Cohen PE, Pollard JW (2001) Regulation of meiotic recombination and prophase I progression in mammals. *Bioessays* 23: 996–1009.
- Yazawa T, Yamamoto T, Nakayama T, Hamada S, Abe S (2000) Conversion from mitosis to meiosis: morphology and expression of proliferating cell nuclear antigen (PCNA) and Dmc1 during newt spermatogenesis. *Dev Growth Differ* 42: 603–611.
- Zhao M, Shirley CR, Mounsey S, Meistrich MI (2004) Nucleoprotein transitions during spermiogenesis in mice with transition nuclear protein Tnp1 and Tnp2 mutations. *Biol Reprod* 71: 1016–1025.
- Keeney S (2001) Mechanism and control of meiotic recombination initiation. *Curr Top Dev Biol* 52: 1–53.
- Rogakou E, Boon P, Redon C, Bonner WM (1999) Megabase chromatin domains involved in DNA double-strand breaks in vivo. *J Cell Biol* 146: 905–916.
- Hunter N, Borner GV, Lichten M, Kleckner R (2001) Gamma-H2AX illuminates meiosis. *Nat Genet* 27: 236–238.
- Turner JM, Aprelikova O, Xu X, Wang R, Kim S, et al. (2004) BRCA1, histone H2AX phosphorylation, and male meiotic sex chromosome inactivation. *Curr Biol* 14: 2135–2142.
- Turner JM, Mahadevaiah SK, Elliott DJ, Garchon HJ, Pehrson JR, et al. (2002) Meiotic sex chromosome inactivation in male mice with targeted disruptions of Xist. *J Cell Sci* 115(Pt 21): 4097–4105.
- Turner JM, Mahadevaiah SK, Fernandez-Capetillo O, Nussenzweig A, Xu X, et al. (2005) Silencing of unsynapsed meiotic chromosomes in the mouse. *Nat Genet* 37: 41–47.
- Ashley T, Plug AW, Xu J, Solari AJ, Reddy G, et al. (1995) Dynamic changes in Rad51 distribution on chromatin during meiosis in male and female vertebrates. *Chromosoma* 104: 19–28.
- Baker SM, Plug AW, Prolla TA, Bronner CE, Harris AC, et al. (1996) Involvement of mouse Mlh1 in DNA mismatch repair and meiotic crossing over. *Nat Genet* 13: 336–342.
- Hunter N, Borts RH (1997) Mlh1 is unique among mismatch repair proteins in its ability to promote crossing-over during meiosis. *Genes Dev* 11: 1573–1582.
- Anderson LK, Reeves A, Webb LM, Ashley T (1999) Distribution of crossing over on mouse synaptonemal complexes using immunofluorescent localization of MLH1 protein. *Genetics* 151:1569–79.
- Boguslawski SJ, Smith DE, Michalak MA, Mickelson KE, Yehle CO, et al. (1986) Characterization of monoclonal antibody to DNA:RNA and its application to immunodetection of hybrids. *J Immunol Methods* 89: 123–130.
- Hu Z, Zhang A, Storz G, Gottesman S, Leppla SH (2006) An antibody-based microarray assay for small RNA detection. *Nucleic Acids Res* 34:e52.
- Page J, de la Fuente R, Manterola M, Parra MT, Viera MT, et al. (2012) Inactivation or non-reactivation: what accounts better for the silence of sex chromosomes during mammalian male meiosis? *Chromosoma* 121: 307–326.
- Fernandez-Capetillo O, Mahadevaiah SK, Celeste A, Romanienko PJ, Camerini-Otero RT, et al. (2003) H2AX is required for chromatin remodeling and inactivation of sex chromosomes in male mouse meiosis. *Dev Cell* 4: 497–508.
- Ichijima Y, Ichijima M, Lou Z, Nussenzweig A, Camerini-Otero RD, et al. (2011) MDC1 directs chromosome-wide silencing of the sex chromosomes in male germ cells. *Genes Dev* 25: 959–971.
- Handel MA (2004) The XY body: a specialized meiotic chromatin domain. *Exp Cell Res* 296: 57–63.
- Wang PJ, Page DC, McCarrey JR (2005) Differential expression of sex-linked and autosomal germ-cell-specific genes during spermatogenesis in the mouse. *Hum Mol Genet* 14: 2911–2918.
- Royo H, Polikiewicz G, Mahadevaiah SK, Prosser H, Mitchell M, et al. (2010) Evidence that meiotic sex chromosome inactivation is essential for male fertility. *Baer Biol* 20: 2117–2123.
- Baarends WM, Wassenaar E, van der Laan R, Hoogerbrugge J, Sladdens-Linkels E, et al. (2005) Silencing of unpaired chromatin and histone H2A ubiquitination in mammalian meiosis. *Mol Cell Biol* 25: 1041–1053.
- Romanienko PJ, Camerini-Otero RD (2000) The mouse Spo11 gene is required for meiotic chromosome synapsis. *Mol Cell* 6: 975–987.
- Pittman DL, Cobb J, Schimenti KJ, Wilson LA, Cooper DM, et al. (1998) Meiotic prophase arrest with failure of chromosome synapsis in mice deficient for Dmcl1, a germline-specific RecA homolog. *Mol Cell* 1: 697–705.
- Cressman VL, Backlund DC, Avrutskaya AV, Leadon SA, Godfrey V, et al. (1999) Growth retardation, DNA repair defects, and lack of spermatogenesis in BRCA1-deficient mice. *Mol Cell Biol* 19: 7061–7075.
- Edelmann W, Cohen PE, Kneitz B, Winand N, Lia M, et al. (1999) Mammalian MutS homologue 5 is required for chromosome pairing in meiosis. *Nat Genet* 21: 123–127.
- Kneitz B, Cohen PE, Avdievich E, Zhu L, Kane MF, et al. (2000) MutS homologue 4 localization to meiotic chromosomes is required for chromosome pairing during meiosis in male and female mice. *Genes Dev* 14: 1085–1097.
- Kolas NK, Svetlanov A, Lenzi ML, Macaluso FP, Lipkin SM, et al. (2005) Localization of MMR proteins on meiotic chromosomes in mice indicates distinct functions during prophase I. *J Cell Biol* 171: 447–458.
- Xu X, Aprelikova OI, Moens P, Deng CX, Furth PA (2003) Impaired meiotic DNA-damage repair and lack of crossing-over during spermatogenesis in BRCA1 full-length isoform deficient mice. *Development* 130: 2001–2012.
- Aguilera A (2005) mRNA processing and genomic instability. *Nat Struct Mol Biol* 12: 737–738.
- Castellano-Pozo M, Garcia-Muse T, Aguilera A (2012) R-loops cause replication impairment and genome instability during meiosis. *EMBO Reports* 13:923–929.
- Gan W, Guan Z, Liu J, Gui T, Shen K, et al. (2011) R-loop mediated genomic instability is caused by impairment of replication fork progression. *Genes Dev* 25: 2041–2056.
- Sordet O, Nakamura AJ, Redon CE, Pommier Y (2010) DNA double-strand breaks and ATM activation by transcription-blocking DNA lesions. *Cell Cycle* 9: 274–278.
- Turner JM (2007) Meiotic sex chromosome inactivation. *Development* 134: 1823–1831.
- McKee BD, Handel MA (1993) Sex chromosomes, recombination, and chromatin conformation. *Chromosoma* 102: 71–80.
- Mahadevaiah SK, Turner JM, Baudat F, Rogakou EP, de Boer P, et al. (2001) Recombinational DNA double-strand breaks in mice precede synapsis. *Nat Genet* 27: 271–276.
- Burgoyne PS, Mahadevaiah T, Turner SK (2009) The consequences of asynapsis for mammalian meiosis. *Nat Rev Genet* 10: 207–216.
- Zhu Q, Pao GM, Huynh AM, Suh H, Tonnu N, et al. (2011) BRCA1 tumour suppression occurs via heterochromatin-mediated silencing. *Nature* 7363: 179–184.

54. Chan W, Costantino N, Li R, Lee SC, Su Q, et al. (2007) A recombineering based approach for high-throughput conditional knockout targeting vector construction. *Nucleic Acids Res* 35: e64.
55. Chou AH (2008) Polyglutamine-expanded ataxin-3 causes cerebellar dysfunction of SCA3 transgenic mice by inducing transcriptional dysregulation. *Neurobiol Dis* 31:89–101.
56. Thomas PS Jr (2006) Loss of endogenous androgen receptor protein accelerates motor neuron degeneration and accentuates androgen insensitivity in a mouse model of X-linked spinal and bulbar muscular atrophy. *Hum Mol Genet* 15:2225–2238.
57. Ditzler S, Stoeck J, LeBlanc M, Kooperberg C, Hansen S, et al. (2003) A Rapid Neurobehavioral Assessment Reveals that FK506 Delays Symptom Onset in R6/2 Huntington's Disease Mice. *Preclinical Research Articles* 1:115–126.
58. Eddy EM (2002) Male Germ cell gene expression. *Recent Prog Horm Res* 57:103–28.

## **APPENDIX II**



## WORLD OF REPRODUCTIVE BIOLOGY

### Senataxin Saves Sperm

A multitasking protein controls chromosomal activities during spermatogenesis in mice, according to a new report. The evolutionarily conserved protein, senataxin, is required for proper homologous recombination during meiosis and helps mediate the silencing of the XY body, which is restricted in a process called meiotic sex chromosome inactivation.

Studies in proliferating mammalian cells and yeast have suggested that senataxin may help co-ordinate replication, transcription, and DNA repair through multiple mechanisms. For instance, the yeast ortholog of senataxin is associated with DNA replication forks, and the mammalian protein binds to proteins involved in transcription. Moreover, senataxin seems to protect the genome from DNA damage by helping to eliminate R loops, RNA:DNA hybrids that form over transcription pause sites.

To further investigate the role of senataxin, Olivier Becherel et al. created mice deficient for this protein. The female mice had reduced fertility and the male mice were completely infertile. The researchers focused their studies on understanding the impairment in males.

The researchers found that in senataxin-deficient spermatocytes, R loops accumulated during meiotic recombination. Perhaps as a consequence of this defective R-loop elimination, DNA double-stranded breaks also accumulated, ultimately resulting in a failure of the essential step in meiosis, crossing over.

Proper formation of the XY body was also impaired. The XY body was transcriptionally active in senataxin-deficient mice, and proteins involved in XY silencing did not localize properly to the XY chromosomes. Senataxin was found to be associated with the XY body, a process that requires DNA repair protein BRCA1. As a result of these meiotic defects, spermatogenesis was arrested in the pachytene stage, resulting in apoptosis and male infertility.

The findings show how DNA-regulating proteins can be deployed for multiple tasks. Other examples include proteins involved in the response to DNA damage that also play essential roles in meiosis, such as BRCA1, MDC1, and H2AX.

—Charlotte Schubert

Becherel OJ, Yeo AJ, Stellati A, Heng EY, Luff J, Suraweera AM, Woods R, Fleming J, Carrie D, McKinney K, Xu X, Deng C, et al. Senataxin plays an essential role with DNA damage response proteins in meiotic recombination and gene silencing. *PLoS Genet* 2013; 9(4):e1003435.

## **APPENDIX III**

# Senataxin protects the genome

## Implications for neurodegeneration and other abnormalities

Martin F. Lavin,<sup>1,2,\*</sup> Abrey J. Yeo<sup>1,3</sup> and Olivier J. Becherel<sup>1,4</sup>

<sup>1</sup>Queensland Institute of Medical Research; Radiation Biology and Oncology; Brisbane, QLD, Australia; <sup>2</sup>University of Queensland Centre for Clinical Research; Herston, QLD, Australia; <sup>3</sup>School of Medicine; University of Queensland; Herston, QLD, Australia; <sup>4</sup>School of Chemistry & Molecular Biosciences; University of Queensland; St. Lucia, QLD, Australia

**A**taxia oculomotor apraxia type 2 (AOA2) is a rare autosomal recessive disorder characterized by cerebellar atrophy, peripheral neuropathy, loss of Purkinje cells and elevated  $\alpha$ -fetoprotein. AOA2 is caused by mutations in the *SETX* gene that codes for the high molecular weight protein senataxin. Mutations in this gene also cause dominant neurodegenerative disorders. Similar to that observed for other autosomal recessive ataxias, this protein protects the integrity of the genome against oxidative and other forms of DNA damage to reduce the risk of neurodegeneration. Senataxin functions in transcription termination and RNA splicing and it has been shown to resolve RNA/DNA hybrids (R-loops) that arise at transcription pause sites or when transcription is blocked. Recent data suggest that this protein functions at the interface between transcription and DNA replication to minimise the risk of collision and maintain genome stability. Our recent data using *SETX* gene-disrupted mice revealed that male mice were defective in spermatogenesis and were infertile. DNA double strand-breaks persisted throughout meiosis and crossing-over failed in *SETX* mutant mice. These changes can be explained by the accumulation of R-loops, which interfere with Holiday junctions and crossing-over. We also showed that senataxin was localized to the XY body in pachytene cells and was involved in transcriptional silencing of these chromosomes. While the defect in meiotic recombination was striking in these animals, there was no evidence of

neurodegeneration as observed in AOA2 patients. We discuss here potentially different roles for senataxin in proliferating and post-mitotic cells.

Autosomal recessive cerebellar ataxias are a class of progressive neurodegenerative disorders that result from cerebellar atrophy and spinal tract dysfunction.<sup>1</sup> One of these, ataxia oculomotor apraxia type 2 (AOA2) is characterized by progressive cerebellar atrophy and peripheral neuropathy, oculomotor apraxia and elevated  $\alpha$ -fetoprotein serum levels, with an onset between 10–20 y of age.<sup>2–4</sup> Brain MRI reveals diffuse cerebellar atrophy and electroneuromyography confirms the peripheral neuropathy.<sup>4</sup> The major clinical features of this disorder are shown in Table 1. In a post-mortem AOA2 case, Criscuolo et al.<sup>5</sup> observed reduced brain size and cerebellar atrophy which was most evident at the level of the vermis and anterior lobe; the cerebellar cortex had marked loss of Purkinje cells and brainstem and spinal cord were slightly reduced. Thus, as with other autosomal recessive ataxias, pathology in the cerebellum features strongly. However, unlike that for the related disorder ataxia telangiectasia (A-T), there is no evidence of increased cancer susceptibility in AOA2.

The gene mutated in AOA2 was initially mapped to chromosome 9q34 and subsequently identified as *SETX*.<sup>6</sup> *SETX* is predicted to code for a 2,667 amino acid protein (senataxin) that contains a highly conserved C-terminal seven-motif domain found in the superfamily 1 of

**Keywords:** Ataxia oculomotor apraxia type 2 (AOA2), *SETX* gene, senataxin, RNA processing, R-loops, DNA double strand breaks, neurodegeneration

Submitted: 05/13/13

Accepted: 05/31/13

Published Online: 06/18/13

Citation: Lavin MF, Yeo AJ, Becherel OJ. Senataxin protects the genome: Implications for neurodegeneration and other abnormalities. *Rare Diseases* 2013; 1:e25230; <http://dx.doi.org/10.4161/rdis.25230>

\*Correspondence to: Martin F. Lavin;

Email: [martin.lavin@qimr.edu.au](mailto:martin.lavin@qimr.edu.au)

Addendum to: Becherel OJ, Yeo AJ, Stellati A, Heng EYH, Luff J, Suraweera AM, et al. Senataxin plays an essential role with DNA damage response proteins in meiotic recombination and gene silencing. *PLoS Genet* 2013; 9:e1003435; PMID:23593030; <http://dx.doi.org/10.1371/journal.pgen.1003435>.

**Table 1.** Ataxia Oculomotor Apraxia Type 2 (AOA2): Clinical Features

Onset second decade
Diffuse cerebellar atrophy (MRI)
Peripheral neuropathy
Early loss of reflexes
Loss of Purkinje cells
Oculomotor apraxia
Extra-neurological features of A-T missing but $\alpha$ -fetoprotein elevated
Autosomal recessive cerebellar ataxia

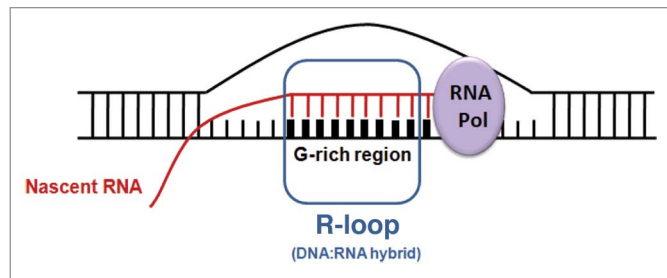


**Figure 1.** R-loop structure. R-loops form at sites when the RNA polymerase complex encounters G-rich sequences such as those found at transcription pause sites, CpG islands in promoter regions, repeat sequences and telomeric regions.<sup>31,32</sup> Pairing of the nascent RNA remains with the ssDNA region behind the elongating RNA polymerase complex leads to R-loop (DNA/RNA hybrid) formation.

**Table 2.** Mutations in *SETX* give rise to different neurodegenerative disorders

Disorder	Age of onset (yr)	Major Clinical Phenotype	Gene/Protein	Inheritance	References
Ataxia oculomotor apraxia type 2 (AOA2)	10–20	Cerebellar ataxia with peripheral neuropathy	<i>Setx/senataxin</i>	Recessive	1–5
Tremor ataxia syndrome (TAS)	3, 13*	Cerebellar ataxia without peripheral neuropathy	<i>Setx/senataxin</i>	Dominant	11
Juvenile Amyotrophic lateral sclerosis (ALS4)	14**	Limb weakness and severe muscle wasting	<i>Setx/senataxin</i>	Dominant	9
Autosomal dominant proximal spinal muscular atrophy (ADSM4)	10–20	Muscular atrophy and weakness	<i>Setx/senataxin</i>	Dominant	10

\*Age of onset for daughter and mother. \*\*Average age of onset.

DNA/RNA helicases and an N-terminal domain important for protein-protein interaction.<sup>7,8</sup> Generally speaking, mutations in a single gene, such as *SETX*, gives rise to one syndrome, which, of course, may show heterogeneity depending on the nature and localization of the mutations. In the case of *SETX*, up to 4 different syndromes are associated with mutations in this gene (Table 2). Juvenile amyotrophic lateral sclerosis (ALS4) is a form of juvenile ALS characterized by distal muscle weakness and atrophy, normal sensation and pyramidal tract signs. The ALS4 locus maps to chromosome 9q34. Chen et al.<sup>9</sup> detected missense mutations in a single allele in the *SETX* gene (which maps to this locus) which segregated with the disease. Subsequent studies have detected *SETX* mutations in additional ALS4 patients. Heterozygous *SETX* gene mutations were also detected in patients with autosomal dominant proximal spinal muscular atrophy.<sup>10</sup> These patients showed proximal and distal muscular atrophy and pareses. While there was overlap with ALS4, this appeared to be a discrete entity. A dominant *SETX*

mutation, causing a cerebellar phenotype termed tremor-ataxia syndrome, has been described for a mother and daughter. These patients showed cerebellar atrophy, oculomotor defects and tremor but no evidence of peripheral neuropathy or pyramidal signs.<sup>11</sup> In short, mutations in *SETX* can give rise to both dominant and recessive disorders with some overlap in features. A greater insight into the function of senataxin and the proteins it interacts with will help to resolve the quandary of several distinct disorders from mutations in a single gene.

Senataxin shares extensive homology with the yeast *Saccharomyces cerevisiae* splicing endonuclease 1 protein (Sen1p), which possesses helicase activity, and is involved in the processing of tRNA, rRNA, small nuclear and small nucleolar RNA.<sup>12</sup> Sen1p also interacts with Rad2, which is required for DNA repair, suggesting that the protein may be involved in protecting the genome.<sup>13</sup> We demonstrated that this might also be the case for senataxin by showing that AOA2 patient cells display sensitivity to DNA damaging agents such as H<sub>2</sub>O<sub>2</sub>, camptothecin and mitomycin C

and the cells had elevated levels of oxidative DNA damage.<sup>8</sup> In support of a role for senataxin in the DNA damage response, it has also been demonstrated that telomere length is constitutively reduced in AOA2 lymphocytes and the rate of telomere shortening by DNA damage is increased in these cells.<sup>14</sup> Interaction of Sen1p with Rnt1p (an endoribonuclease required for RNA maturation) suggested that Sen1p is also involved in RNA processing and transcription.<sup>13</sup> We provided evidence for a similar role in human cells by identifying novel senataxin-interacting proteins, the majority of which are involved in transcription and RNA processing, including RNA polymerase II.<sup>15</sup> Binding of RNA polymerase II to candidate genes was significantly reduced in senataxin deficient cells and this was accompanied by decreased transcription of these genes, suggesting a role for senataxin in the regulation/modulation of transcription. RNA polymerase II-dependent transcription termination was defective in cells depleted of senataxin in keeping with the observed interaction of senataxin with poly(A) binding proteins 1 and 2. Splicing

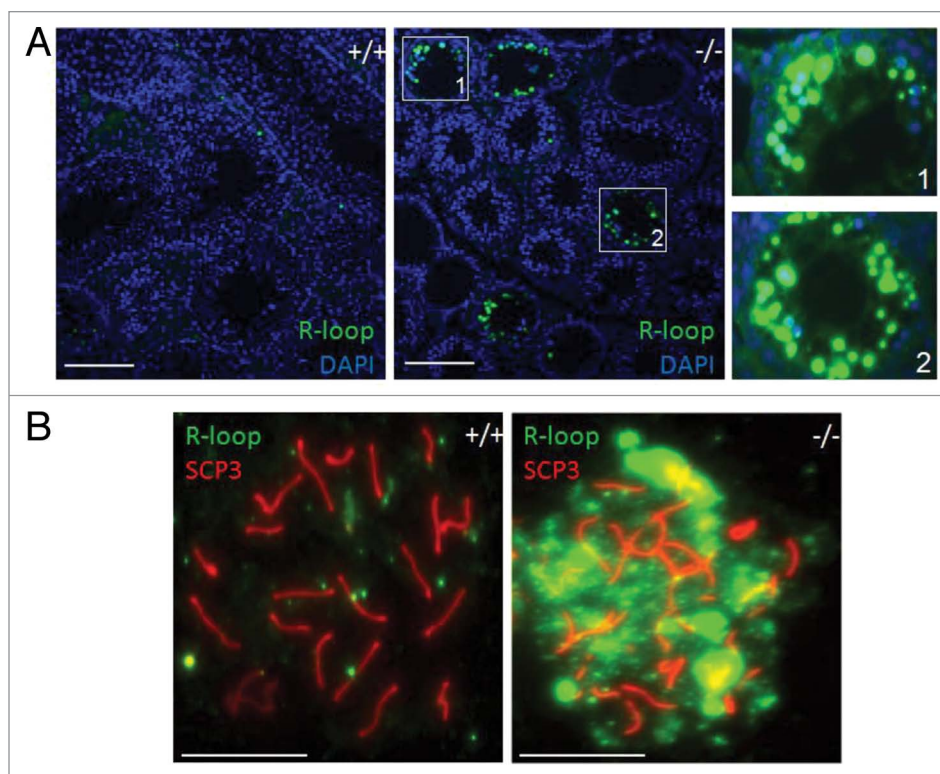


**Figure 2.** Accumulation of R-loops in *Setx*<sup>-/-</sup> germ cells. **(A)** Immunostaining of testes cross-sections from wildtype (+/+) and *Setx* knockout (-/-) mice with the S9.6 DNA/RNA (R-loop) antibody. Nuclei were stained with Hoechst 33342. Scale bar, 100  $\mu$ m. Regions 1 and 2 show magnifications. **(B)** Immunostaining of pachytene spermatocytes from wildtype (+/+) and *Setx* knockout (-/-) with S9.6 antibody shows a dramatic accumulation of R-loops in senataxin deficient germ cells. SCP3 was used to stain for the synaptonemal complex and identify pachytene stage cells. Scale bar, 20  $\mu$ m.

efficiency of specific mRNAs and alternate splice-site selection of both endogenous genes and artificial minigenes were altered in senataxin-depleted cells.<sup>15</sup> A role for senataxin in transcription elongation and termination is further supported by a report showing that cells with senataxin knockdown displayed an increase in RNA read-through and Pol II density downstream of the Poly (A) site and also exhibited increased levels of R-loop formation.<sup>16</sup> R-loops are RNA/DNA hybrids that form over transcription pause sites by interaction with a ssDNA template behind an elongating Pol II complex (Fig. 1). These structures are potentially harmful and can cause genomic instability if left unresolved.<sup>16-18</sup> The yeast ortholog of senataxin Sen1p, has also been shown to protect its heavily transcribed genome from R-loop-mediated DNA damage.<sup>19</sup> More recently, Hazelbaker et al.<sup>20</sup> showed that kinetic competition between elongating RNA pol II and Sen1p helicase likely explains the temporal and spatial window for early Pol II termination. Loss of Sen1p results in

transient R-loop accumulation, giving rise to transcription-associated recombination and genome instability. More insight into this was provided recently by Alzu et al.<sup>21</sup> who showed that Sen1p associates with DNA replication forks to protect their integrity across RNA Pol II – transcribed genes. Thus, Sen1p plays an important role in coordinating replication with transcription to protect the genome. Support for a similar role for the human ortholog, senataxin, was provided recently by Yuce-Petronczki and West<sup>22</sup> who showed that senataxin localized to distinct nuclear foci in S/G2 phase cells and that the number of these foci increased in response to impaired replication. These data suggest that senataxin localizes to collision sites between the transcription apparatus and components of the replisome.

All of the investigations above have described a role for senataxin in preventing collision between DNA replication forks and ongoing transcription to preserve genome integrity in proliferating cells. However, the major phenotype in

AOA2 patients is progressive neurodegeneration in post-mitotic tissue. Under those conditions, ongoing transcription will not encounter DNA replication forks. What then is the role of senataxin in the brain? Vantaggiato et al.<sup>23</sup> provided evidence that senataxin plays a role in neurogenesis and cytoprotection during neuronal differentiation which is mediated by fibroblast growth factor 8. However, since this is a progressive disease, it is unlikely that the role of senataxin is restricted to development. To address this further, we disrupted the *SETX* gene in a mouse model for AOA2, which was the subject matter of our recent publication.<sup>24</sup> Unfortunately, we did not observe a neurodegenerative phenotype in the *Setx*<sup>-/-</sup> mice and there was no evidence of more subtle behavioral differences in these mice, which limited investigation into the nature of the defect in the brains of these mice. This was not altogether surprising since knockout of several of the genes causing autosomal recessive ataxias in humans fails to re-capitulate the phenotype in mouse

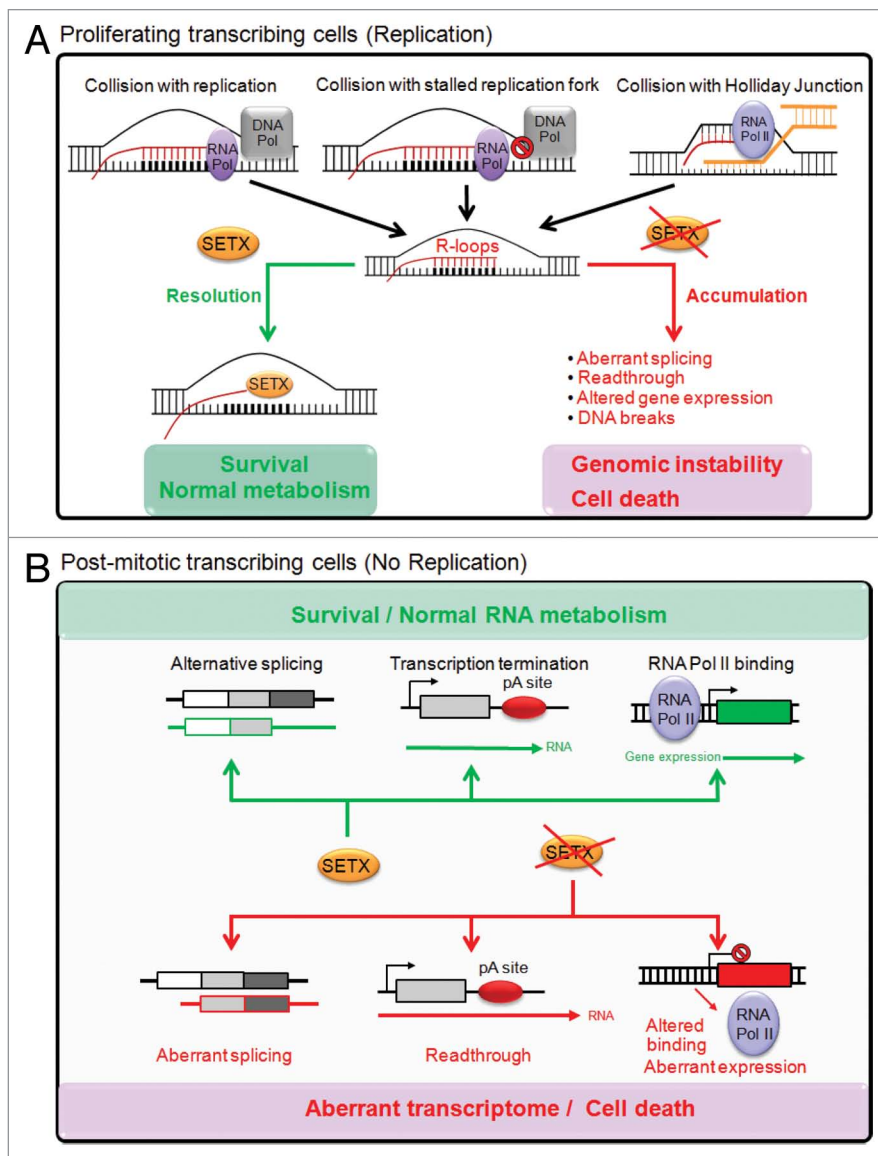


**Figure 3.** Protection of the genome by senataxin in proliferating vs. post-mitotic cells. **(A)** In proliferating cells, collision of the transcription apparatus (RNA Pol) with replication forks (DNA Pol), stalled replication forks following DNA damage exposure, or Holliday junctions during homologous recombination, lead to the formation and accumulation of R-loop structures. In the presence of senataxin, R-loops are effectively resolved by its putative DNA/RNA helicase activity, thus leading to normal cellular metabolism and cell survival. In the absence of senataxin, R-loops accumulate and impact on RNA metabolism through the alteration of mRNA splicing, the inhibition of transcription termination, the promotion of readthrough, the alteration of gene expression and the formation of DNA breaks. The accumulation of these defects drives genomic instability and ultimately cell death. **(B)** In contrast, in post-mitotic cells, such as neurons, the absence of DNA replication and homologous recombination, and the lack of R-loops accumulation suggest senataxin's role in protecting the genome may be directly due to its effect on mRNA splicing, transcription termination and the modulation of gene expression through its interaction with RNA binding proteins.

models.<sup>25</sup> However, we observed that *Setx*<sup>-/-</sup> male mice were infertile and fertility was reduced in females. While there is no information on male fertility in AOA2, there are a few reports of hypogonadism in females. Criscuolo et al.<sup>4</sup> reported two

patients who entered menopause in early adulthood which was also observed in a separate study.<sup>5</sup> Ovarian failure has also been observed in a patient with AOA2<sup>26</sup> and another patient had a diagnosis of polycystic ovarian syndrome.<sup>27</sup> We

subsequently showed that senataxin had an essential role in spermatogenesis in mice and in its absence these cells failed to progress past the pachytene stage of prophase 1 of meiosis.<sup>24</sup> The DNA double-strand breaks (DSB) introduced by Spo11 in readiness for meiotic recombination were inefficiently repaired on autosomes, resulting in a failure to complete crossing-over. During the process of crossing-over, autosomes remain transcriptionally active, so it was possible that in the absence of senataxin, R-loops would accumulate in the vicinity of unrepaired DNA DSB leading to collapse of Holiday junctions and inhibition of the crossing-over step. Indeed this was the case since we detected elevated levels of R-loops in both spermatocyte spreads and testes sections (Fig. 2). Wild-type mice showed a very much reduced level of signal. So in the case of spermatocyte differentiation, the R-loops that accumulate in the absence of senataxin appear to collide with Holiday junctions rather than with advancing replication forks. We also screened for the presence of R-loops in the brains of *Setx* mutant mice but failed to detect these structures by immunofluorescence (unpublished data). This was not altogether surprising since neither DNA replication nor DNA recombination is taking place in this tissue. It is possible that persistence of DNA damage in post-mitotic cells might lead to the accumulation of these structures, which in turn could contribute to the neurodegenerative changes in AOA2 patients. However, we and others have provided evidence for a broader role for senataxin in transcription and other cellular processes. Senataxin plays an important role in transcription termination to prevent RNA readthrough, which may or may not be related to R-loop resolution.<sup>15,16</sup> The presence of significant readthrough of mRNA may lead to inefficient or aberrant protein synthesis and consequently cell toxicity. Senataxin has also been shown to play a role in the regulation of splicing<sup>15</sup> and deficiency of the SR splicing factor ASF/SF2 leads to R-loop accumulation and genome instability.<sup>18</sup> This in turn may interfere with the fidelity of the transcriptome in AOA2 cerebellum.

AOA2 is just one of several neurodegenerative disorders characterized by

defects in RNA metabolism that impact either gene transcription, pre-mRNA splicing, ribonucleoprotein complex formation, mRNA transport, RNA translation or RNA degradation.<sup>28</sup> One form of the motor neuron disease, amyotrophic lateral sclerosis (ALS) is caused by defects in TDP-43 and FUS/TLS, both of which contain RNA-binding motifs<sup>29</sup> and spinal muscular atrophy (SMA) is caused by deletion or mutation in survival of motor neuron 1 (SMN1). Profound loss of spliceosome integrity is a critical mechanism common to ALS and SMA.<sup>30</sup> It is also of interest that we previously identified SMN as one of the proteins that interact with senataxin, pointing to an overlapping role in RNA processing.<sup>15</sup>

In summary, much progress has been made recently on the function of senataxin and its yeast ortholog Sen1p in resolving potential conflict between transcription

and DNA replication in proliferating cells. Resolution of R-loops is prominent in that role but it is evident that senataxin has a broader involvement in RNA processing (Fig. 3). Its role in post-mitotic cells is not clear, but it is likely that this will be on some aspect of RNA metabolism to protect the integrity of the genome/transcriptome. What remains intriguing is how mutations in a single gene *SETX*, often in close proximity to one another, can cause both autosomal dominant and recessive disorders. However, while mutations in *SETX* give rise to what appears to be 4 different syndromes, it is also evident that there is some overlap across these disorders. To date, several senataxin-interacting proteins have been identified, all of which are involved in some aspect of RNA processing.<sup>15</sup> Mutations in some of these also give rise to other neurodegenerative disorders.<sup>28</sup> It seems likely that these

proteins function in complexes to control RNA metabolism and different mutations in the various subunits may impact differently on the function of the complex(es), giving rise to the heterogeneity of neurodegenerative disorders observed. The challenge that lies ahead is to understand the relationships of these proteins to one another in the complexes and how they function to control processes in neurons and other cell types in the brain to minimise the risk of neurodegeneration.

#### Disclosure of Potential Conflicts of Interest

No potential conflict of interest was disclosed.

#### Acknowledgments

We thank the Australian National Health and Medical Research Council for funding support and Tracey Laing for assistance in preparation of this manuscript.

#### References

- Palau F, Espinós C. Autosomal recessive cerebellar ataxias. *Orphanet J Rare Dis* 2006; 1:47; PMID:17112370; <http://dx.doi.org/10.1186/1750-1172-1-47>
- Le Ber I, Bouslam N, Rivaud-Péchois S, Guimarães J, Benomar A, Chamayou C, et al. Frequency and phenotypic spectrum of ataxia with oculomotor apraxia 2: a clinical and genetic study in 18 patients. *Brain* 2004; 127:759-67; PMID:14736755; <http://dx.doi.org/10.1093/brain/awh080>
- Fogel BL, Perlman S. Clinical features and molecular genetics of autosomal recessive cerebellar ataxias. *Lancet Neurol* 2007; 6:245-57; PMID:17303531; [http://dx.doi.org/10.1016/S1474-4422\(07\)70054-6](http://dx.doi.org/10.1016/S1474-4422(07)70054-6)
- Anheim M, Monga B, Fleury M, Charles P, Barbot C, Salih M, et al. Ataxia with oculomotor apraxia type 2: clinical, biological and genotype/phenotype correlation study of a cohort of 90 patients. *Brain* 2009; 132:2688-98; PMID:19696032; <http://dx.doi.org/10.1093/brain/awp211>
- Criscuolo C, Chessa L, Di Giandomenico S, Mancini P, Saccà F, Grieco GS, et al. Ataxia with oculomotor apraxia type 2: a clinical, pathologic, and genetic study. *Neurology* 2006; 66:1207-10; PMID:16636238; <http://dx.doi.org/10.1212/01.wnl.0000208402.10512.4a>
- Moreira MC, Klur S, Watanabe M, Németh AH, Le Ber I, Moniz JC, et al. Senataxin, the ortholog of a yeast RNA helicase, is mutant in ataxia-ocular apraxia 2. *Nat Genet* 2004; 36:225-7; PMID:14770181; <http://dx.doi.org/10.1038/ng1303>
- Chen YZ, Hashemi SH, Anderson SK, Huang Y, Moreira MC, Lynch DR, et al. Senataxin, the yeast Sen1p orthologue: characterization of a unique protein in which recessive mutations cause ataxia and dominant mutations cause motor neuron disease. *Neurobiol Dis* 2006; 23:97-108; PMID:16644229; <http://dx.doi.org/10.1016/j.nbd.2006.02.007>
- Suraweera A, Becherel OJ, Chen P, Rundle N, Woods R, Nakamura J, et al. Senataxin, defective in ataxia oculomotor apraxia type 2, is involved in the defense against oxidative DNA damage. *J Cell Biol* 2007; 177:969-79; PMID:17562789; <http://dx.doi.org/10.1083/jcb.200701042>
- Chen YZ, Bennett CL, Huynh HM, Blair IP, Puls I, Irobi J, et al. DNA/RNA helicase gene mutations in a form of juvenile amyotrophic lateral sclerosis (ALS4). *Am J Hum Genet* 2004; 74:1128-35; PMID:15106121; <http://dx.doi.org/10.1086/421054>
- Rudnik-Schöneborn S, Eggermann T, Kress W, Lemmink HH, Cobben JM, Zerres K. Clinical utility gene card for: proximal spinal muscular atrophy. *Eur J Hum Genet* 2012; 20; PMID:22510849; <http://dx.doi.org/10.1038/ejhg.2012.62>
- Bassuk AG, Chen YZ, Batish SD, Nagan N, Opal P, Chance PF, et al. In cis autosomal dominant mutation of Senataxin associated with tremor/ataxia syndrome. *Neurogenetics* 2007; 8:45-9; PMID:17096168; <http://dx.doi.org/10.1007/s10048-006-0067-8>
- Ursic D, Himmel KL, Gurley KA, Webb F, Culbertson MR. The yeast SEN1 gene is required for the processing of diverse RNA classes. *Nucleic Acids Res* 1997; 25:4778-85; PMID:9365256; <http://dx.doi.org/10.1093/nar/25.23.4778>
- Ursic D, Chinchilla K, Finkel JS, Culbertson MR. Multiple protein/protein and protein/RNA interactions suggest roles for yeast DNA/RNA helicase Sen1p in transcription, transcription-coupled DNA repair and RNA processing. *Nucleic Acids Res* 2004; 32:2441-52; PMID:15121901; <http://dx.doi.org/10.1093/nar/gkh561>
- De Amicis A, Piane M, Ferrari F, Fanciulli M, Delia D, Chessa L. Role of senataxin in DNA damage and telomeric stability. *DNA Repair (Amst)* 2011; 10:199-209; <http://dx.doi.org/10.1016/j.dnarep.2010.10.012>
- Suraweera A, Lim Y, Woods R, Birrell GW, Nasim T, Becherel OJ, et al. Functional role for senataxin, defective in ataxia oculomotor apraxia type 2, in transcriptional regulation. *Hum Mol Genet* 2009; 18:3384-96; PMID:19515850; <http://dx.doi.org/10.1093/hmg/ddp278>
- Skourtis-Stathaki K, Proudfoot NJ, Gromak N. Human senataxin resolves RNA/DNA hybrids formed at transcriptional pause sites to promote Xrn2-dependent termination. *Mol Cell* 2011; 42:794-805; PMID:21700224; <http://dx.doi.org/10.1016/j.molcel.2011.04.026>
- Aguilera A, Gómez-González B. Genome instability: a mechanistic view of its causes and consequences. *Nat Rev Genet* 2008; 9:204-17; PMID:18227811; <http://dx.doi.org/10.1038/nrg2268>
- Li X, Manley JL. Inactivation of the SR protein splicing factor ASF/SE2 results in genomic instability. *Cell* 2005; 122:365-78; PMID:16096057; <http://dx.doi.org/10.1016/j.cell.2005.06.008>
- Mischo HE, Gómez-González B, Grzechnik P, Rondón AG, Wei W, Steinmetz L, et al. Yeast Sen1 helicase protects the genome from transcription-associated instability. *Mol Cell* 2011; 41:21-32; PMID:21211720; <http://dx.doi.org/10.1016/j.molcel.2010.12.007>
- Hazelbaker DZ, Marquardt S, Wlotzka W, Buratowski S. Kinetic competition between RNA Polymerase II and Sen1-dependent transcription termination. *Mol Cell* 2013; 49:55-66; PMID:23177741
- Alzu A, Bermejo R, Begnis M, Lucca C, Piccini D, Carotenuto W, et al. Senataxin associates with replication forks to protect fork integrity across RNA-polymerase-II-transcribed genes. *Cell* 2012; 151:835-46; PMID:23141540; <http://dx.doi.org/10.1016/j.cell.2012.09.041>
- Yüce O, West SC. Senataxin, defective in the neurodegenerative disorder ataxia with oculomotor apraxia 2, lies at the interface of transcription and the DNA damage response. *Mol Cell Biol* 2013; 33:406-17; PMID:23149945; <http://dx.doi.org/10.1128/MCB.01195-12>
- Vantaggiato C, Bondioni S, Airoldi G, Bozzato A, Borsani G, Rugarli EL, et al. Senataxin modulates neurite growth through fibroblast growth factor 8 signalling. *Brain* 2011; 134:1808-28; PMID:21576111; <http://dx.doi.org/10.1093/brain/awr084>
- Becherel OJ, Yeo AJ, Stellati A, Heng EY, Luff J, Suraweera AM, et al. Senataxin plays an essential role with DNA damage response proteins in meiotic recombination and gene silencing. *PLoS Genet* 2013; 9:e1003435; PMID:23593030; <http://dx.doi.org/10.1371/journal.pgen.1003435>
- Lavin MF. The appropriateness of the mouse model for ataxia-telangiectasia: Neurological defects but no neurodegeneration. *DNA Repair (Amst)* 2013; In press; PMID:23731731; <http://dx.doi.org/10.1016/j.dnarep.2013.04.014>

26. Lynch DR, Braastad CD, Nagan N. Ovarian failure in ataxia with oculomotor apraxia type 2. *Am J Med Genet A* 2007; 143A:1775-7; PMID:17593543; <http://dx.doi.org/10.1002/ajmg.a.31816>
27. Fogel BL, Lee JY, Perlman S. Aberrant splicing of the senataxin gene in a patient with ataxia with oculomotor apraxia type 2. *Cerebellum* 2009; 8:448-53; PMID:19727998; <http://dx.doi.org/10.1007/s12311-009-0130-8>
28. Strong MJ, Volkening K. TDP-43 and FUS/TLS: sending a complex message about messenger RNA in amyotrophic lateral sclerosis? *FEBS J* 2011; 278:3569-77; PMID:21810174; <http://dx.doi.org/10.1111/j.1742-4658.2011.08277.x>
29. Fiesel FC, Kahle PJ. TDP-43 and FUS/TLS: cellular functions and implications for neurodegeneration. *FEBS J* 2011; 278:3550-68; PMID:21777389; <http://dx.doi.org/10.1111/j.1742-4658.2011.08258.x>
30. Tsuiji H, Iguchi Y, Furuya A, Kataoka A, Hatsuta H, Atsuta N, et al. Spliceosome integrity is defective in the motor neuron diseases ALS and SMA. *EMBO Mol Med* 2013; 5:221-34; PMID:23255347; <http://dx.doi.org/10.1002/emmm.201202303>
31. Wongsurawat T, Jenjaroenpun P, Kwok CK, Kuznetsov V. Quantitative model of R-loop forming structures reveals a novel level of RNA-DNA interactome complexity. *Nucleic Acids Res* 2012; 40:e16; PMID:22121227; <http://dx.doi.org/10.1093/nar/gkr1075>
32. Ginno PA, Lott PL, Christensen HC, Korf I, Chédin F. R-loop formation is a distinctive characteristic of unmethylated human CpG island promoters. *Mol Cell* 2012; 45:814-25; PMID:22387027; <http://dx.doi.org/10.1016/j.molcel.2012.01.017>